GEORGIA INSTITUTE OF TECHNOLOGY
Engineering Experiment Station

PROJECT INITIATION

Date: June 21, 1972

Project Title: An Investigation of the Accuracy of Far-Field Radiation Patterns Determined from Near-Field Measurements.

Project No.: A-1433*

Project Director: Dr. C. P. Burns (Principal Investigator)

Sponsor: U. S. Army Missile Command

Effective . . June 5, 1972. . . . . Estimated to run until: . . . April 4, 1973. (End Work Period)

Type Agreement: . . Contract No. DAAH01-72-C-0930 . . . . . Amount: $ . . 31,772* . . . . .

*Constitutes sub-project under E-21-621 (School of EE), Dr. E. B. Joy & Dr. C. P. Rodrigue Co-Project Directors, budgeted for $26,283. Total Contract estimate is $58,055

REPORTS REQUIRED: Final Technical Report

SPONSOR CONTACT PERSONS: Technical Matters
Chief, Advanced Sensors Directorate for
Research, Development, Engineering &
Missile Systems Laboratory
U. S. Army Missile Command
Redstone Arsenal, Ala 35809
Contractual Matters
(Thru GTRI)
Mr. R. J. Whitcomb (ACO)
ONR Resident Representative
Campus

Defense Priority Rating: DO-A2 under DMS Reg. 1

Assigned to . . . . . RADAR . . . . . Division

COPIES TO:

Project Director	Photographic Laboratory
Director	Security, Property, Reports Coordinator
Assistant Director	EES Accounting
GTRI	EES Supply Services
Division Chief(s)	~~Library~~
Service Groups	Rich Electronic Computer Center
Patent Coordinator	Project File
	Other Dr. E. B. Joy/Dr. C. P. Rodrigue, Co-Project Directors

RI DDC
Service Required

RA-62

GTA

GEORGIA INSTITUTE OF TECHNOLOGY
Engineering Experiment Station

PROJECT TERMINATION

Date September 21, 1973

PROJECT TITLE: An Investigation of the Accuracy of Far Field Radiation Patterns Determined From Near Field Measurements

PROJECT NO: A-1139*

PROJECT DIRECTOR: Dr. C. E. Baum (Principal Investigator)*

SPONSOR: U. S. Navy (Office of Naval Research)

TERMINATION EFFECTIVE: [illegible] 1973 (Contract Expiration)

CHARGES SHOULD CLEAR ACCOUNTING BY: September 30, 1973

Contract Closeout Items Pertaining: Final Invoice & Closing Documents
Final Report of Inventions
Government Property Inventory & Cert.
Classified Material Cert.

*Institution sub-contract under N-21-022, School of [illegible]
Dr. [illegible] Roy and Mr. C. E. Baum, Co-Project Directors.

PATENT DIVISION

COPIES TO:

Project Director
Director
Associate Director
Assistant Directors
Division Chief
Branch Head
Accounting
Engineering Design Services

General Office Services
Photographic Laboratory
Purchasing
Report Section
Library ✓
Security
Rich Electronic Computer Center

rm EES 402 (R10—62)

GEORGIA INSTITUTE OF TECHNOLOGY
OFFICE OF RESEARCH ADMINISTRATION

RESEARCH PROJECT INITIATION

all reports will come from the A project A-1433

Date: June 21, 1972

Project Title: An Investigation of the Accuracy of Far-Field Radiation Patterns Determined from Near-Field Measurements

Project No: E-21-621*

Principal Investigator Dr. E. B. Joy and Dr. G. P. Rodrigue

Sponsor: U. S. Army Missile Command

Agreement Period: From June 5, 1972 Until April 4, 1973 (End Work Period)

Type Agreement: Contract No. DAAH01-72-C-0950 S

Amount: $26,283*

*Project includes sub-project A-1433 (EES) budgeted for $31,772 with Mr. C. P. Burns PrincipalInvestigator. Total contract estimate is $58,055.

Reports Required:
Final Technical Report

Sponsor Contact Person (s): Technical Matters
Chief, Advanced Sensors Directorate
for Research, Development Engineering &
Missile Systems Laboratory
U. S. Army Missile Command
Redstone Arsenal, Alabama 35809

Contractual Matters
(Thru GTRI)
Mr. R. J. Whitcomb (ACO)
ONR Resident Representative
Campus

Assigned to: Electrical Engineering

Defense Priority Rating: DO-A2 under DMS Reg. 1

COPIES TO:

Principal Investigator	Library
School Director	Rich Electronic Computer Center
Dean of the College	Photographic Laboratory
Director, Research Administration	Project File
Director, Financial Affairs (2)	
Security-Reports-Property Office	
Patent Coordinator	Other Mr. C. P. Burns (Principal Investigator A-1433)

RA-3 (6-71)

GEORGIA INSTITUTE OF TECHNOLOGY

OFFICE OF RESEARCH ADMINISTRATION

RESEARCH PROJECT TERMINATION

Date: September 21, 1973

Project Title: An Investigation of the Accuracy of Far-Field Radiation Patterns Determined from Near-Field Measurements

Project No: E-21-621

Principal Investigator: Dr. E. B. Joy & Dr. G. P. Rodrigue

Sponsor: U.S. Army Missile Command; Redstone Arsenal, Alabama

Effective Termination Date: 9/4/73 (Contract Expiration)

Clearance of Accounting Charges: by 9/30/73

grant/closeout actions remaining: Final Invoice & Closing Documents
Final Report of Inventions
Gov't. Property Inventory & Cert.
Classified Material Cert.

NOTE: Includes Sub-Project A-1433 EES.

School of Electrical Engineering

COPIES TO:

Principal Investigator
School Director
Dean of the College
Director of Research Administration
Associate Controller (2)
Security-Reports-Property Office ✓
Patent and Inventions Coordinator
Library, Technical Reports Section
Rich Electronic Computer Center
Photographic Laboratory
Terminated Project File No. _____
Other _____

RA-4 (5/70)

AN INVESTIGATION OF THE ACCURACY OF FAR-FIELD RADIATION PATTERNS DETERMINED FROM NEAR-FIELD MEASUREMENTS

G. P. Rodrigue, E. B. Joy,
and C. P. Burns

Georgia Institute of Technology
Atlanta, Georgia

August 1973

Advanced Sensors Directorate
Research, Development, Engineering and Missile Systems Laboratory
U. S. Army Missile Command
Redstone Arsenal, Alabama

AN INVESTIGATION OF THE ACCURACY OF FAR-FIELD RADIATION PATTERNS DETERMINED FROM NEAR-FIELD MEASUREMENTS

G. P. Rodrigue
E. B. Joy
C. P. Burns

August 1973

FOREWORD

This study of the accuracy of far-field radiation patterns of microwave antennas as determined from near-field measurements was conducted under Contract No. DAAH01-72-C-0950 from the U. S. Army Missile Command. The work reported was performed at Georgia Tech in the School of Electrical Engineering and in the Radar Division of the Engineering Experiment Station during period from June 1972 to July 1973.

In addition to Georgia Tech personnel, special acknowledgement is made to Scientific Atlanta for their cooperation in scheduling their Gwinnett County Antenna Range and to Mr. William G. Spaulding of the Advanced Sensors Directorate, RDE and Missile Systems Laboratory, who was AMC's Technical Representative on this project.

ABSTRACT

The results reported herein show that far-field antenna patterns determined on the near-field range are as accurate as those determined on a far-field range. The patterns of a single plane, monopulse antenna, operated at 5.45 GHz were measured on a near-field range and two different far-field ranges, and detailed comparisons were made.

The results of a computer-aided simulation study to determine the effects of various near-field measurement errors on the far-field patterns are also described. It was found that some near-field parameters are relatively critical; point source reflections are very deleterious. Far-field accuracy was found to be surprisingly insensitive to many near-field parameters.

Comparisons of near-field and far-field techniques indicate several additional, non-technical, advantages of the near-field approach.

Recommendations are made for future work to demonstrate the near-field techniques on phased array antennas, and to improve the data processing procedures so as to increase the resolution of far-field patterns obtained from near-field measurements.

TABLE OF CONTENTS

LIST OF FIGURES

LIST OF FIGURES (Continued)

LIST OF FIGURES (Continued)

LIST OF FIGURES (Continued)

LIST OF FIGURES (Continued)

LIST OF FIGURES (Continued)

LIST OF FIGURES (Continued)

LIST OF FIGURES (Continued)

LIST OF FIGURES (Continued)

LIST OF FIGURES (Continued)

LIST OF FIGURES (Continued)

LIST OF TABLES

SECTION 1

INTRODUCTION

1.1 Program Goals

This final report on Contract No. DAAH01-72-C-0950 contains the results of a program conducted at the Georgia Institute of Technology for the U. S. Army Missile Command. The goal of this program has been the demonstration of the accuracy of a near-field measurement technique in determining the far-field antenna patterns of microwave antennas.

While several earlier programs of investigation have been conducted on near-field measurements, there has been a noticeable lack of conclusive corroborative data of far-field patterns determined on qualified far-field ranges and on near-field ranges. Additionally, antennas measured in previous programs have not generally conformed to the high-performance standards of modern missile system radars. Thus, in this program, the emphasis has been on the collection of comparable sets of data on an antenna designed to have pattern characteristics comparable to those of a modern high gain monopulse radar antenna.

Since neither the near-field antenna range nor any far-field antenna range has infinite accuracy, a portion of this effort has also been allocated to the determination of the accuracy of the measurements conducted on both the near-field range and the far-field ranges. Error tolerances can be established for each set of these measurements, and the final results can then be compared with respect to agreement within those assigned errors. In addition, two sets of far-field measurements were taken to compare also the agreement achievable on different far-field ranges.

1.2 Description of Program

The test antenna used was, in the interest of time and money, a single plane monopulse antenna. It consisted of a four foot paraboloidal dish reflector fed by two horns so as to form sum and difference patterns in the azimuth plane. The details of the design of this antenna are contained in Section 4.

Measurements were taken in the following sequence. First, the antenna pattern characteristics were obtained on a 1000 foot range at Georgia Tech. Second, the far-field pattern was determined from near-field measurements in the near-field laboratory at Georgia Tech. Finally, a second set of far-field patterns was measured on Scientific-Atlanta's Gwinnett County range.

In the final analysis then, it is possible to compare the far-field patterns determined from the near-field measurements with the far-field patterns determined on either of the far-field ranges. Furthermore, it is possible to compare the far-field patterns measured on two outdoor ranges with one another.

The accuracy of a far-field range can be determined by field probe measurements to check for spurious or multipath reflections on the range. In the near-field facility no such direct measurement is possible, and, in general, it is mathematically impossible to relate in a deterministic way the influence of certain near-field measurement errors on specific far-field parameters.

To quantify the accuracy of far-field patterns determined from near-field measurements a simulation study was conducted wherein a wide range of near-field pattern errors were modeled mathematically, and the resultant errors produced in the computed far-field patterns

determined. The simulation study not only allows the quantification of the accuracy of the far-field patterns determined from the near-field measurements but also allows the establishment of accuracy criteria for each near-field parameter.

It is to be emphasized that the simulation study serves this dual role and therefore is more than simply a means of justifying the accuracy of far-field patterns determined on the near-field facility. The simulation results have general applicability in the specification of required near-field measurement accuracy, not only on this program but also on any future application of the near-field technique. Inasmuch as errors of the near-field range are generally prescribed with respect to wavelength criteria, these same results could be extended to frequencies other than the C-band frequencies used in these experiments, and can provide valuable information as to which near-field parameters are critically important and which are relatively less so. In future applications of the near-field technique, these results can provide very valuable insight into where equipment expenditures can most wisely be made, and can prevent unnecessary and costly expenditures in certain areas of the near-field range where the justification of such cost is not borne out by the influence of those inaccuracies on the far-field patterns.

The results obtained in this study fully substantiate the accuracy of this near-field measurement approach. All pattern parameters were found to be measurable within the accuracy of the far-field range, and valuable insight into the accuracy requirements on near-field measurements were obtained from the simulation study.

1.3 Outline of Report

This report is divided into several sections and their contents are briefly described below. The background of near-field measurement techniques as embodied in earlier work is summarized in Section 2 with extensive references to previous work. This information provides some insight into the reason for the recent rapid advance of near-field techniques.

Section 3 outlines the simulation study conducted on this program with regard to the mathematical models used, the near-field measurement errors simulated, and the far-field parameters determined and tabulated. The principle results of this simulation study are presented in graphical form showing the influence of the magnitude of each near-field error on the error produced in various far-field parameters. Complete simulation results are contained in Appendix A.

Section 4 contains a description of the antenna design used in this study including one feed designed for a deep difference pattern null and low sidelobe levels and a second feed designed to produce a better compromise between sum and difference patterns and to more accurately represent those characteristics achievable on a high-performance radar antenna.

Section 5 contains a description of each far-field antenna range, the quality of that range as determined from field probe measurements, procedures used in collection of data, and the principal results of the far-field patterns. Additional graphs of far-field patterns determined on the far-field ranges are contained in Appendix B. The near-field range is described in Section 6, and the control of this facility by the Nova computer is presented in block diagram form.

The principal sources of error on the near-field range are also described in this section. Representative near-field data collected and computed far-field patterns are also shown in this section.

Section 7 contains a comparison of the results of the far-field patterns determined both on the two far-field ranges and on the near-field range. Comparative, superposed, pattern cuts are displayed and derived numerical data are displayed in tabular form.

Section 8 discusses the relative advantages and disadvantages of the two types of measurements as presently seen. Recommendations on future work are also contained in Section 8.

SECTION 2

NEAR-FIELD MEASUREMENT BACKGROUND

2.1 Development of Near-Field Measurements

The determination of the far-field radiation pattern from near-field measurements is an old concept. The equations relating the near-field of an antenna to the far-field of the same antenna were in print in the 1930's.

Early work in near-field measurements attempted to directly implement Huygens' principle of secondary spherical waves (1-4). Use of Huygens' principle required measurement of both the tangential electric and magnetic fields on a near-field surface. As the magnetic field was difficult to measure with accuracy, it was assumed to be directly proportional to the measured electric field as in a plane wave.

Huygens' principle also required knowledge of the direction of propagation of the field at each point on the measurement surfaces. As the unknown direction of propagation could not be determined directly, it was assumed to be normal to the measurement surface.

The near-field measuring probe was assumed to be ideal, measuring exactly the undistorted tangential electric field. The near-field measurement spacings were chosen to obtain smooth near-field measurement graphs on a trial and error basis. The amount of near-field data was usually very large and almost no data minimization was used.

Experimentally, early work in near-field measurement was directed toward development of an ideal near-field measuring probe. Richmond and Tice (5) stated that an ideal probe should possess the following qualities:

(1) The probe should not distort the field being measured.

(2) The probe should be small enough to essentially measure the field at a point.

(3) The probe should be linearly polarized.

(4) The probe should provide the measuring equipment with an adequate signal.

Two general classes of probes were developed to measure the tangential electric field. The first class provided a direct sample of the field. The second class provided an indirect sample of the field by measuring the backscattering from a small probe located on the measurement surface.

Whiteside and King (6), Borts (7), and Woonton (8) worked with direct measurement probes and developed small dipole probes which closely approximated the ideal probe at low frequencies. Richmond and Tice (5) developed small dielectrically loaded waveguide probes which were useful in the microwave region and provided a good estimate of the field without probe correction.

Justice and Rumsey (9), Harrington (10) and Plonsey (11) developed near-field scatterers and scattering systems which measured the near-field indirectly. The significance of this method of measurement is that the probe size can be greatly reduced, reducing the distortion of the field due to the presence of the probe.

In all of these early near-field measurement systems, measurement of the relative phase of the electromagnetic field was time-consuming and usually inaccurate.

Although sophisticated probes and measuring systems were developed, many unjustifiable assumptions concerning the properties of the field being measured remained, until Booker (12) and Clemmow (13) reformulated

the far-field determination problem in terms of plane wave expansions. They showed that only two components of the tangential electric field were required to determine the complete far-field and that knowledge of the direction of propagation at each near-field measurement point was not required.

Brown (14) and Jull (15-17), working with line sources and using cylindrical wave expansions of the electromagnetic fields, also showed that only two components of the tangential electric field needed to be measured and that the direction of propagation of the measured field was not needed.

In summary, four problems prevented the near-field measurement technique of far-field determination from being viable. The problems were as follows:

a. The far-field computation process required lengthy integral evaluations, which, even with fast digital computers, were costly.

b. A mathematical description of the interaction of the near-field probe and the near-field being measured was needed to accurately calculate the far-field pattern.

c. A sample spacing criterion was needed to specify the required distance between near-field samples.

d. Near-field measurement and data recording equipment were needed to measure amplitude and phase and to record large amounts of data quickly and accurately in a format compatible with a digital computer.

2.2 Recent Advances in Near-Field Technology

The solutions to these problems have come from many sources and

have recently been combined and implemented at Georgia Tech.

The solution to the first problem came from the use of the plane wave expansion technique to describe the electromagnetic field in its transition from the near-field to the far-field instead of the previously used Huygens' Principle, a spherical wave expansion. The major computational requirement of the plane wave expansion technique is the Fourier Transform of an equally incremented two-dimensional complex array of near-field data. The recently developed Fast Fourier Transform algorithm now performs this computation in an almost insignificant amount of computer time. Previous computation times of one to two hours have been reduced to approximately five to ten seconds.

The solution to the second problem was originated by Kerns (18) and Dayhoff (19) at NBS.* Using the plane wave expansion technique of far-field determination and neglecting second reflections between the near-field probe and the test antenna, they solved a linear system of plane wave matrix equations resulting in an easily implemented technique for correction. The probe correction technique, however, introduced an additional requirement into this far-field determination procedure. The far-field pattern, or equivalently the wavenumber spectrum, of the near-field probe was required to be known.

The solution to the third problem, the sampling problem, was originated by Joy (20) at Georgia Tech. The sample spacing for near-field measurements made on a planar surface was found to be a function of the distance from the test antenna to the near-field measurement plane and of the dynamic amplitude range of the near-field measurement equipment. The sample spacing was found to monotonically increase with increasing separation, reaching an upper bound of one-half wavelength.

* National Bureau of Standards, Boulder, Colorado

The solution to the fourth problem was the development of a new generation of microwave receivers by Scientific Atlanta, Inc. The newly developed receivers can measure the amplitude and relative phase easily, accurately, and quickly. Associated automated probe positioning, data conversion, and recording equipment allow recording large quantities of data and facilitate transfer of data to digital computers.

Among the most recent published near-field measurement results have been the results of Ph.D. dissertation research by Joy (20-23) and Leach (24), both of Georgia Tech. Joy measured the near-field of two antennas, over a planar surface; whereas, Leach measured the near-field of a single antenna over a cylindrical surface. The attached bibliography is a comprehensive summary of near-field publications.

BIBLIOGRAPHY

1. S. Silver, Microwave Antenna Theory and Design, McGraw-Hill Book Company, New York, Chapters 5 and 6, 1949.

2. N. J. Gamara, "Pattern Predictability on the Basis of Aperture Phase and Amplitude Distribution Measurements," Tech. Rep. EDL-M247, Contract DA 36-039 SC-S5402, (DDC No. AD-236298) Electronic Defense Lab, Mountain View, California, March 25, 1960.

3. M. Hu, "Study of Near-zone Fields of Large Aperture Antennas," Final Report on Contract No. AF 30(602)-928, Syracuse University Research Institute, April 1957.

4. D. T. Paris, "Digital Computer Analysis of Aperture Antennas," IEEE Transactions on Antennas and Propagation, Vol. AP-16, No. 2, pp. 262-264, March 1968.

5. J. H. Richmond and T. E. Tice, "Probes for Near-field Measurements," IRE Transactions on Microwave Theory and Propagation, Vol. 3, No. 3, pp. 32-34, April 1955.

6. H. Whiteside and R. W. P. King, "The Loop Antenna as a Probe," IEEE Transactions on Antennas and Propagation, Vol. AP-12, No. 3, pp. 291-297, May 1964.

7. G. A. Woonton, "The Probe Antenna and the Diffraction Field," Technical Report 17, Eaton Elec. Res. Lab., McGill University, July 1952.

8. R. B. Borts and G. A. Woonton, "The Effect of the Directivity of the Probe Upon the Measurement of Aperture Fields," Technical Report 21, (DDC No. AD 28506) Eaton Elec. Tes. Lab., McGill University, July 1952.

9. R. Justice and V. H. Rumsey, "Measurement of Electric Field Distribution," IRE Transactions on Antennas and Propagation, Vol. AP-3, No. 4, pp. 177-180, October 1955.

10. R. F. Harrington, "Small Resonant Scatterers and Their Use for Field Measurements," IRE Transactions on Microwave Theory and Techniques, Vol. MTT-10, No. 3, pp. 166-174, May 1962.

11. R. Plonsey, "Surface Current Measurements with an Electric Probe," IRE Transactions on Microwave Theory and Techniques, Vol. MTT-10, No. 3, pp. 214-217, May 1962.

12. H. G. Booker and P. C. Clemmow, "The Concept of an Angular Spectrum of Plane Waves, and its Relation to that of Polar Diagram and Aperture Distribution," Proceedings IEE, Vol. 97, Part 3, pp. 11-17, January 1950.

13. P. C. Clemmow, The Plane Wave Spectrum Representation of Electromagnetic Fields, Pergamon Press, Ltd., London, 1966.

14. J. Brown, "A Theoretical Analysis of Some Errors in Aerial Measurements," Proceedings IEE, Vol. 105, Part C, pp. 343-351, February 1959.

15. E. V. Jull, "An Investigation of Near-field Radiation Patterns Measured with Large Antennas," IRE Transactions on Antennas and Propagation, Vol. AP-10, No. 4, pp. 363-369, July 1962.

16. E. V. Jull, "The Estimation of Aerial Radiation Patterns from Limited Near-field Measurements," Proceedings IEE, Vol. 110, No. 3, pp. 501-506, March 1963.

17. J. Brown and E. V. Jull, "The Prediction of Aerial Radiation Patterns from Near-field Measurements," Proceedings IEE, Vol. 105, Part B., No. 42, pp. 635-644, November 1961.

18. D. M. Derns, "Antenna Measurements with Arbitrary Measruing Antennas at Arbitrary Distances," High Frequency and Microwave Field Strength Precision Measurements Seminar, National Bureau of Standards, Boulder, Colorado, Session 3, Lecture 1, 1966.

19. D. M. Kerns and E. S. Dayhoff, "Theory of Diffraction in Microwave Interferometry," Journal of Research of the National Bureau of Standards - B. Mathematics and Mathematical Physics, Vol. 64B, No. 1, January-March 1960.

20. E. B. Joy, "Spatial Sampling and Filtering in Near-field Measurements," Ph.D. Dissertation, Georgia Institute of Technology, 1970.

21. E. B. Joy and D. T. Paris, "Spatial Sampling and Filtering in Near-field Measurements," IEEE Transactions on Antennas and Propagation, Vol. AP-20, No. 3, May 1972, pp. 253-261.

22. E. B. Joy, "Far-field Calculation From Near-field Measurements," Proceedings of the Eleventh Symposium on Electromagnetic Windows, Atlanta, Georgia, August 1972, pp. 253-261.

23. E. B. Joy and D. T. Paris, "A Practical Method for Measuring the Complex Polarization Ratio of Arbitrary Antennas," accepted for publication in the IEEE Transactions on Antennas and Propagation.

24. W. M. Leach, "Probe Compenstated Near-field Measurements on a Cylinder," Ph.D. Dissertation, Georgia Institute of Technology, 1972.

SECTION 3

NEAR-FIELD MEASUREMENT ERROR SIMULATION STUDY

3.1 Introduction

The integral relationships existing between the near-field and the far-field of an antenna are of sufficient complexity that straightforward statistical or deterministic evaluation of the effects of near-field measurement error on the calculated far-field pattern can only be done for the simplest types of errors. Therefore, as an alternative method of quantifying the effects of near-field measurement errors on the calculated far-field pattern of an antenna, a computer simulation of these errors was carried out.

The purpose of the simulation is to put bounds on the many possible near-field measurement errors which take place in an actual near-field measurement environment. Viewed differently, the results of the computer simulation should, for a given required far-field pattern accuracy, specify the required environment for performing near-field measurements as well as specify the maximum allowable inaccuracies of the associated microwave source, transmission lines, mechanical positioners, and data measuring and recording equipment.

The simulation uses a base model on which perturbations are made. The base model is a hypothetical, well defined near-field distribution. The near-field distribution is entered as two, two-dimensional complex arrays. One array for the X-component of the near-field and one array for the Y-component of the near-field. Each array is complex, meaning that the amplitude and phase of each near-field component must be specified. Each near-field array contains 64 x 64 = 1096 complex near-

field samples spaced at intervals of 2/3 wavelength in both the X and Y directions. The near-field area being sampled is approximately 43 wavelengths square. Using the hypothetical near-field distributions, a far-field pattern is calculated and stored within the computer. To determine the effect of a near-field error, the hypothetical near-field distribution is corrupted by the error. As an example, suppose the dynamic range of the near-field measurement receiver was so poor that it could only measure amplitudes which were within a -10 dB range from the peak of the near-field distribution. The far-field of the modified distribution would then be calculated using the same computer program as before, and the results compared to the stored far-field pattern calculated from the error-free hypothetical distribution. The differences between the far-field patterns would then be recorded as far-field pattern errors. The error relationships can then be shown in tabular form. A parametric evaluation of this type of near-field measurement error could be made by repeating the above computations for dynamic ranges of - 15 dB, -20 dB, -25 dB, -30 dB, -35 dB, -40 dB, -45 dB, -50 dB. The results of this parametric study could then be graphed to display the effect on the far-field predictions of the dynamic range of the near-field receiver.

3.2 Hypothetical Model

The hypothetical model used in the simulation study simulates an azimuth plane monopulse antenna with sum and difference far-field patterns. In many respects the hypothetical antenna is similar to the antenna which was designed, constructed and measured, and which will be described in more detail later. For simplicity the difference

pattern has only two main lobes instead of the usual four. This allows direction determination in only the horizontal plane and not in the vertical plane, but illustrates the basic monopulse system well. The hypothetical distribution may be thought of as being generated by a paraboloidal dish reflector antenna fed by two horn antennas. In the sum mode the horns are fed in phase and in the difference mode the horns are fed 180 degrees out of phase.

It must be emphasized that the hypothetical distribution is not meant to accurately depict any actual antenna, but rather to represent a general class of antennas with a closed form distribution. The following steps were used to arrive at the hypothetical near-field distribution. First, assume that if only one of the two feed horns were present it would produce a Taylor distribution with -20 dB sidelobes. The equation for this near-field distribution is given by

$$E_Y(x,y) = 0.707 \left(1 - (x^2 + y^2)/R^2\right)^2 \qquad (1)$$

where: $R = 0.6094$

(x,y) = aperture position in meters

If the feed horn were tilted by a small angle $\frac{\alpha}{2}$ radians, the far-field pattern would shift by an angle $\frac{\alpha}{2}$ radians, and the near-field distribution would be correspondingly modified by a phase shift factor as follows:

$$E_Y(x,y) = 0.707 \left(1 - (x^2 + y^2)/R^2\right)^2 e^{-j\beta \, x \sin(\alpha/2)} \qquad (2)$$

where: $\beta = 2\pi/\lambda$

If a second horn antenna were added, placed in the center of the parabola, and then shifted by an angle $-\frac{\alpha}{2}$ radians, the total near-field distribution would be the sum of the two near-field distributions and

would be given by

$$E_{YS}(x,y) = 1.414 \left(1 - (x^2 + y^2)/R^2\right)^2 \cos\left(\beta \times \sin(\alpha/2)\right) \quad (3)$$

If the phase of the second feed horn were changed by 180 degrees to produce a monopulse difference pattern, the difference near-field distribution would be

$$E_{YD}(x,y) = j\ 1.414 \left(1 - (x^2 + y^2)/R^2\right)^2 \sin\left(\beta \times \sin(\alpha/2)\right) \quad (4)$$

To this point we have assumed that the feed horns were linearly polarized. Now let it be further assumed that each of the feed horns has a polarization ratio defined by

$$T = \frac{E_X(x,y)}{E_Y(x,y)} \quad (5)$$

Thus, in summary, the X and Y components of the hypothetical near-field distributions are as follows:

SUM Pattern

1. Y component; $E_{YS}(x,y) = 1.414 \left(1 - (x^2 + y^2)/R^2\right)^2 \cos\left(\beta \times \sin(\alpha/2)\right)$ (6)

2. X component; $E_{XS}(x,y) = T\ E_{YS}(x,y)$

DIFFERENCE Pattern

1. Y component; $E_{YD}(x,y) = j\ 1.414 \left(1 - (x^2 + y^2)/R^2\right)^2 \sin\left(\beta \times \sin(\alpha/2)\right)$ (7)

2. X component; $E_{XD}(x,y) = T\ E_{YD}(x,y)$

These near-field distributions are used throughout the near-field measurement simulation. The sum far-field power pattern is calculated and stored, and the difference far-field power pattern is calculated and stored. The bulk of the simulation can be summarized as modifying

the hypothetical near-field distributions to simulate various near-field measurement errors followed by computation of the associated far-field patterns. The far-field patterns are then compared with the stored far-field patterns and various far-field errors are tabulated.

3.3 Near-field Errors

Near-field errors are most often produced in a complicated fashion. For example, a measurement receiver may be nonlinear, it may also add a random amplitude and phase to the signal, and it may have a limited dynamic range. Although it is not difficult to simulate a specific receiver with known characteristics, the result of such simulation could not be projected to other types of receivers with different characteristics. The approach taken in this analysis is to simulate errors which are a function of a single parameter. If enough of the single-parameter errors are simulated, a complicated near-field error can be synthesized as a combination of the simpler errors. This calculation of the effects of combined errors has been carried out for those errors estimated to exist in Georgia Tech's near-field laboratory.

Based on five years of experience in making near-field measurements and on an examination of the types and forms of the various near-field measurement errors, fifteen constitutive types of errors were formulated. Each error is a function of a single parameter, and thus far-field errors associated with each type of error can be tabulated as a function of a single parameter. What follows is a brief discussion of each of the fifteen types of near-field errors used in the sumulation.

3.3.1 Random amplitude error

Random amplitude errors are usually associated with measurement noise. Random amplitude errors can also be generated at the source

and in data conversion and recording equipment. In the simulation the amplitude of each sample of the hypothetical near-field distribution is determined and to the amplitude is added a random decibel error. The error is uniformly distributed between the limits of $\pm$ DBE dB. The uniform distribution is generated by a random number generation program which is incorporated within the simulation program. The range of DBE used is from 0 dB to 6 dB.

3.3.2 Amplitude error which is linear with respect to the true amplitude

This type of error is associated with the measurement receiver and data conversion equipment. It is one form of nonlinearity possessed by almost all measuring devices. The amplitude of each sample is determined and to it is added a dB error which is linearly proportional to the amplitude in decibels. The error for a zero dB amplitude is zero, and the error for a -40 dB amplitude is DB40L. The range of DB40L is from -10 dB to +10 dB.

3.3.3 Amplitude error which is quadratic with respect to the true amplitude

This error is another form of nonlinearity found in most receivers and data conversion equipment. The amplitude of each sample of the hypothetical distribution is determined and to it is added a decibel error which is directly proportional to the square of the amplitude in decibels. The error for a zero dB amplitude is zero dB and the error for a -40 dB amplitude is DB40Q. The range of DB40Q is from -10 dB to +10 dB.

3.3.4 Amplitude errors which are linear with time

This type of error simulates the drift of equipment with time. The most common source of this type of error is the microwave source; however,

receivers and data conversion equipment can also produce this type of error. At the start of the near-field measurement this error is zero, and at the end of the measurement the error is TDB dB. The range of TDB is from zero to 6 dB.

3.3.5 Amplitude truncation with respect to the true amplitude

This type of error simulates the errors associated with the dynamic range limitation of the receiver, data conversion equipment and data recording equipment. The amplitude of each sample of the hypothetical distribution is determined, and if the amplitude is greater than TLEVEL dB down from the maximum of the near field distribution it is unchanged; however, if it is less, it is set equal to zero (-200 dB). The range of TLEVEL is from -10 dB to -50 dB.

3.3.6 Random phase error

Random phase errors are usually associated with the receiver as measurement noise. Random phase errors may occur in other ways too, such as random flexing of coaxial cables, random motion of the test antenna or the probe antenna, noise in data conversion and data recording equipment. Random phase error may also be caused by jitter of the phase lock mechanism of the source. The phase of each sample of the hypothetical distribution is determined and to it is added a randomly distributed phase angle in degrees. The random phase is uniformly distributed with limits $\pm$ PHE degrees. The range of PHE used is from zero degrees to 20 degrees.

3.3.7 Phase error which is linearly proportional to the true phase

The true phase of each sample of the hypothetical distribution is determined and to it is added a phase error in degrees which is linearly

proportional to the true phase. If the true phase is zero, zero degrees are added to the phase. If the true phase is 180 degrees, PH180L degrees are added to the phase. The range of PH180L used in the simulation was -10 degrees to +10 degrees.

3.3.8 Phase error which is quadratic with respect to the true phase

This is another type of nonlinearity associated with measurement receivers, data conversion equipment, and data recording equipment. The true phase of each sample of the hypothetical distribution is determined and to it is added a phase error in degrees which is directly proportional to the square of the true phase. If the true phase is zero, zero degrees are added to the phase. If the true phase is 180 degrees, PH180Q degrees are added to the phase. The range of PH180Q used in the simulation was from -10 degrees to +10 degrees.

3.3.9 Phase error which is linear with time

Drift of the receiver and slow warping of mechanical positioners can cause a gradually increasing or decreasing phase error to be produced. The true phase of each sample of the hypothetical distribution is determined and to it is added a phase which is linearly proportional to the time since measurement began. The first sample receives no phase error and the last sample receives a phase error of TPHASE degrees. The range of TPHASE used in the simulation was from zero degrees to 20 degrees.

3.3.10 Phase error which is quadratic with amplitude

The phase accuracy of a phase/amplitude receiver is a nonlinear function of the amplitude of the received signal. For moderate and large amplitude signals the phase error of the receiver is small and almost independent of the signal strength. For low amplitude signals the phase

error increases rapidly with decreasing amplitude. In simulating this error, the phase and amplitude of each sample of the hypothetical distribution is determined. To the phase of the sample is added an error which is a quadratic function of the amplitude of the sample. If the amplitude of the sample is zero dB, zero phase error is added. If the amplitude of the sample is -40 dB, PHE40 degrees are added to the phase. The range of PHE40 used in the simulation was from -20 degrees to +20 degrees.

3.3.11 Random X and Y probe position errors

The probe is positioned to specified positions in the XY plane in order to measure the response of the probe to the near field at the specified positions. Due to random mechanical vibrations, random thermal variations and random inaccuracies inherent in the positioning drives and indicators, the X and Y positions are not accurately known. This uncertainty in positioning is simulated by adding to the true X and Y positions a random X position error and a random Y position error. The X position error is uniformly distributed between $\pm$ XYE wavelengths and the Y position error is uniformly distributed between $\pm$ XYE wavelengths. Using the modified positions the distribution functions (Equations 6 and 7) are evaluated and used in place of the values previously determined at the true X and Y positions. The range of XYE used in the simulation was from one thousandth of a wavelength to one third of a wavelength. Due to the fact that data is taken for all X positions for a single Y position, the Y position error is changed only when the probe is positioned to a new Y position. The X position error is changed for each sample, however.

3.3.12 Deterministic Z position error

The probe positioner is supposed to position the near-field probe

throughout the Z = constant plane. The Z position error for the particular XY positioner used at Georgia Tech has been tabulated and is used in this simulation. As the Z position error is less than 40 thousandths of an inch, it is assumed that only the phase of the signal is affected by this error. It is further assumed that the phase error is linearly proportional to the Z position error. This assumption is only true for fields which are propagating in the Z direction. For other directions of propagation the error is less, reaching zero error for directions of propagation parallel to the XY plane. Thus, this simulation will be a worst case simulation, and the true error would be equal to or less than that simulated.

The phase of each sample of the hypothetical distribution is determined and to that phase is added an error which is linearly proportional to the Z position error at the sample location. If the Z position error is zero, the phase error is zero. If the Z position error is forty thousandths of an inch (0.040) the phase error is Z40 degrees. The range of Z40 used in the simulation was from zero to 115.2 degrees.

3.3.13 Near-field measurement area truncation error

The theory of near-field measurement states that the whole XY plane must be sampled. Such complete sampling is impossible, and something less than the whole near-field plane is measured. As mentioned previously, a 43 wavelength by 43 wavelength square sector of the XY plane is being sampled in this simulation. To quantify the effects of further reduction in the size of the measurement area, the square center portion comprising AREA percent of the measurement area is used in the calculations. The amplitude of each sample of the hypothetical near-field distribution is determined, and if it is within the central

square area its amplitude is unchanged, if the sample is outside the central square area, its amplitude is set to zero (-200 dB). The range of AREA used in the simulation is from 100 percent to 5 percent.

3.3.14 Amplitude and phase errors due to motion of the near-field probe

The near-field probe is positioned in a continuous manner in X, and data is received and converted in a continuous manner. Data is recorded, however, only when the probe is passing a specified sample point. The main factor limiting the speed of the probe in measuring a single near-field is the speed of the probe positioner. If the antenna being measured could rapidly switch its near-field distributions the limiting factor in the near-field measurement process would be the time constant of the receiver. The receiver is modeled as having a simple RC time constant, and an exponential weighting factor is employed. The true amplitude and phase of each sample of the hypothetical distribution is determined and to it is added the value of the last sample weighted by an exponential time function with time constant of 50 milliseconds. The time increment between samples is DELT seconds. The range of DELT used in the simulation is from 500 milliseconds to 10 milliseconds.

3.3.15 Amplitude and phase errors due to point source reflections in the near-field measurement environment

Reflections are always present to some degree on a far-field or a near-field measurement range. The simplest form of a reflection is a point source reflector. More complicated forms of reflections can be formed as a composite of point source reflections. In this error simulation a point source may be located at any XR, YR, ZR position. The amplitude of the point source is specified as its amplitude measured

at the center of the near-field (XY) measurement plane. The amplitude is specified as being RDB dB down from the maximum amplitude of the hypothetical near-field distribution. The range of RDB used in the simulation was from 10 dB to 50 dB. The amplitude and phase of each sample of the hypothetical distribution is determined and to it is added the amplitude and phase of the spherical wave produced by the point source.

3.4 Far-Field Quantities Determined

Fifteen far-field parameters are extracted from the far-field power and field patterns to quantify the effects of near-field errors on the far-field patterns. The fifteen parameters were chosen to place emphasis on the important features of the monopulse sum and difference patterns and to conform to standard far-field pattern nomenclature. In what follows a brief description of each far-field parameter is given.

3.4.1 Relative gain of sum pattern main beam

The gain of the error-free sum far-field elevation component power pattern is arbitrarily set equal to zero decibels by normalizing the pattern by the largest value of the pattern and then converting to decibels. The sum far-field power pattern calculated from the near-field with errors is then normalized by the same normalizing coefficient and converted to decibels. The maximum value of the far-field with errors is then the relative gain of the sum far-field power patterns with respect to the far-field pattern without errors.

3.4.2 Sum pattern -3.0 dB azimuth width

The azimuth width in degrees of the sum far-field elevation power pattern is determined on the azimuth principal plane slice of the far-field

pattern. Since the pattern is smooth in the main beam region, linear interpolation of the far-field data values is used where necessary to determine intermediate values of the power pattern. The width is determined at the -3 dB contour of the pattern, using the peak of the main beam as zero dB.

3.4.3 Sum pattern -10 dB azimuth width

The determination of this parameter is the same as above except that the -10 dB contour of the sum power pattern is used.

3.4.4 Complex polarization ratio of the sum pattern main beam

The complex azimuth and elevation components of the far-field patterns are used to determine the complex polarization ratio of the peak of the main beam of the sum far-field pattern. The direction of the peak of the sum pattern main beam is determined as the direction of the maximum value of the power pattern of the elevation component. (The elevation component was chosen as the antenna is approximately linearly polarized at this point of the pattern.) The complex polarization ratio is then formed as the complex value of the azimuth component of the far-field pattern divided by the complex value of the elevation component in the specified direction.

3.4.5 Depth of difference pattern null

The depth of the difference power pattern central null is determined in the azimuth principal plane slice of the elevation component of the difference far-field power pattern. The depth of the null is determined in decibels with respect to the maximum value of the difference power pattern of the elevation component. For greater precision in the determination of the depth of the null the three data values on the

positive azimuth side of the null are fitted with a parabola, and the three data values on the negative azimuth side of the null are fitted with a parabola, with the lowest data value being used as one of the three points used on the negative side. The intersection point of the two parabolas determines the depth of the difference null as well as the direction of the difference null. In the event the parabolas do not intersect, the two points on the positive azimuth side of the null are fitted with a straight line, and the two points on the negative azimuth side of the null are fitted with a straight line. The intersection of the straight lines then determines the depth and azimuth location of the difference null.

3.4.6 Direction of difference pattern null

The azimuth direction of the elevation component of the difference power pattern null is determined in the azimuth principal plane slice of the power pattern as described above (3.4.5).

3.4.7 Monopulse error slope

The monopulse error slope is determined using the azimuth principal plane slice of the difference far-field power pattern of the elevation component. The monopulse error slope is here defined as the slope of the above difference pattern at the difference pattern null expressed as volts per degree, using one volt at the peak of the difference pattern as a voltage reference. The slope is determined from the slopes of the parabolas or straight lines used in the determination of the difference null depth and azimuth direction. The average of the absolute values of the slopes of the two parabolas or the two straight lines evaluated at the point of intersection is used as the monopulse error slope.

3.4.8 First azimuth null locations of the sum pattern

The first positive azimuth null location and the first negative azimuth null location with respect to the main beam of the sum power pattern of the elevation component are determined in the azimuth principal plane. No interpolation of the far-field pattern is used. The azimuth location of the first minimum values on each side of the main beam in the principal plane are used.

3.4.9 Relative gain of the maximum sum pattern sidelobe

The sum power pattern of the elevation component is used to determine the maximum sidelobe level parameter. The entire two dimensional pattern is searched to find the second largest local maximum. (The largest local maximum is the peak of the main beam.) The amplitude of the second largest local maximum is determined in decibels with respect to the peak of the main beam.

3.4.10 Direction of the maximum sum pattern sidelobe

The azimuth and elevation directions of the second largest local maximum of the sum far-field power pattern of the elevation component is determined as described above.

3.4.11 Complex polarization ratio of the peak of the maximum sum pattern sidelobe

The complex value of the azimuth far-field component is divided by the complex value of the elevation far-field component of the sum pattern in the direction specified for the peak of the maximum sum pattern sidelobe to form the complex polarization ratio.

3.4.12 Relative gain of maximum difference pattern sidelobe

The third largest local maximum of the difference power pattern of

the elevation component is defined as the maximum difference pattern sidelobe. (The first two local maxima are the twin peaks of the difference power pattern.) The level of this sidelobe is specified in decibels using the peak of the difference pattern as reference.

3.4.13 Direction of the maximum difference pattern sidelobe

The azimuth and elevation coordinates of the third largest local maximum of the difference power pattern of the elevation component is defined as the direction of the maximum difference pattern sidelobe.

3.4.14 Complex polarization ratio of the peak of the maximum difference pattern sidelobe

The complex azimuth component is divided by the complex elevation component of the difference far-field pattern in the direction specified for the peak of the maximum difference pattern sidelobe to obtain this complex polarization ratio.

3.4.15 RMS sidelobe level

The RMS sidelobe level of the sum power pattern of the elevation component is calculated using all values of the power pattern in a rectangular region with specified azimuth and elevation center point and with a specified azimuth and elevation width. In this simulation the azimuth and elevation centers were each 15 degrees and the azimuth and elevation widths were each 10 degrees. The RMS value is calculated as an average power value in the specified region and converted to decibels using the peak of the sum power as reference.

3.5 Simulation Results

3.5.1 Individual near-field errors

Table 3-1 shows the tabular printout from a typical simulation run. The fifteen far-field pattern parameters described in Section 3.4 are

Table 7-1. Typical Tabular Printout of Simulation Study for a Single Error Parameter.

FAR FIELD PATTERN PARAMETERS
DBE = 3.000

PARAMETER		WITH NEAR FIELD ERRORS	TRUE PATTERN	CHANGE IN PARAMETER
1. RELATIVE GAIN OF SUM PATTERN MAIN BEAM :		.254 DB	.000 DB	-.254 DB
2. SUM PATTERN -3.0 DB AZIMUTH WIDTH :		4.357 DEGREES	4.343 DEGREES	-.013 DEGREES
3. SUM PATTERN -10.0 DB AZIMUTH WIDTH :		7.725 DEGREES	7.707 DEGREES	-.018 DEGREES
4. COMPLEX POLARIZATION RATIO OF SUM MAIN BEAM :	MAGNITUDE :	-28.891 DB	-28.891 DB	-.000 DB
	PHASE :	-34.279 DEGREES	-34.290 DEGREES	-.010 DEGREES
5. DEPTH OF DIFFERENCE PATTERN NULL :		-41.422 DB	-168.120 DB	-126.697 DB
6. DIRECTION OF DIFFERENCE PATTERN NULL :	AZIMUTH :	.000 DEGREES	.000 DEGREES	.000 DEGREES
7. MONOPULSE ERROR SLOPE :		-.71731 VOLTS/DEG	-.73032 VOLTS/DEG	-.01301 VOLTS/DEG
8. FIRST AZIMUTH NULL LOCATION OF SUM PATTERN :	PLUS AZIMUTH :	6.730 DEGREES	6.730 DEGREES	.000 DEGREES
	MINUS AZIMUTH :	-6.730 DEGREES	-6.730 DEGREES	.000 DEGREES
9. RELATIVE GAIN OF MAXIMUM SUM PATTERN SIDELOBE :		-31.951 DB	-29.160 DB	2.791 DB
10. DIRECTION OF PEAK OF MAXIMUM SUM PATTERN SIDELOBE :	AZIMUTH :	-1.351 DEGREES	.000 DEGREES	23.671 DEGREES
	ELEVATION :	6.054 DEGREES	6.054 DEGREES	.000 DEGREES
11. COMPLEX POLARIZATION RATIO OF PEAK OF MAXIMUM SUM PATTERN SIDELOBE :	MAGNITUDE :	-29.418 DB	-28.898 DB	.520 DB
	PHASE :	-35.477 DEGREES	-32.979 DEGREES	2.49805 DEGREES
12. RELATIVE GAIN OF MAXIMUM DIFFERENCE PATTERN SIDELOBE :		-25.111 DB	-24.944 DB	.167 DB
13. DIRECTION OF MAXIMUM DIFFERENCE PATTERN SIDELOBE :	AZIMUTH :	7.408 DEGREES	7.408 DEGREES	.000 DEGREES
	ELEVATION :	1.343 DEGREES	1.343 DEGREES	.000 DEGREES
14. COMPLEX POLARIZATION RATIO OF PEAK OF MAXIMUM DIFFERENCE PATTERN SIDELOBE :	MAGNITUDE :	-28.287 DB	-28.285 DB	.002 DB
	PHASE :	-33.374 DEGREES	-33.351 DEGREES	.023 DEGREES
15. RMS SIDELOBE LEVEL :		-47.305 DB	-70.128 DB	-22.823 DB
CENTER OF SAMPLE REGION :	AZIMUTH =	15.000 DEGREES		
	ELEVATION =	15.000 DEGREES		
SIZE OF SAMPLE REGION :	AZIMUTH WIDTH =	10.000 DEGREES		
	ELEVATION WIDTH =	10.000 DEGREES		

listed at the end of each run in three columns. Column 1 lists the values of that far-field parameter obtained with the simulated near-field error. Column 2 lists that pattern parameter obtained with the ideal, hypothetical near-field illumination, and Column 3 lists the change in the far-field pattern parameter.

Note that the ideal (or "true") pattern is unrealistic in many respects in that the indicated performance of the mathematical model is superior to what might reasonably be expected on any real antenna. For example, a difference pattern null of -168.120 dB is unrealistically deep, and a RMS sidelobe level of -70.128 dB is unrealistically low for any practical antenna. Such numbers result from the mathematical perfection of the illumination function chosen as the base. It does, however, provide a very sensitive measure of the effects of various imperfections in the near-field parameters. The fact that practical antennas never achieve such levels of performance is simply a manifestation of the fact that practical antennas invariably have errors in their near-field illumination function.

In order to facilitate a comprehension of the voluminous results of the simulation program the data are presented in a series of graphs where the change in the various far-field pattern parameters are plotted as a function of the amplitude of the error for each of several possible near-field errors. These results then permit an allowable error to be set in any near-field parameter based on the desired accuracy in the specified far-field parameter. Of the fifteen far-field parameters tabulated, twelve are of a form that can be represented graphically. The directions of the maximum sum and the maximum difference pattern sidelobes are not parameters that can be presented in a meaningful way

in graphical form. Similarly, the complex polarization ratios of the maximum sum pattern sidelobe and maximum difference pattern sidelobe are not meaningful when represented in graphical form as different sidelobes become maximum during the simulation. On the other hand, some parameters listed in the table, e.g., first null locations of the sum pattern require two graphs, one for the positive azimuth reading and one for the negative azimuth reading.

Figures 3-1 through 3-4 present the results of the simulation program wherein the near-field error is a point source reflection of variable amplitude. The twelve far-field parameters are plotted as a function of the magnitude of this reflection in these figures.

Figure 3-1 shows the dependence of various errors in the sum pattern main beam parameters resulting from the presence of point source reflections. The point source reflections were allowed to vary in amplitude from a low value of -50 dB to a high value of -5 dB. These dB levels are explained in Section 5.2 as referenced to the maximum value of the unperturbed near-field illumination in the near-field plane. Polarization ratio is shown in this figure as a solid line and plotted with data points indicated. In plotting all these data the true pattern minus the error indicated equals the far-field parameter obtained with near-field errors. In other words, the polarization ratio of the unperturbed pattern is -28.891 dB. If a point source error of -10 dB (10 dB below the maximum of the near-field direct signal) is present, an error of -13 dB is obtained. This indicates that the point source results in a polarization ratio of (-28.891 dB) - (-13 dB) or about -16 dB. The presence of a point source reflection at a -10 dB level results in a gain error of

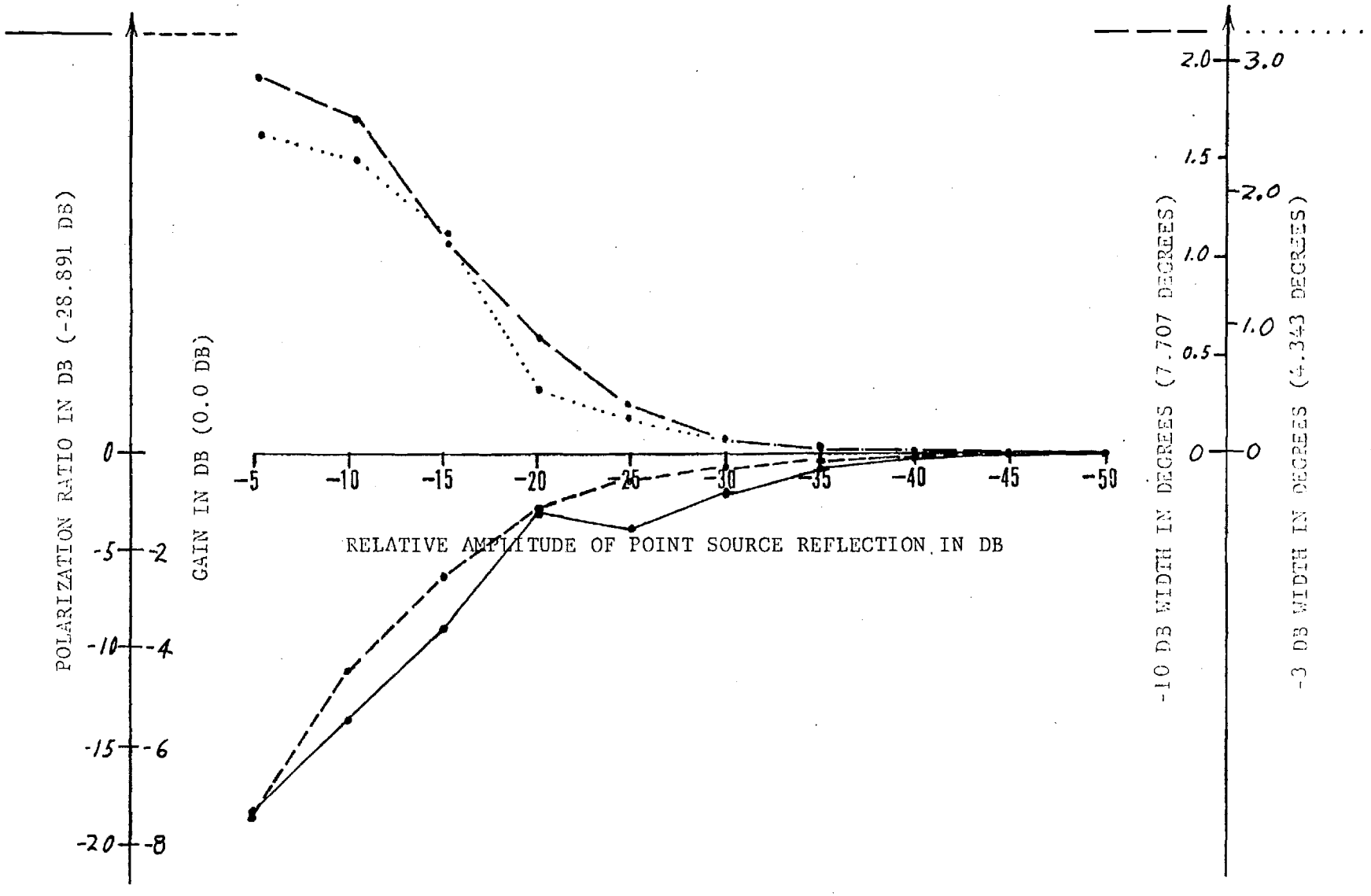

FIGURE 3-1. ERRORS IN SUM PATTERN MAIN BEAM PARAMETERS (TRUE VALUES)

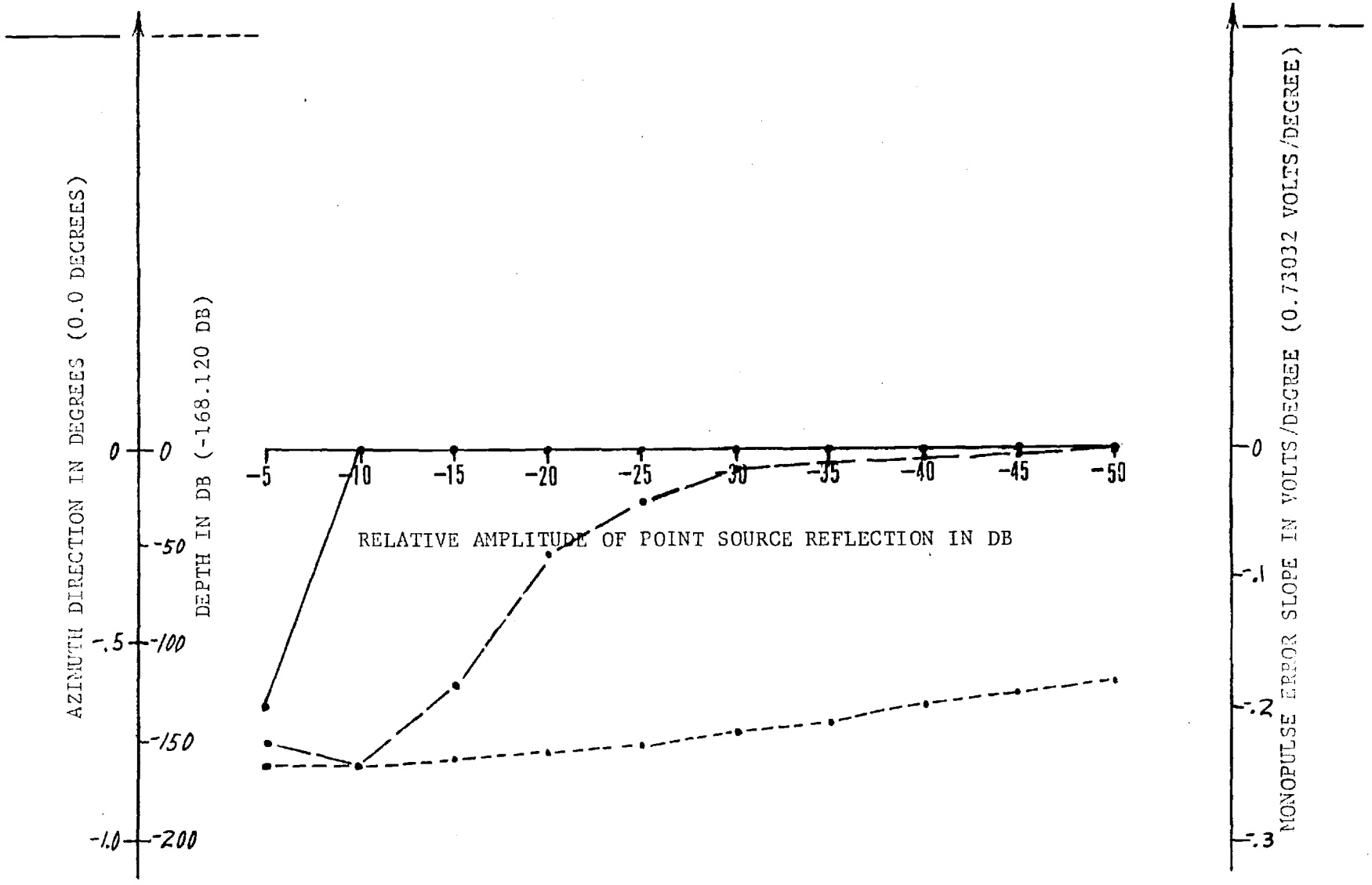

FIGURE 3-2. ERRORS IN DIFFERENCE PATTERN NULL PARAMETERS (TRUE VALUES)

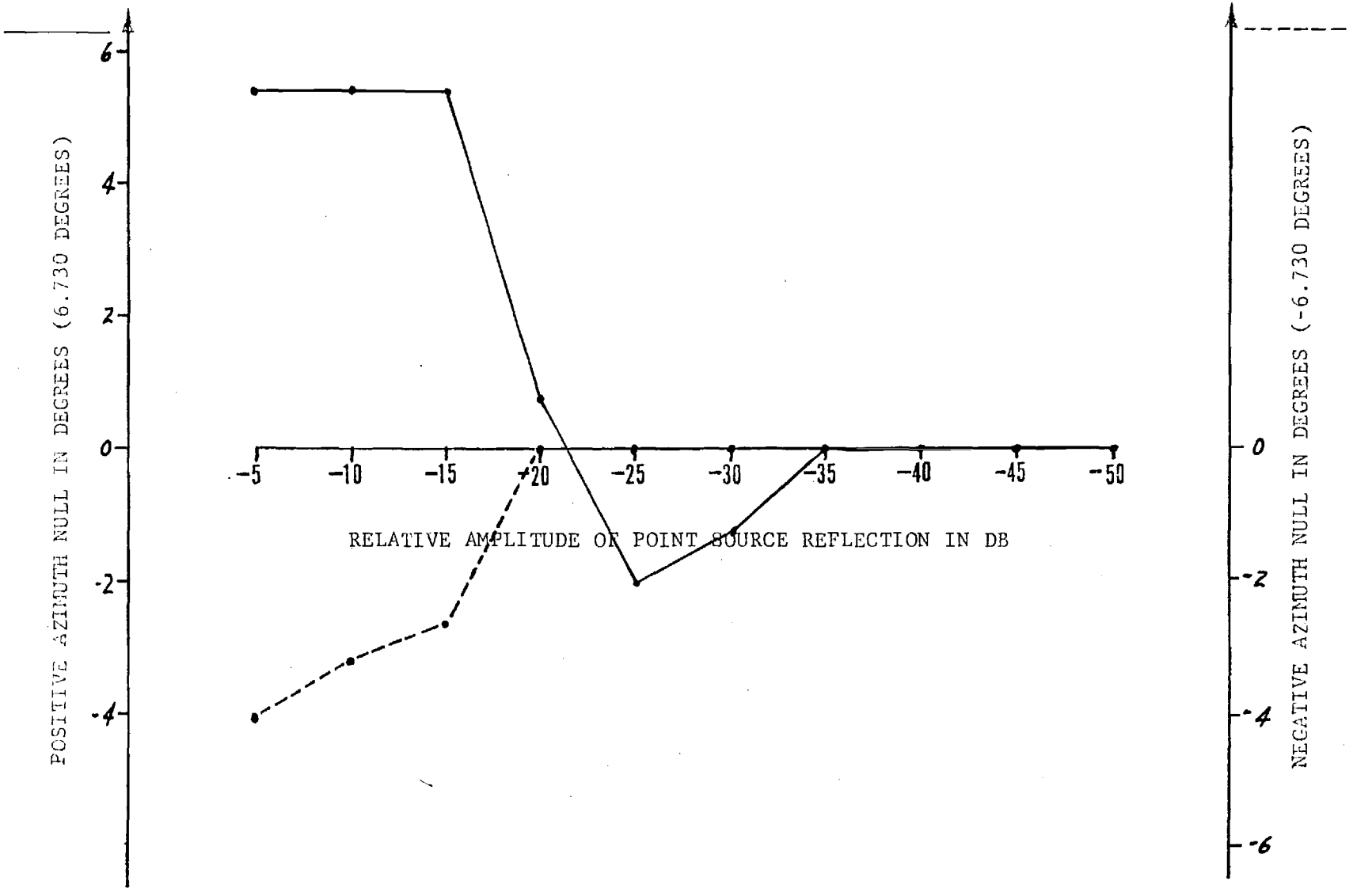

FIGURE 3-3. ERRORS IN SUM PATTERN FIRST NULL LOCATIONS (TRUE VALUES)

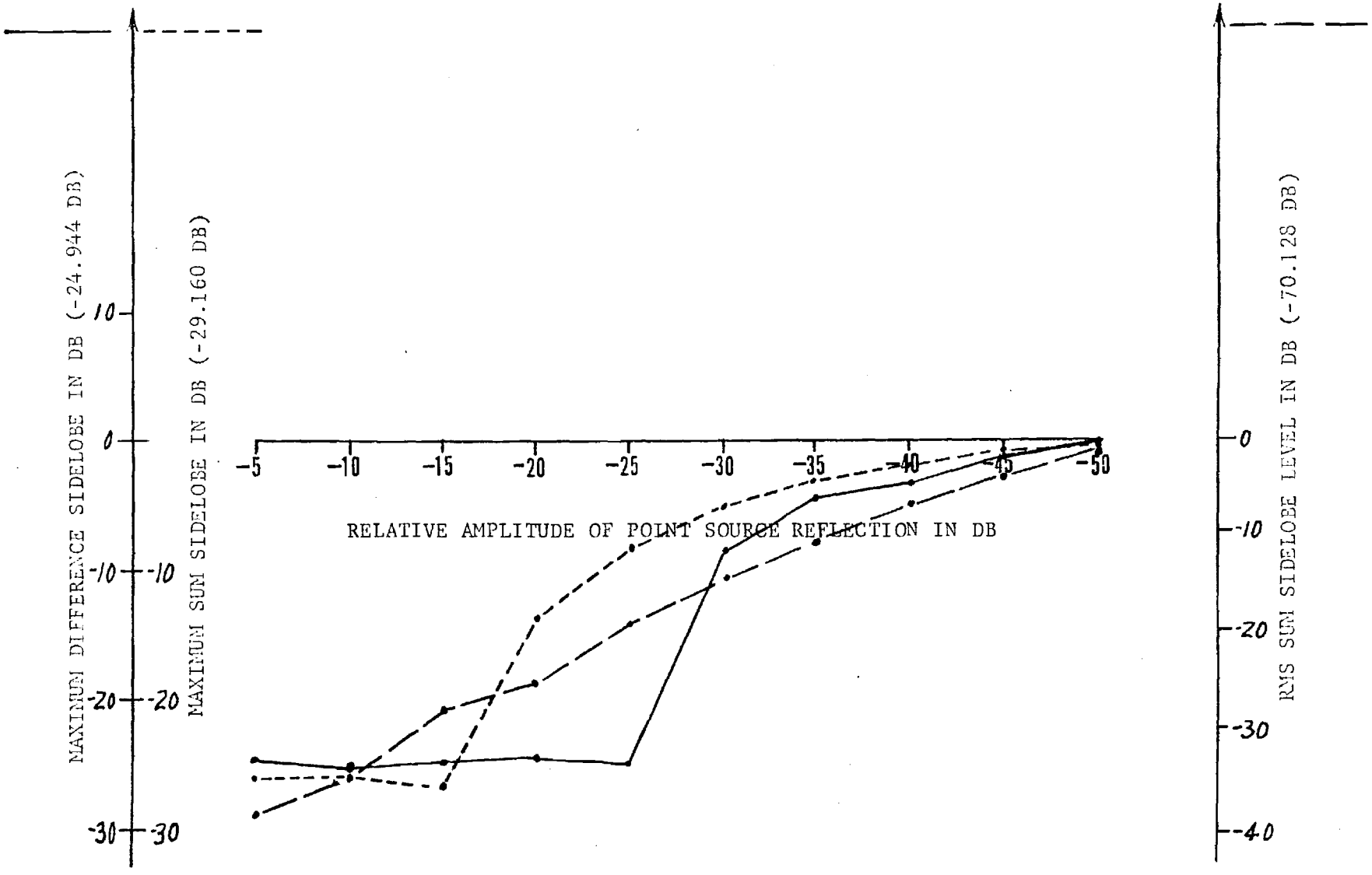

FIGURE 3-4. ERRORS IN SIDELOBE LEVELS (TRUE VALUES)

approximately -4.5 dB or the gain of the antenna is 0 dB + 4.5 dB, or 4.5 dB above the unperturbed value. The error in gain is plotted as series of dashed lines. The effect of point source reflections on the 3 dB and 10 dB beamwidths are also indicated in Figure 3-1. The 10 dB width, originally specified as 7.707 degrees, would be narrowed by approximately 1.75 degrees by the presence of a point source reflection with the magnitude of 10 dB. The 3 dB beamwidth, originally 4.343 degrees, would be narrowed by 2.3 degrees by the introduction of a point source reflection 10 dB down, and would have a resulting width of about 2.0 degrees. It might be noted that a -10 dB point source reflection is unrealistically large and values of -40 dB are more reasonable.

Figure 3-2 plots errors introduced in the principal null of the difference pattern parameters by the presence of a point source reflection on the near-field range. The range of point source reflection is maintained at the same level of -50 dB to -5 dB. The azimuth direction (solid line) plotted in degrees is shown to be independent of point source errors until a level of -5 dB is reached. The zero error level is indicated by the presence of data points along the azimuth in this plot. The null depth is strongly affected by the presence of point source reflections, as one would anticipate, and even for a level of -50 dB an error of approximately -120 dB is obtained. It must be borne in mind that the reference null depth is that of the ideal pattern, -168.120 dB. Thus for a -40 dB reflection, with associated error of approximately -130 dB, the measured value of null depth would be -168.120 dB -(-130 dB) or a null depth value of approximately -38 dB. This represents the minimum null depth one would anticipate being able to measure in an environment

with point source reflections at the -40 dB level. Monopulse error slope results are plotted as dashed lines and indicate a relative independence until point source reflections on the order of -25 dB are encountered. Monopulse error slope then increases.

Figure 3-3 shows errors in the sum pattern first null locations as a function of the same point source reflection. The positive azimuth null error is shown as a solid line and is independent of point sources below -35 dB. The negative azimuth null, at -6.73 degrees when unperturbed, shows an independence of point source reflections until the level of -20 dB is obtained. The reason for the asymmetric behavior of the point source reflection on azimuth null locations is found in the fact that the point source reflections are off center and considered to be located at a point X = .866, Y = 0.0, Z = 4.92 meters with respect to the Z = 0 near-field measurement plane.

The effect of point source reflections on sidelobe levels are indicated in Figure 3-4 where true levels, i.e., levels for the ideal antenna, are shown in every case in parentheses. The maximum difference pattern sidelobe (solid line) is shown as having a negative error of 3.0 dB for a point source reflection 40 dB down. The maximum difference pattern sidelobe in the presence of that reflection would be approximately -22 dB instead of the -24.9 dB for the ideal pattern. The maximum sum pattern sidelobe also rises with the presence of point reflections, and the sum pattern sidelobe level for a -40 dB reflection has an error in the order of -2.0 dB, indicating a maximum sum pattern sidelobe value with the reflection present of -27 dB. RMS sidelobe levels are relatively sensitive to point source reflections, and for the -40 dB level an RMS sidelobe error of -7.5 dB is obtained. Thus the RMS sidelobe

level of the pattern with the near-field error present would be approximately -62.5 dB.

It should be pointed out that on the various graphs which follow, and those contained in Appendix A as well, the scales of the far-field pattern error may vary considerably from one simulation to the next, so that a casual visual inspection of these graphs can be misleading.

Figures 3-5 through 3-16 contain some of the more interesting results of the simulation study. A complete summary of the results is contained in the 60 plots shown in Appendix A. In many instances, however, the errors introduced were so small as to be of little practical interest. The results contained in this chapter are intended to indicate some of the more significant or more interesting outgrowths of this study.

One of the more significant equipment errors simulated was that of a possible linear amplitude error in the receiver. These results are shown in Figures 3-5, 3-6, and 3-7. The error simulated is such that for a received signal strength at the -40 dB level in the receiver, the receiver is assumed to introduce an error in dB equal to that plotted on the abscissa, and it is further assumed that this error varies linearly with receiver dB reading. In this plot zero error is located at the center, hence all tabulated far-field patterns show no error at this point. Polarization ratio (Figure 3-5) appears to approximate an even function of receiver linear amplitude error. The polarization error introduced is relatively small in realistic receiver error ranges. The gain of the main beam is appreciably affected by a linear amplitude error as small as 1 dB. A 1 dB linear amplitude error introduces a 0.25 dB error in the main beam gain, and the main beam gain error is

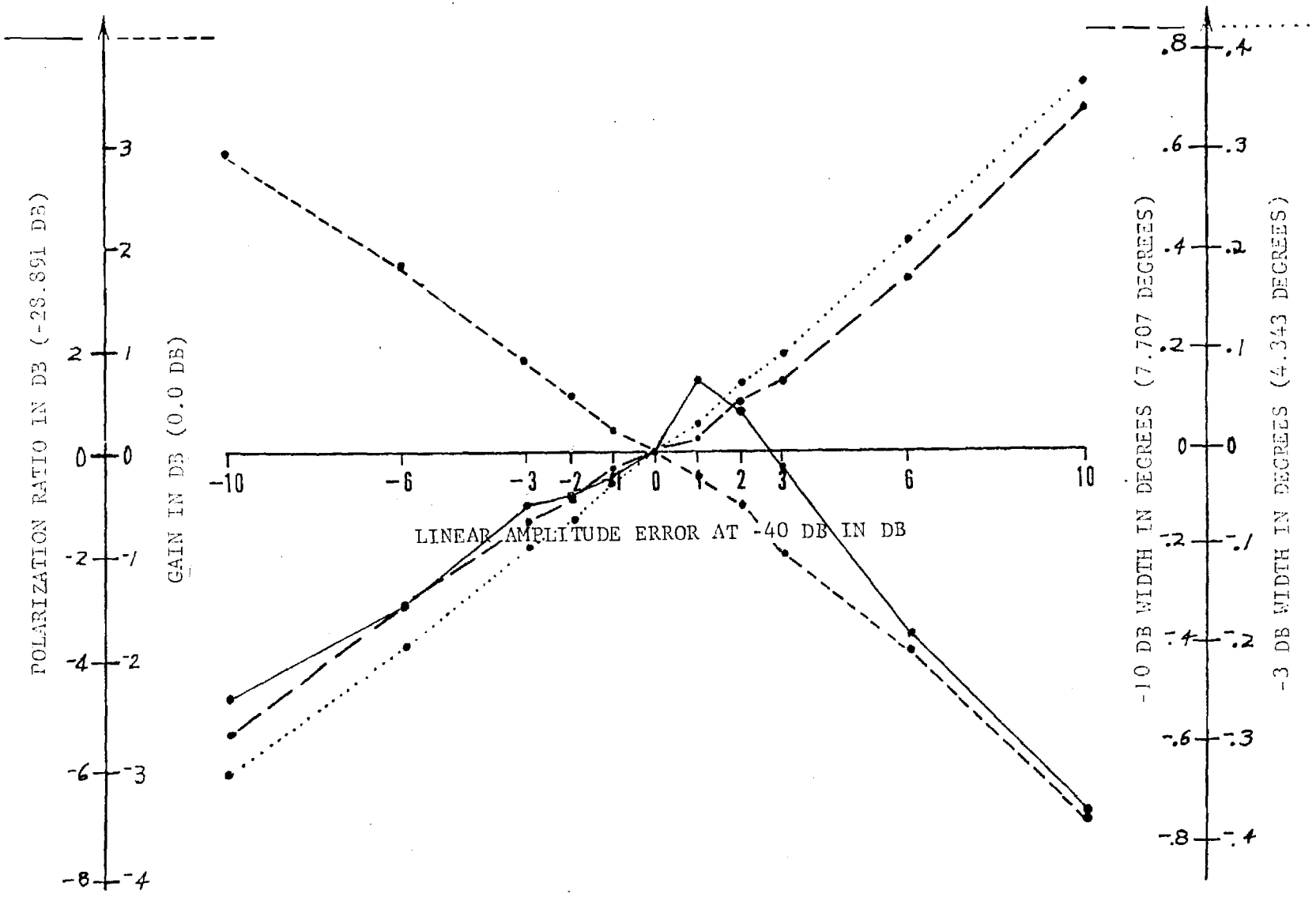

FIGURE 3-5. ERRORS IN SUM PATTERN MAIN BEAM PARAMETERS (TRUE VALUES)

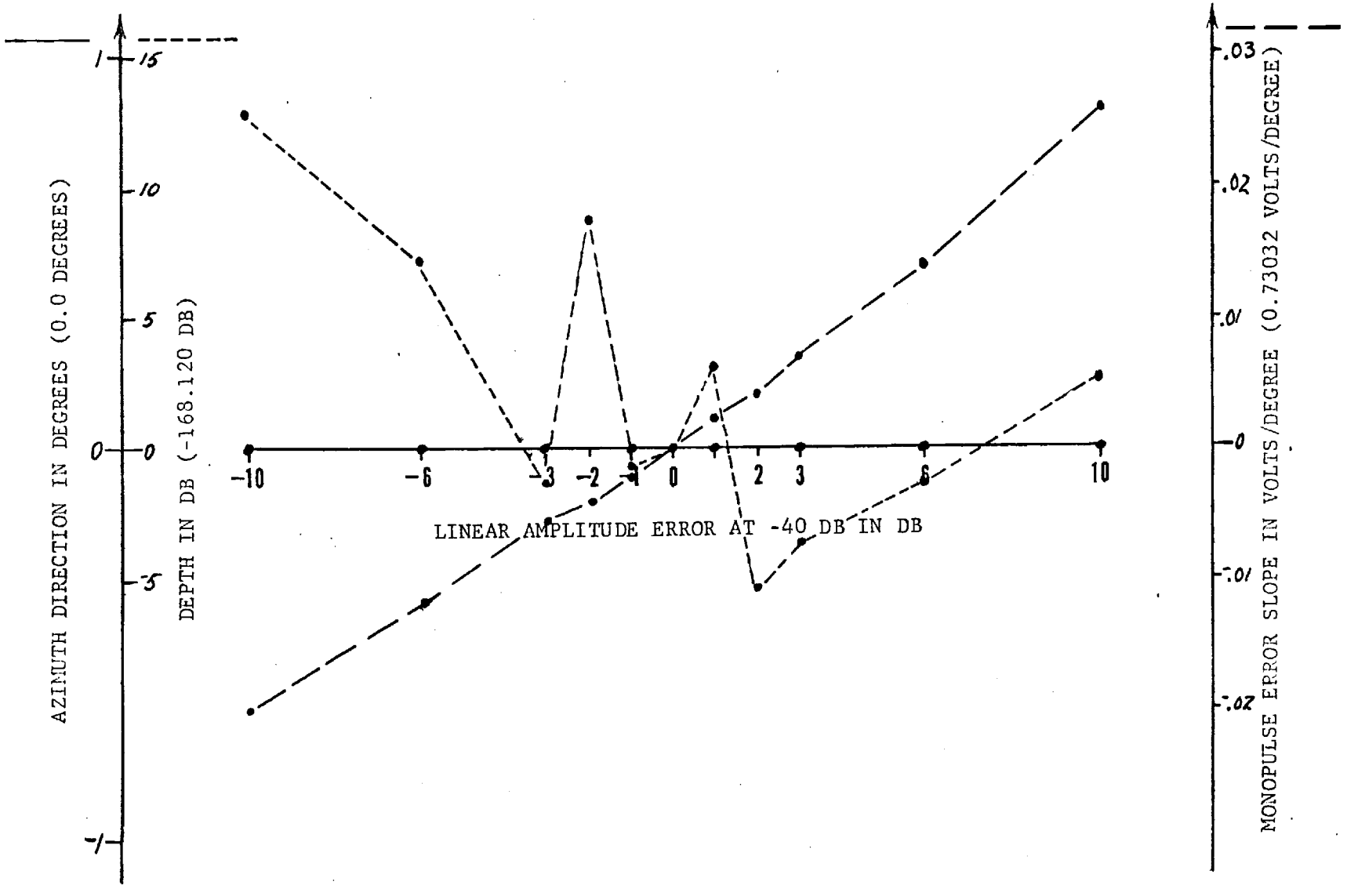

FIGURE 3-6. ERRORS IN DIFFERENCE PATTERN NULL PARAMETERS (TRUE VALUES)

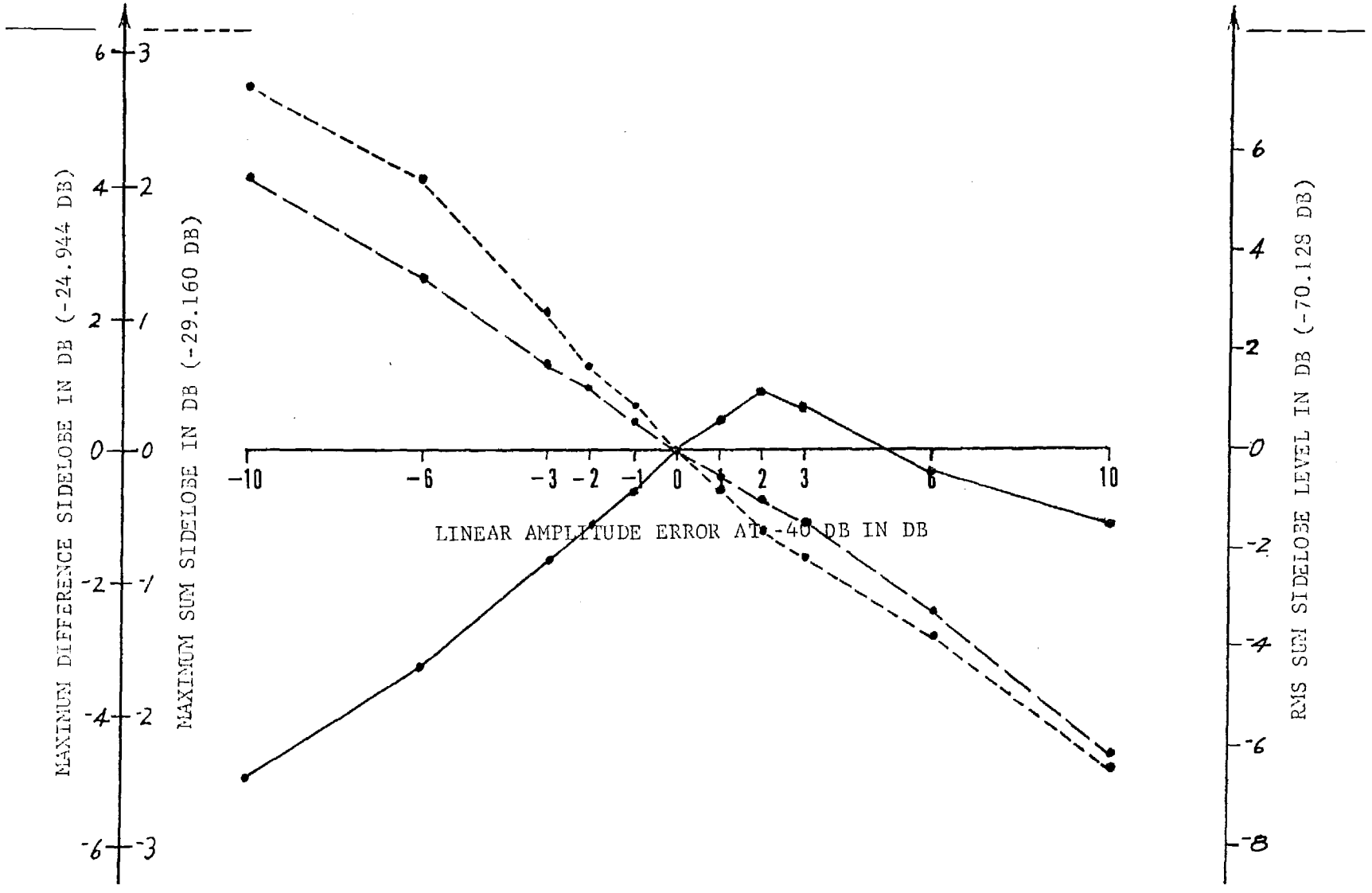

FIGURE 3-7. ERRORS IN SIDELOBE LEVELS (TRUE VALUES)

an odd function of receiver error. The three and ten dB beamwidths are both also odd functions of linear amplitude error.

The linear amplitude errors introduced no error in azimuth direction as indicated in Figure 3-6, where the data points all lie along the abscissa. This, of course, is to be expected inasmuch as a linear amplitude error does not disturb the symmetry of the pattern. The depth of the minimum is also little affected. Note that this scale, unlike that of Figure 3-2, extends only over a range of -5 dB to +15 dB out of the total of 168 dB. These errors are almost random.

The monopulse error slope is seen to be an odd function of linear amplitude error with error slope increasing for negative amplitude errors and decreasing for positive amplitude errors. It should be noted here that the change in monopulse error slope is small in every case, the full range of this graph of Figure 3-6 being from -0.2 to +0.03 volts per degree.

The effect on sidelobe levels (Figure 3-7) of a linear amplitude error is again relatively small. The maximum difference pattern sidelobe changes by approximately 0.5 dB for a linear amplitude error of 1 dB. The maximum sum pattern sidelobe changes by approximately 0.3 dB for a 1 dB linear amplitude error. The RMS sidelobe level of the sum pattern changes by approximately 0.6 dB (out of 70 dB) for a 1 dB linear amplitude error.

In summary, the primary effects of a linear amplitude error are in the gain of the main beam.

Figures 3-8, 3-9, and 3-10 indicate errors in far-field patterns incurred by the finite response time of the receiver. In this case, as explained in the preceding section, the response time of the receiver

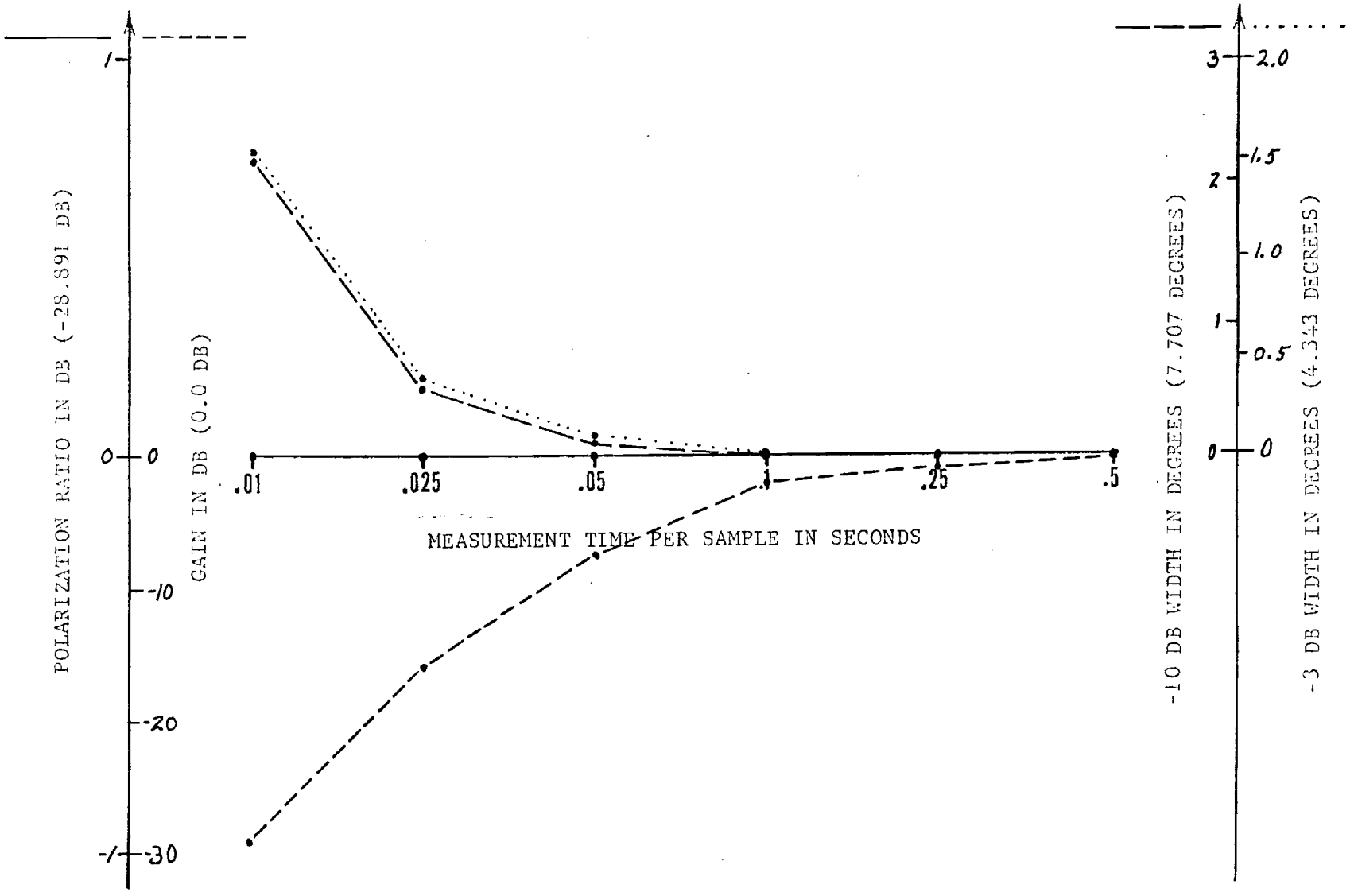

FIGURE 3-8. ERRORS IN SUM PATTERN MAIN BEAM PARAMETERS (TRUE VALUES)

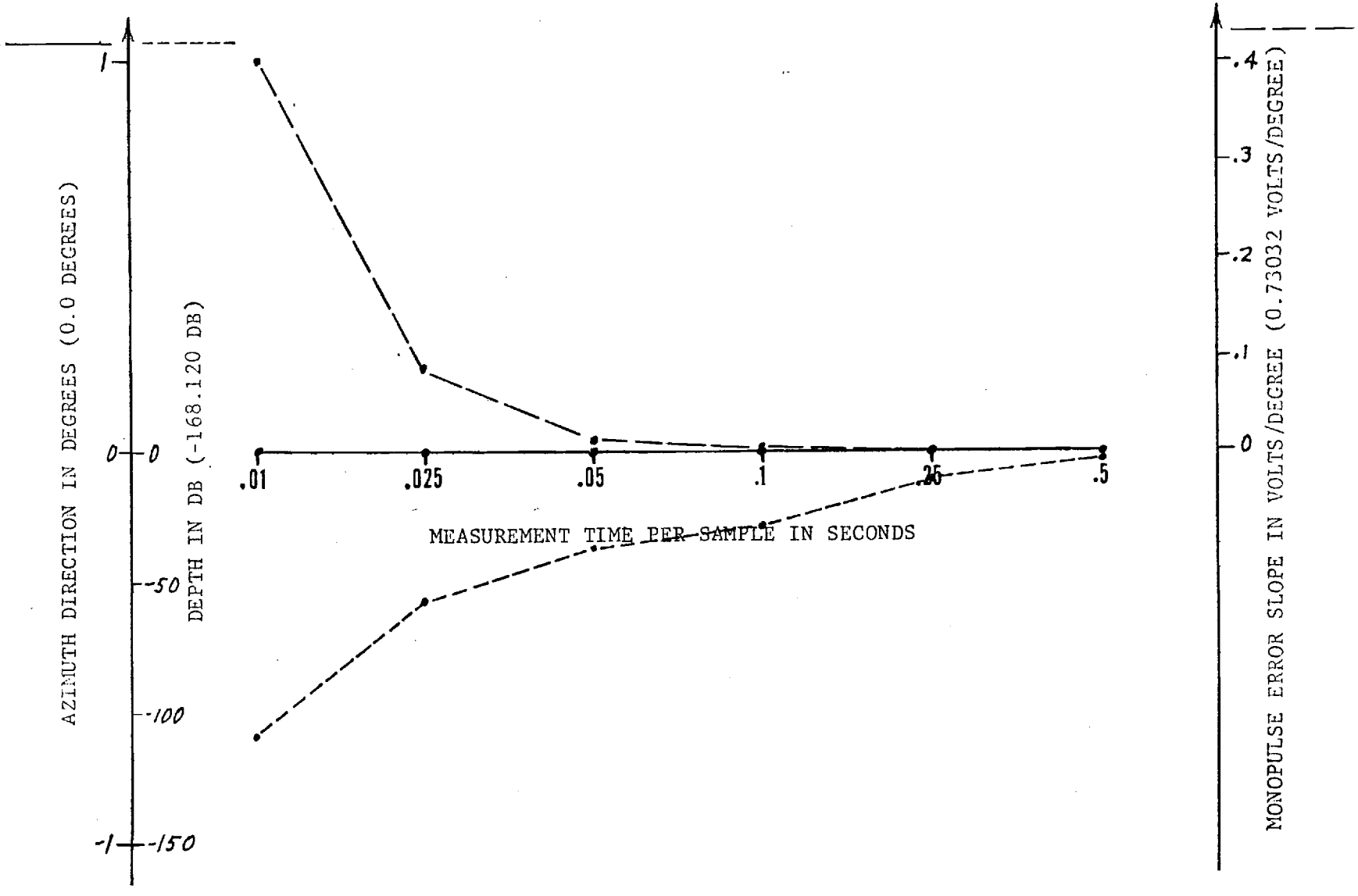

FIGURE 3-9. ERRORS IN DIFFERENCE PATTERN NULL PARAMETERS (TRUE VALUES)

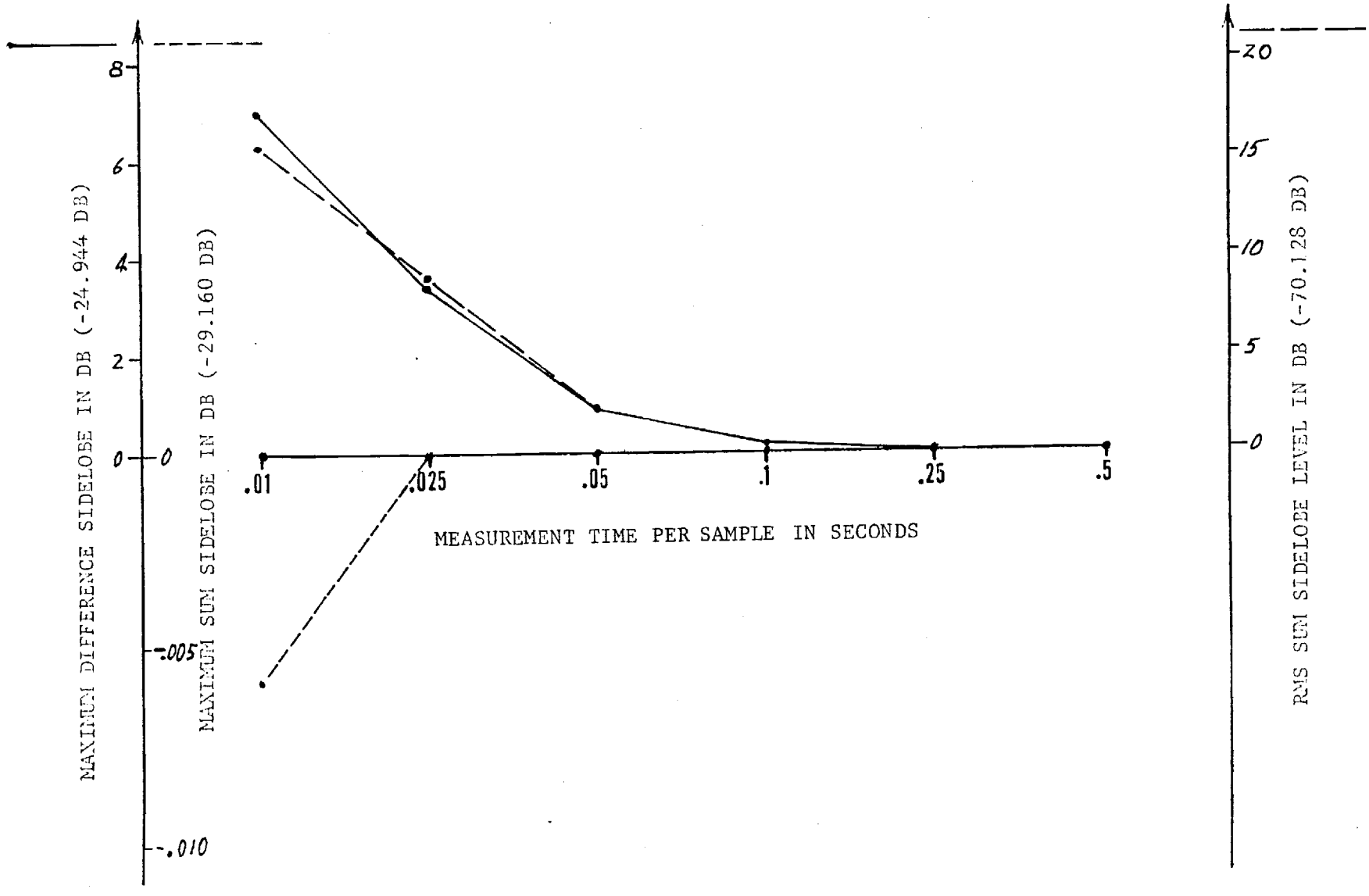

FIGURE 3-10. ERRORS IN SIDELOBE LEVELS (TRUE VALUES)

is modeled as a simple RC response with a time constant of 50 milliseconds. The measurement time between samples (in seconds) was allowed in this simulation to vary from 0.5 seconds to 10 μsec. and the resulting error introduced in pattern parameters is presented here. Figure 3-8 shows that as the measurement time becomes shorter than the response time of the RC circuit a large error in overall gain is introduced. Even at a measurement time of 0.33 sec., which corresponds to that used on the present measurement program, the effect on the main beam is to increase the gain by approximately 1 dB.

The cause of this relatively large error is found in the simulation model used, which does not fully represent the real receiver. In the simulation the product of the amplitude value of the last data point and the time constant weighting factor is added to the amplitude value of the new data point. Thus if the amplitude at two adjacent points is actually the same, this method of simulation would cause it to increase. If the actual receiver data is constantly updated, and if no change in amplitude occurs, the output value would always be correct no matter how rapidly samples are taken. The simulation technique used leads to a pessimistic conclusion, but is felt to be more indicative of the results one would obtain on a phased array when beam switching is used between points, and hence amplitude and phase might vary considerably between points.

The 0.33 second measurement time does not influence the beam width or the polarization ratio to any appreciable extent. In fact, polarization ratio is completely insensitive to the measurement time.

Figure 3-9 shows that the measurement time also influences the depth of the indifference pattern null, although in this case the

dependence is not great. The 0.33 second measurement time produces roughly a 10 dB decrease in the depth of the null, but this decrease is small compared to the reference level of -168.12 dB. Azimuth pointing direction is unaffected, and the monopulse error slope is affected only to a small extent, which is a reflection of the change in the gain of the main beam.

The sidelobes are seen in Figure 3-10 to be effected to a relatively small extent, and even for measurement times equal to the sampling time the effect on sidelobes is relatively small. RMS sidelobe levels are, in fact, lowered by approximately 2 dB (out of 70 dB) for a measurement time equal to the sampling time.

Far-field parameters are notably insensitive to amplitude truncation in the near field. Amplitude truncation is shown in Figure 3-11 to influence the gain to only a very small degree. For a truncation at the -40 dB level (all signals less than -40 dB are set equal to -200 dB) the gain of the main beam is reduced by approximately 0.05 dB. Polarization ratio is also relatively unaffected by this truncation error as are beam widths for truncations less than 30 dB.

The null depth is seen in Figure 3-12 to be insensitive to truncation. The indicated error of 13 dB (out of 168 dB) is negligible in practical antennas. Such errors are largely overshadowed by those from other sources. Azimuth direction is completely unaffected by truncation.

Figure 3-13 shows the effect of amplitude truncation on the sidelobe levels. Largest error is in RMS sidelobes where a 5 dB error is introduced by a -40 dB truncation level, i.e., if the amplitude is truncated at the -40 dB level, RMS sidelobe levels would be increased

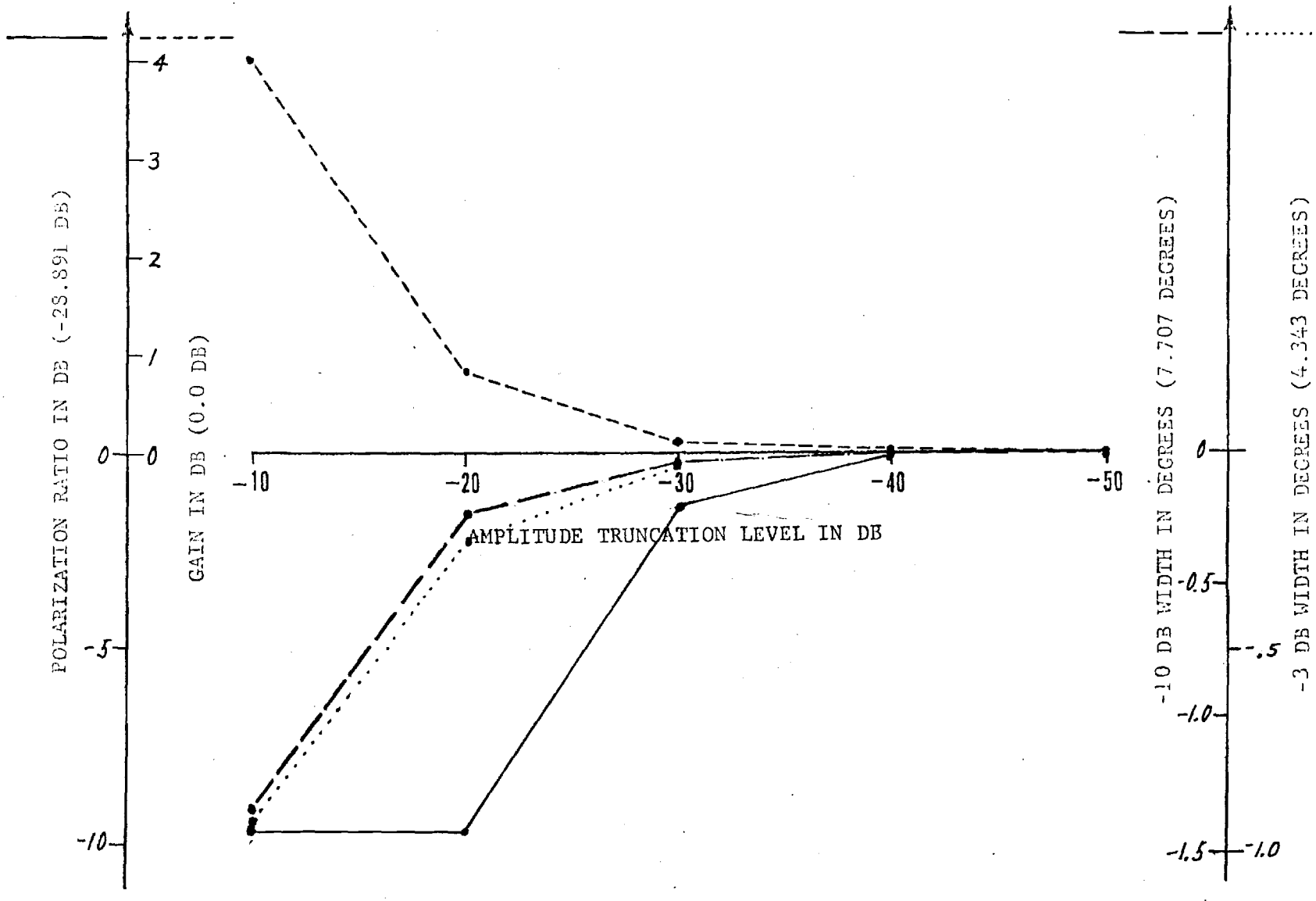

FIGURE 3-11. ERRORS IN SUM PATTERN MAIN BEAM PARAMETERS (TRUE VALUES)

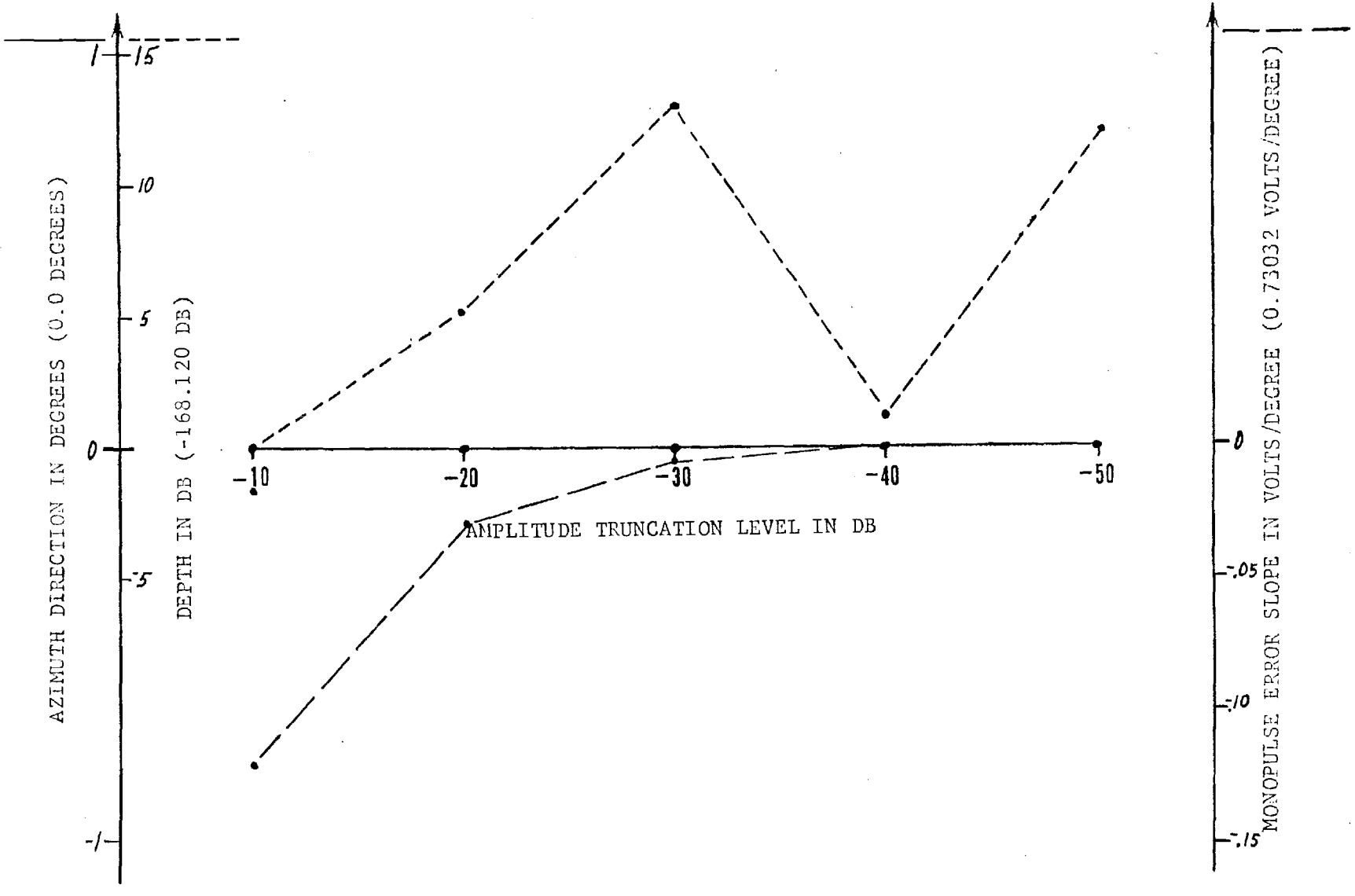

FIGURE 3-12. ERRORS IN DIFFERENCE PATTERN NULL PARAMETERS (TRUE VALUES)

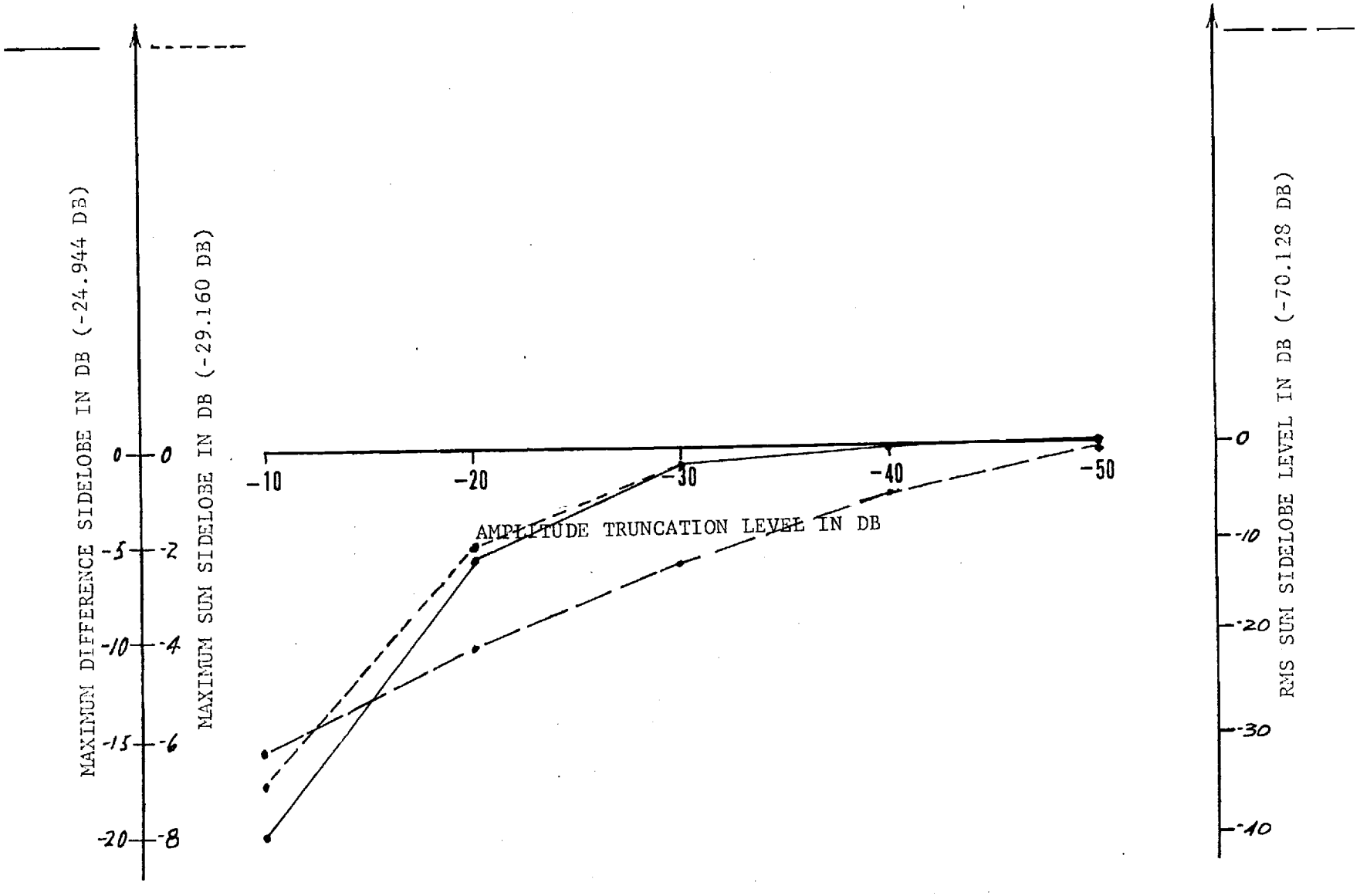

FIGURE 3-13. ERRORS IN SIDELOBE LEVELS (TRUE VALUES)

approximately to -65 dB from -70 dB. Maximum sum and difference pattern sidelobes are essentially unaffected by a -40 dB level truncation.

Random phase errors influence the gain of the main beam to a negligibly small extent even for phase errors as large as $\pm$ 2 degrees, and in the equipment normally used a random phase error of $\pm$ 0.6 dB is a realistic estimate. Similarly, random phase errors produce virtually no beamwidth error as the much magnified error graphs of Figure 3-14 indicate. As is to be expected, the primary effects of random phase error are on null depth and sidelobe levels as shown in Figures 3-15 and 3-16. A $\pm$2 degree random phase error would raise the difference pattern null by approximately 105 dB (out of 168 dB) and the RMS sidelobe level would be raised from -70 dB to -62 dB.

Table 3-2 presents an overall, qualitative, summary of the simulation study results. Near-field errors are listed in the left hand column and their effect on each of the twelve far-field parameters is indicated by a letter, S - sensitive, I - insensitive, M - moderate.

3.5.2 Composite near-field errors

Simulation runs were also conducted using as input a composite of all fifteen possible near-field errors. The parameter chosen for each near-field error was a "best estimate" of the actual error on the near-field range. Thus the far-field pattern parameter errors obtained in this run are indicative of the accuracy to be expected on the Georgia Tech near-field range as presently configured.

The specified near-field errors input to the program are listed in Table 3-3 and the output of the program is reproduced in Table 3-4.

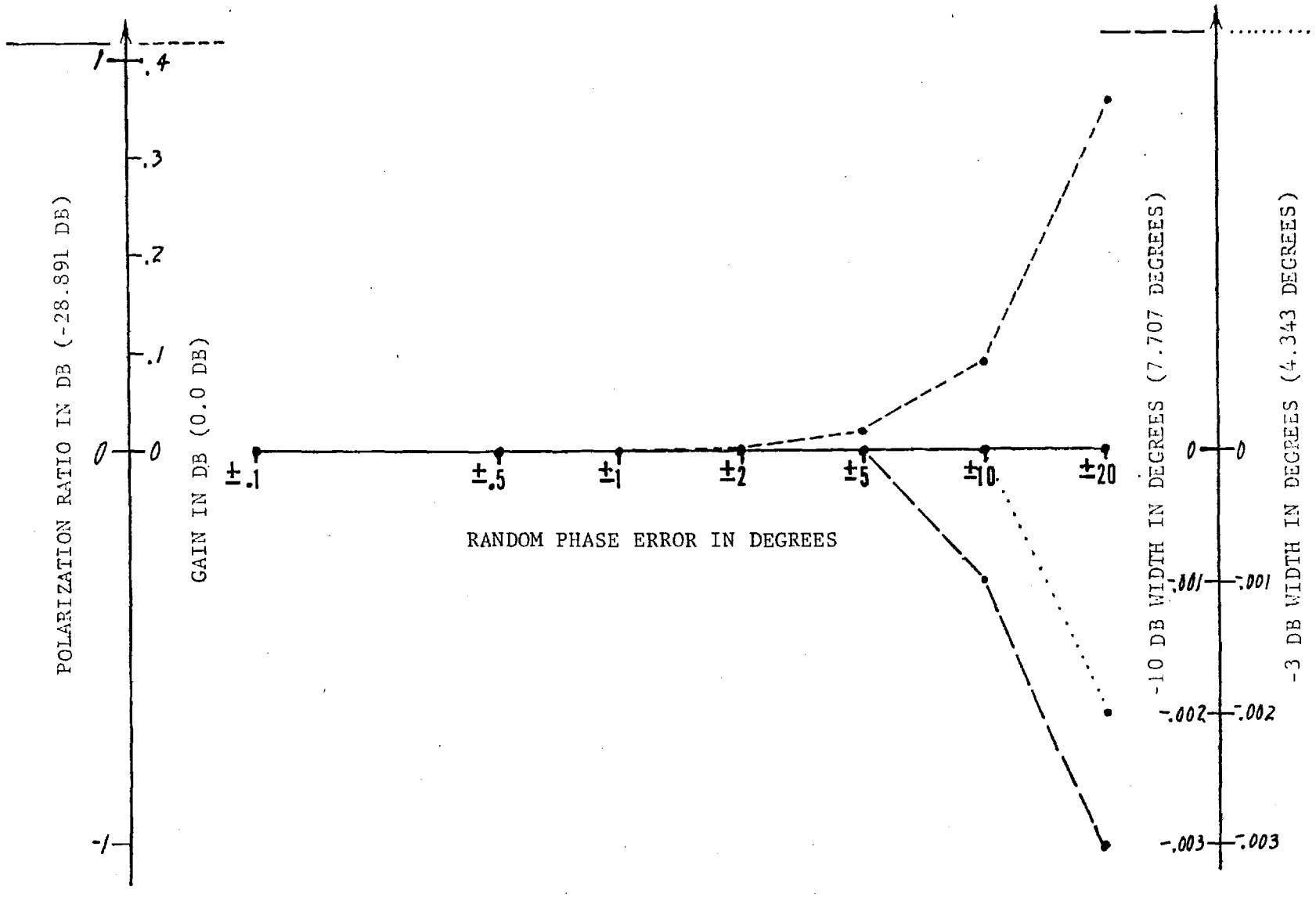

FIGURE 3-14. ERRORS IN SUM PATTERN MAIN BEAM PARAMETERS (TRUE VALUES)

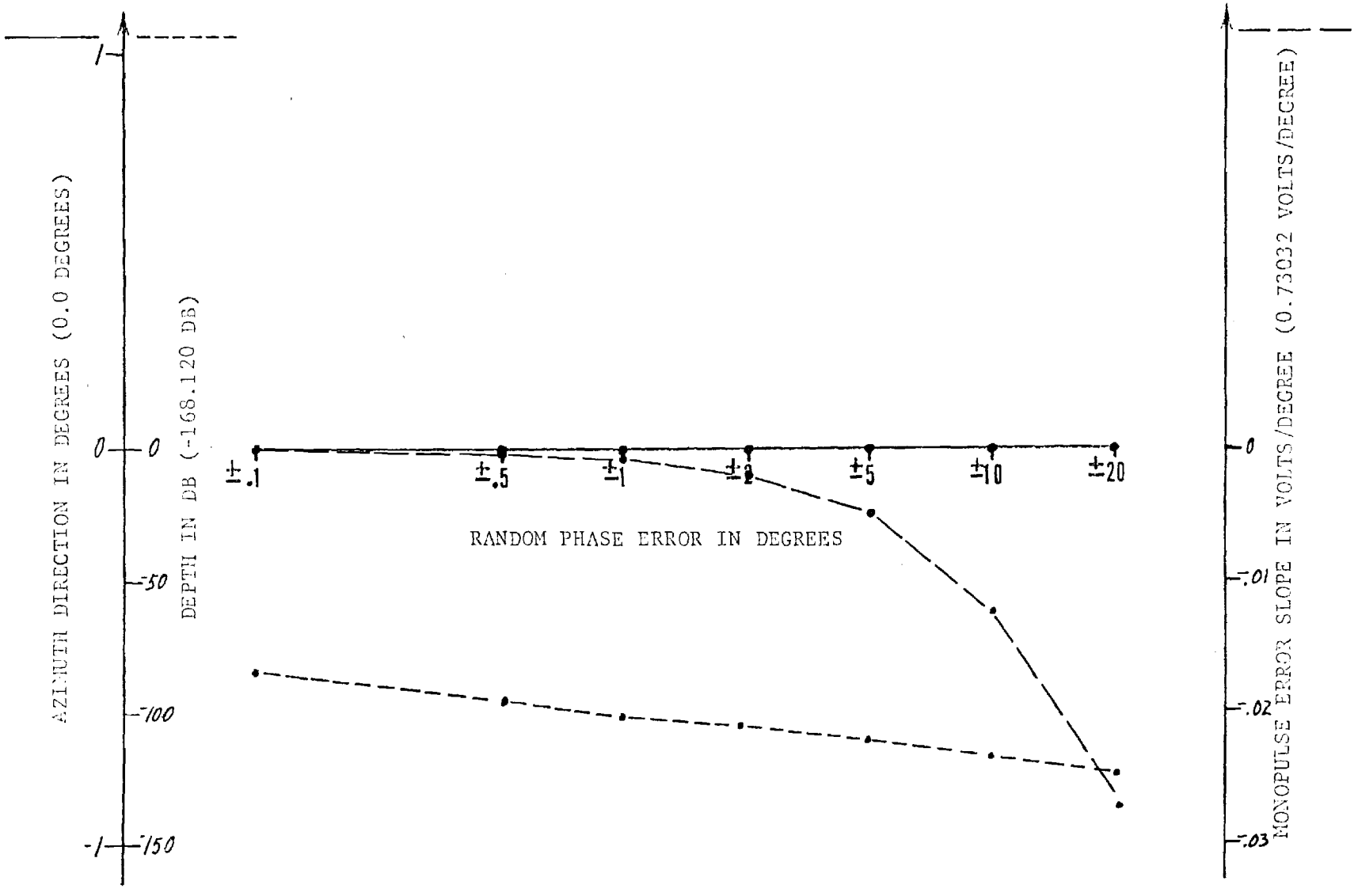

FIGURE 3-15. ERRORS IN DIFFERENCE PATTERN NULL PARAMETERS (TRUE VALUES)

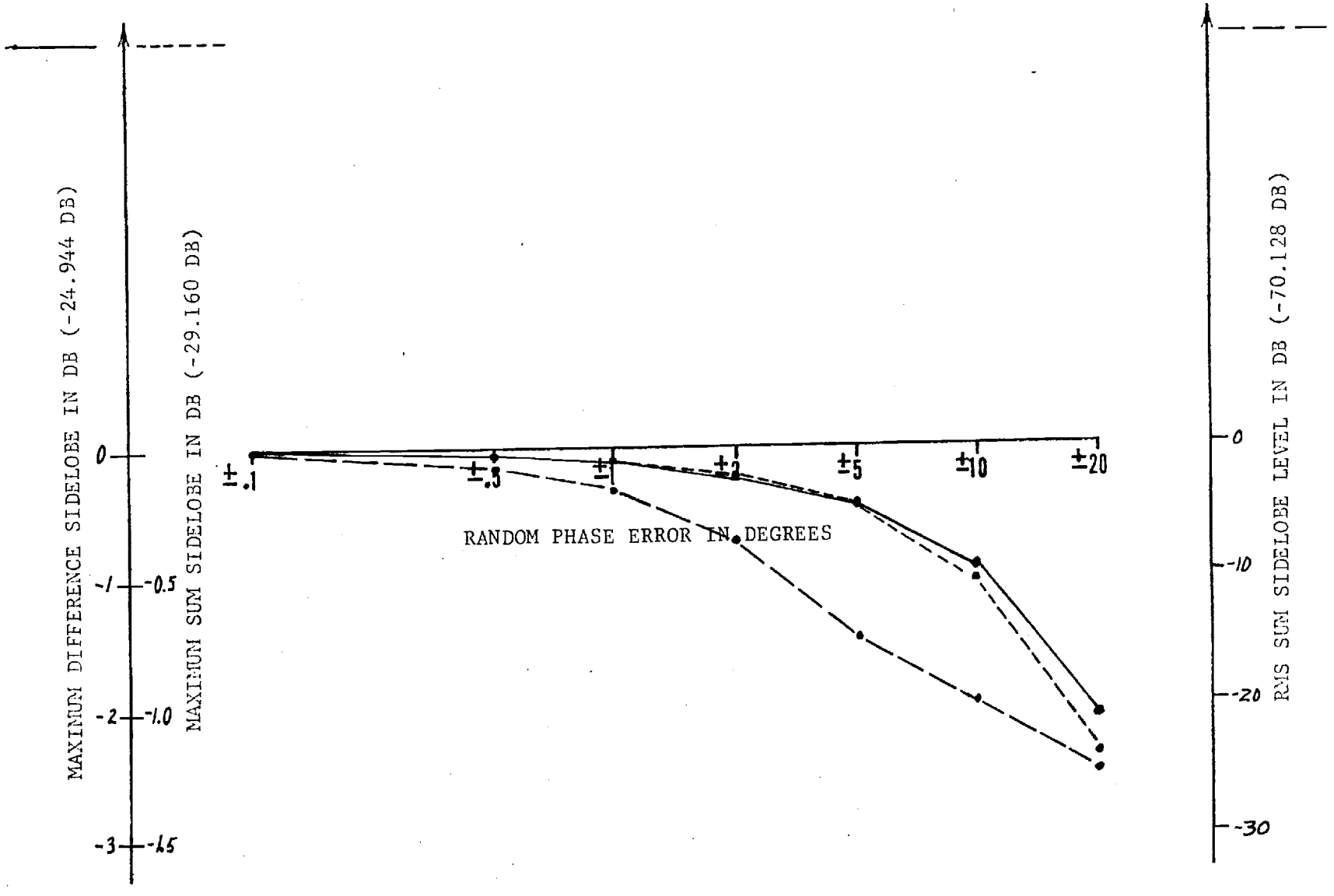

FIGURE 3-16. ERRORS IN SIDELOBE LEVELS (TRUE VALUES)

Table 3-2. Qualitative Summary of Near-field Error Simulation

Far-field Parameters / Near-field Error	Σ PATTERN				Δ PATTERN NULL			Σ PAT. 1st NULL		SIDELOBE LEVELS		
	Polarization	Gain	10db BW	3db BW	Direction	Depth	Error Slope	+Az	-Az	Max ΔSL	Max ΣSL	RMS SL
Random Amplitude	I	I	I	I	I	S	I	I	I	I	M	S
Linear Amplitude	M	S	M	M	I	I	M	M	M	M	I/M	I/M
Quadratic Amplitude	M	M	I/M	I	I	I	I	I	I	I/M	I	I
Linear Amplitude Drift	I	S	I	I	I	M	I	I	I	I	I	I
Amplitude Truncation	S/M	S/M	I	I	I	I	I	I	I	I/M	I	M
Random Phase	I	I	I	I	I	S	M	I	I	I/M	I/M	M
Linear Phase	I	I	I	I	I	S	M	I	I	I	I	I
Quadratic Phase	I	I	I	I	I	S	I	I	I	I	I	I
Total Phase Drifts	I	M	I	I	I	I	I	I	I	I	I	I
Quadratic Phase Error @ 40 db	M	I	I	I	I	I	I	I	I	I	I	I
Random X-Y	I	I	I	I	I	I	I	I	I	I	I	I
Z - Position Error	I	I	I	I	I	S/M	I	I	I	I	I	I
% of Measurement Area	I	I	I	I	I	I/M	I	I	I	I	I	I/M
Measurement Time/sample	I	S	I	I	I	M	M	I	I	I	I	I
Relative Amplitude Point Source	S	S	M	M	I	S	S			S	S	M

S - Sensitive I - Insensitive M - Moderate

Table 3-3. Composite Errors

Random Amplitude	$\pm$0.1 db
Linear Amplitude @ -40 db	-0.1 db
Quadratic Amplitude @ -40 dB	-0.5 db
Linear Amplitude drifts	0.1 db
Amplitude truncation	-55.0 db
Random Phase Error	$\pm$2.0 db
Linear Phase Error @ $\pm$180 degrees	0.1 degrees
Quadratic Phase Error @ $\pm$ 180 degrees	0.2 degrees
Total phase drift	5.0 degrees
Quadraic Phase Error @ -40 db	4.0 degrees
Random X and Y position (in λ)	$\frac{1}{360}$
Z-Position Error	$\pm$0.02
Percentage of Measurement Area	90.0%
Measurement Time per sample (in sec.)	0.2 sec.
Relative Amplitude of Point Sources	-45.0 db

Table 3-4. Results of Simulation Run Using Composite Errors.

FAR FIELD PATTERN PARAMETERS

TOTAL = *******

PARAMETER		WITH NEAR FIELD ERRORS	TRUE PATTERN	CHANGE IN PARAMETER
1. RELATIVE GAIN OF SUM PATTERN MAIN BEAM :		.137 DB	.000 DB	-.137 DB
2. SUM PATTERN -3.0 DB AZIMUTH WIDTH :		4.332 DEGREES	4.343 DEGREES	.012 DEGREES
3. SUM PATTERN -10.0 DB AZIMUTH WIDTH :		7.693 DEGREES	7.707 DEGREES	.014 DEGREES
4. COMPLEX POLARIZATION RATIO OF SUM MAIN BEAM :	MAGNITUDE :	-27.985 DB	-28.891 DB	-.906 DB
	PHASE :	-41.135 DEGREES	-34.290 DEGREES	6.846 DEGREES
5. DEPTH OF DIFFERENCE PATTERN NULL :		-35.737 DB	-168.120 DB	-132.383 DB
6. DIRECTION OF DIFFERENCE PATTERN NULL :	AZIMUTH :	.000 DEGREES	.000 DEGREES	.000 DEGREES
7. MONOPULSE ERROR SLOPE :		-.74389 VOLTS/DEG	-.73032 VOLTS/DEG	.01277 VOLTS/DEG
8. FIRST AZIMUTH NULL LOCATION OF SUM PATTERN :	PLUS AZIMUTH :	6.730 DEGREES	6.730 DEGREES	.000 DEGREES
	MINUS AZIMUTH :	-6.730 DEGREES	-6.730 DEGREES	.000 DEGREES
9. RELATIVE GAIN OF MAXIMUM SUM PATTERN SIDELOBE :		-28.074 DB	-29.160 DB	-1.087 DB
10. DIRECTION OF PEAK OF MAXIMUM SUM PATTERN SIDELOBE :	AZIMUTH :	-.675 DEGREES	.000 DEGREES	.675 DEGREES
	ELEVATION :	-6.054 DEGREES	6.054 DEGREES	12.108 DEGREES
11. COMPLEX POLARIZATION RATIO OF PEAK OF MAXIMUM SUM PATTERN SIDELOBE :	MAGNITUDE :	-21.889 DB	-28.898 DB	-7.008 DB
	PHASE :	-156.691 DEGREES	-32.979 DEGREES	123.713 DEGREES
12. RELATIVE GAIN OF MAXIMUM DIFFERENCE PATTERN SIDELOBE :		-23.962 DB	-24.944 DB	-.982 DB
13. DIRECTION OF MAXIMUM DIFFERENCE PATTERN SIDELOBE :	AZIMUTH :	-5.398 DEGREES	7.408 DEGREES	12.806 DEGREES
	ELEVATION :	-4.705 DEGREES	1.343 DEGREES	-3.362 DEGREES
14. COMPLEX POLARIZATION RATIO OF PEAK OF MAXIMUM DIFFERENCE PATTERN SIDELOBE :	MAGNITUDE :	-15.686 DB	-28.285 DB	-12.599 DB
	PHASE :	161.452 DEGREES	-33.351 DEGREES	-194.804 DEGREES
15. RMS SIDELOBE LEVEL :		-61.835 DB	-70.128 DB	-8.293 DB
CENTER OF SAMPLE REGION :	AZIMUTH =	15.000 DEGREES		
	ELEVATION =	15.000 DEGREES		
SIZE OF SAMPLE REGION :	AZIMUTH WIDTH =	10.000 DEGREES		
	ELEVATION WIDTH =	10.000 DEGREES		

EM: 150787 MLSEE

The error in main beam gain of 0.137 dB arises largely from the receiver response time error. In a subsequent composite error run with the measurement interval increased to 2.0 sec. (from .29 sec.), all computed far-field pattern parameters were virtually identical except for main beam gain, whose error was then reduced to 0.084 dB. Thus roughly half of the main beam gain error of Table 3-4 arises in the receiver response time, and as mentioned above in 3.5.1 the method of modeling the receiver does not truly represent the actual receiver.

Sum pattern beamwidths at -3 and -10 dB points are accurate to routhly 0.015 degrees (~.3 milliradian). The complex polarization ratio of the sum pattern main beam is also quite accurately determined.

The large error in difference pattern null depth is again the result of the idealized model used for the "true pattern." These results show that the difference pattern null depth of a test antenna could be measured down to -35 dB with respect to the difference pattern maximum. If the null was deeper than this, then near-field range errors would limit its determination. These estimates are corroborated by the data of Section 7.

The difference pattern null direction and sum pattern first null locations have no measurable error resulting from the composite errors simulated. Monopulse error slope has a small (~2%) error.

The sum pattern sidelobe structure incurred a small error, 1 dB at the -30 dB level, and the location of the largest sidelobe is shifted from (Az 0.0; EL 6.054 degrees) to (Az - 0.675 degrees; EL - 6.054 degrees), where the negative elevation sidelobe has been raised so that it moves from second to first place in relative size. With this change in sidelobe, a change in polarization ratio of the

sidelobe also occurs. A similar effect is produced in the difference pattern where the sidelobe at (Az - 5.398 degrees; EL + 4.705 degrees), grows to replace that at (Az 7.408; EL 1.343 degrees) as the largest difference pattern sidelobe. The polarization ratio, of course, also changes to a major degree. Of more interest from a systems standpoint is the RMS sidelobe level that, with errors, increases to -61.8 dB from -70.1 dB. This result clearly shows that the near-field range does not limit the accuracy with which RMS sidelobe level can be determined.

In summary, the near-field composite error simulation yields results whose accuracy compares favorably with those of a far-field range, except perhaps in the measurement of main beam gain where receiver recovery time seems a chief limitation.

SECTION 4

TEST ANTENNA DESIGN

This section describes the test antenna design and boresighting techniques developed for use in the experimental phase of this accuracy study.

4.1 Antenna Fabrication

A four foot diameter C-band reflector antenna with a two-horn monopulse feed was designed and constructed for use as the test antenna. A single-plane monopulse system was chosen for simplicity since a single plane system would be smaller and lighter than a two-plane system and would still allow a comparison of near-field/far-field measurement accuracy of the critical parameters, monopulse error slope, difference null depth, and boresight error. The design of the feed system and reflector support structure emphasized a high degree of mechanical rigidity without appreciably reducing the electrical performance of the antenna. Any mechanical movement of the feed relative to the reflector, or reflector deformation would alter the true antenna pattern and thus effect the comparison between the near-field and far-field measurements. The antenna and support structure are shown in Figure 4-1.

Design goals for the test antenna are summarized in Table 4-1.

4.1.1 First feed

In the interest of simplicity, the first feed design (Feed 1) used two C-band waveguide horns mounted side-by-side, and connected directly at the feed to a folded hybrid coupler. Since the sum and difference signals are processed directly at the feed, most of the

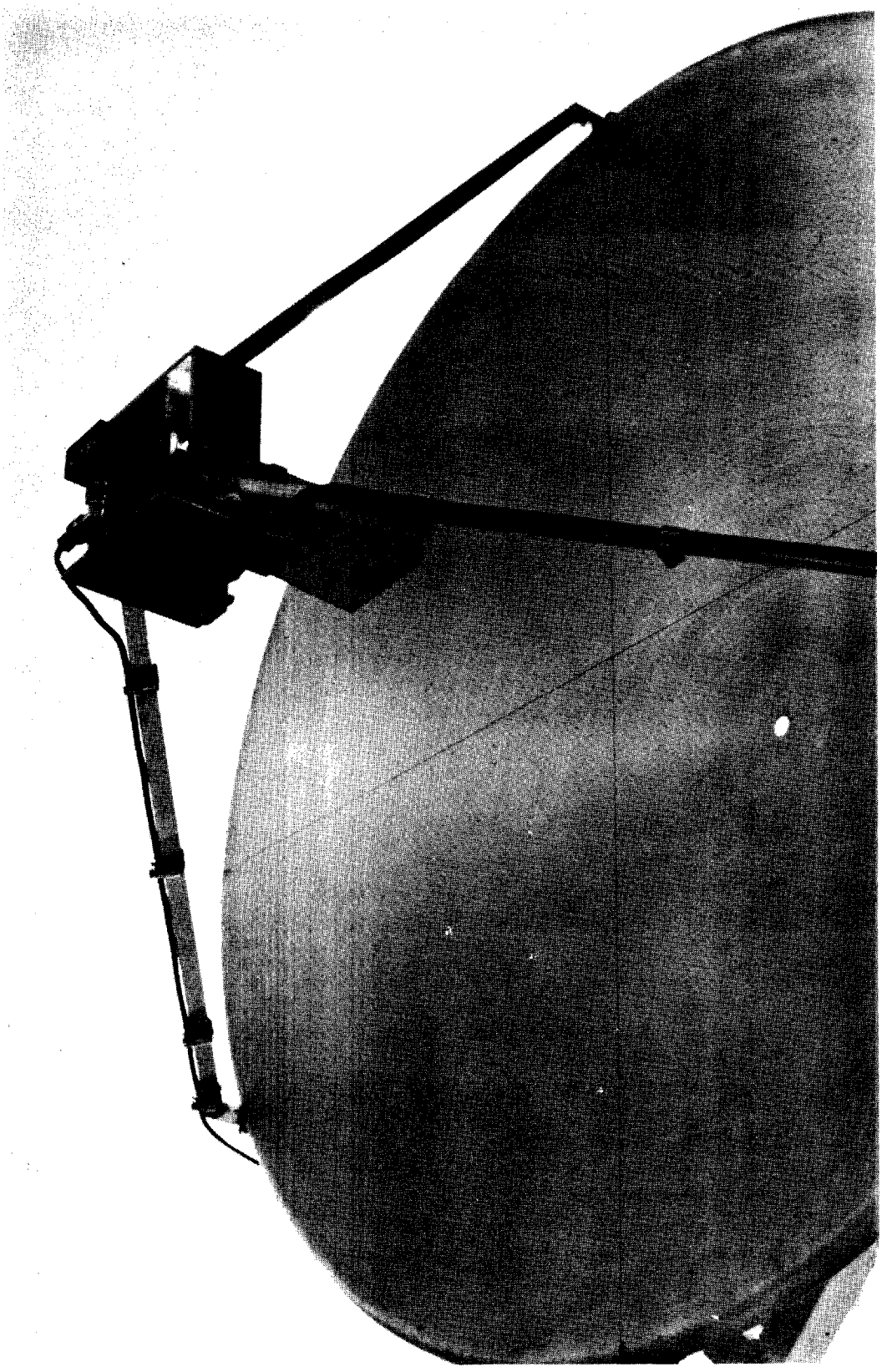

Figure 4-1. The test antenna and support structure mounted on the Georgia Tech far-field range.

TABLE 4-1

DESIGN GOALS FOR MONOPULSE TEST ANTENNA

Gain	30 dB
3 dB Beamwidth	3.0 degrees
First Sidelobe	20 dB below peak sum main beam
Far Out Sidelobes	-40 dB RMS over 20° x 20° sector 30° from main beam
Difference Null	30 dB below peak sum main beam

phase matching problems associated with processing the sum and difference channels behind the reflector are eliminated. In this way, motion of the feed line does not affect the difference channel null. This was considered important because the antenna must be moved between antenna ranges. Semi-rigid coax was used to bring the sum and difference signals to the hybrid and was rigidly attached to the feed support rods.

Design emphasis, in the case of Feed 1, was placed on the difference pattern, since a more demanding comparison between measurement accuracies could be made using the difference null depth and boresight error than could be achieved with the sum pattern parameters. The resultant difference pattern is shown in Figure 4-2. Null depth was greater than 40 dB, and the first sidelobe level was -27 dB. The sum pattern is shown in Figure 4-3. As shown in the figure, the sum pattern main beam has a pronounced dip caused by too low a crossover level between the feed horn patterns. Because this sum pattern does not represent those used in practical systems (and could affect the credibility of the test program), a second feed was designed with a better compromise between sum and difference patterns.

4.1.2 Second feed

The second feed (Feed 2) used the same basic design as the first but used dielectrically loaded horns. This reduced the horn-to-horn spacing by a factor of two and raised the crossover point above 3 dB. The sum pattern is shown in Figure 4-4 and meets all the design goals. The difference pattern is shown in Figure 4-5. Although the difference

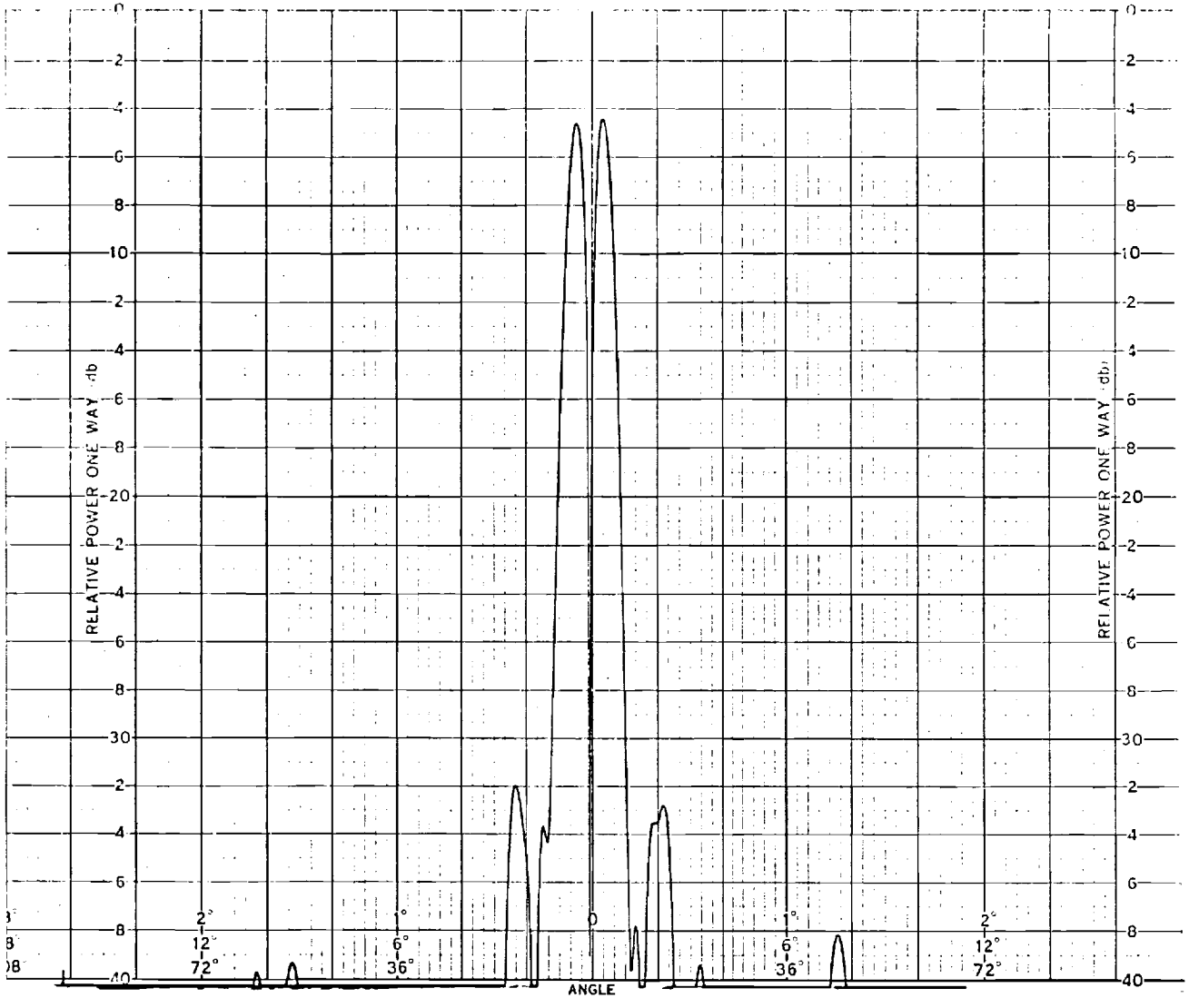

Figure 4-2. Far-field pattern for the first feed, difference pattern principal plane azimuth cut, twelve degrees per major division.

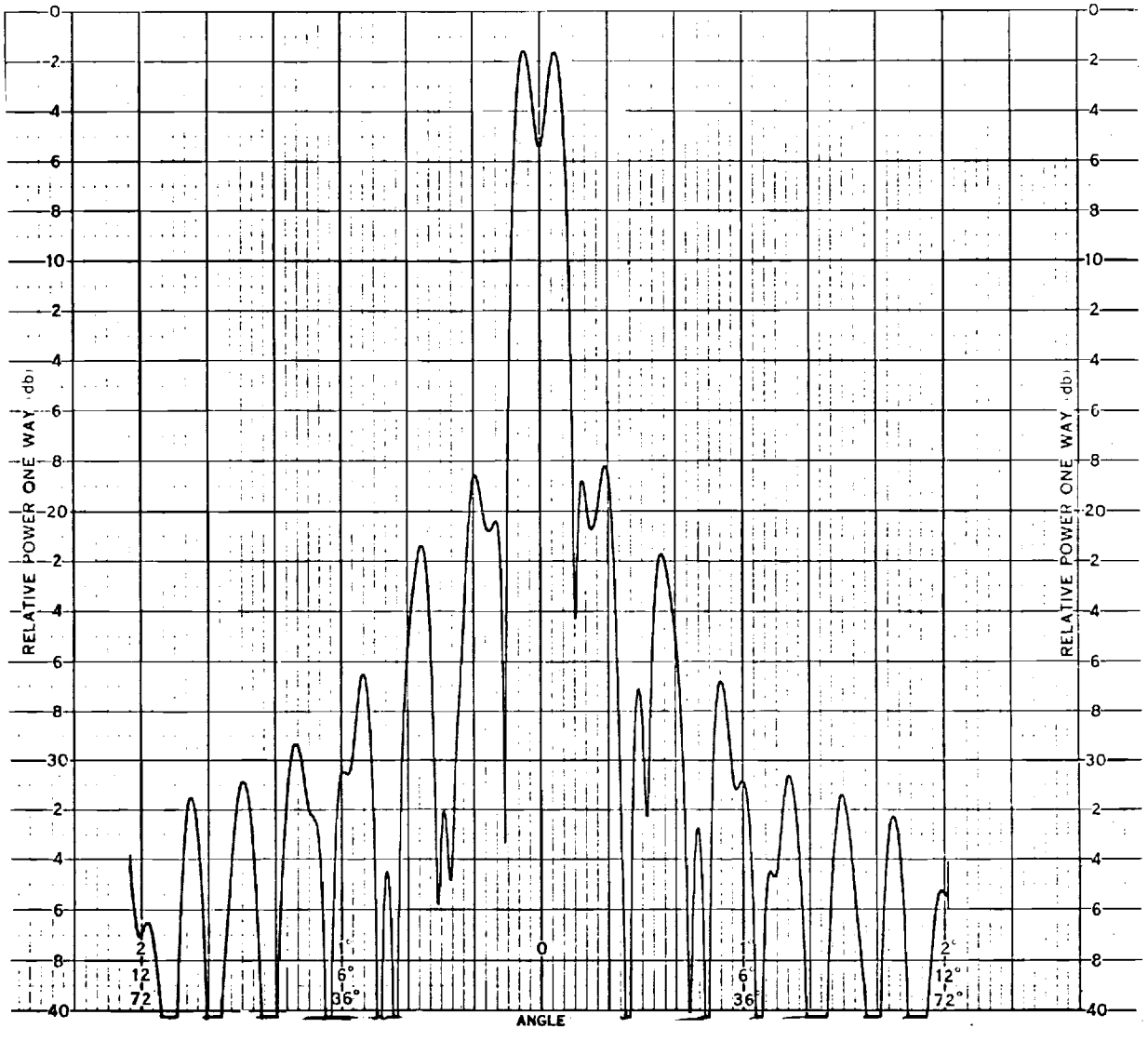

Figure 4-3. Far-field pattern for the first feed, sum pattern principal plane azimuth cut, twelve degrees per major division.

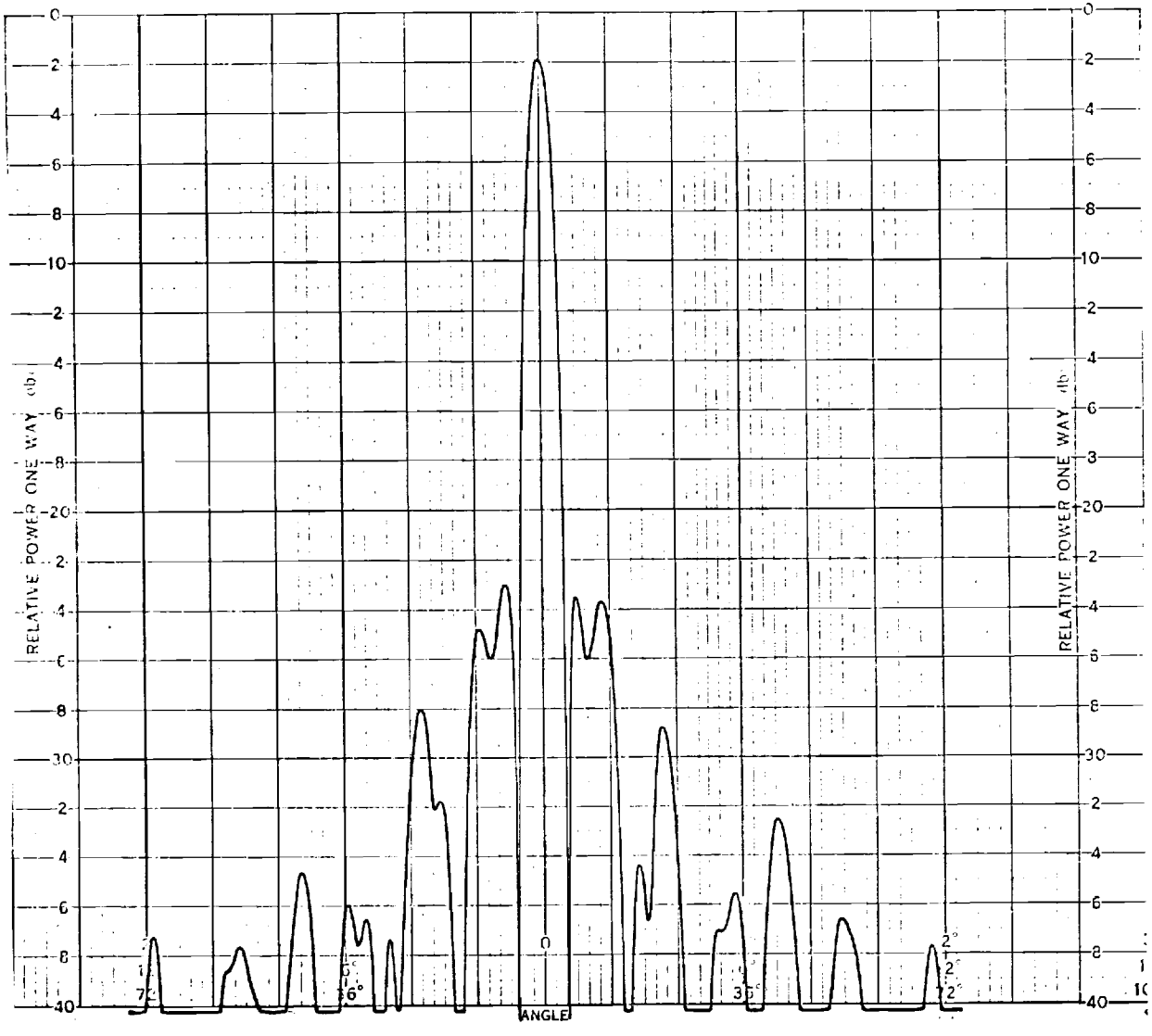

Figure 4-4. Far-field pattern for the second feed, sum pattern principal plane azimuth cut, twelve degrees per major division.

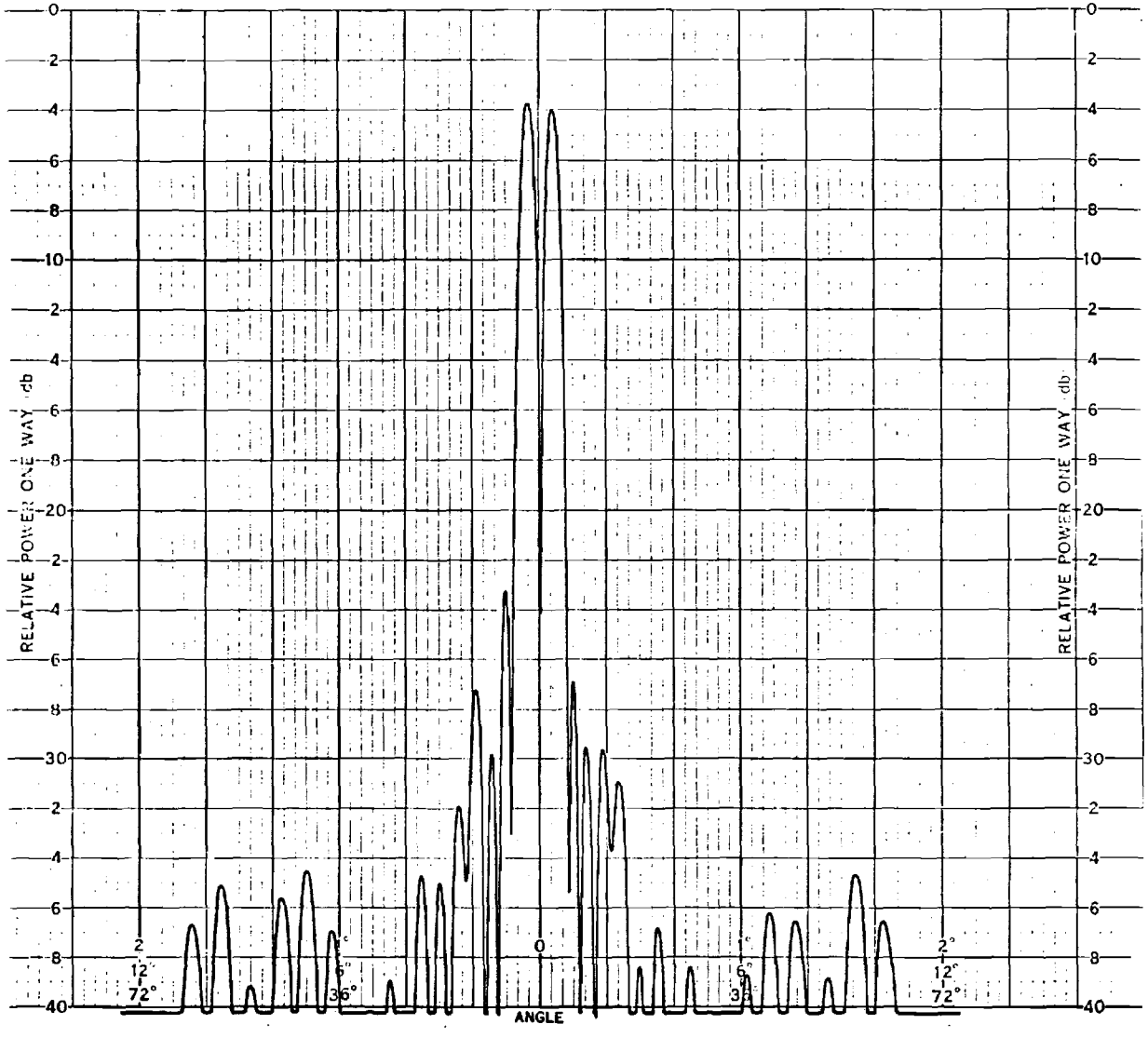

Figure 4-5. Far-field pattern for the second feed, difference pattern principal plane azimuth cut, twelve degrees per major division.

null depth is less than 30 dB, it is of sufficient depth to provide an adequate test of the near-field measurement technique.

It was decided that near-field and far-field measurements at Georgia Tech should be made on both feeds, since the feeds were of similar design and could be switched without changing the feed support structure. The first feed design provided a more stringent test of the ability of the near-field technique to reproduce the deep null depth of the difference pattern and the irregular sum pattern dip in the main beam. The second feed provides a test of a more conventional antenna with more practical parameters which would not be controversial in any way.

4.2 Boresighting Techniques

An important part of the measurement program was a test of the boresight error measurement capability of the near-field measurement system. Standard optical alignment techniques utilizing a theodolite and a mirror mounted on the antenna frame were used on the far-field range, but a special technique had to be developed for the near-field system. Far-field angular resolution was limited by the antenna pedestal synchro dials to ± 0.01 degrees (≈ 0.2 millirad.).

4.2.1 Near field

In the near-field boresight alignment depends on the alignment of the measurement plane and the plane of the antenna as shown in Figure 4-6. Any misalignment translates to boresight error in the far-field. An eight inch square mirror was rigidly attached to a one inch thick aluminim plate approximately one foot square. The mirror and plate were attached to the frame of the test antenna using four adjustable rods. With the antenna mounted in front of the near-field

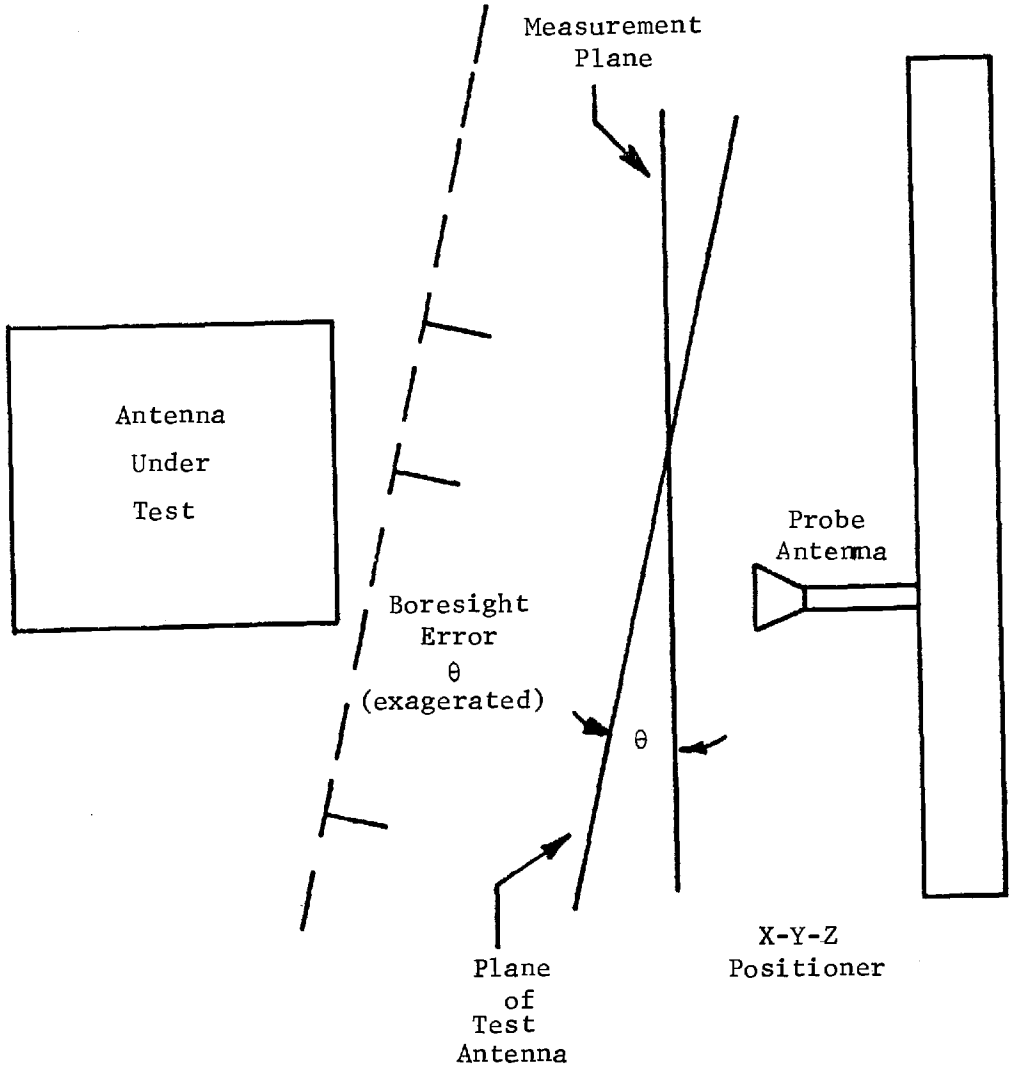

Figure 4-6. Misalignment of the measurement plane and the plane of the test antenna corresponds to boresight error in the far field.

probe, the plane of the mirror was aligned with the plane of the probe by adjusting the four mounting rods. A feeler gauge was attached to the near-field probe and used in the alignment procedure. The total variation in or out of the measurement plane was measured by moving the feeler gauge around the four corners of the mirror and was within 0.0025 inches. This corresponds to a potential angular error in the far-field of 0.32 milliradian ($\approx$0.02 degrees).

The probe antenna was also aligned using a mirror. A theodolite was used to obtain a true horizontal line, and the probe was rotated until the theodolite image could be seen. In this way the probe position could be set to the same position with excellent accuracy. Since the probe horn must also be aligned for cross polarization measurements, a 45 degree prism with a reflective coating was placed in the probe after it was rotated 80 degrees, and the probe again adjusted until the theodolite image could be seen. Thus cross polarization measurements are referenced to a 90 degree rotation determined from this 45 degree prism.

4.2.2 Far field

The boresighting technique used for far-field measurements at both ranges is illustrated in Figure 4-7. The mirror which was aligned with the near-field measurement plane was used as the boresight reference. The theodolite was aligned with the transmitter antenna feed horn, corrected for parallax in the azimuth plane. Estimated angular accuracy for the far-field boresight alignment is $\pm$0.05 degrees; a one foot error in parallax correction corresponds to an angular error (for the Georgia Tech 1000 foot range) of

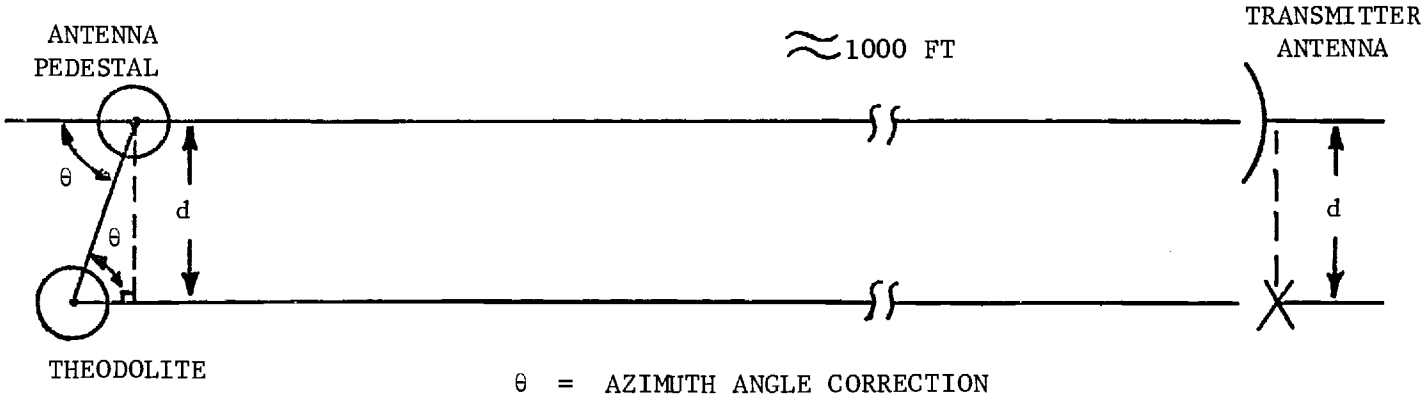

Figure 4-7. Far-field boresight alignment technique used on both outdoor antenna ranges.

$$a = \frac{1 \text{ ft}}{1000 \text{ ft}} (57.3 \text{ degrees/radian}) = 0.057 \text{ degrees}$$

A comparison of the boresight error measurements on the two far-field ranges and the near-field range will be presented in Section 7. Agreement between the near-field and far-field boresight error measurements is well within the estimated accuracy of the far-field alignment techniques.

SECTION 5

FAR-FIELD RANGE MEASUREMENTS

5.1 Description of Far-field Ranges and Their Qualification

Measurements of the test antenna pattern were made on two different far-field ranges so that two independent far-field measurements could be compared with each other as well as with the pattern based on near-field measurements. Both far-field ranges are operated as elevated ranges. Chronologically, the first set of far-field data was collected on a range at Georgia Tech, and subsequently measurements were carried out at Scientific-Atlanta's Gwinnett County range.

5.1.1 Georgia Tech far-field range

The Georgia Tech far-field range operates between two buildings (Harry L. Baker and Physics). The transmitter, located on the roof of the Baker Building, employed a 4 foot diameter paraboloidal reflector with a beamwidth of approximately 3 degrees. The receive station, located atop the Physics Building Tower, is raised approximately 100 feet above the transmitter. Figure 5-1 is a photograph of the transmitter site from the receiving site. The range is 1000 feet long, and the transmitter beam is thus directed at an elevation angle of about 5 degrees above the horizontal.

The receiver uses a Scientific-Atlanta Model 1742 wide range receiver operated in the coherent mode using a reference channel. The antenna frame as shown in Figure 5-2 was mounted on an azimuth-over-elevation-over-azimuth pedestal. Angular readings were not corrected for parallax on the far-field plots, and a very small error (less than 4 milliradians for worst case and zero for principal

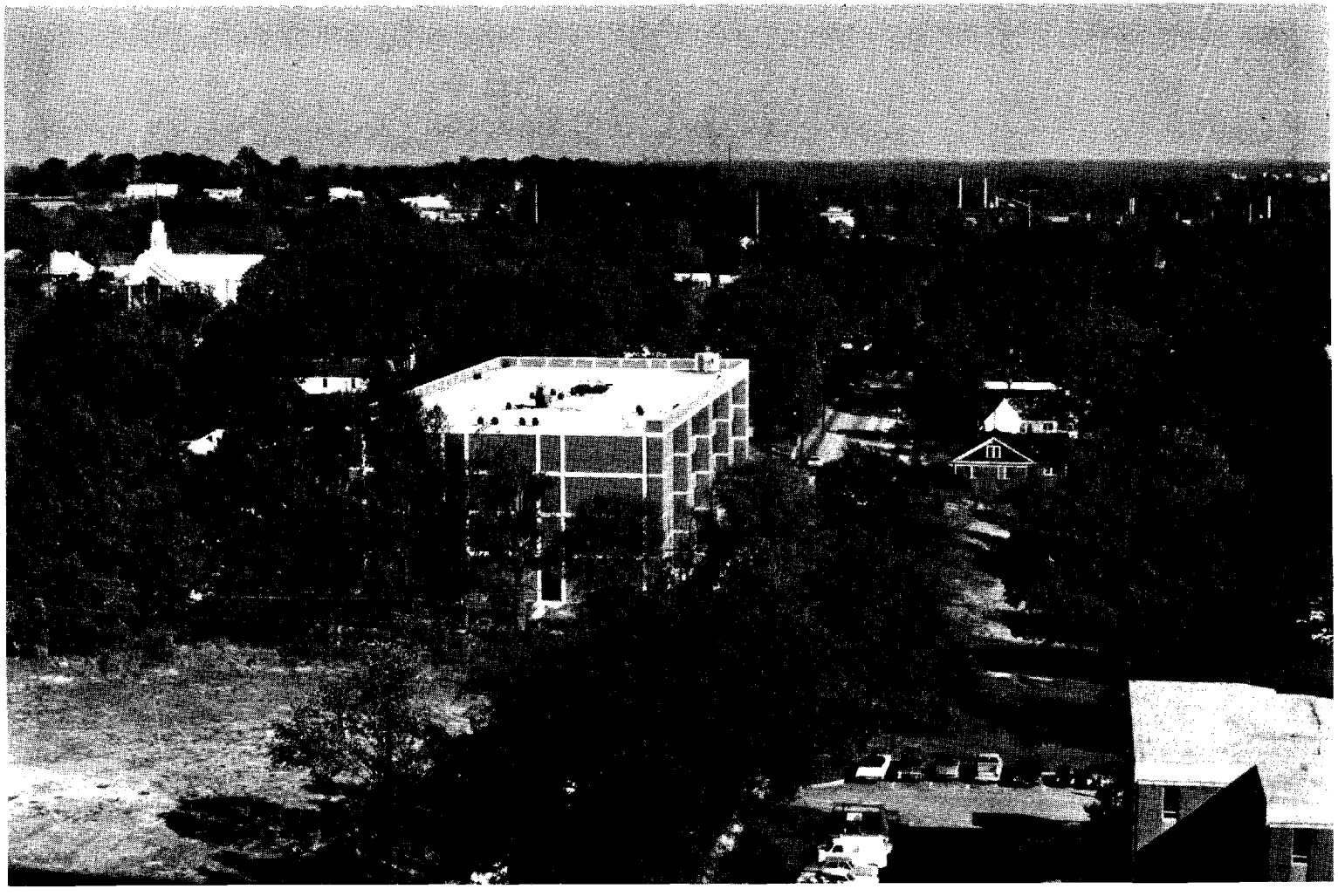

Figure 5.1. View of Georgia Tech far-field range looking from receiving site to transmitter site.

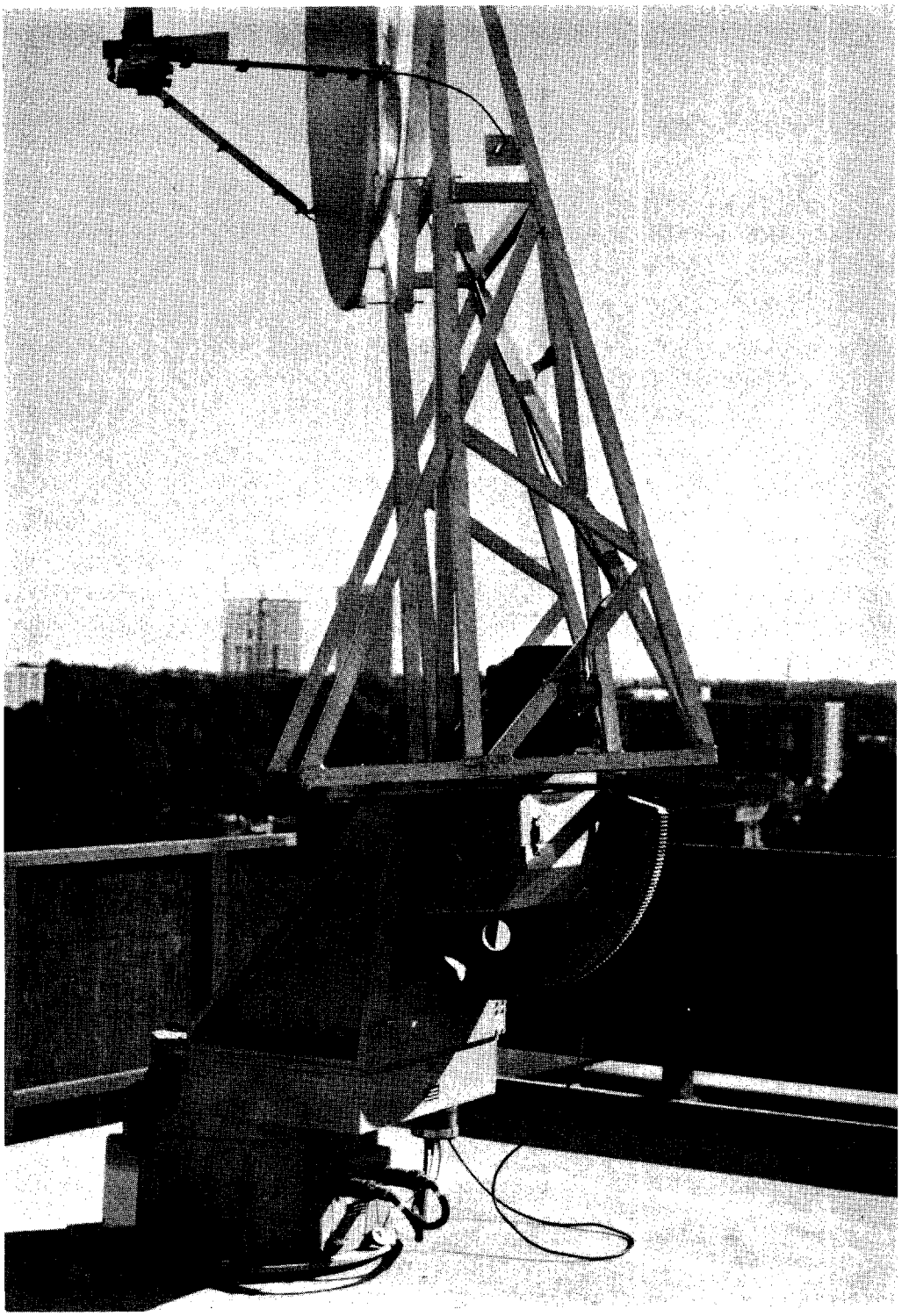

Figure 5.2. Test antenna and support frame mounted on antenna pedestal at Georgia Tech far-field range.

plane cuts) is residual in the far-field data as compared to the near-field derived data.

A field probe was used to scan the electromagnetic fields existing on the far-field range at the test frequency of 5.45 GHz and at the plane of the receiving antenna. Figures 5-3 and 5-4 show data recorded on the Georgia Tech range in a vertical scan section and a horizontal scan section, respectively, by the field probe. An open-ended C-band waveguide was used as the receiving antenna. This waveguide with a gain of 2 dB is in essence an isotropic receiver when viewed over the angles subtended by point reflections on the range.

The vertical field probe results indicate two reflections, one with a period of about 0.3 feet and the other a longer period of approximately 4 feet. The peak-to-peak amplitudes of these signals are approximately 1.5 dB and 1.0 dB, respectively. These correspond respectively to extraneous reflections about 22 dB and 25 dB below the direct beam of the source or transmitting antenna. The higher frequency ripple is apparently caused by a reflection from structural members on the receiving building, while the lower frequency (and lower level) reflection originates from the coping on the building used as a transmitter site. This allocation is based on the observed period of the two ripples and the angle computed from that periodicity. It should be noted that when a standrad gain horn having a gain of 15 dB is used as the probe, no ripple is observed in the pattern. For a high-gain receive antenna in conjunction with the high-gain transmitter the range quality is on the order of 50 dB. In a worst case analysis, however, the numbers of 22 dB and 25 dB are more

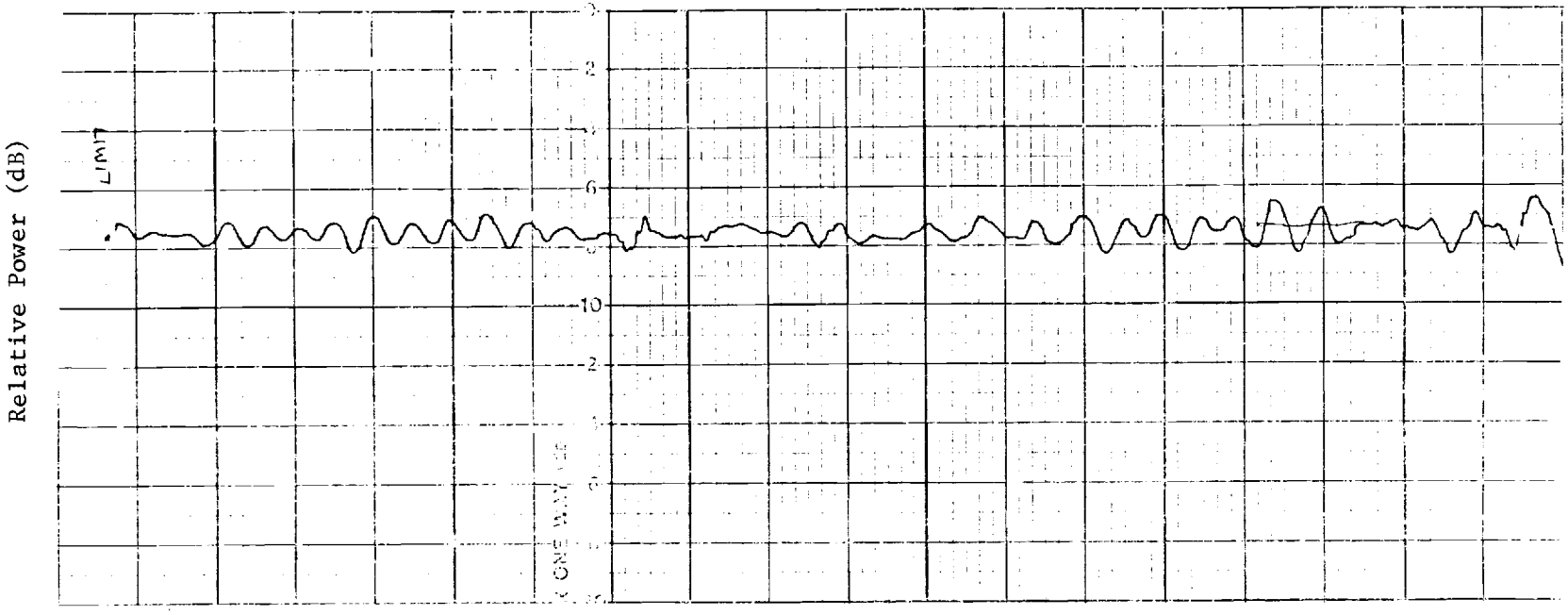

Figure 5-3. Field probe response on Georgia Tech far-field range for vertical cut.

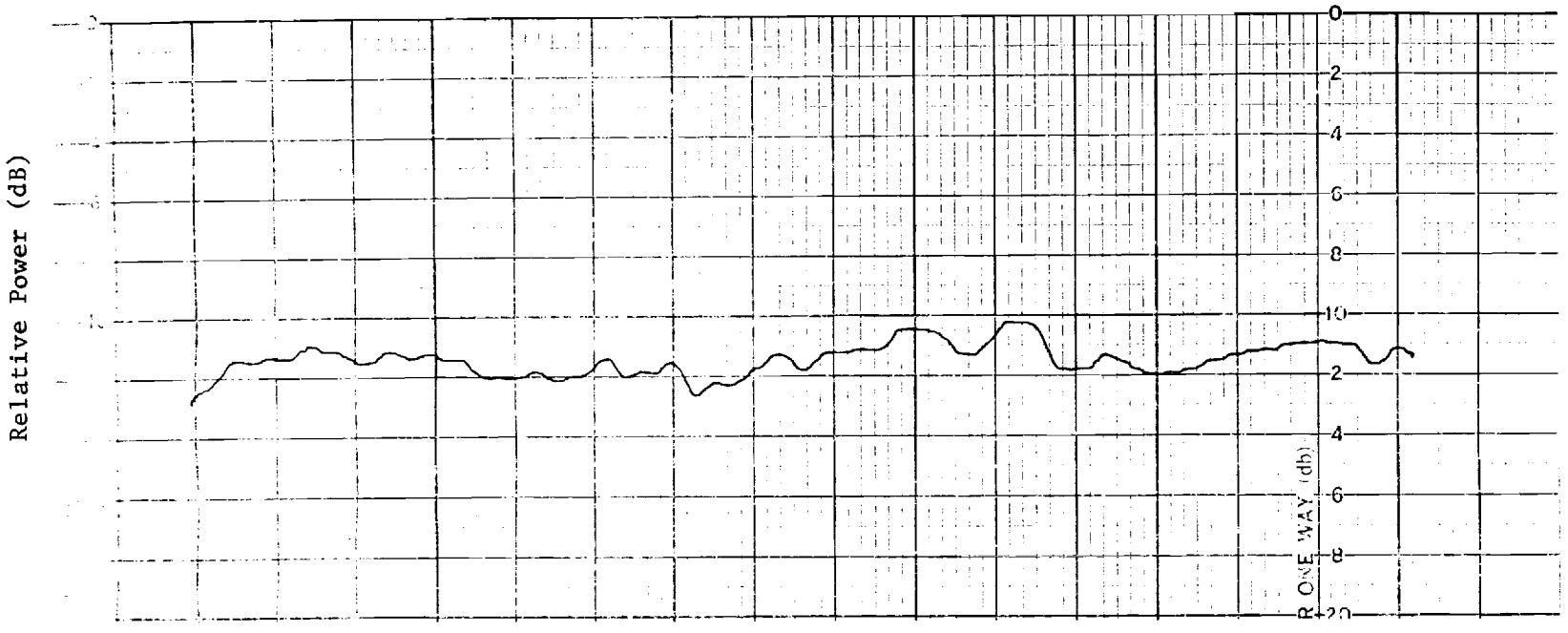

Figure 5-4. Field probe response on Georgia Tech far-field range for horizontal cut.

representative of the effects point reflections on the range would have on measured pattern characteristics. The horizontal scan (Figure 5-4) shows a similar amplitude though less systematic variation. This cut was taken with the probe horn in closer proximity to the test antenna and probably reflects coupling to that structure.

For the spurious reflection 22 dB below the direct signal, a negligibly small error in the measured gain of the main beam is expected. The inaccuracy associated with this reflection would lead to an error of $\pm$.08 dB in the measured gain of the main beam. For sidelobes on the order of 40 dB down, however, measurement errors on the order of $\pm$.7 dB would be incurred due to the range reflection. This $\pm$.7 dB error corresponds to the condition obtained when the gain of the test antenna in the direction of the main beam and in the direction of the point reflections are equal. If the gain of the beam in the direction of the spurious reflection were greater than that in the direction of the source by on the order of 10 or 15 dB, then errors as large as $\pm$3 dB might be observed in the measurements. In taking elevation cuts the main beam of the receiver (or test) antenna occasionally pointed at ground, and in those cases even larger range errors might be expected.

The computed errors resulting from the 25 dB reflection are correspondingly lower. Here it is found that the error in the main beam is approximately the same, $\pm$.07 dB, while the effect on sidelobes is on the order of $\pm$.5 dB under the assumption that the gain is the same pointing at the source and at the point reflections. Again, if the gain in the direction of the point reflection is larger than that of the source, errors up to $\pm$3 dB could be incurred.

In summary far-field data obtained on the Georgia Tech outdoor range should be accurate in main beam gain measurements to $\pm$.1 dB (exclusive of gain calibration errors). Sidelobe peak levels should be accurate to approximately $\pm$1.0 dB, while sidelobe skirts should be within $\pm$4 dB. These range errors arise from range reflections only and do not include angular errors, etc.

5.1.2 Scientific Atlanta Gwinnett County range

Scientific Atlanta's Gwinnett County range is a 1500 foot range specially constructed on levelled open ground. The receiver station is located atop a 50 foot tower. The transmitter employs an 8 foot diameter paraboloidal reflector with a beamwidth of approximately 1.5 degrees. The transmitter is raised about 10 feet above ground level and its beam is inclined upward 2 degrees with respect to the horizontal when pointing at the receive antenna. The receiving equipment included a Scientific Atlanta Model 1742 wide range receiver operated in the coherent mode. At this facility the transmitter site includes a rotatable mount for cross polarization measurements. All measured far-field cross polarization measurements were made on this range,as Georgia Tech's transmitting facility is not so equipped. The Gwinnett facility also uses an azimuth-over-elevation-over-azimuth mount. As previously mentioned a small parallax error is residual in the far-field range data when compared to the Georgia Tech far- and near-field range data, but its magnitude is quite small.

Figure 5-5 shows a vertical field probe plot taken on the Gwinnett County range. The ripple amplitude (once the probe leaves the immediate vicinity of support structures) is on the order of 0.1 db peak-to-peak. This would indicate spurious levels 39 db below the main

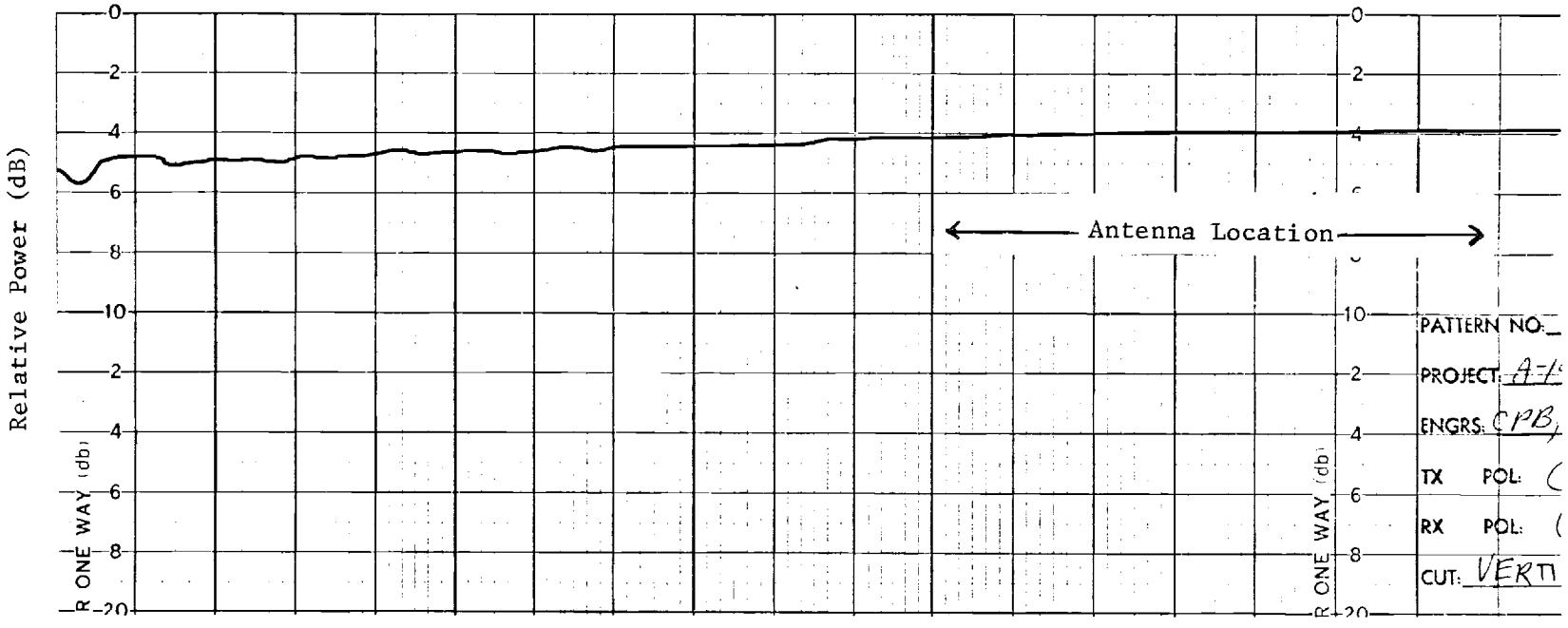

Figure 5-5. Field probe response for vertical cut at Gwinnett County range.

beam. In this case, however, a small horn was used as the probe, and its gain of approximately 7 dB discriminates against spurious reflections. Thus a more realistic estimate of range quality would be on the order of -30 dB extraneous reflection levels. This corresponds to an error in peak sidelobe levels from range reflections of approximately $\pm$0.5 dB.

5.2 Far-field Measurements Procedures

The general procedures used on both far-field ranges are described below.

The first step in the far-field measurements was to locate the optical boresight of the system as described in Section 4.2. Secondly, gain measurements were made of the monopulse antenna and referenced to a standard gain horn. The transmitting antenna used was a 4 foot paraboloidal reflector in one case and an 8 foot reflector in the other. Received signal levels were measured on boresight using both the standard gain horn and the monopulse antenna. The difference between the two received signal levels was recorded, and added to the known gain of the standard gain horn to obtain the sum channel, boresight gain of the monopulse antenna. This maximum boresight gain was then set to -2 dB on a Scientific Atlanta rectangular pattern recorder. All patterns taken on each range are referenced to this sum boresight level.

Antenna difference boresight cuts were taken to detect any discrepancy between the electrical and optical boresights. The Scientific Atlanta positioner control units used at both antenna ranges have direct dial readings in degrees of both the azimuth and elevation angles. Direct readout to one-tenth degree is provided

on the indicators, and interpolations to approximately .01 degree can be made. These indicators and the pattern recorders were set such that zero degrees corresponded to the optical boresight. Expanded difference azimuth cuts were taken, and the null location compared to the "zero degrees" marking on the pattern paper. Agreement between optical and electrical boresight was found to be within 0.03 degree.

For all recorded cuts the levels are referenced to the sum boresight level. No normalization of the recorded patterns was made. All difference cuts are also referenced to the sum boresight level. This same reference is applied to the off-axis cuts and to the RMS sidelobe sections. For off-axis regions where the signal level is low, 20 dB of attenuation was removed to raise the pattern level. Some of the off-axis and all of the RMS sidelobe cuts were raised. However, the reference of these cuts to the sum boresight signal level is preserved when the 20 dB offset is properly taken into account. Patterns recorded in this manner are marked "raised 20 dB." In addition, all angles on the recorded patterns are referenced to the optical boresight discussed earlier.

Cross polarized patterns in both the sum and difference modes are referenced to the peak of the parallel polarized pattern. For the difference mode, the cross polarized pattern is referenced to the parallel difference pattern which is in turn referenced to the sum parallel pattern.

Using the above procedures, all recorded information is exactly referenced to the optical boresight in angle and to the sum parallel boresight level in amplitude. This method prevents ambiguity in

data analysis. Since the procedure followed was identical for both outdoor ranges, the data can be compared by using a simple overlay technique as is done in much of the presentation of Section 7.

5.3 Far-field Patterns

Sample far-field pattern cuts are displayed in Figures 5-6 through 5-10. All these are data recorded on Feed 2 at the Scientific Atlanta range. More complete outdoor range data is contained in Appendix B both for Feed 1 and for Feed 2. (Comparisons of far-field range results with near-field results on both Feed 1 and Feed 2 are made in Section 7.)

Figure 5-6 shows a principal azimuth plane cut for the sum channel of Feed 2. Main beam gain was determined (via standard gain horn calibration) to be 30.2 dB. First sidelobe levels are down 22 dB. Figure 5-7 shows the principal elevation plane cut also of the sum channel. First sidelobes are here seen to be about 18 dB down. The difference channel of Feed 2 is shown in a principal azimuth plane cut in Figure 5-8. The difference pattern null is about 22.5 dB below the difference pattern maximum, which is in turn 2.8 dB below the maximum sum channel gain. Difference pattern first sidelobes are about 20 dB below the principal maximum.

In addition to the principal plane cuts numerous off-axis pattern cuts were made, and one sample is shown in Figure 5-9. This particular graph is an azimuth cut taken at an elevation angle of -8 degrees.

To determine RMS sidelobe levels pattern cuts were taken over an azimuth angular width of 20 degrees and at 0.5 degree angular increments in elevation so as to cover a 20 degree spread in elevation. One series of such curves is reproduced in Figure 5-10 where the azimuth angles run from zero degrees to -20 degrees and elevation angles are

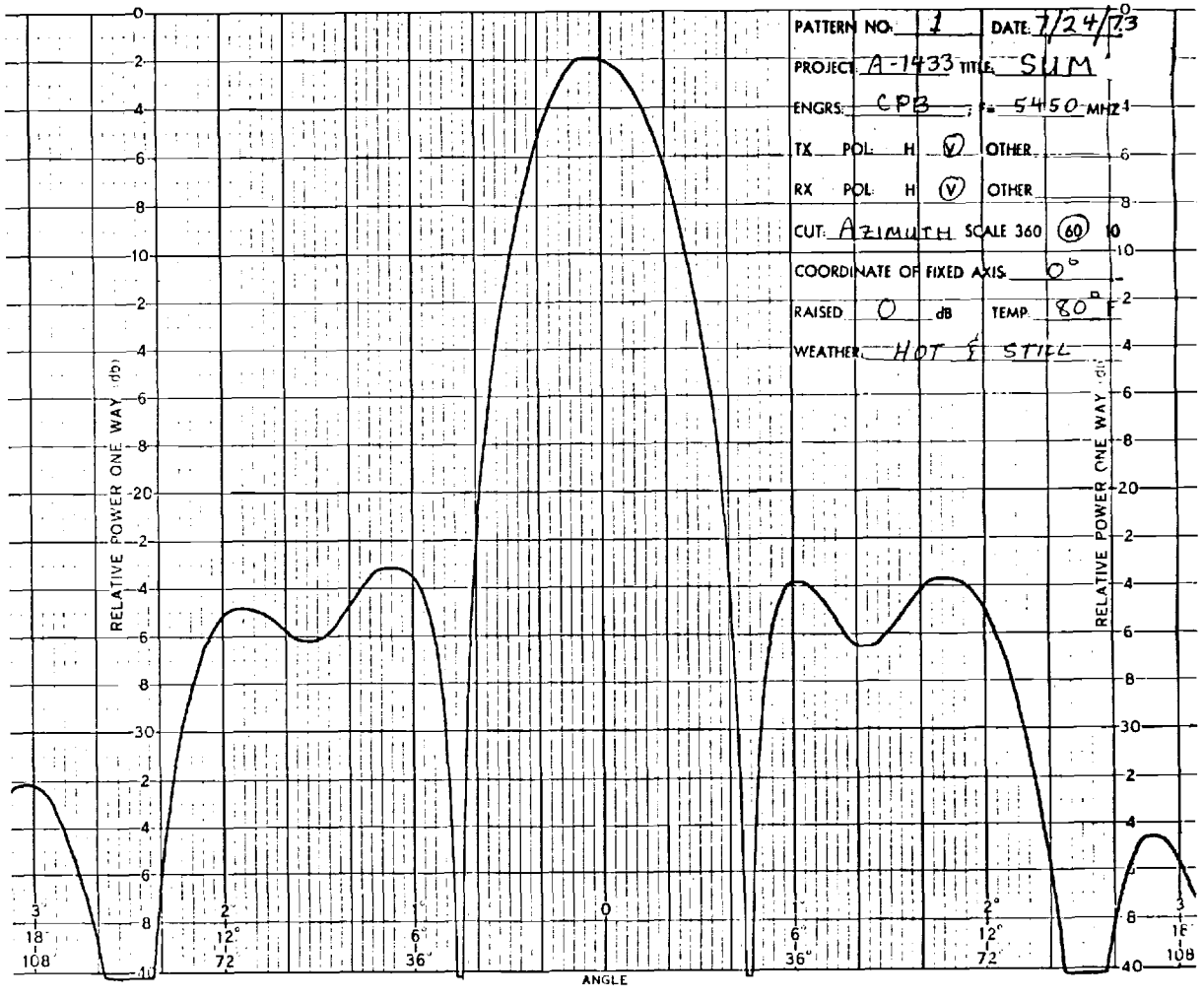

Figure 5.6. Far-field sum pattern cut in principal azimuth plane taken on Feed 2 at SA range, 12 degrees per major division.

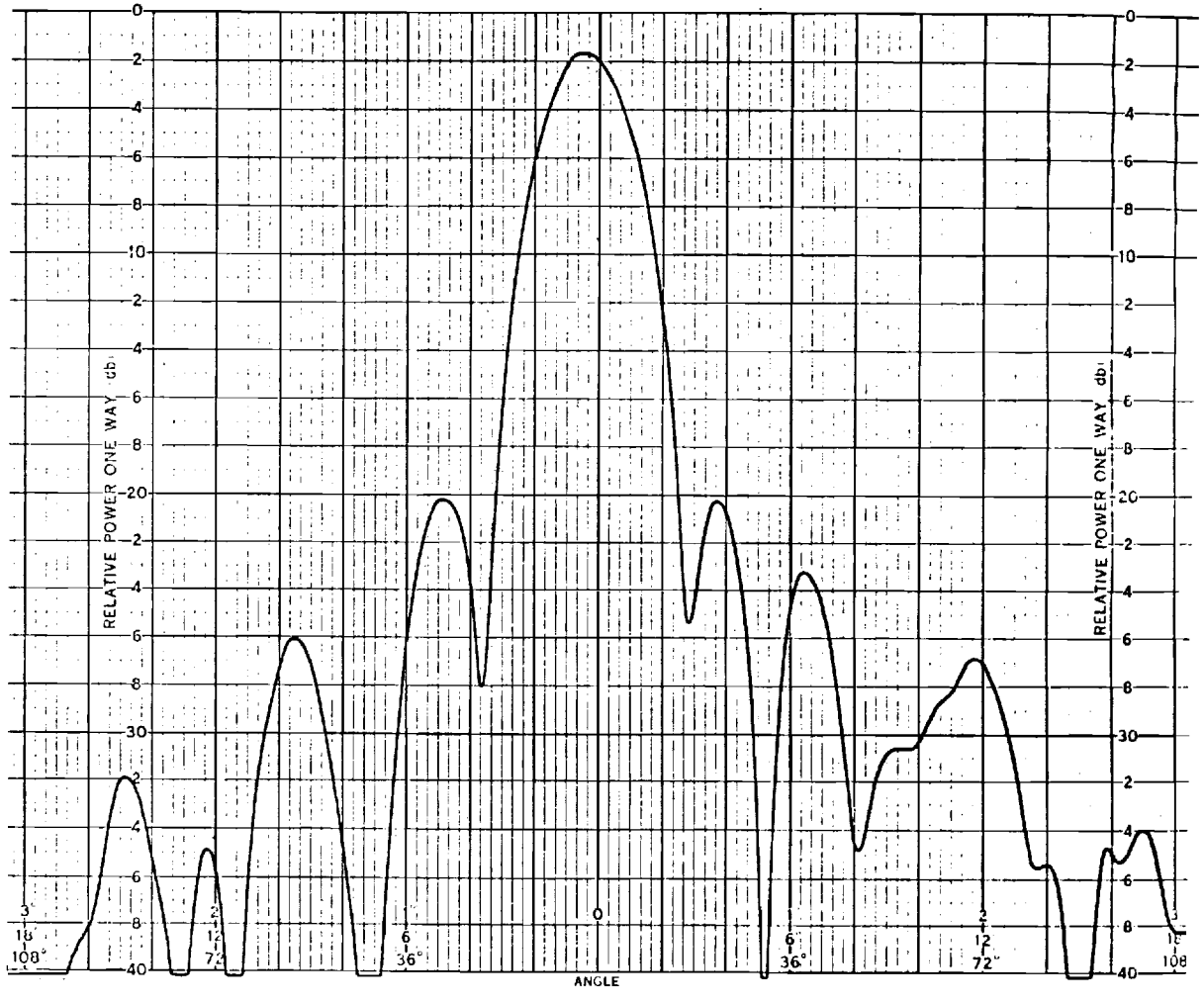

Figure 5.7. Far-field sum pattern cut in principal elevation plane taken on Feed 2 at SA range, 12 degrees per major division.

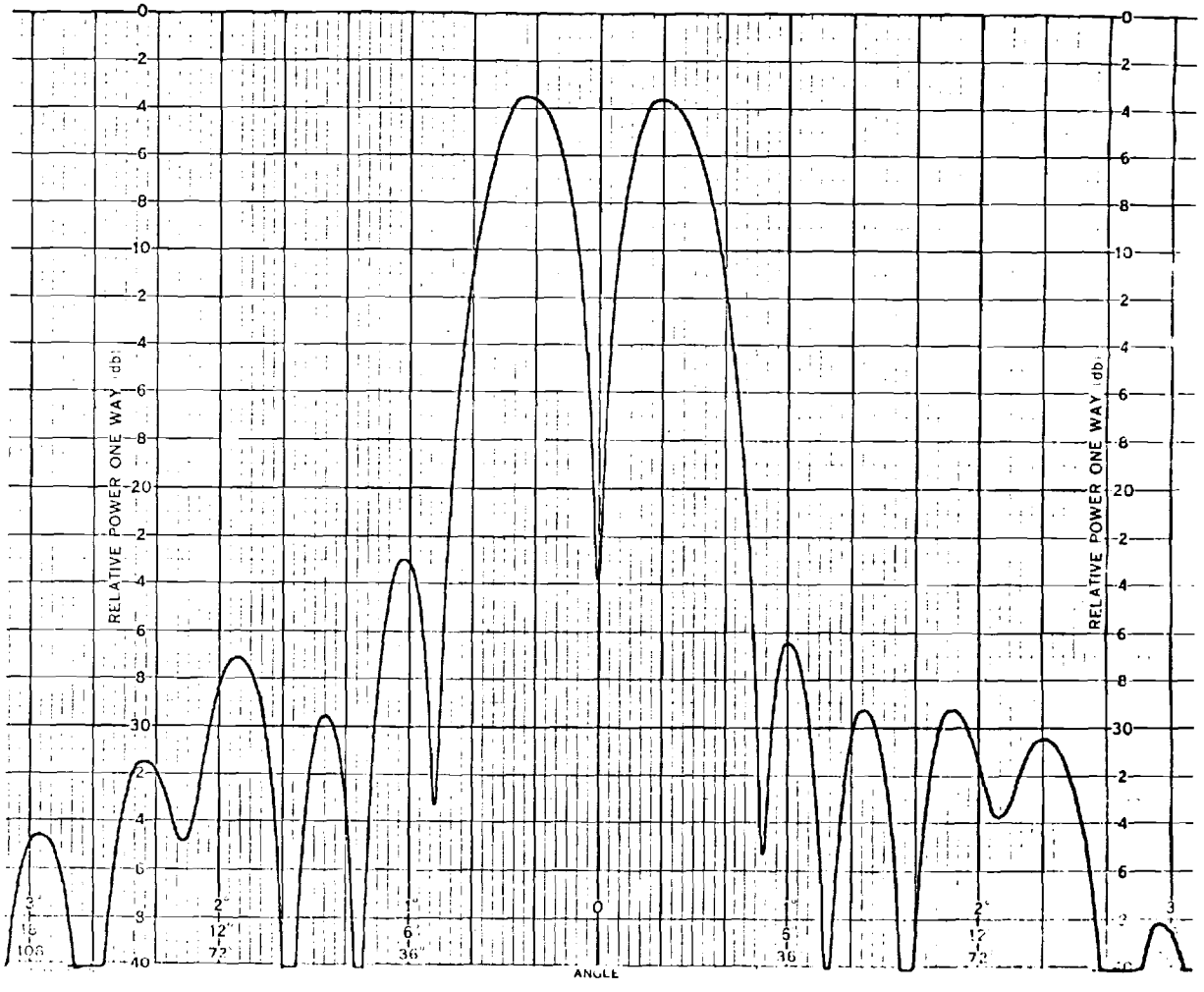

Figure 5.8. Far-field difference pattern cut in principal azimuth plane taken on Feed 2 at SA range, 12 degrees per major division.

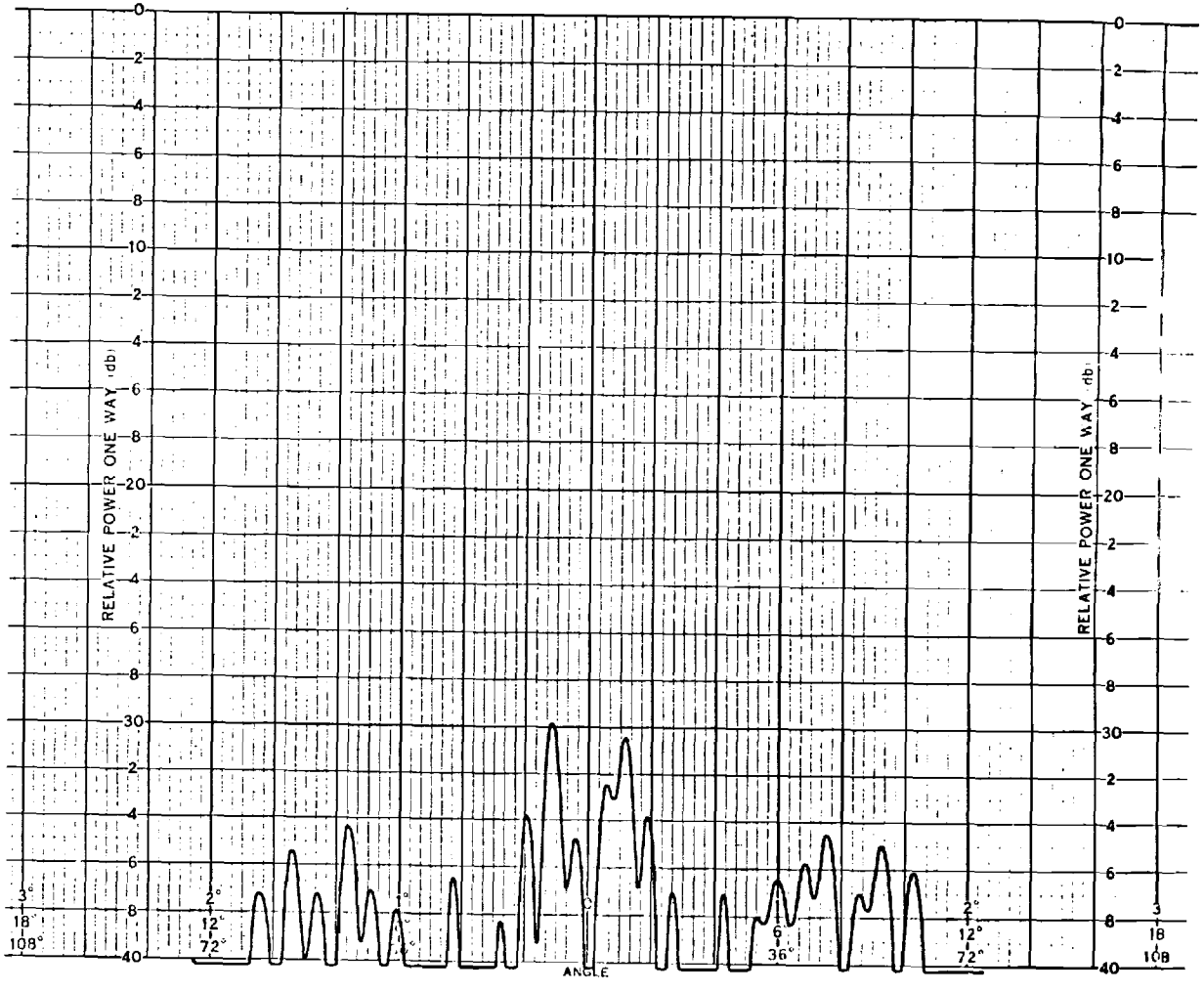

Figure 5.9. Far-field difference pattern cut in azimuth plane at elevation angle of -8 degrees, 12 degrees per main division.

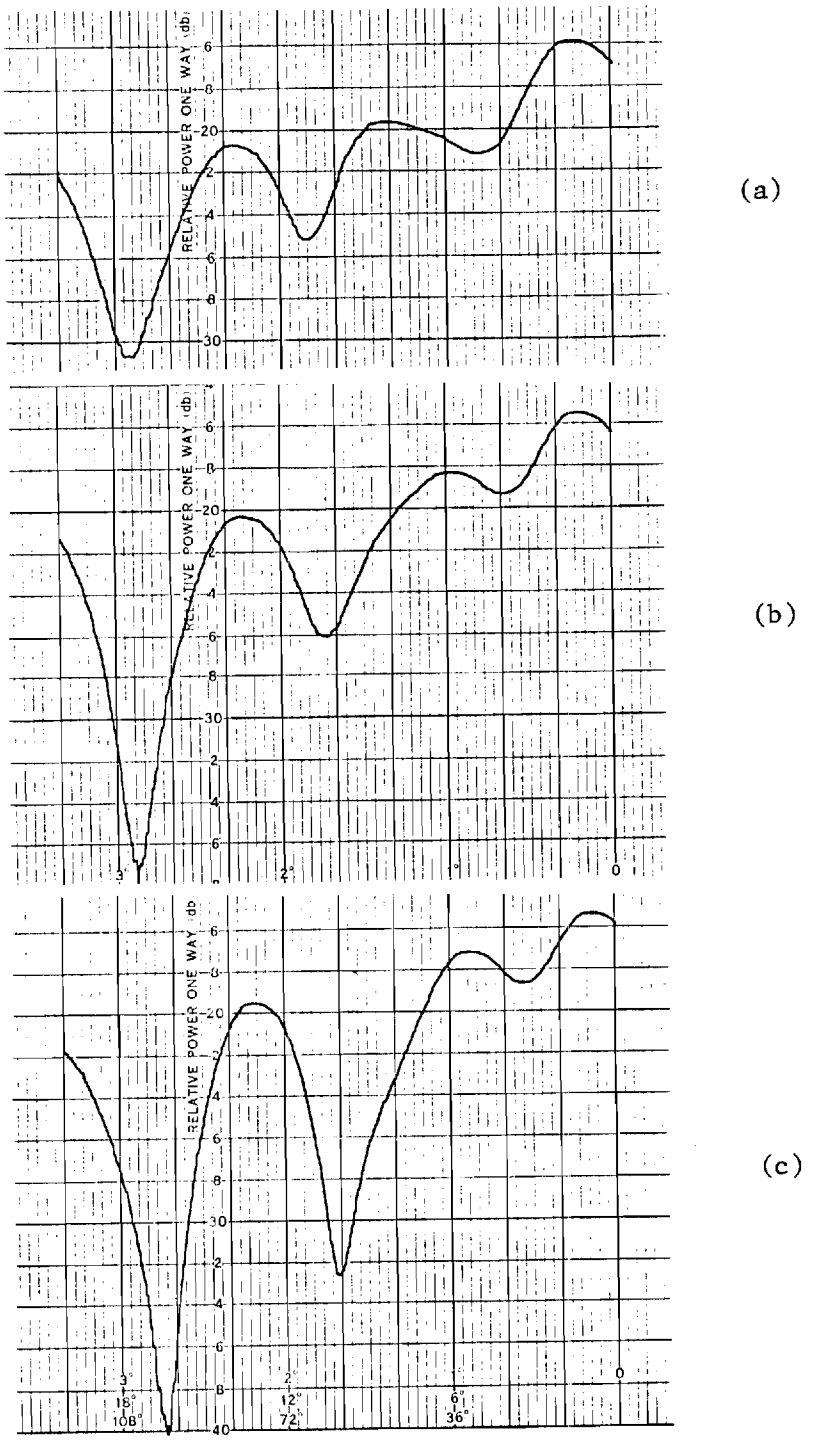

Figure 5.10. Examples of azimuth cuts taken for RMS sidelobe determination. Elevation angles: (a) -25.5°; (b) -26.0°; (c) -26.5°; twelve degrees per main division.

-25.5 degrees, 26.0 degrees, and 26.5 degrees. From complete sets covering 20 degree by 20 degree square blocks, gain readings at 0.5 degree increments in both azimuth and elevation are obtained, and the RMS value of the 1600 data points is calculated as the RMS sidelobe level for that particular angular section.

SECTION 6

NEAR-FIELD RANGE MEASUREMENTS

6.1 Near-field Measurement System

The near-field measurement system used to measure the amplitude and phase of two orthogonal components of the near-fields of the test antenna is described. A schematic diagram of this system is given in Figure 6-1, and a photograph of the system is shown in Figure 6-2.

6.1.1 Mechanical equipment

The near-field probe, used as a receiving antenna, is held in position by a rotary probe holder capable of complete rotation without changing the amplitude or phase of the signal passing through it. The rotary probe holder is a hollow aluminum tube, 30 inches long and 3.5 inches in diameter. The holder houses a C-band waveguide mounted on eight centering posts, a waveguide-to-coaxial connector, a 10-inch section of RG-212U coaxial cable, a Scientific-Atlanta Series 14-2 mixer connected in series with a Scientific-Atlanta Series 10-1 Rotary Joint. The rotary probe holder is transported to any point in a 100 by 100 inch plane by a Scientific Atlanta XY-motion Unit and associated Series 4100 Position Control and Indicator Unit. Two NORDEN OADC 35/1000P/INC optical incremental encoders monitor the X and Y positions of the near-field probe.

A mechanical scissor unit built into the XY-motion unit connects the rotary probe holder to a stationary point on the XY-motion unit via RG-214U RF cable and three rotary joints. This scissor unit enables movement of the receiving antenna throughout a 100 by 100

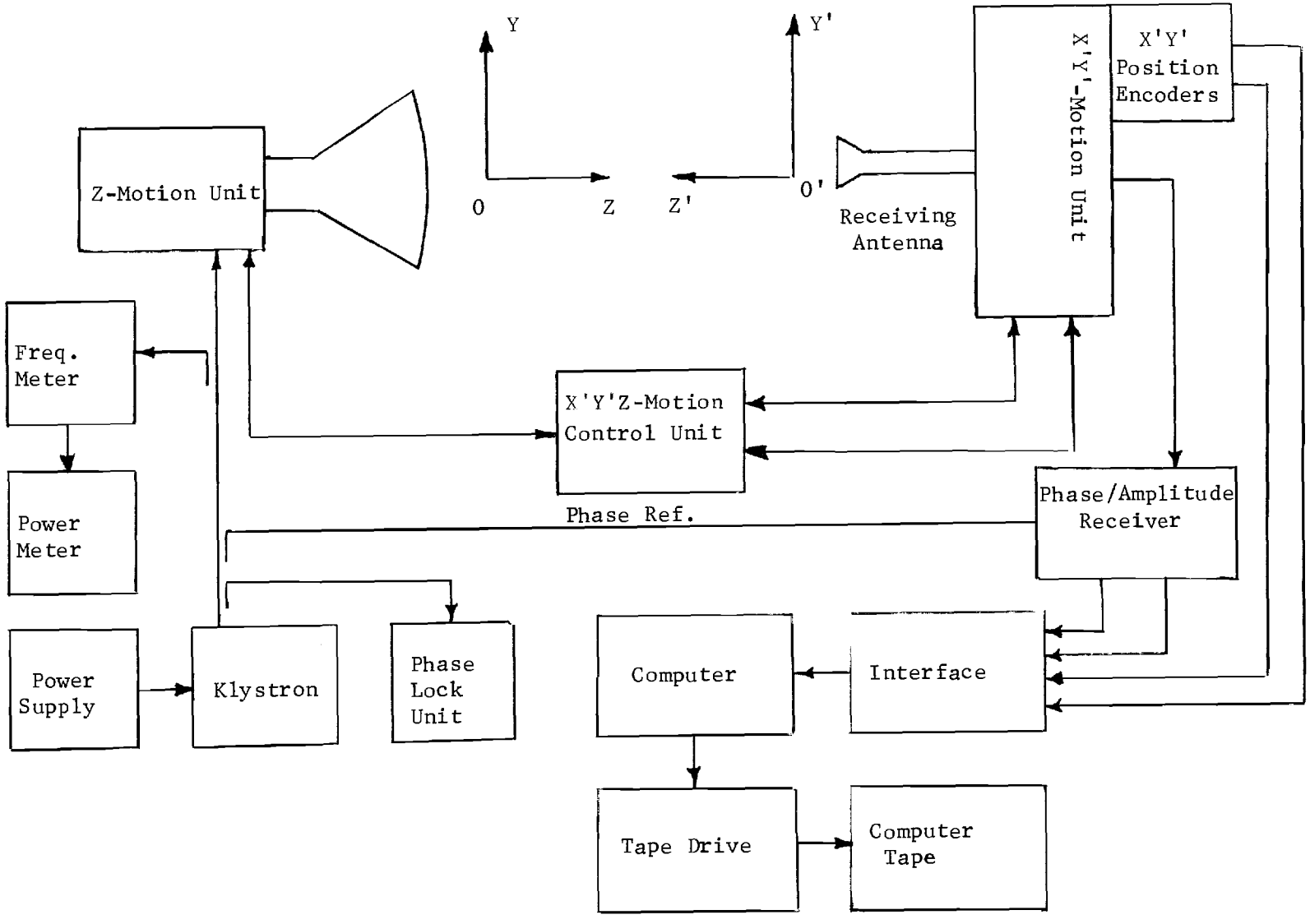

Figure 6-1. Block diagram of near-field measurement system.

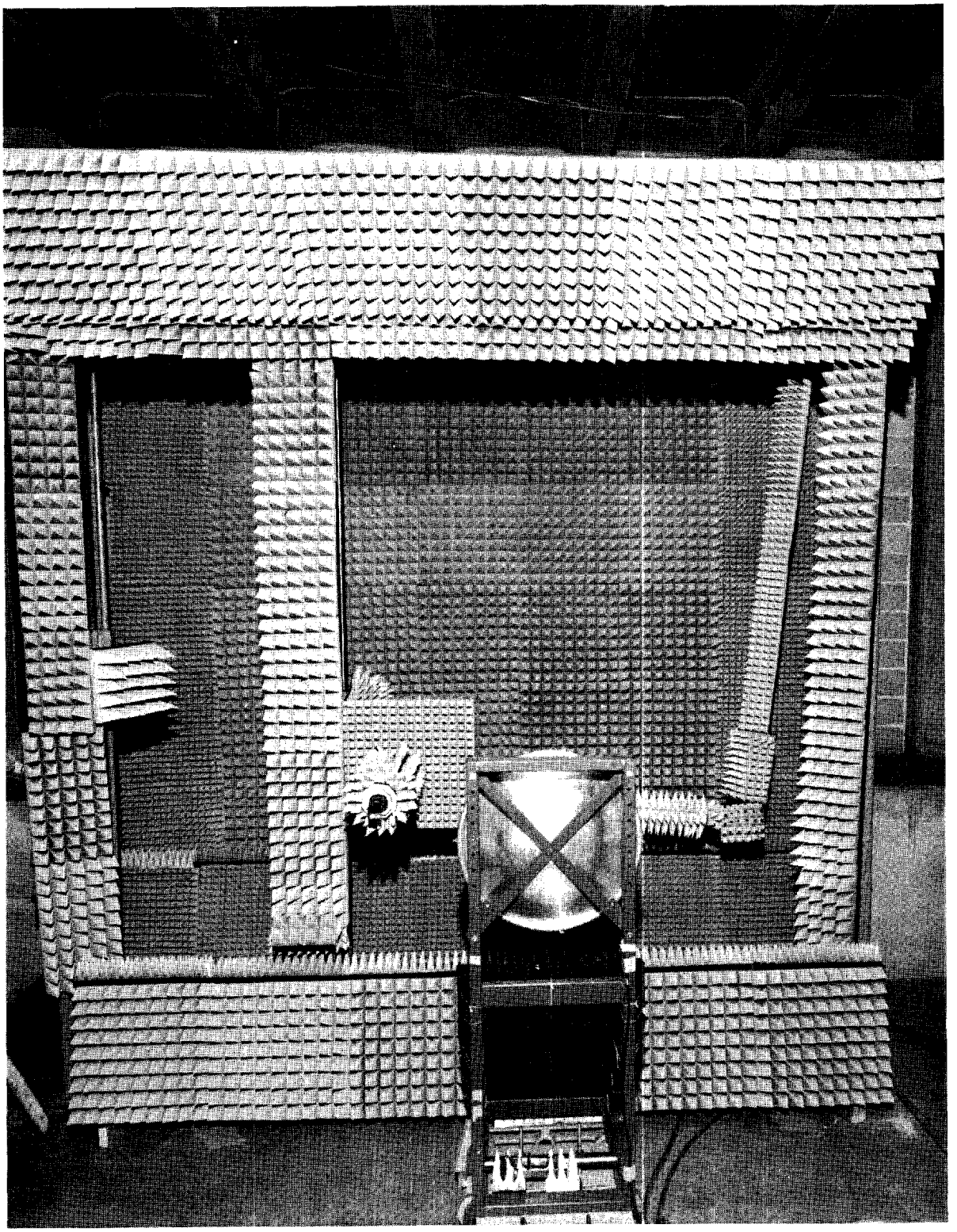

Figure 6.2. Near-field measurement area.

inch plane without changing the amplitude or phase of the received signal due to XY motion.

6.1.2 Electrical equipment

Microwave energy passes from the XY-motion unit to a Scientific Atlanta Series 1750 Wide Range Phase/Amplitude Receiving System through RG-214U RF cable lashed to rigid supports. The receiver provides voltages proportional to the relative amplitude of the received signal and to the relative difference in phase between the received signal and the phase of the microwave source output. A digital interfacing unit is connected to the receiver and position sensors on the XY-motion unit.

The computer interface provides positional, amplitude, and phase information in digital form to a Supernova mini-computer. When the computer is ready to receive data it starts the interface. The interface then accepts a 4-bit digital word which it uses to determine which of the four types of data to transmit to the computer. Finally, the interface sends the proper 16-bit word to the computer and signals completion. Cycle time for this operation is 1 millisecond for position and amplitude information and an average of 2 milliseconds for phase information.

Each position encoder has two outputs in a quadrature time relationship. Hence, distance information as well as directional information is obtained. The encoders are geared so that the encoder shaft rotates once for every 5.0 inches moved. The output of the encoders is 1000 pulses for every shaft revolution. Thus there is one encoder pulse for each 0.05 inch moved. The interface contains counters which are controlled by the encoders. The output of

the counters thus represents the absolute position of the probe in digital form.

The amplitude channel output of the phase-amplitude receiver-amplitude modulates a 1000 Hz sine wave. The output of the receiver goes directly into the interface where it is amplified and detected. Finally, the output of the detector is converted to a 12-bit digital word. This number bears a linear relationship to the output of the receiver. Considering system noise and overall equipment stability, a useful dynamic range of 55 dB is obtained.

The phase channel of the computer interface makes use of the digital phase information output from the receiver to obtain resolution of 0.1 degree. The phase-amplitude receiver provides a free-running clock output with a frequency of 1.0 MHz. A counter in the phase channel of the interface counts the number of clock pulses between start and stop signals from the receiver. The contents of the counter at the stop signal bears a direct relationship to the relative phase of the signals received by the receiver. A phase difference of -180.0 degrees corresponds to zero counts in the interface counter, and +179.9 degrees corresponds to 3599 counts. Since the phase-amplitude receiver provides the digital phase information, the phase information at the output of the interface is as accurate as the phase information at the input.

Data is taken row-by-row since a more consistant probe speed is possible in the X axis. At the end of each row the operator moves the probe to the proper position in the Y axis (with the aid of read-outs from the interface) and begins scanning another row. As the probe is moved in the X axis the computer continuously checks the

position and determines when a data point is reached. At each data point amplitude, phase, and X and Y position information are stored in a buffer in memory. When the buffer is full it is copied onto tape automatically. The average time per complete near-field scan is 3 hours. Each scan consists of 128 rows with 128 data points per row.

The test antenna is used as a transmitting antenna and is mounted on a Scientific-Atlanta Z-motion Unit. The XY position of the test antenna is fixed by its mounting structure; however, its Z-position may be varied by the Control and Position Indicator Unit. The test antenna is connected to a 2K43 klystron, operating at 5.45 GHz, by a stationary RG-212URF cable. The klystron is powered by a Narda Microwave Corporation Model 438 Klystron Power Supply. The output of the klystron is phase locked to a crystal frequency reference with a FEL Model 133-AK Klystron Synchronizer, and its power output is continuously monitored with a Hewlett-Packard Model 431 Power Meter to insure constant output energy. The frequency of the klystron is initially set and periodically checked with a Hewlett-Packard J532A Frequency Meter connected in series with the power meter.

The XY-motion unit, the Z-motion unit, the rotary probe holder, and three of the four walls surrounding the XY-motion unit are covered with B. F. Goodrich VHP-8 microwave absorbing material with a normal incident minimum absorption of 45 dB at C-band. The receiver, XYZ-motion Control and Position Indicator Unit, the digital interfacing unit, the klystron, klystron power supply, synchronizer, frequency meter, and power meter are located behind a 4 foot wall of

absorbing material away from the measurement area.

6.2 Electrical Accuracy

The receiver, the digital interfacing unit, the rotary joints, the klystron, stray radiation and mechanical alignment inaccuracy each contribute to amplitude and phase measurement inaccuracy.

The amplitude and phase accuracy of the receiver was measured using precision attenuators and phase shifters. The results of these tests demonstrated that the receiver inaccuracy was a composite of many types of inaccuracies. The principal types of errors were identified and are discussed below.

(1) Random Amplitude Error: This amplitude error varies randomly with time. This error was estimated to vary uniformly between ± 0.05 dB.

(2) Linear Amplitude Error: This amplitude error varies linearly with the amplitude level being measured with the error increasing from zero dB at level of zero dB to -0.1 dB at -40 dB.

(3) Quadratic Amplitude Error: The amplitude error varies quadratically with the amplitude level (in dB) being measured, with the error increasing from zero dB at level of zero dB to -0.5 dB at -40 dB.

(4) Linear Amplitude Drift: This amplitude error varies linearly with measurement time with a starting value of zero and an ending value of 0.05 dB.

(5) Amplitude Truncation: This amplitude error is zero for all amplitude measurements above -55 dB. Below -55 dB all amplitude measurements are recorded as -55 dB.

(6) Random Phase Error: This phase error varies randomly with time. This error was estimated to vary uniformly between $\pm$1.0 degrees.

(7) Linear Phase Error: This phase is linearly proportional to the phase being measured. The error is zero at zero degrees phase and increases to a maximum of $\pm$.1 degree at $\pm$180 degrees, respectively.

(8) Quadratic Phase Error: This phase error is quadratically porportional to the phase being measured. The error is zero at zero degrees phase and increases to 0.2 degrees at $\pm$180 degrees.

(9) Total Phase Drift: This phase error varies linearly with time with a starting value of zero and a final value of 5.0 degrees.

(10) Quadratic Phase/Amplitude Error: This phase error varies quadratically with amplitude. This error is zero at zero dB and increases to 4.0 degrees at -40 dB.

The digital interfacing unit has an amplitude truncation level of approximately -55 dB and a zero phase error as explained previously.

The amplitude and phase variation of each of the four rotary joints in the system were measured with the receiver and found to have a maximum of 0.05 dB amplitude variation and a maximum of 0.2 degrees phase variation at the operating frequency.

The klystron was continuously monitored in amplitude and found not to vary more than 0.1 dB during the measurement. The klystron synchronizer is specified to maintain a frequency stability of one part in 10^6 for long term operation. To analyze the effect of a

small frequency change on the relative phase difference between the received signal and the reference signal, the two electrical path lengths are calculated in wavelengths. The difference between the direct reference path from source to receiver and the path from source to transmitting antenna to receiving antenna to receiver is approximately 700 wavelengths. An increase or decrease in frequency of one part in 10^6 produces a corresponding decrease or increase in the number of wavelengths of one part in 10^6, yielding a change of phase of $\pm 700 \times 10^{-6} \times 360 \approx \pm 0.25$ degree. This phase drift is approximately linear with time for short time durations.

Stray radiation is substantially reduced through application of absorbing material and use of absorbing rings on the near-field probes. Absorbing material is used to cover all reflecting objects in the measurement area. Remaining reflectors are tested to determine if they are contributing stray radiation at the receiving antenna by means of the following absorption test: A set of measurements is taken for various positions of the receiving and transmitting antennas; the suspected reflector is covered with absorbing material and the measurements repeated. Any difference in the measurements indicate absorbing material is required to cover the reflector. It is estimated that the stray radiation level is equal to or below the reflection coefficient of the absorbing material, which is -45 dB.

The mechanical alignment accuracy of ± 0.005 inch for each of the three spectral coordinates produces a maximum radial position error of ± 0.0087 inch. At a frequency of 5.45 GHz this positional error produces a maximum phase error of ± 1.45 degrees.

Considering the above sources and the magnitude of amplitude and phase measurement errors, a composite error table was formed and is given in Table 3-3.

6.3 Mechanical Alignment Accuracy

A precision bubble level is used to align the Z-axis of the Z-motion unit and the X-direction traverse bar of the XY-motion unit parallel to the earth with an accuracy of five arc-minutes. A precision clinometer is used to align the Y-direction traverse bars of the XY-motion unit perpendicular to the earth with an accuracy of 30 arc-seconds. A transit and a precision square are used to set the Z-axis of the Z-motion unit perpendicular to the X-axis of the XY-motion unit with an accuracy of five arc-minutes.

The Z-position of the near-field probe holder as it traverses the XY plane is aligned and deviations from a true plane measured using the following procedure. An optical target is mounted on the side of the rotary probe holder and a precision transit is aligned in an XY-plane of the XY-motion unit such that the optical target appears at the same point in the transit sight at each end of the Y-minimum, X-traverse of the rotary probe holder. With the transit level, an elevation sweep of the transit sight then forms an XY-plane perpendicular to the earth and contains the X-axis of the XY-motion unit. The XY-motion unit is further adjusted to make the optical target appear at the same point of the transit sight at three of the four corners of the 100 by 100 inch measurement area. Using the transit, the deviation of the probe location from a true plane is recorded throughout the measurement area at the intersections

of a square lattice, five inches in horizontal and vertical spacings, with an accuracy of five-thousandths of an inch. Figure 6-3 is a graph of the Z-position error of the rotary probe holder in thousandths of an inch. The maximum error is found to be 40-thousandths of an inch. The error graph is tabulated and used to correct probe position information as part of the far-field computation process.

The X and Y positions of the near-field probe are known to the accuracy of the optical position encoders, which is $\pm$.005 inch. With the measured Z-position error data known, the Z-position of the near-field probe is specified as a function of the X and Y position and is also accurate to within $\pm$.005 inch.

The alignment of the measurement plane of the antenna is shown in Figure 4-3. Any misalignment between these planes translates to boresight error in the far-field. The alignment procedure is outlined again here. An eight-inch square mirror was rigidly attached to a one-inch thick aluminum plate approximately one foot square. The mirror and plate were attached to the frame of the test antenna using four adjustable rods. With the antenna mounted on the Z-position unit in front of the near-field probe, the plane of the mirror was aligned with the plane of the probe by adjusting the four mounting rods. A feeler gauge was attached to the near-field probe and used in the alignment procedure. The total variation in or out of the measurement plane was measured by moving the feeler gauge around the four corners of the mirror, and was within 0.0025 inches. This corresponds to a potential angular error in the far-field of $\pm$0.32 milliradian ($\approx \pm$0.02 degrees).

The near-field probe is centered to an accuracy of two-thousandths

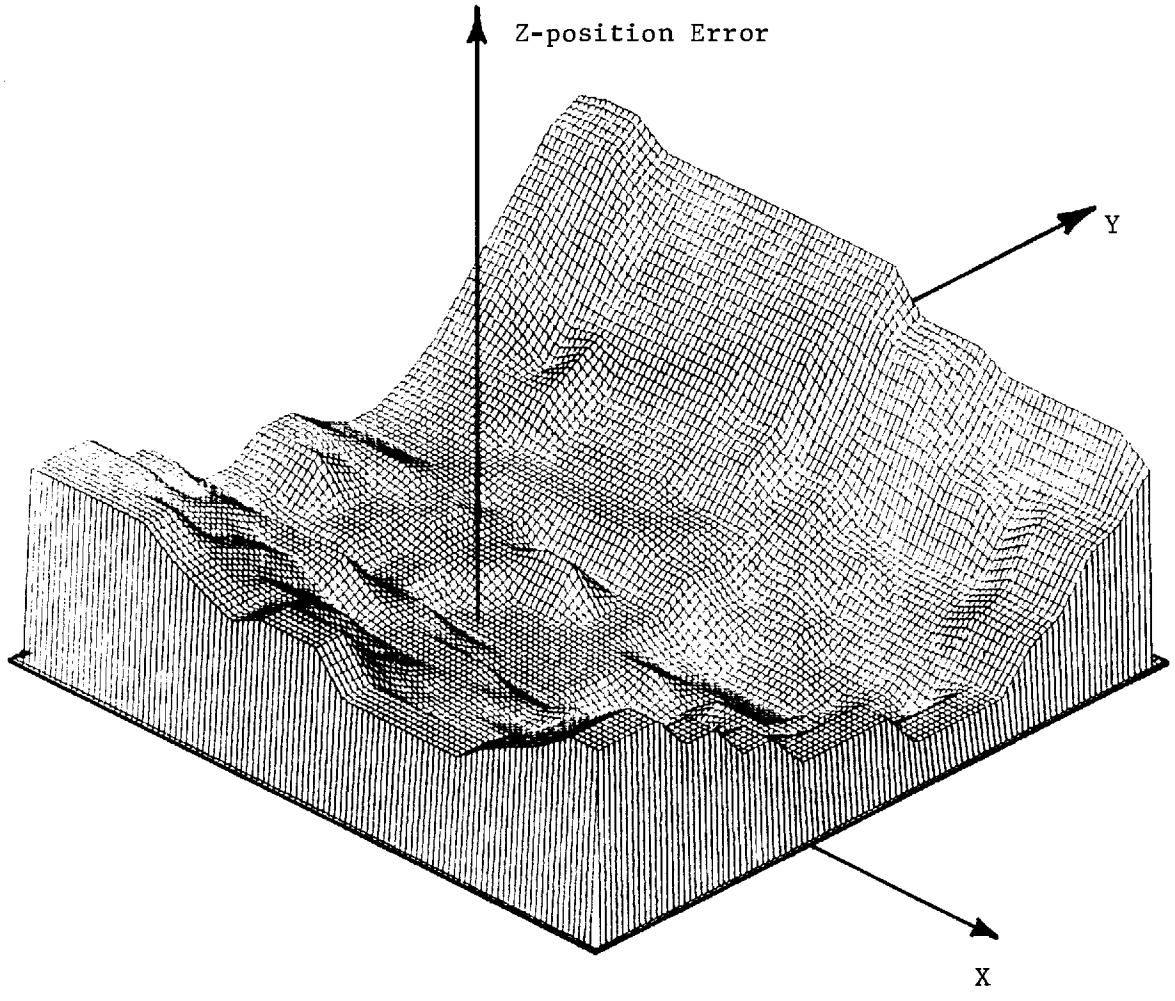

Figure 6-3. Z-position error of the near-field measurement plane.

of an inch in the rotary probe holder using a dial guage. The probe holder is leveled with a small bubble level to an accuracy of five arc-minutes.

The rotary position of the near-field probe is aligned using a mirror. A leveled theodolite image is seen. In this way the rotary position of the probe could be set with excellent accuracy. Since the probe must be rotated 90 degrees for cross polarization measurements, a 45 degree prism with a reflective coating was placed on the probe and probe rotated 90 degrees until the theodolite image could be seen. The accuracy of these theodolite measurements using the mirror and prism is dependent on the flatness of the mirrors, the parallelism of the mirror plane with the flat surface of the near-field probe, and the construction of the prism. Considering the above, it is estimated that the angular inaccuracies of the near-field probe are less than ± 1.0 milliradian ($\approx \pm 0.06$ degree).

6.4 Procedures

Prior to performing near-field measurements a computer program called NEAR V must be inputed into the near-field measurement minicomputer, and data specifying sample spacings and the location of the near-field measurement origin must be read into the computer. Also, the mechanical alignment of the near-field measurement system must be accomplished as described previously (Section 4.2). Two measurements of the near-field are required, one for each of two orientations of the near-field probe. The two orientations normally used differ by a 90 degree rotation of the probe about its Z-axis. (See Figure 6-3.)

Before taking data the probe is moved to the point to be called the origin, and the position counters are reset. The origin, the lower-left hand corner of the positioner when viewed from the antenna, is the starting point for a scan. The only calibration required is that of the amplitude channel in the interface. This involved slightly adjusting the gain and bias of the input to the analog-to-digital converter in the interface. Normally, setup time is negligible. With the aid of the mini-computer the near field of the test antenna is sampled in amplitude and phase while the near-field probe is continuously moved in the X direction. At the end of each X transverse the probe is positioned to a new Y-position and another X transverse is made only this time in the negative X direction. This scanning process is continued until data from all pre-determined sampling locations has been obtained. Next, the probe is returned to the origin, and the amplitude and phase of this point is remeasured to check for drift of the amplitude and phase. The amplitude and phase are adjusted to be equal to the first measurement, and the probe is rotated 90 degrees to begin the second measurement. The same scanning procedure is performed and data recorded for the second measurement.

The computer tape generated by the mini-computer, referred to as the "raw data tape" is taken to the Georgia Tech Univac 1108 computer for processing. The processing by the Univac may be broken down into three separate programs called SNDATA, LOOK, and MAIN.

SNDATA reads the raw data tape, converts the phase and amplitude data into complex components, and records them onto another tape referred to as the "processed data tape." The position information

is not recorded on the processed tape, since its function is to positively identify points on the raw data tape which may not be in a standard format. Optionally SNDATA produces a printout of each data point.

LOOK reads the processed data tape and produces information necessary to generate 3-dimensional plots of the near-field data. The plotting is done by a Calcomp plotter owned by the computer center at Georgia Tech.

MAIN reads the processed data tape and calculates the far-field antenna pattern.

MAIN also has as options printing out statistics about the far-field pattern, plotting 3-dimensional plots of the far-field pattern, and/or plotting conventional single slices of the far-field pattern. MAIN requires, in addition to the near-field data, the complex vector far-field pattern of the near-field probe and the Z-position error map data.

6.5 Near-field Amplitude and Phase Distributions

The measured near-field amplitude and phase distributions for the second feed are shown in Figures 6-4 through 6-7. The near-field amplitude and phase distributions for the sum pattern are shown in Figures 6-4 and 6-5 respectively. As expected, the amplitude distribution is relatively uniform in the center of the measurement area. The amplitude decreases to -40 dB near the edges of the measurement plane (92 inches square). The phase distribution is uniform over the central portion of the measurement plane, roughly corresponding to the outline of the dish. The amplitude distribution

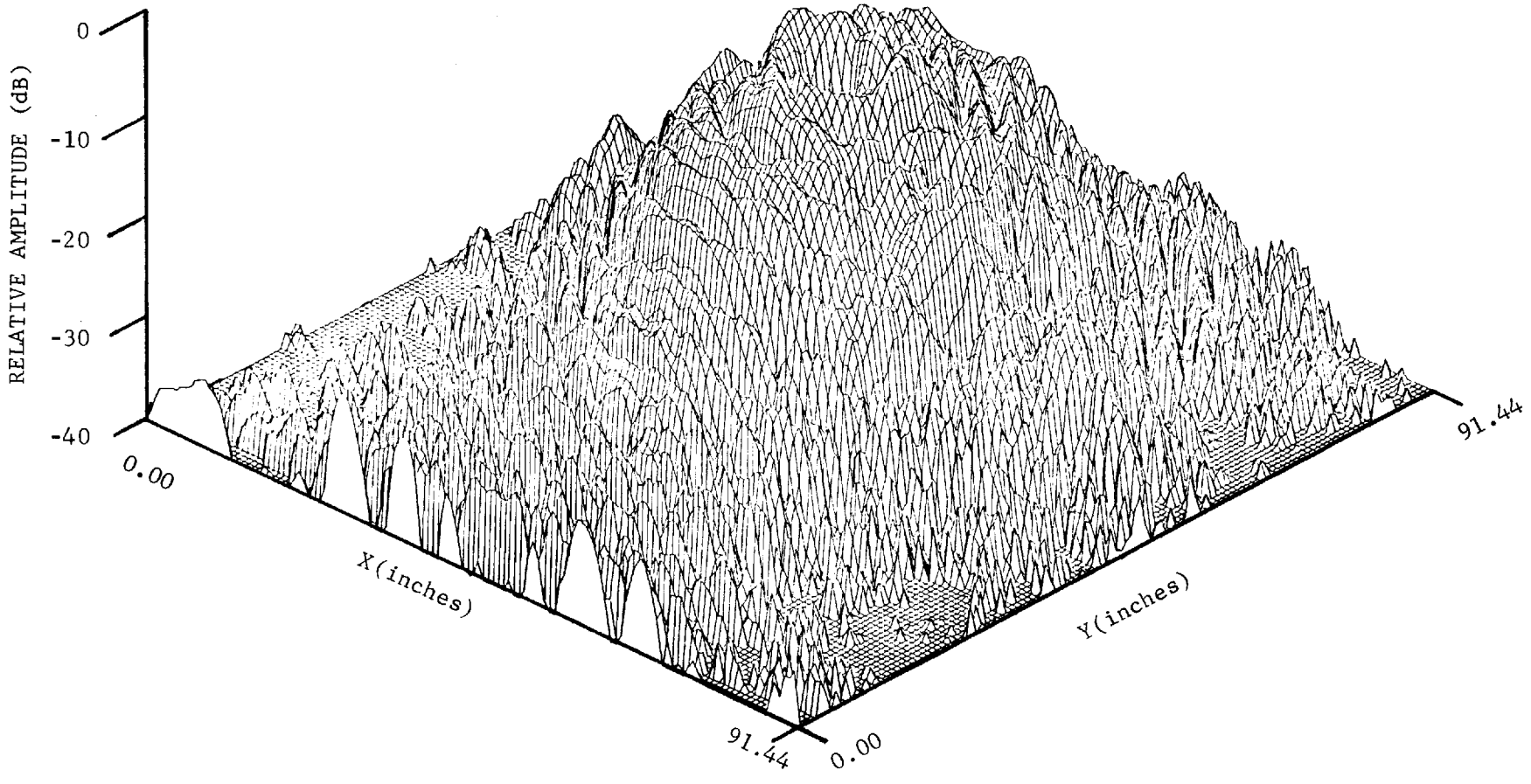

Figure 6-4. Relative amplitude of parallel component of near field of test antenna in sum mode.

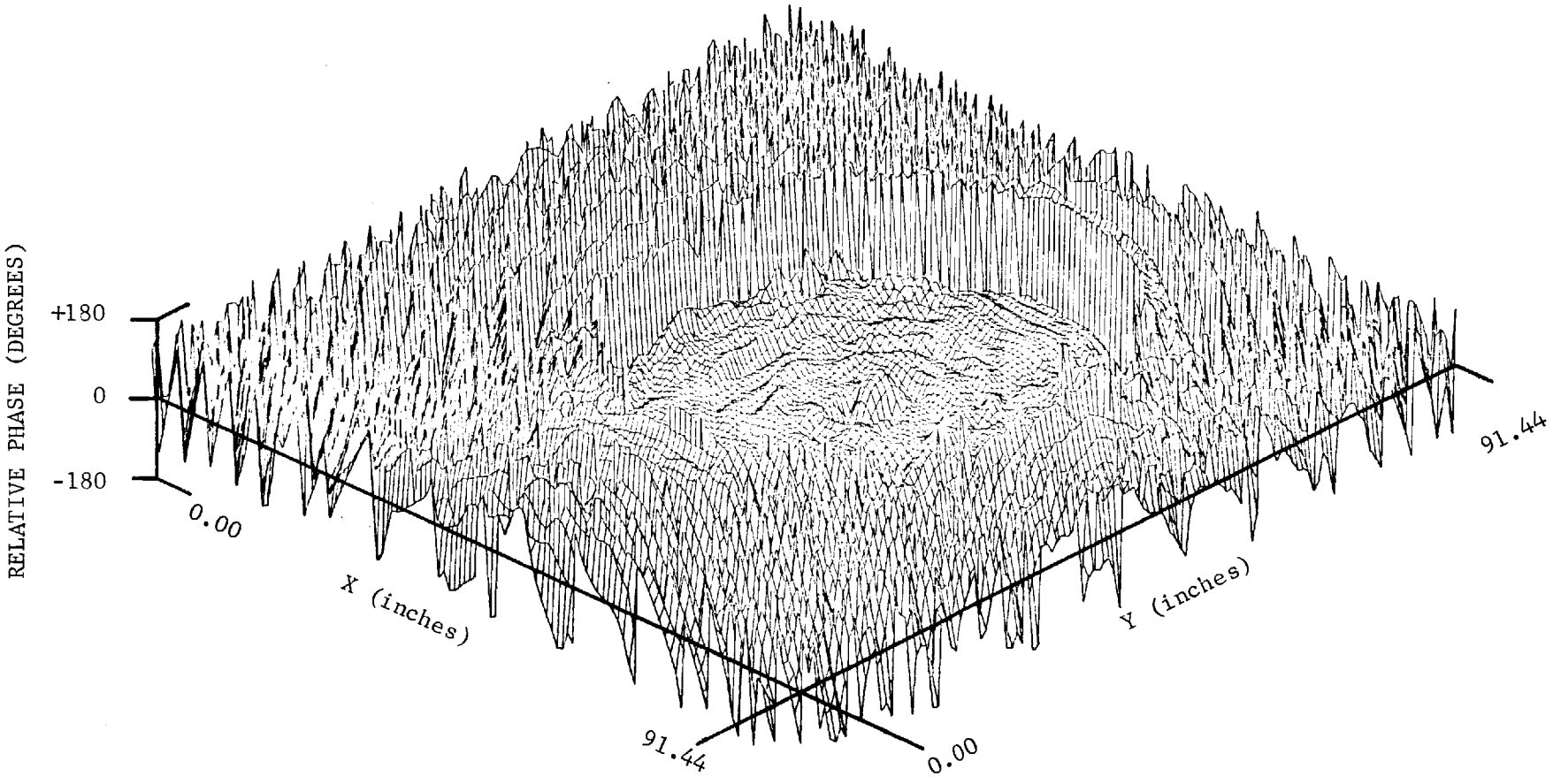

Figure 6-5. Relative phase of parallel component of near field of test antenna in sum mode.

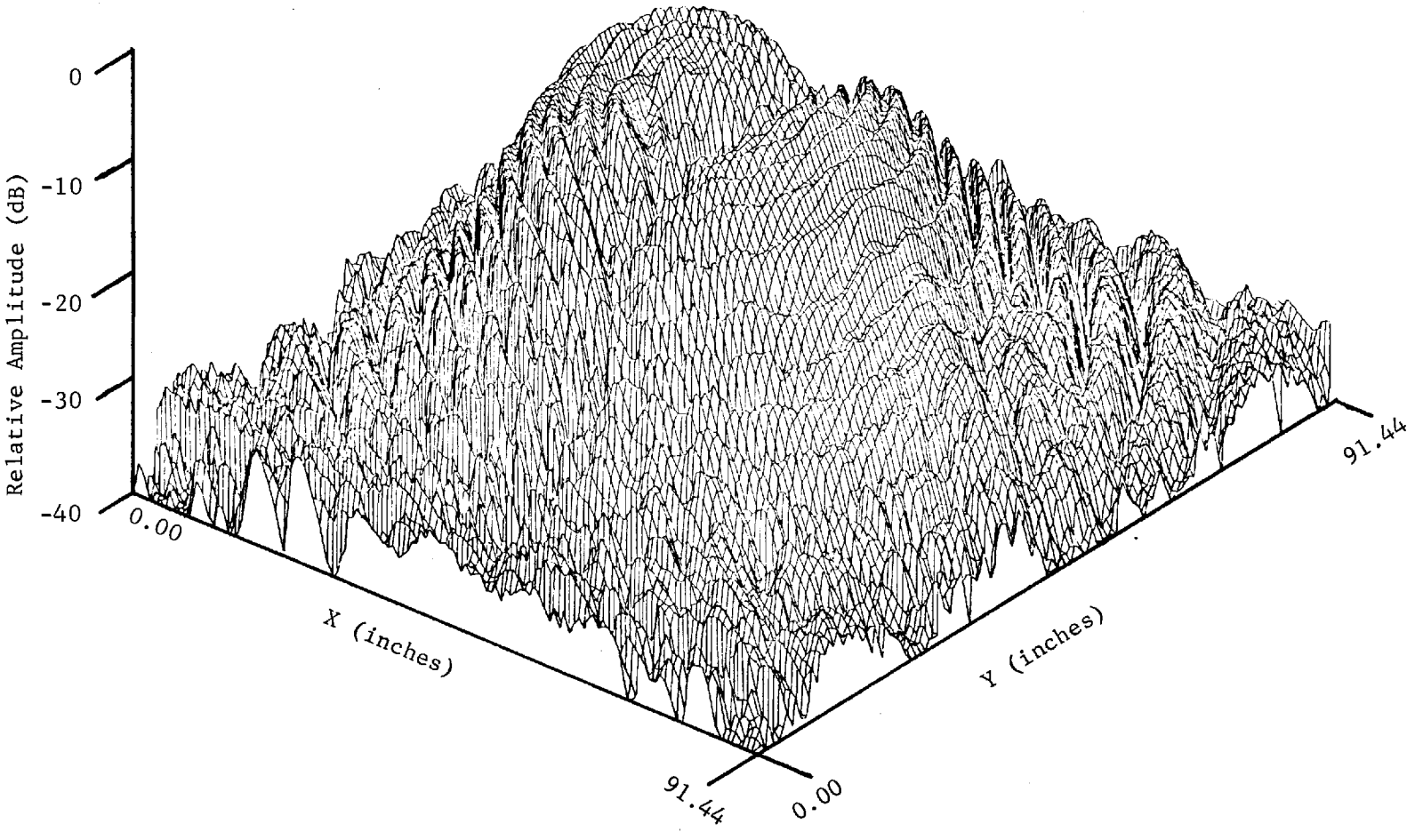

Figure 6-6. Relative amplitude of parallel component of near field of test antenna in difference mode.

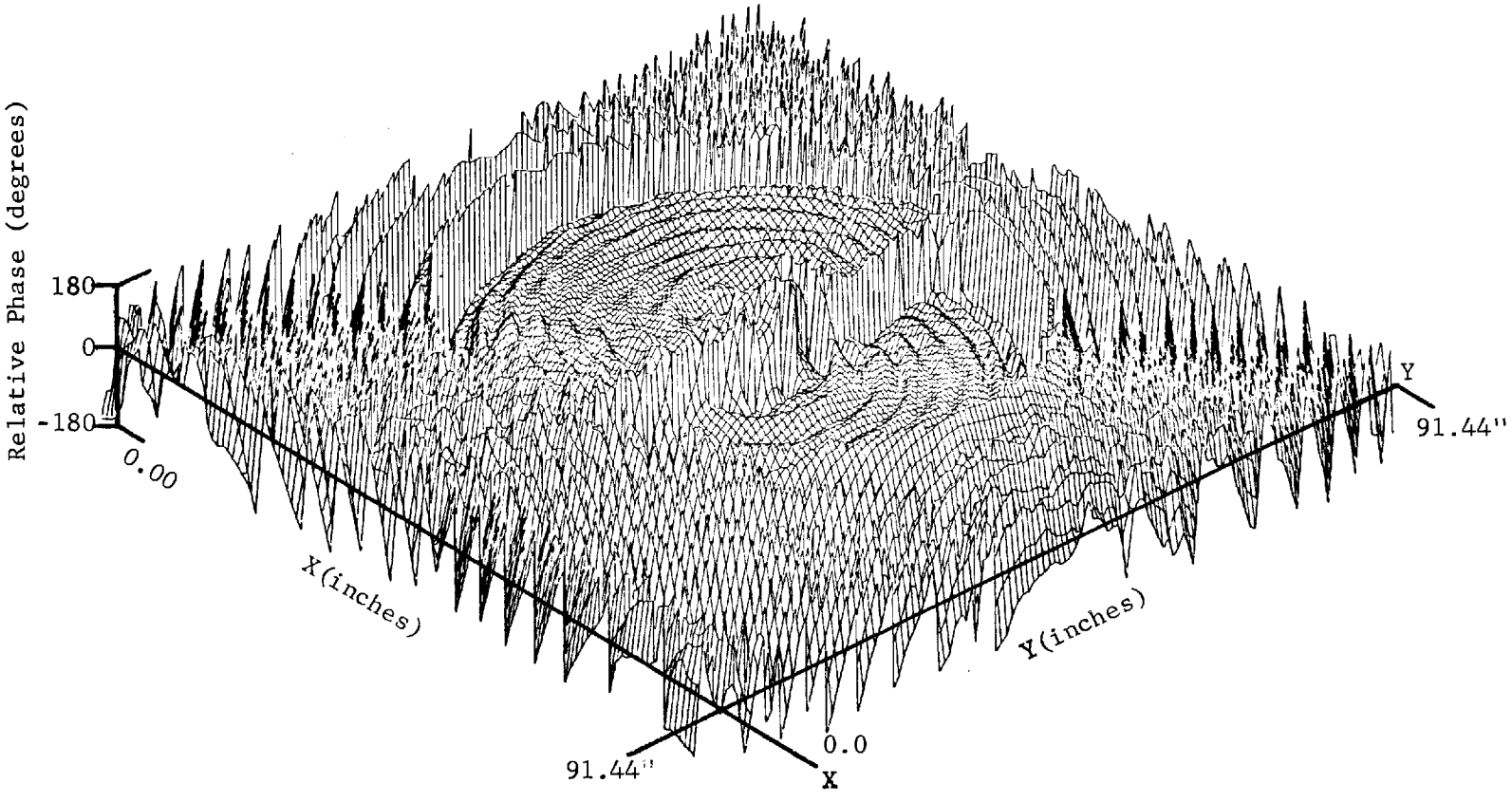

Figure 6-7. Relative phase of parallel component of near field of test antenna in difference mode.

for the difference pattern, shown in Figure 6-6, is similar to the sum pattern amplitude distribution, but the difference pattern phase distribution clearly shows the 180 degree discontinuity in the azimuth plane (Figure 6-7).

6.6 Far-field Patterns Predicted from Near-field Measurements

Far-field patterns predicted from near-field measurements are available in many formats and some sample results are included here. A typical 3-D plot in wave number space is shown in Figure 6-8.

Figures 6-8 through 6-11 show the capability of the far-field computation to depict wide angle information present in the far-field power pattern of a test antenna. The wide angle capability is important in determining the presence of wide angle high level sidelobes in both the parallel and cross components. High level cross polarized sidelobes are particularly difficult to spot on conventional far-field ranges. This presentation also gives an impression of the overall merit of a test antenna in achieving design goals.

Figures 6-12 and 6-13 show respectively the sum and difference power patterns of the test antenna using high resolution for angles close to the main beam. Figures 6-14 and 6-15 show the same power patterns for still higher resolution computations. Higher resolution may in principle, be applied to any small angular sector of the far-field pattern.

Examples of far-field pattern cuts computed from near-field data are shown in Figures 6-16 through 6-19. These principal azimuth plane cuts of the difference pattern demonstrate the use of filtering

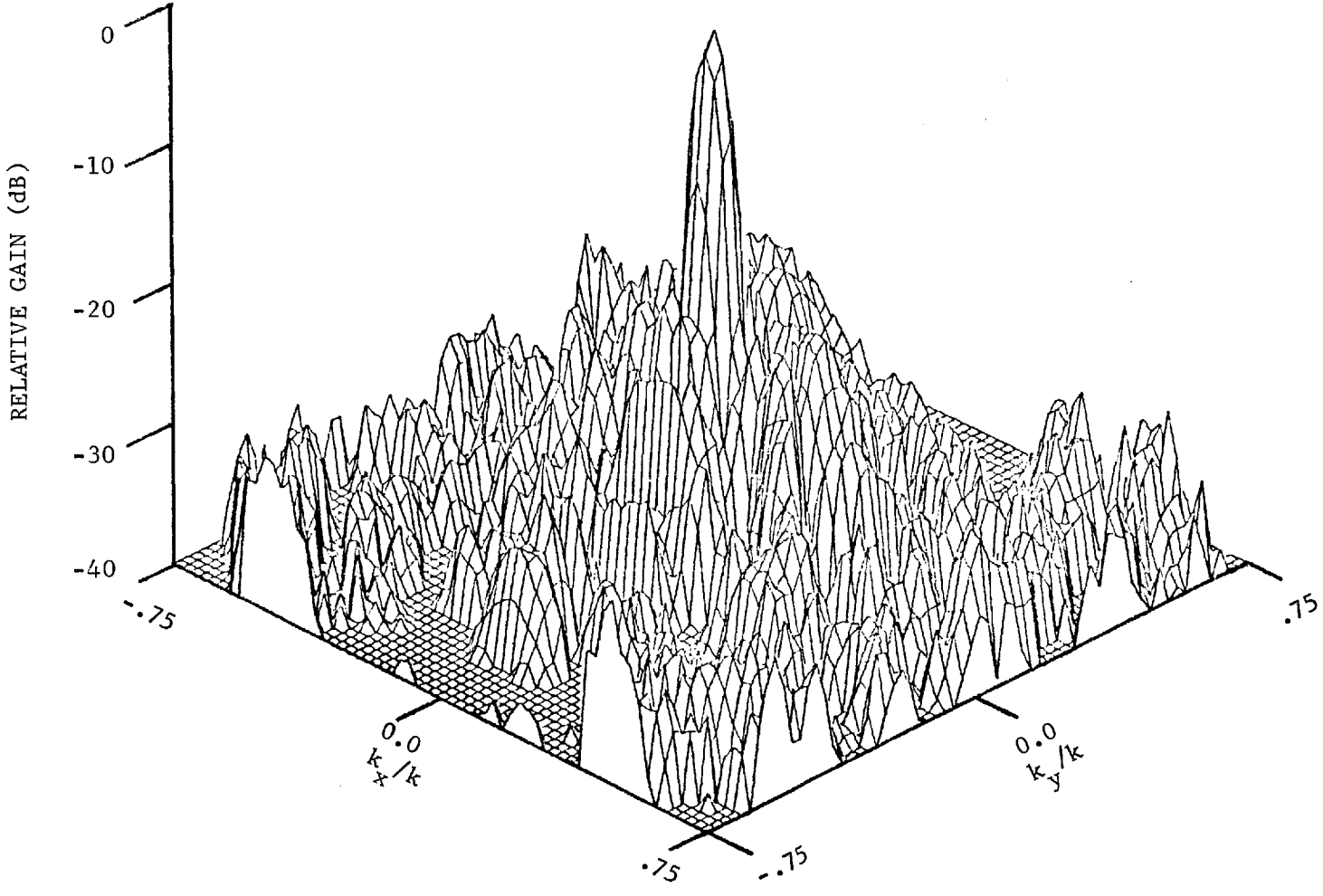

Figure 6-8. Far-field power pattern of parallel component of test antenna in sum mode.

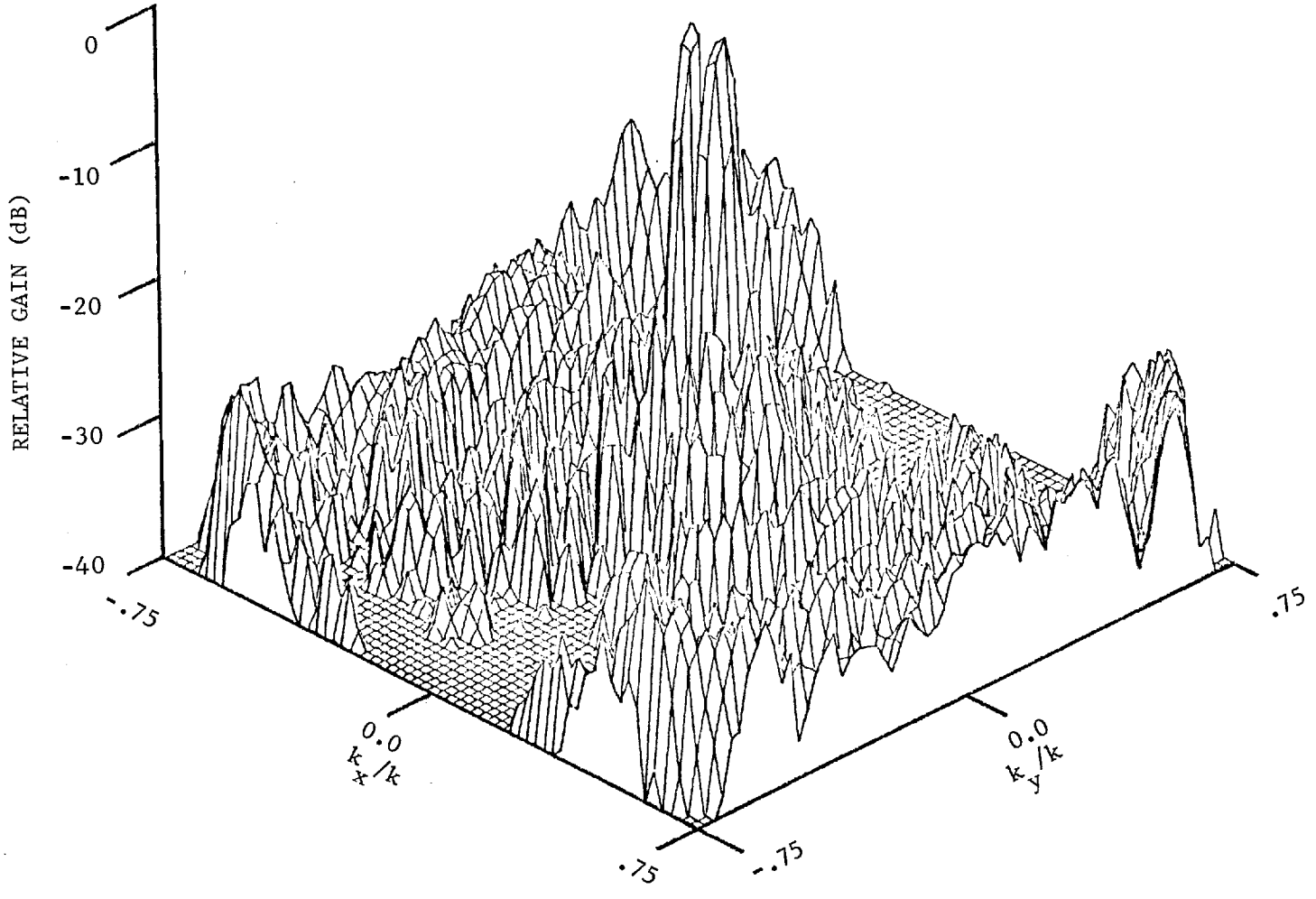

Figure 6-9. Far-field power pattern of parallel component of test antenna in difference mode.

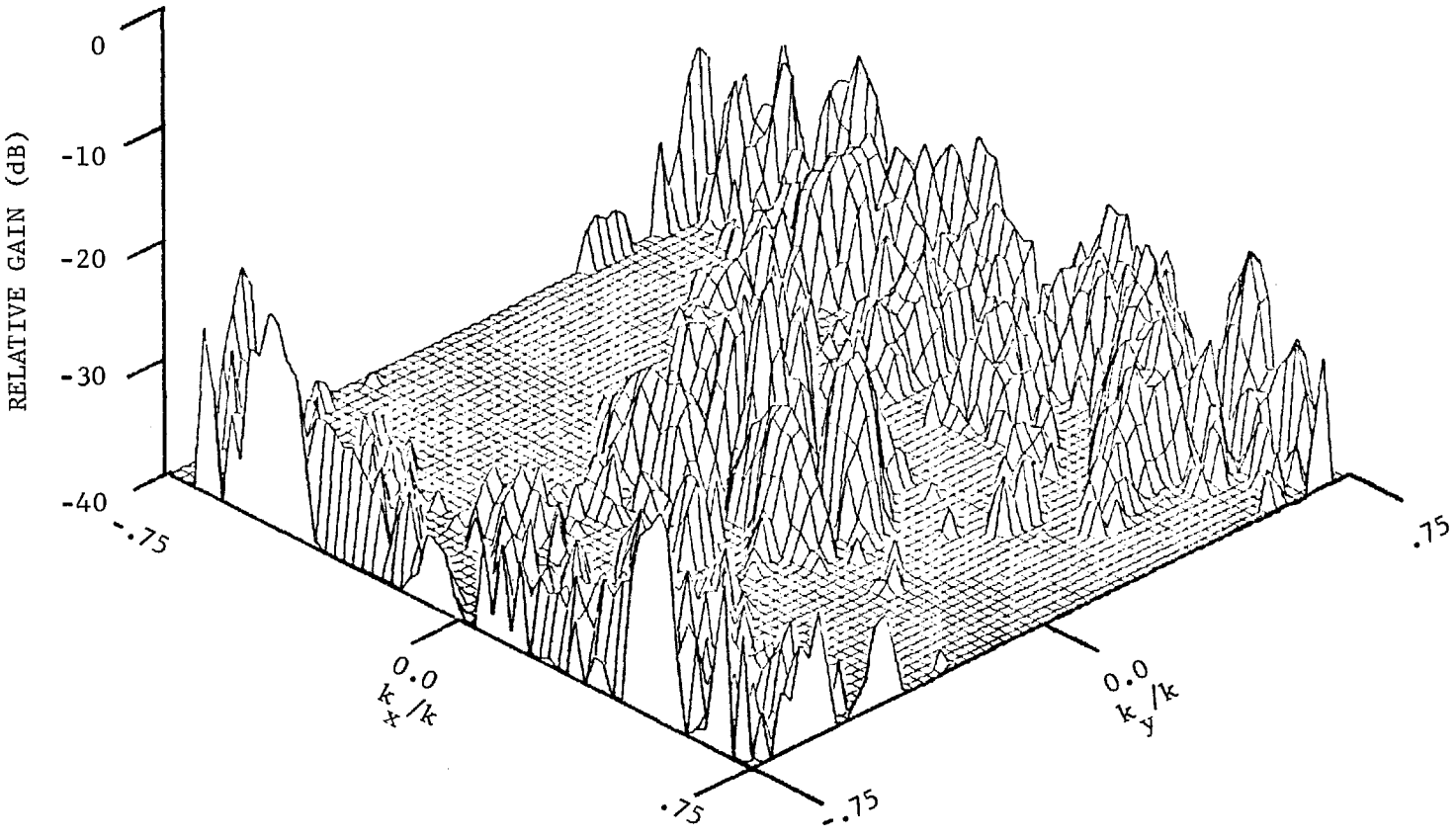

Figure 6-10. Far-field power pattern of cross component of test antenna in sum mode.

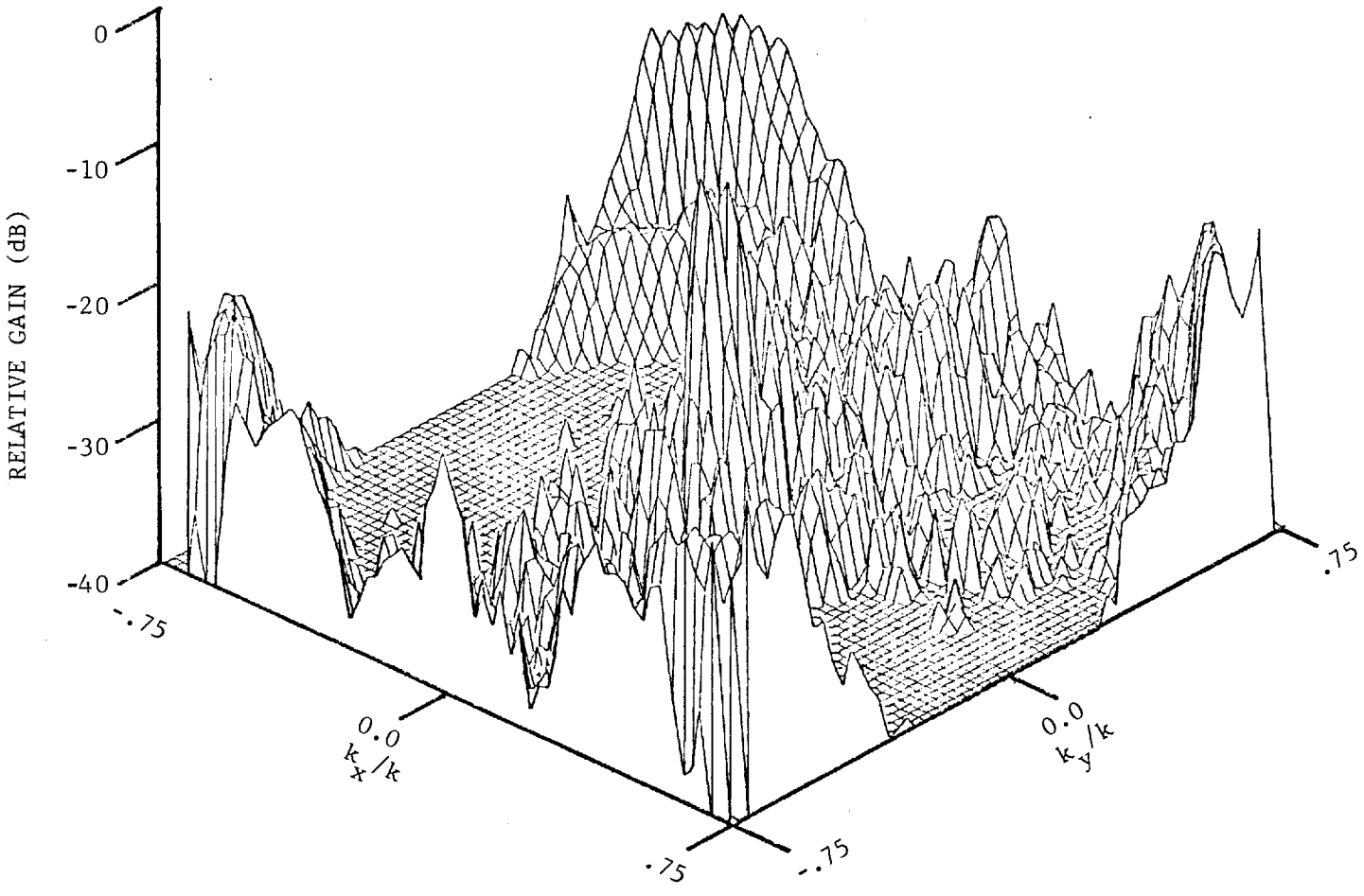

Figure 6-11. Far-field power pattern of cross component of test antenna in difference mode.

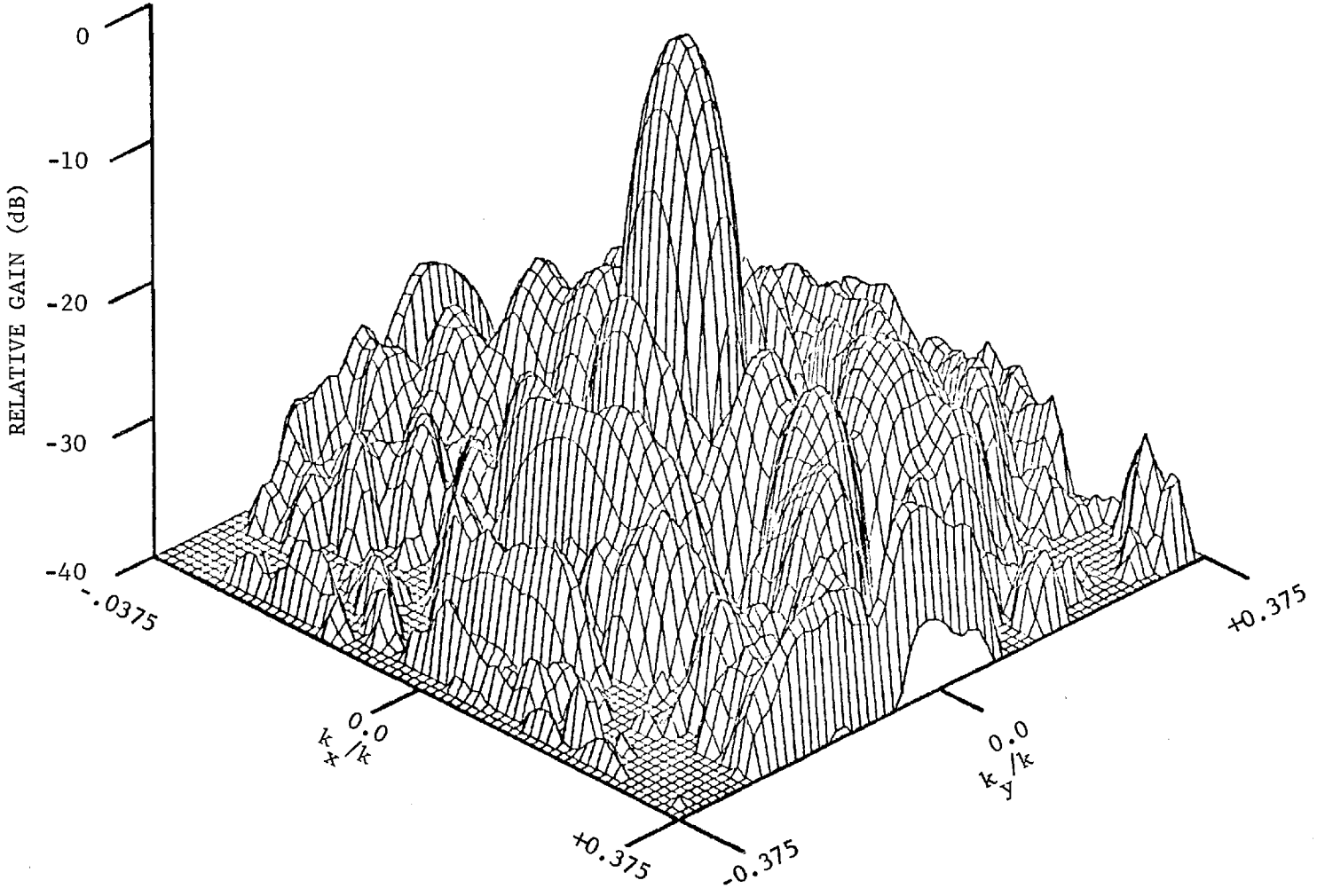

Figure 6-12. Far-field power pattern of parallel component of test antenna in sum mode with increased resolution.

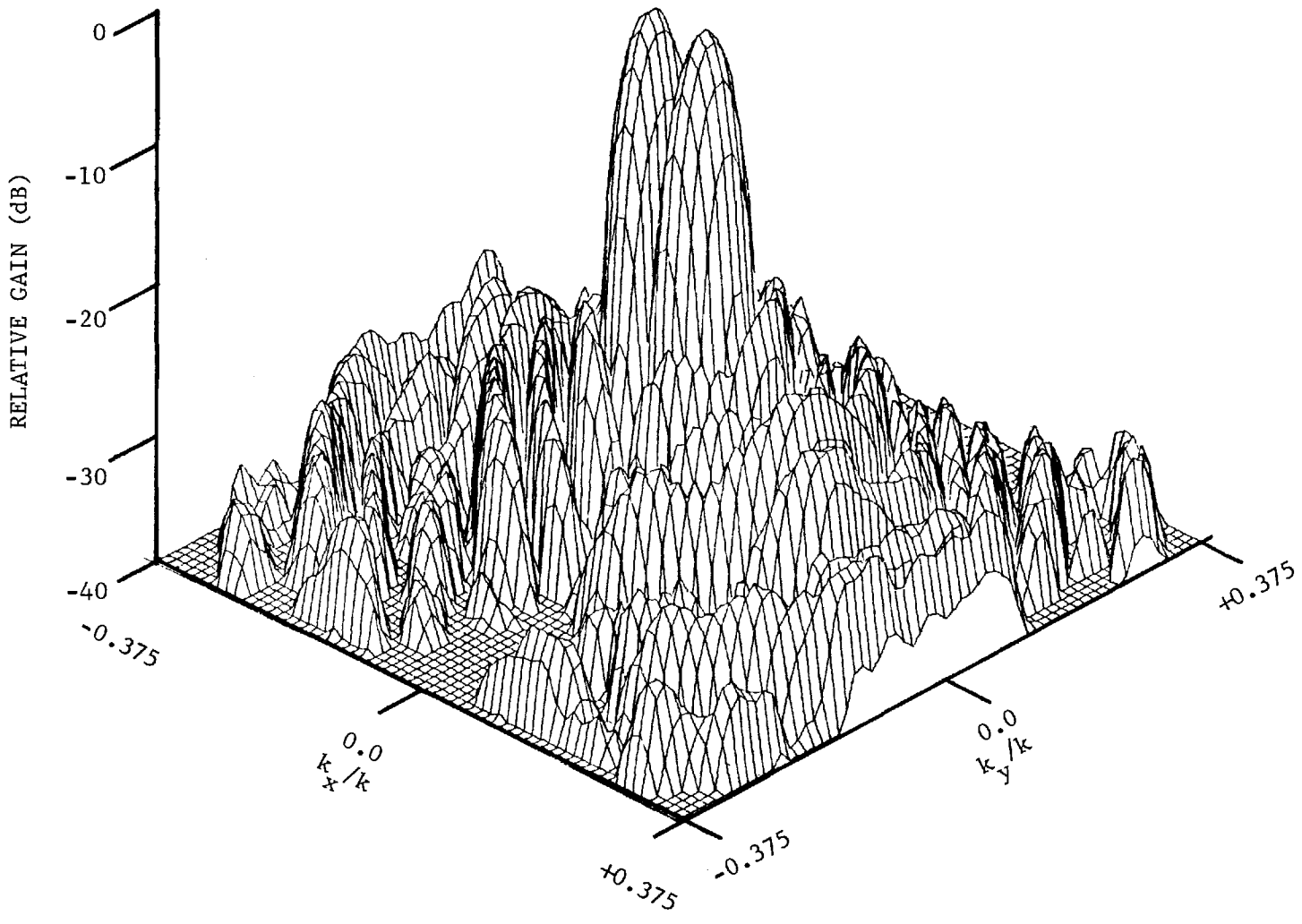

Figure 6-13. Far-field power pattern of parallel component of test antenna in difference mode with increased resolution.

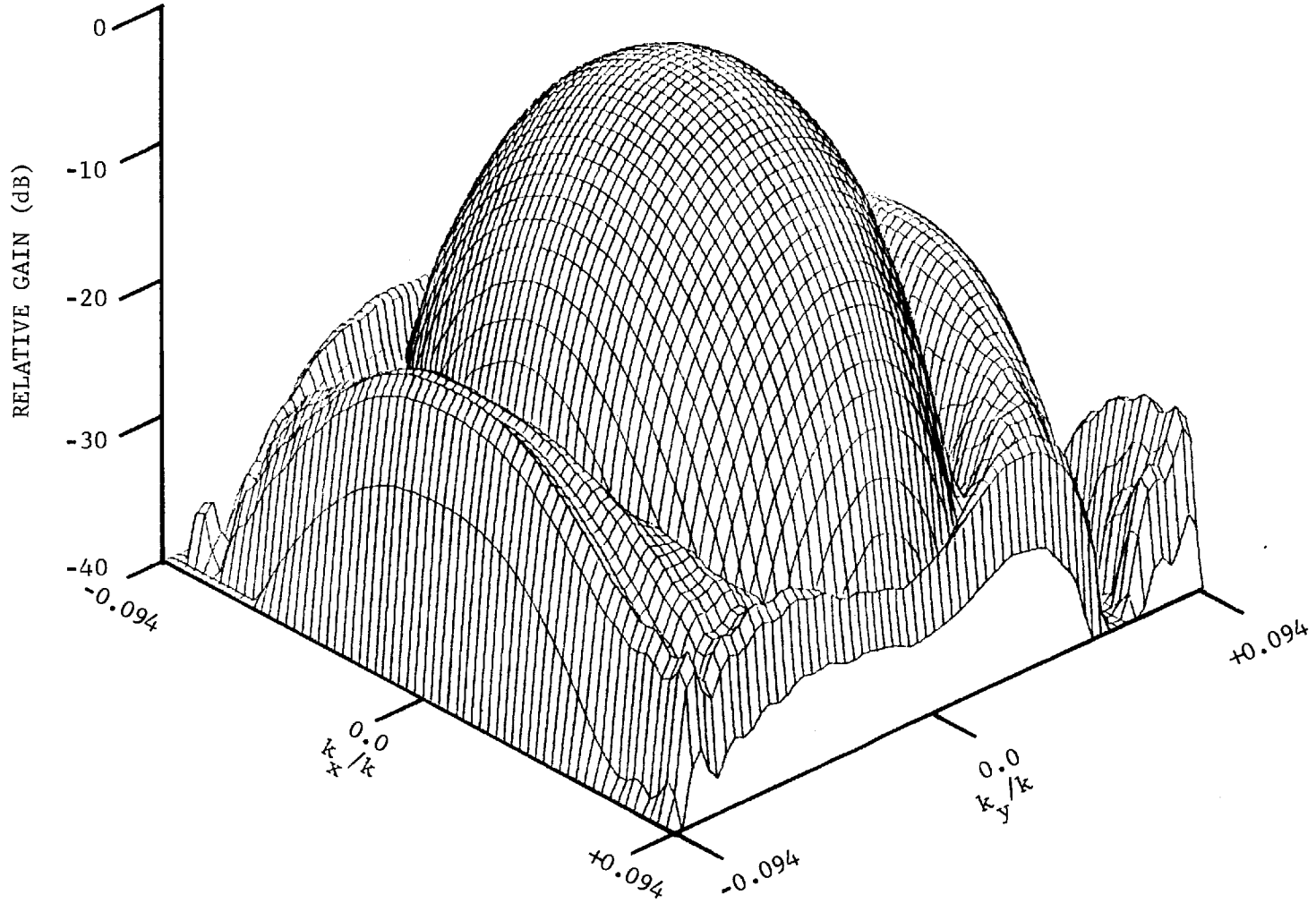

Figure 6-14. Far-field power pattern of parallel component of test antenna in sum mode showing details in vicinity of main lobe.

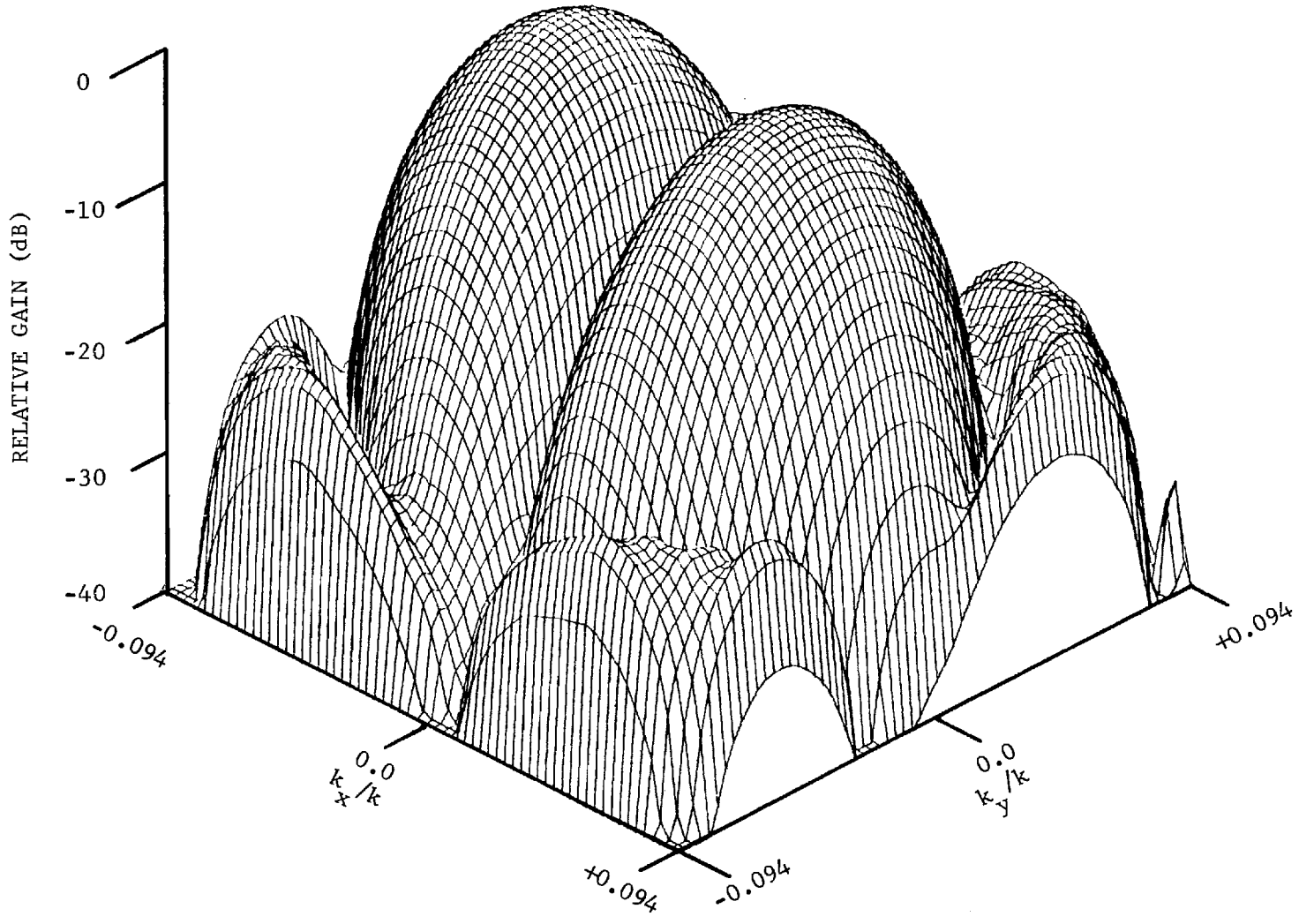

Figure 6-15. Far-field power pattern of parallel component of test antenna in difference mode showing details in vicinity of main lobes.

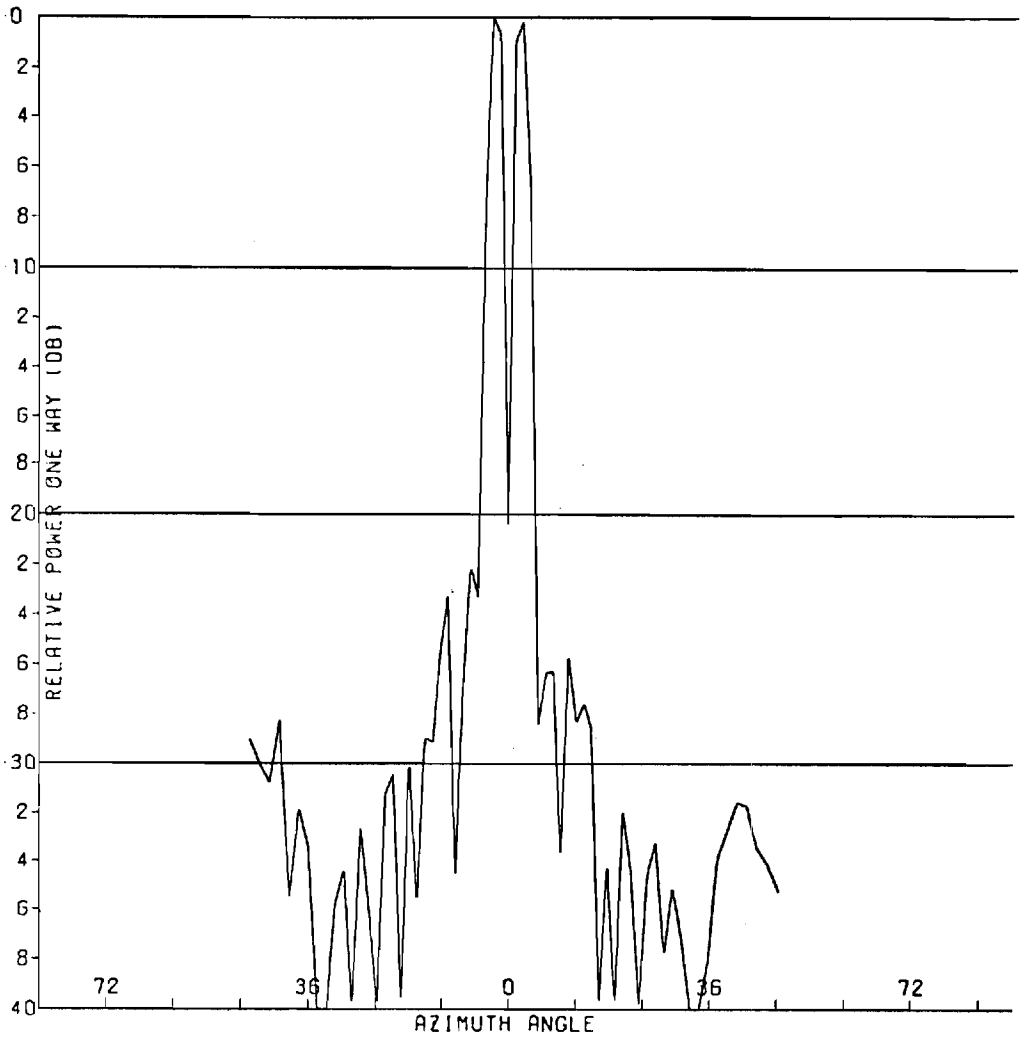

Figure 6-16. Far-field difference pattern predicted from near-field measurements for Feed 2 showing widest angular coverage and least resolution.

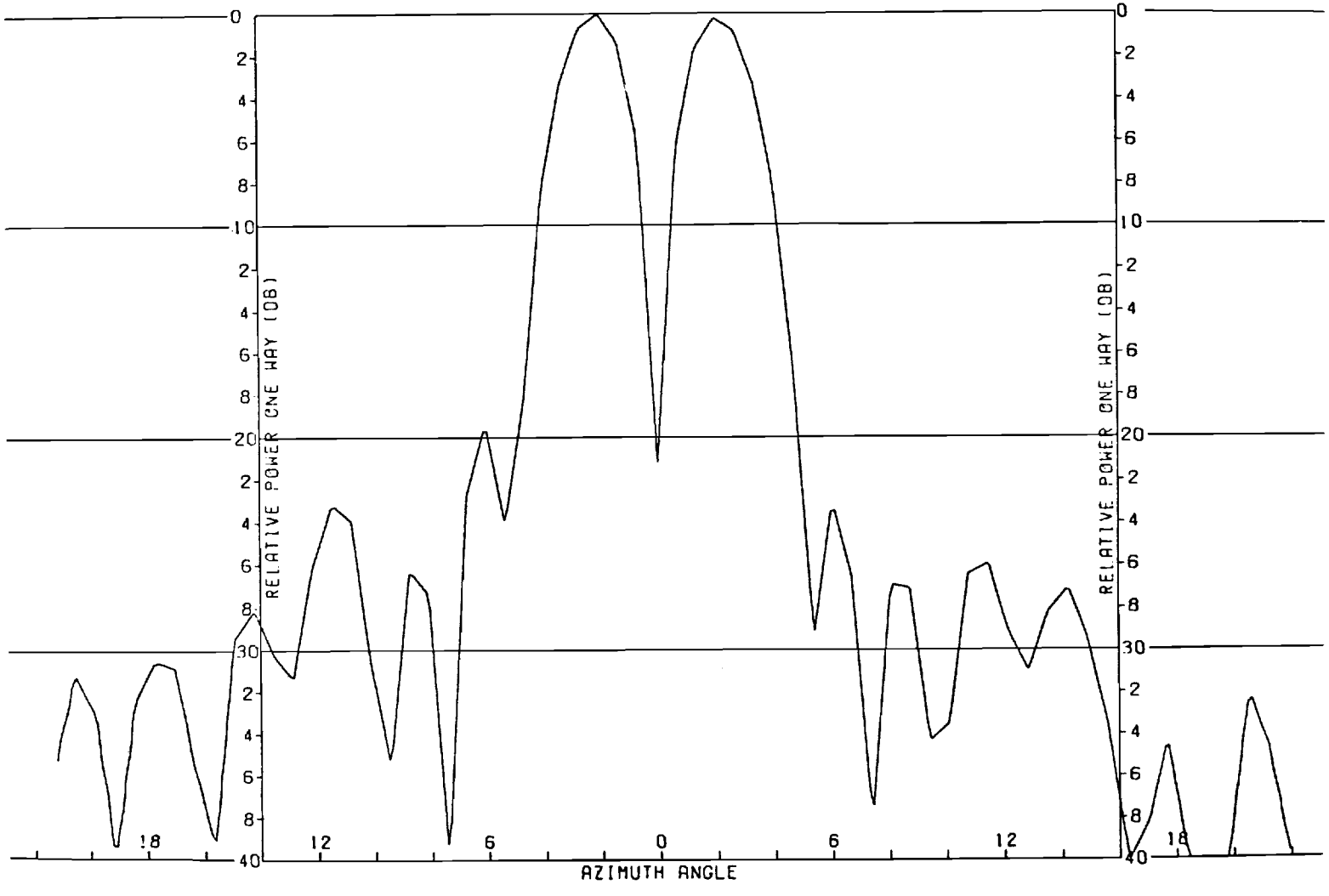

Figure 6-17. Far-field difference pattern predicted from near-field measurements for Feed 2 showing improved resolution by low-pass filtering.

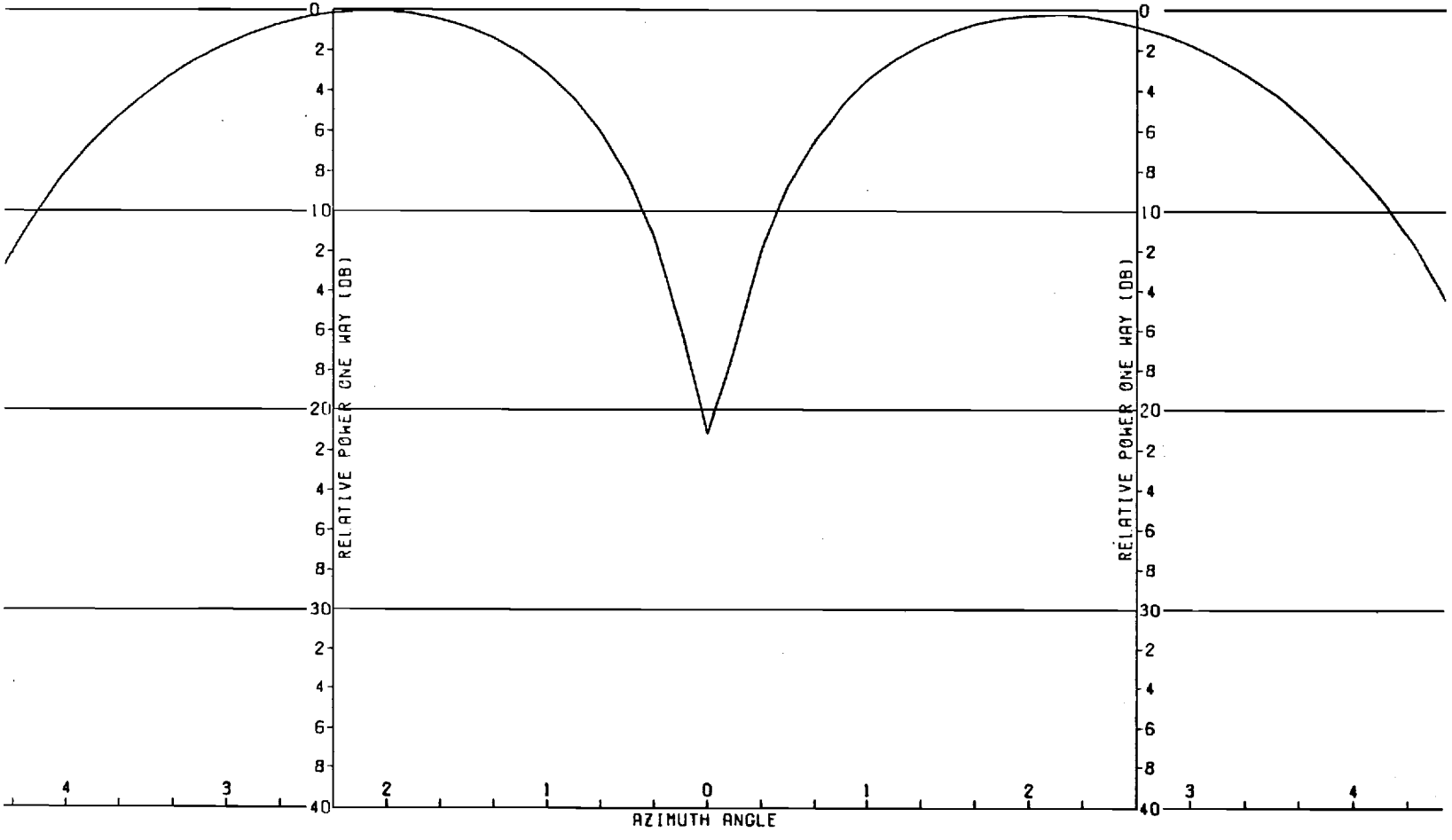

Figure 6-18. Far-field difference pattern predicted from near-field measurements for Feed 2 using three low-pass filter operations to improve resolution.

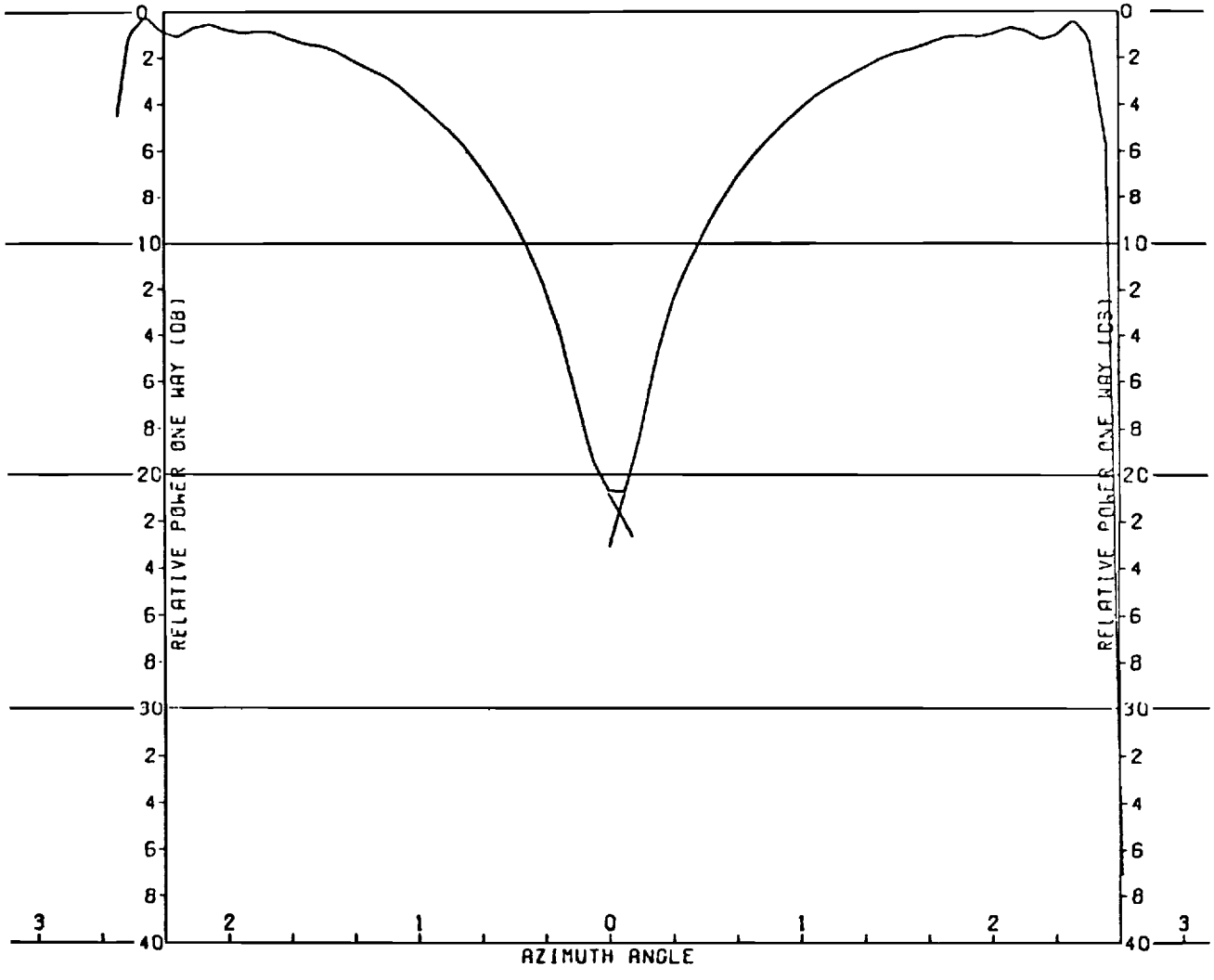

Figure 6-19. Far-field difference pattern predicted from near-field measurements for second feed using four-low pass filter operations to improve resolution.

to increase resolution while sacrificing angular coverage. Figure 6-16 covers azimuth angles of $\pm$ 48 degrees, and the point-to-point nature of the plot is quite evident. One filter stage (Figure 6-17) results in a reduction of angular coverage to $\pm$ 24 degrees with an accompanying improvement in resolution as the number of data points per angular width is doubled. In Figure 6-18 the angular width is only $\pm$ 4 degrees, and greater detail on the difference pattern null is obtained by three stages of filtering. Finally, in Figure 6-19 the results of four smoothing operations is shown. The angular width here is only $\pm$ 2.5 degrees. In this figure ripple distortion produced near band edges is noticeable. Some distortion always occurs near band edges so that the outermost five-to-ten percent of near-field curves is usually ignored. This ripple distortion increases with increasing numbers of filter stages.

It should be stressed that the various presentations, 3-dimensional patterns, different pattern cuts, or tabular formats, are all obtained from the single original set of near-field data. Only reprocessing of the data is used. The original near-field data contains all information about the complete pattern, and it is only necessary to modify the data processing to obtain different details of the far-field pattern. Computer times for these calculations are quite short, about 90 seconds including the generation of plotting tapes.

SECTION 7

COMPARISON OF FAR-FIELD PATTERNS OBTAINED FROM NEAR-FIELD MEASUREMENTS AND FROM FAR-FIELD MEASUREMENTS

The far-field patterns of the test antennas (Feed 1 and Feed 2) obtained on each of the far-field ranges and on the near-field range are compared in this section in various ways. Most comparisons are made on the basis of pattern cuts and in most cases the results are presented as graphs showing superposed curves. Data was taken on Feed 2 on the near-field range and on both the Georgia Tech and Scientific-Atlanta far-field ranges. For Feed 1 only the Georgia Tech near- and far-field ranges were used. Also on Feed 1 optical boresighting was not employed, and on the outdoor range only parallel polarization results are available. Feed 1 was primarily designed for a deep difference pattern null, and the ability of the near-field technique to track such a deep null was of principal interest. Because more thorough comparisons are possible with the data of Feed 2, they will be described first, and subsequently Feed 1 with its optimized difference pattern will be covered.

7.1 Comparisons of Feed 2 Patterns

In interpreting the results shown in this section (7.1) it should be noted that in this data all angular readings are derived from the optical boresighting and all gains referenced to the peak gain of the sum pattern of each range. No effort was made on this program to establish main beam gain accuracy from near-field data, and the expediency of referencing all plots to the peak of the main beam was followed. No other adjustments or fudge factors were employed.

Figure 7-1 shows some results of the three sets of measurements. The sum pattern, principal azimuth plane cut is shown here. The far-field data obtained on Scientific-Atlanta's Gwinnett County range is plotted as a solid line, that obtained on Georgia Tech's far-field range as a dashed line, and the data determined from near-field measurements is plotted as a short dashed line. It is noted that over the main lobe the agreement of all three techniques is exact, and, as in any instance where there is agreement, a single solid line is plotted. The Georgia Tech near- and far-field range data depart from the solid line only when some disagreement occurs. It is seen here that the near-field data agrees with the Scientific-Atlanta far-field range data to within the same accuracy as obtainable on the far-field ranges. The only exceptions to this occur at the first null to the left of the main beam, where the near-field data, plotted in a straight line from one point to the next, skips over this first null. This sort of error can be reduced by increased resolution. Other disagreements in the near-field data tend to occur at the edges of the band where the effects of the filtering process used lead to somewhat larger errors as the band limits are approached. This effect of filters can be improved with future development of a higher quality filter. With these two exceptions it is seen that the near-field data agrees with far-field data to within less than 1 dB at levels approximately 25 dB down and within 2 dB even on the sides of sidelobes. In fact, it appears that the near-field data obtained at Georgia Tech agrees with the far-field data obtained at Scientific-Atlanta to a higher degree of accuracy than does the other far-field measurements. This is notable on the right hand

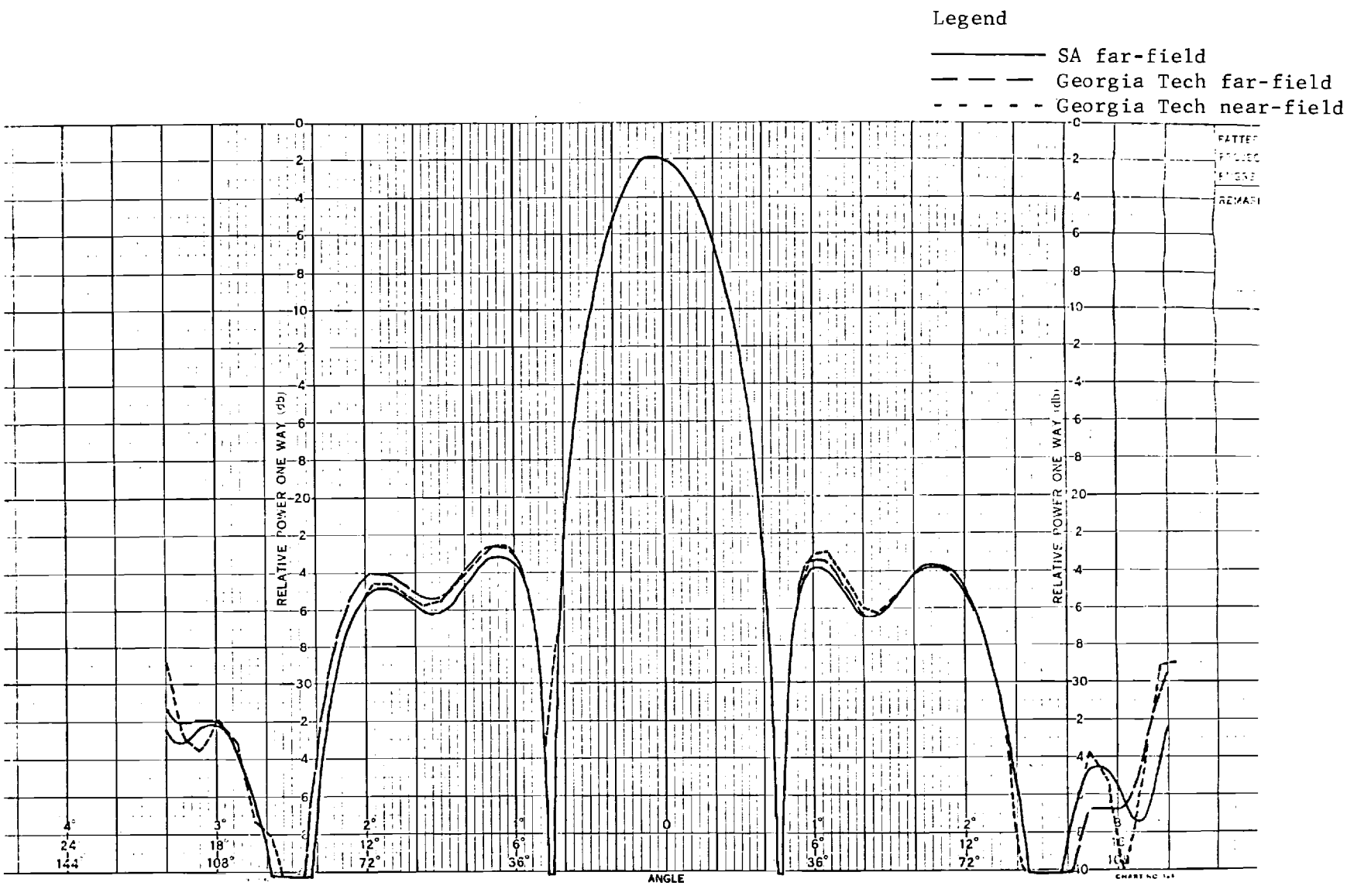

Figure 7-1. Comparison of sum pattern principal azimuth plane cuts for Feed 2 taken in three independent measurements.

side of this plot at an angle of approximately 18 degrees where range effects on the Georgia Tech far-field range distort the sidelobe occurring there.

Figure 7-2 is a principal elevation plane cut of the sum pattern where again the Scientific-Atlanta range is plotted as a solid line and the Georgia Tech data on near- and far-field ranges as the short and long dashes, respectively. Once again it is seen that the agreement among the measurements is very good with the exception of some sharp nulls occurring close to the main lobe where the near-field data jumps from one point to the next. This type of error could be considerably reduced if the number of data points plotted were doubled as can be accomplished with modification of the computer program. Far-field data to the right of the main beam suffers in accuracy because in that orientation the main beam points at ground reflections.

Figure 7-3 is a plot obtained on Scientific-Atlanta's range of the difference pattern measured as a function of azimuth angle over a range of approximately $\pm$ 24 degrees. This same data as derived from near-field measurements is shown in Figure 7-4. The point-to-point nature of the plot is again evident, and it is seen that for this difference pattern null (approximately 21 dB below the difference pattern maximum) the near-field data is able to track. Because the data points are connected on point-to-point basis, RMS sidelobe levels are somewhat lower than they would be if the points were connected by smooth curves. One form of comparison is shown in Figure 7-5, where the computed far-field points (as determined on the near-field range) are plotted as data points on the measured

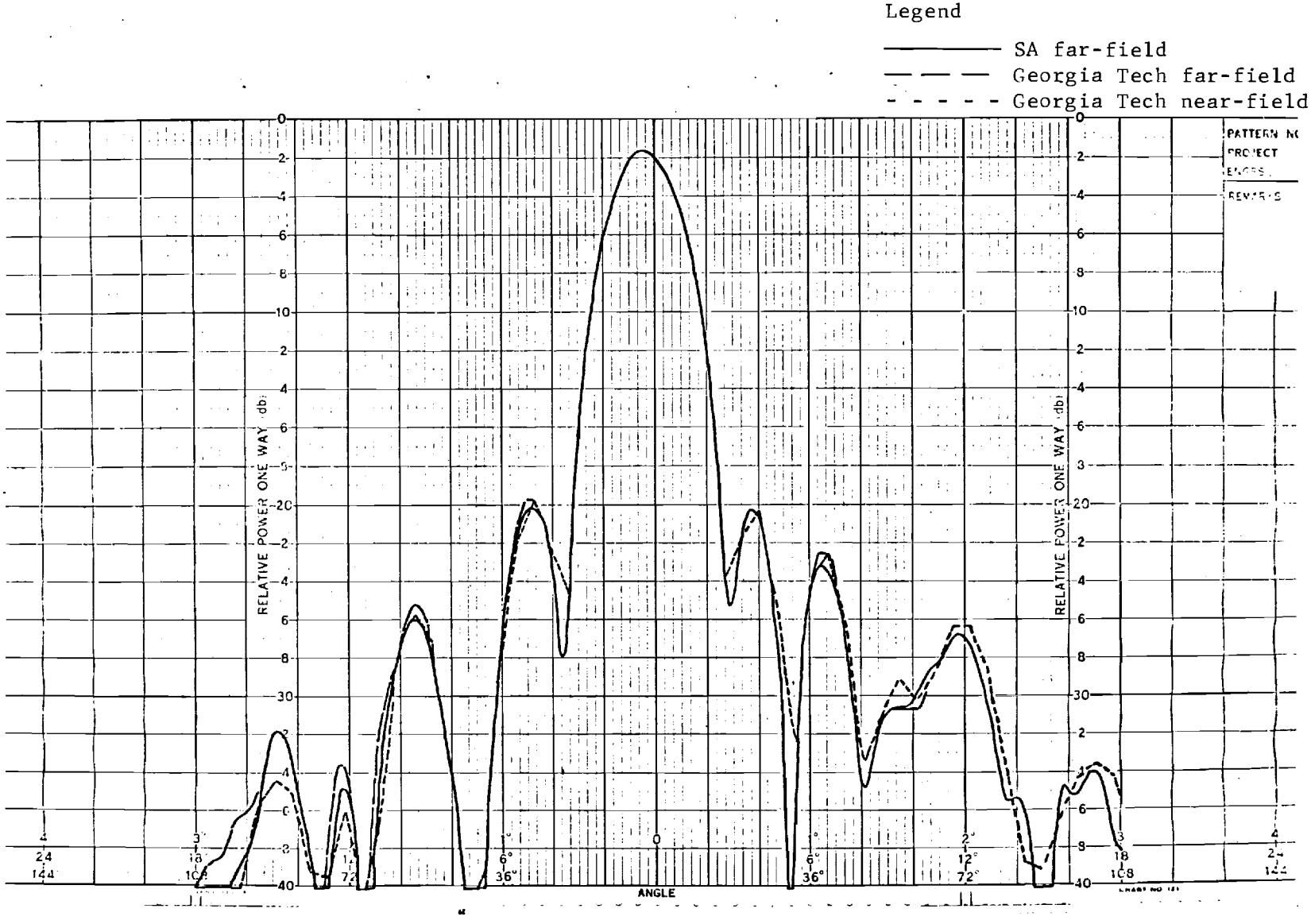

Figure 7-2. Comparison of sum pattern principal elevation plane cuts for Feed 2 taken on three ranges.

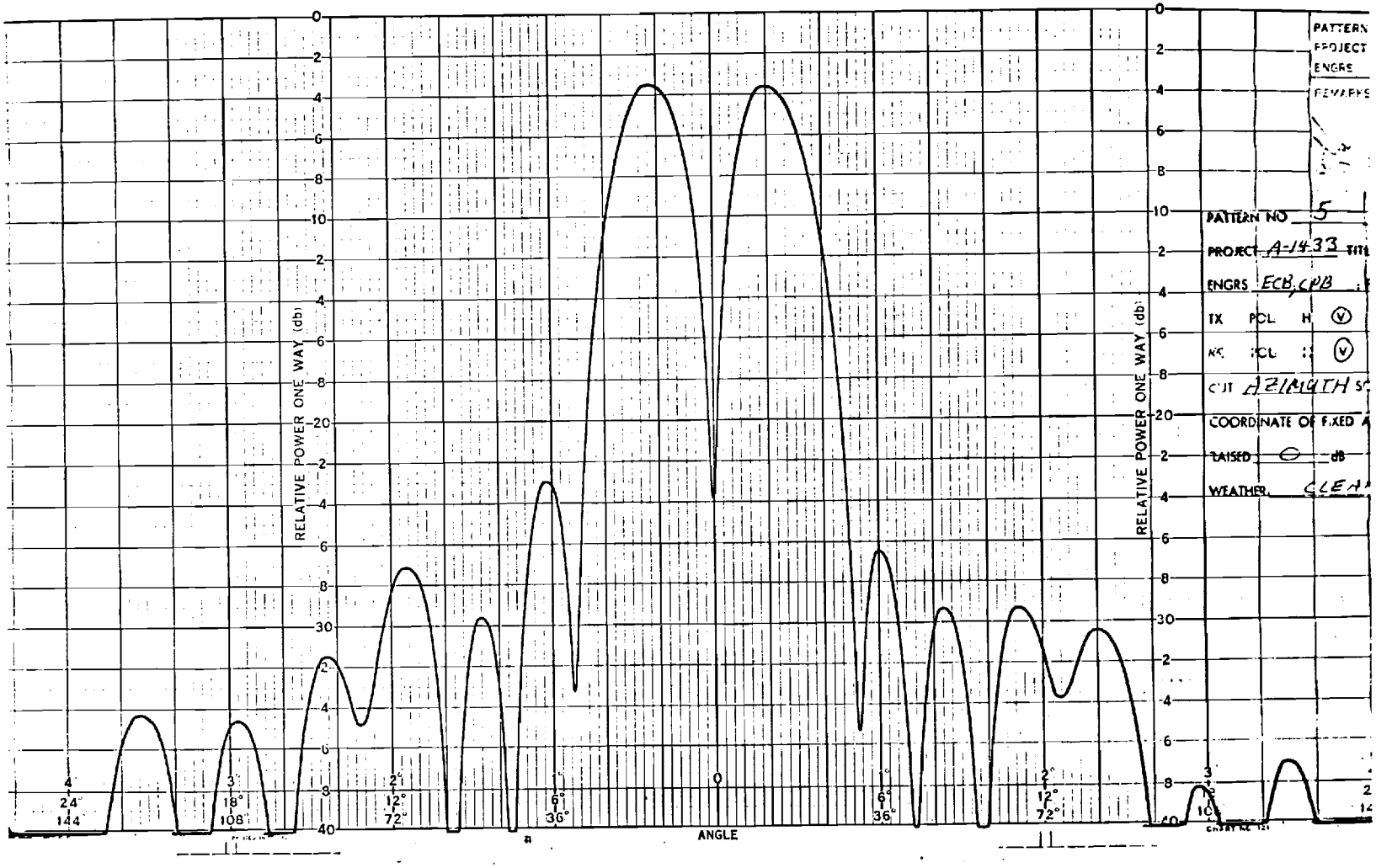

Figure 7-3. Principal azimuth plane cut of difference pattern for Feed 2 measured on Scientific Atlanta far-field range.

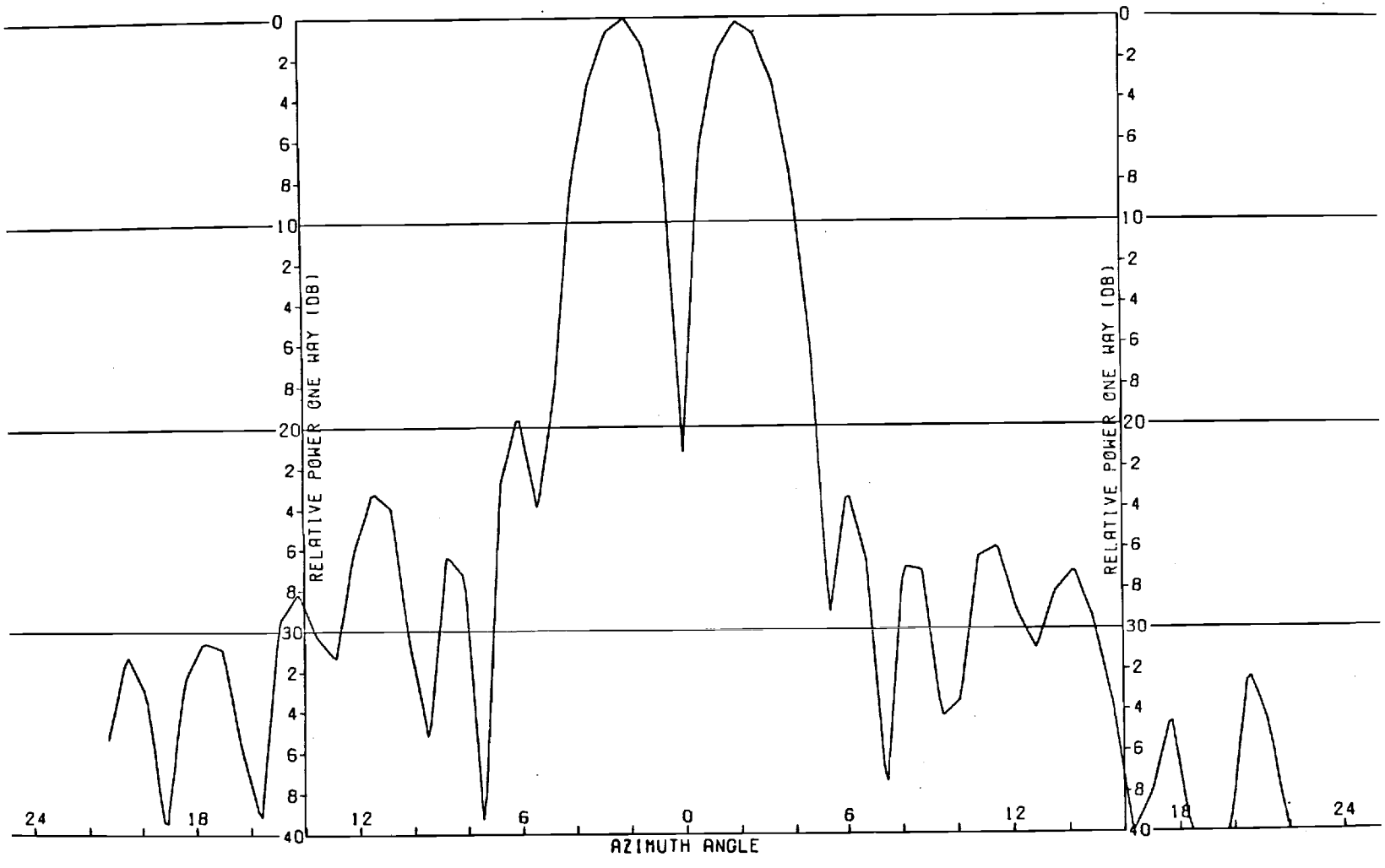

Figure 7-4. Principal azimuth plane cut of difference pattern for Feed 2 derived from near-field measurements.

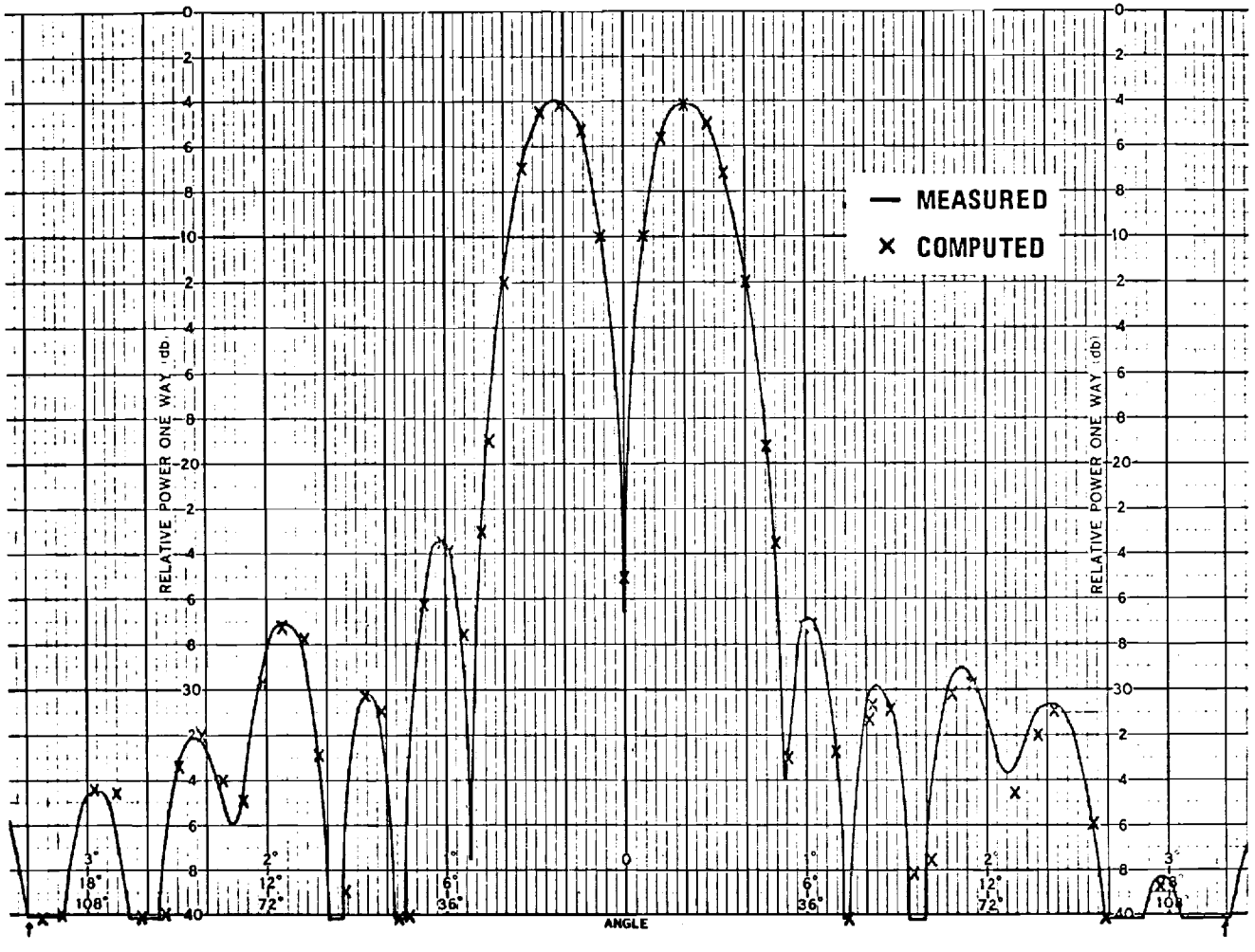

Figure 7-5. Principal azimuth plane cut of difference pattern for Feed 2 showing comparison of near- and far-field results.

far-field data, drawn as a solid line. In this form it is seen that data points fall almost precisely on the far-field plot. Figure 7-6 shows the full cut comparison. Again it should be emphasized that the only registration of angle used was the optical boresighting employed and that the only normalization used was that of the gain of the main beam. It is noted that the agreement between the Scientific-Atlanta far-field range (a solid line) and the Georgia Tech near-field range (small dashes) is comparable to that obtained between the two far-field ranges. (A single solid line indicates a coincidence of data.) Note that the depth of the principle null is approximately 2 dB greater for data taken on the Georgia Tech far-field range than for either the Scientific-Atlanta range or the near-field range. Similarly, the Georgia Tech far-field range indicates that the first null at the left is approximately 4 dB lower than that measured on the Scientific-Atlanta range. The near-field data shows discrepancies in instances where the point-to-point nature of the plots causes a straight line to be drawn across a null. This occurs on the two nulls to either side of the difference pattern principal maxima and occasionally in the sidelobe structure. Also the point-to-point nature of the plots tends to result in slightly lower gain values throughout the sidelobe region. It is noted, however, that the agreement throughout the area is excellent with sidelobes on the order of 30 dB down agreeing with 0.5 to 1.0 dB.

Figure 7-7 is a narrow angle plot of the difference pattern null. This plot covers the angular spread of $\pm$ 2 degrees in azimuth. On this curve the solid line is data obtained at Scientific-Atlanta. The dots and dashes are data obtained on Georgia Tech's far-field range and the

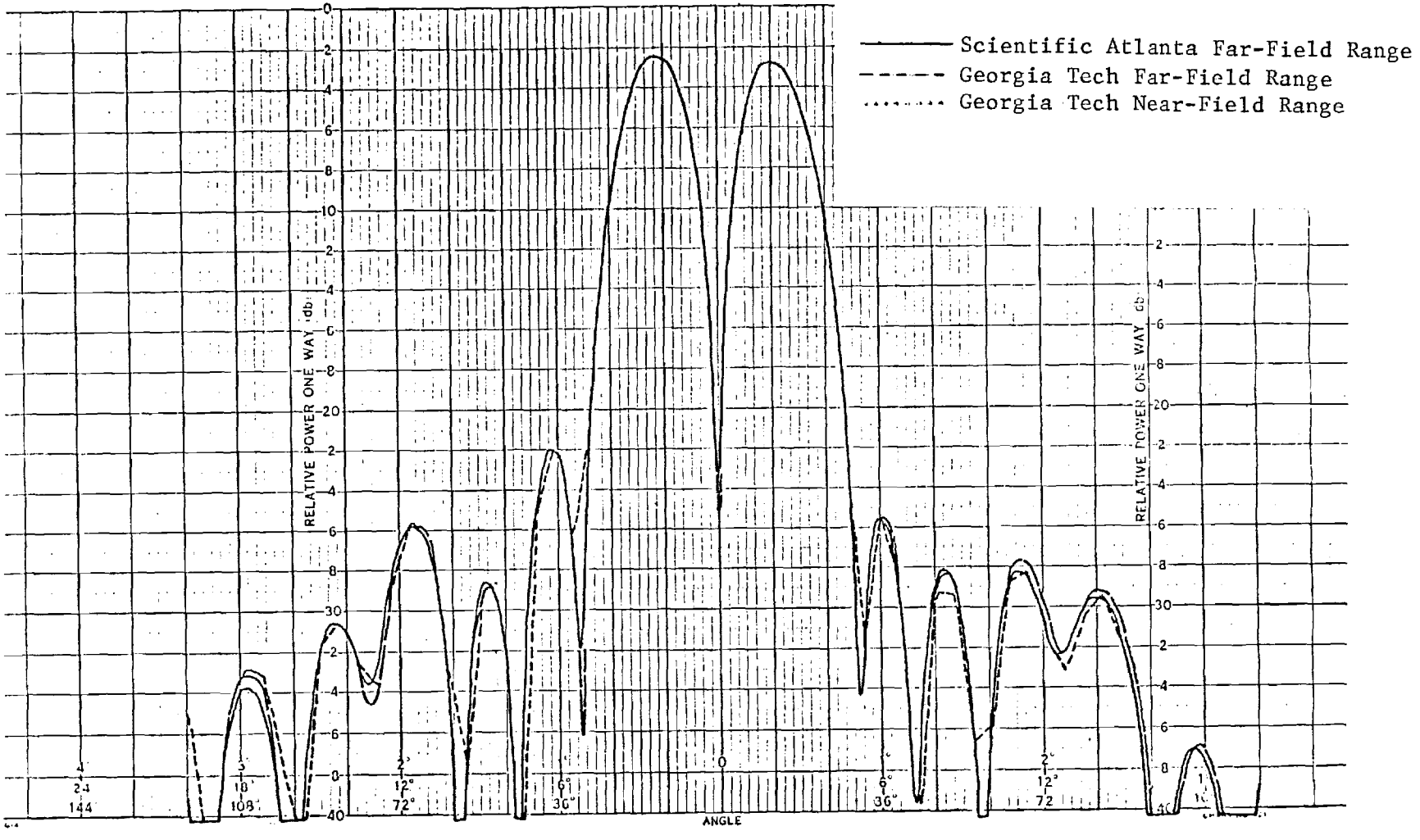

Figure 7-6. Principal azimuth plane cut of difference pattern for Feed 2 showing comparison of three independent measurements.

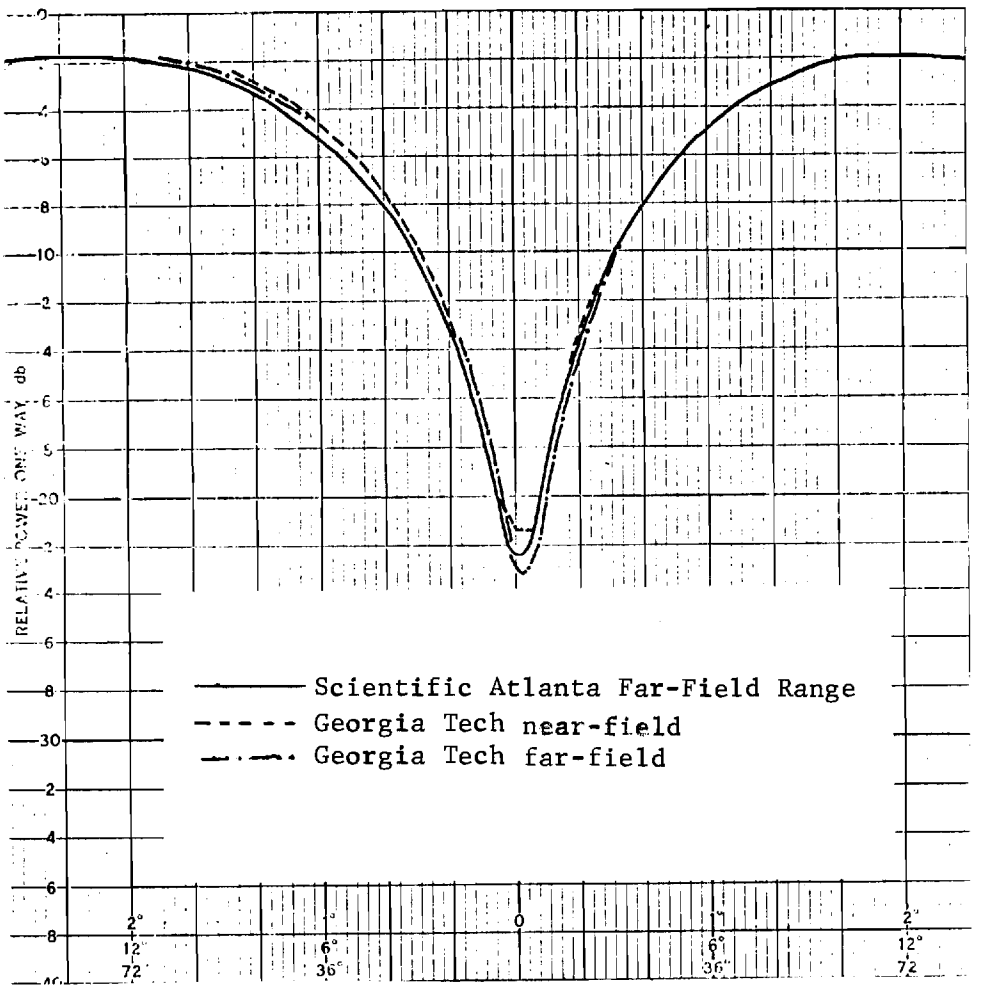

Figure 7-7. Difference pattern null for Feed 2 with increased resolution of near-field results.

dashes are data obtained from measurements on the near-field range. The agreement of boresight is within 0.03 degrees or approximately 0.5 milliradian. This error includes errors in optical boresighting as well. Also included here would be actual deformations that may have occurred in the feed structure over the six month period between measurements. Because of the rigid design of the antenna, these should be negligibly small. Figure 7-8 shows the effects of increasing resolution of the near-field data. In this plot the solid line is Scientific-Atlanta range data, and the two dashed curves represent the near-field predicted data for different degrees of resolution.

Figure 7-9 indicates comparisons obtained in patterns off principal planes. For this data the elevation angle is -2 degrees and azimuth angles are swept approximately $\pm$ 60. The near-field data shown here includes the angular spread of approximately $\pm$ 24 degrees. Again the agreement in shape and contour as well as sidelobe level is quite good, and the relative accuracy of the far-field ranges and near-field range appear to be equivalent. It should be borne in mind that these off-axis slices are made through the sides of lobes and small angular errors can lead to large dB errors. Moreover, since in many casea dajacent peaks may be pointing at ground reflections, the accuracy of the far-field results is probably no better than 2 to 3 dB.

On the near-field plots some distortion is seen near the limit of the band edge ($\pm$ 24 degrees) and should not be interpreted as an inherent near-field error. Again, the Scientific-Atlanta and near-field range data more closely agree than do the two far-field sets.

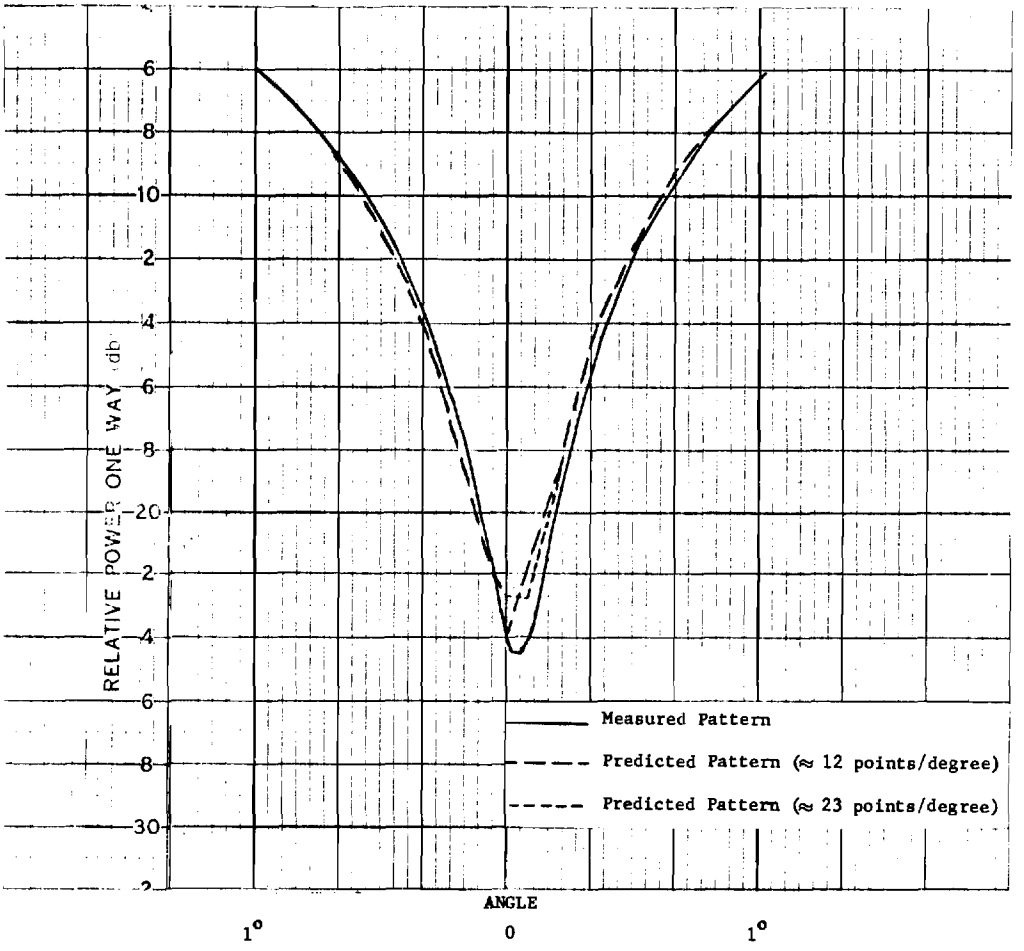

Figure 7-8. Difference null for Feed 2 with increasing resolution of near-field compared to SA range data.

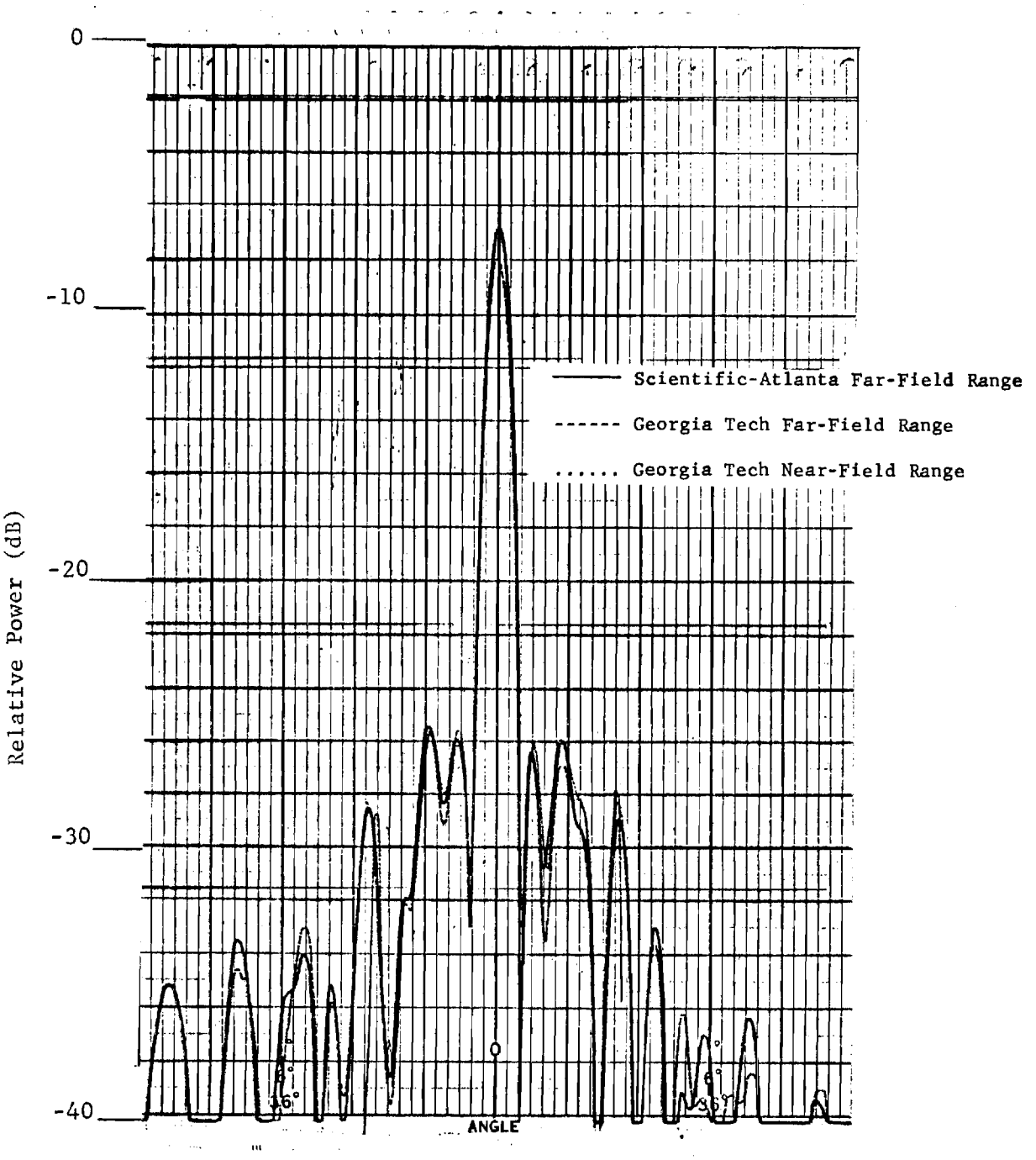

Figure 7-9. Feed 2 sum pattern azimuth plane cuts at elevation angle of -2 degrees taken on three different ranges, 12 degrees per major division.

In Figures 7-10 through 7-20 near-field off-axis cuts are superposed on Scientific-Atlanta far-field data. In each case the Georgia Tech far-field data agreed to the same degree shown in Figure 7-9. Only one far-field plot is shown in this set to make the superposed curves less confusing.

Figure 7-10 shows Scientific Atlanta (solid line) and near-field (dotted line) results for a sum channel elevation cut taken at a fixed azimuth angle of -2 degrees. The near-field data covers elevation angles of $\pm$ 24 degrees, since main beam interception of ground reflections is not a problem in near-field measurements. The Scientific-Atlanta range data covers elevations from +5 to -70 degrees. No fitting of curves was used; only boresighting and gain reference to sum peak.

Figures 7-11 and 7-12 are similar elevation cuts for azimuth angles of -4 and -6 degrees.

Azimuth off-axis cuts are shown in Figures 7-13 through 7-16 for the sum channel of Feed 2. Far-field (solid line) cuts include the full $\pm$ 70 degree angular range. Near-field (dotted line) results cover only the $\pm$ 24 degree range, because one stage of filtering is used to improve resolution. The agreement noted in Figure 7-16 is all the more notable in view of the fact that this contour is 8 degrees of the principal axis in a region of rapidly varying small sidelobes.

Difference channel off-axis azimuth cuts for Feed 2 are shown in Figures 7-17 through 7-20 for elevation angles from -2 to -8 degrees. Here also the Scientific Atlanta range data covers the angular width $\pm$ 70 degrees, while near-field results cover $\pm$ 24 degrees for reasons

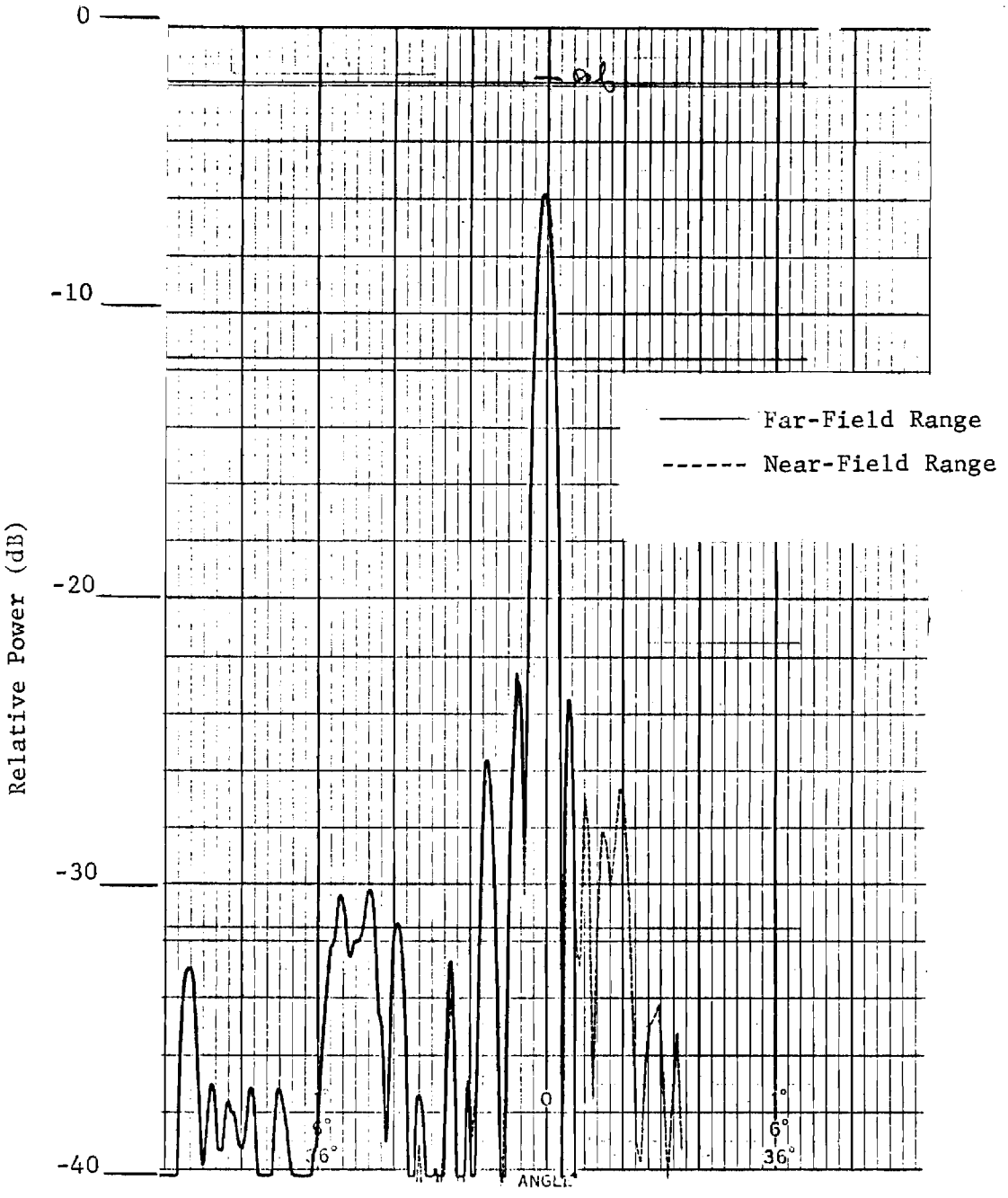

Figure 7-10. Feed 2 sum pattern elevation cuts at azimuth angle of -2 degrees taken on far-field and near-field ranges, 12 degrees per major division.

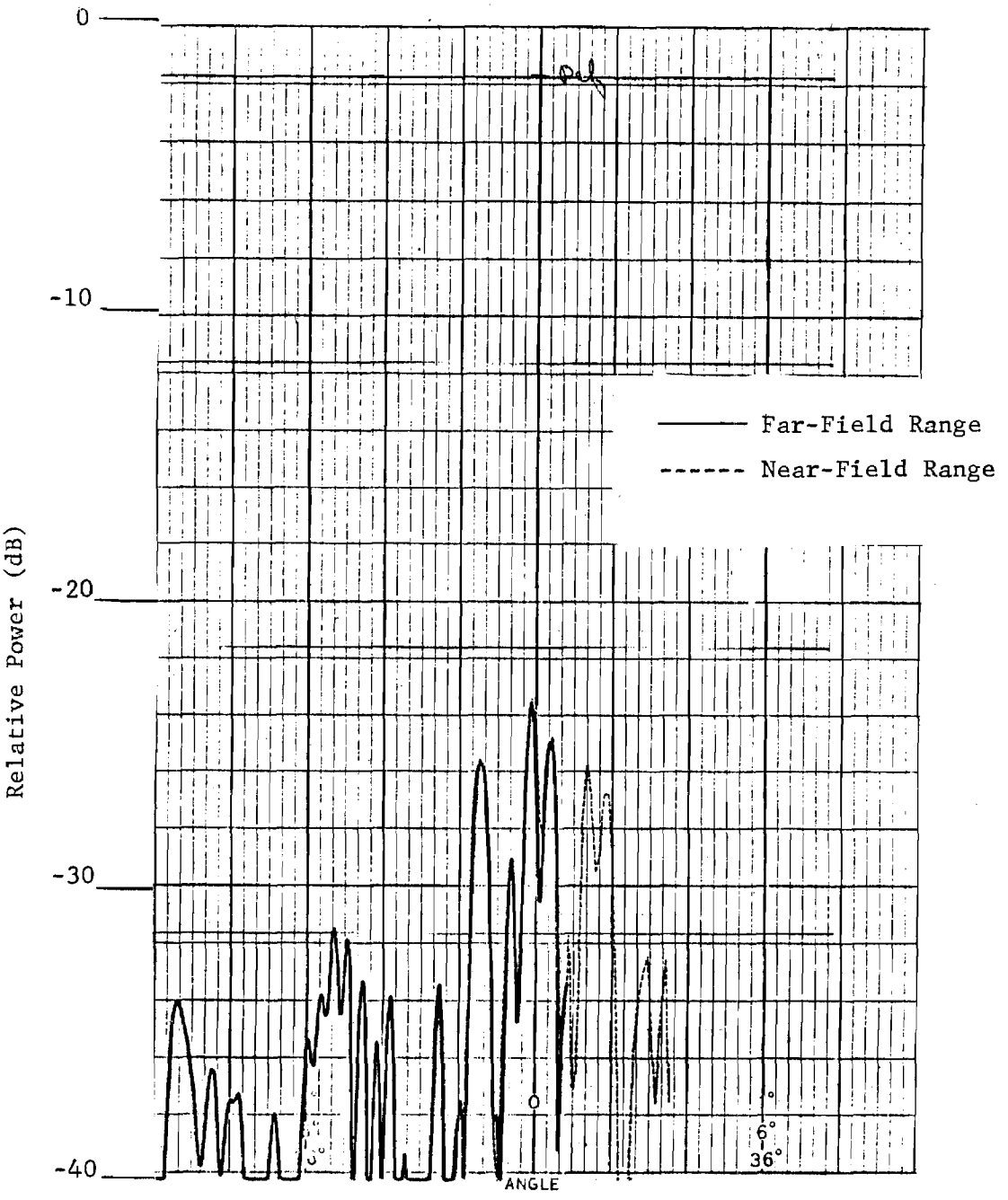

Figure 7-11. Feed 2 sum pattern elevation cuts at azimuth angle of -4 degrees taken on far-field and near-field ranges, 12 degrees per major division.

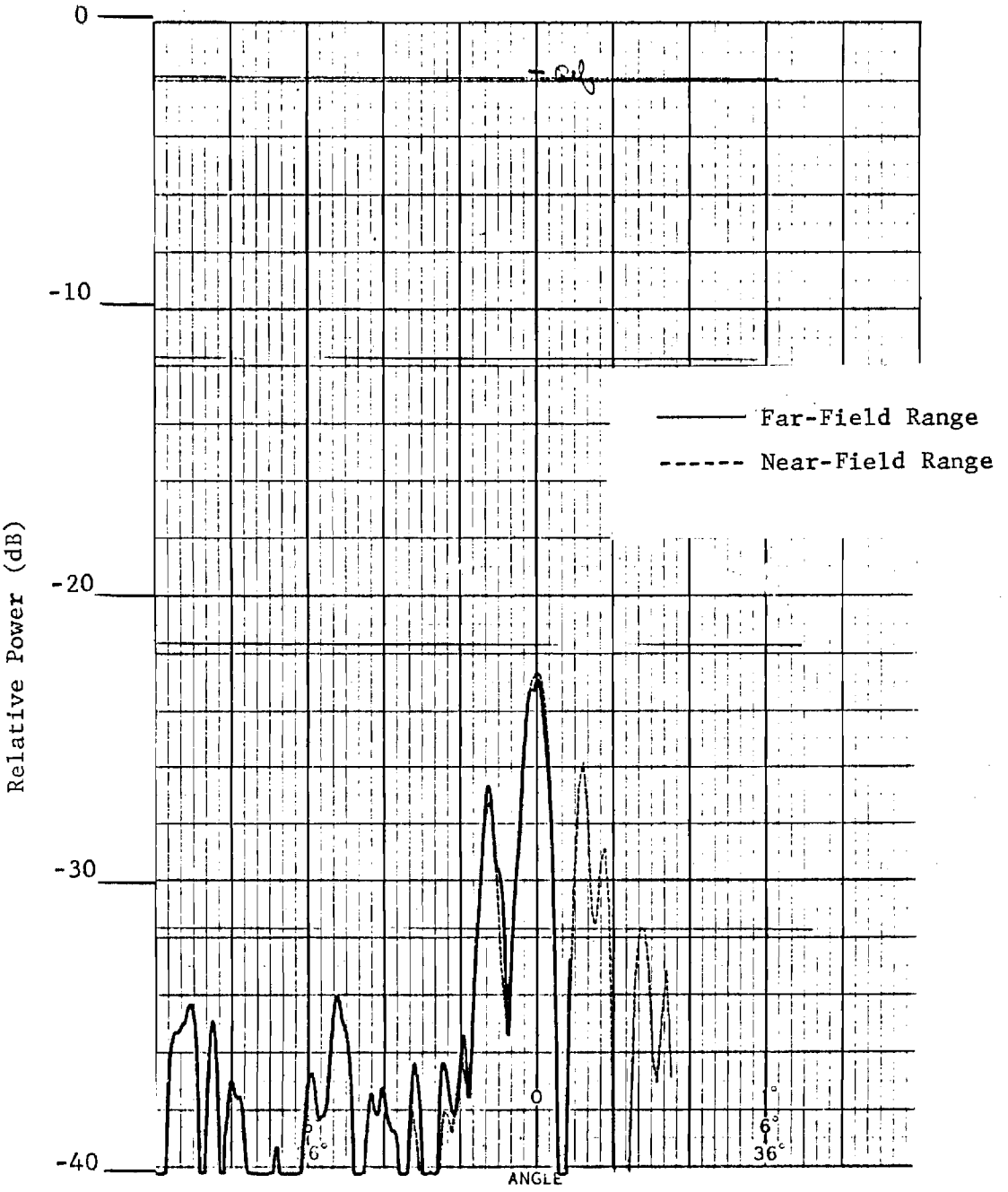

Figure 7-12. Feed 2 sum pattern elevation cuts at azimuth angle of -6 degrees taken on far-field and near-field ranges, 12 degrees per major division.

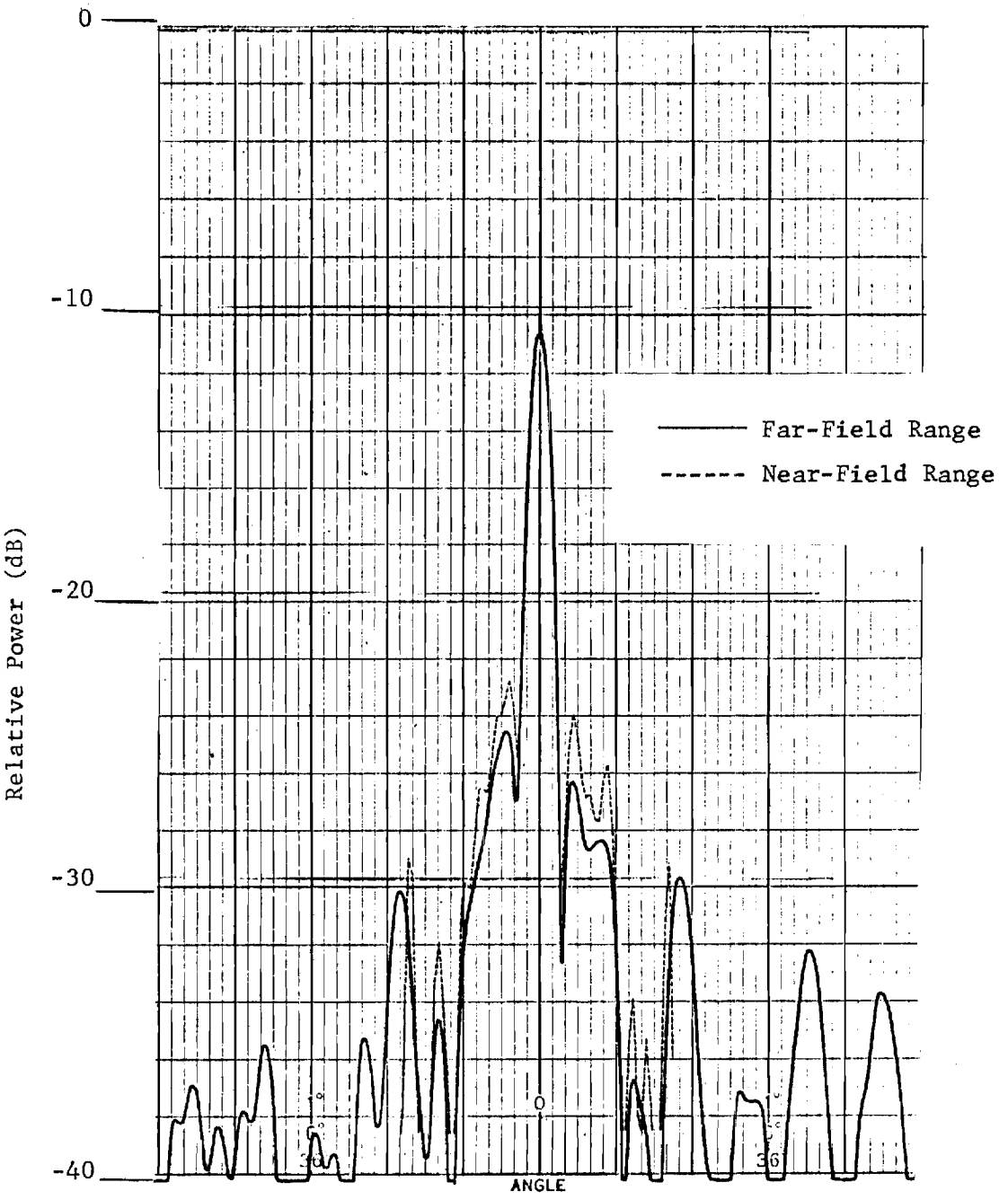

Figure 7-13. Feed 2 sum pattern azimuth cuts at elevation angle of -2 degrees taken on far-field and near-field ranges, 12 degrees per major division.

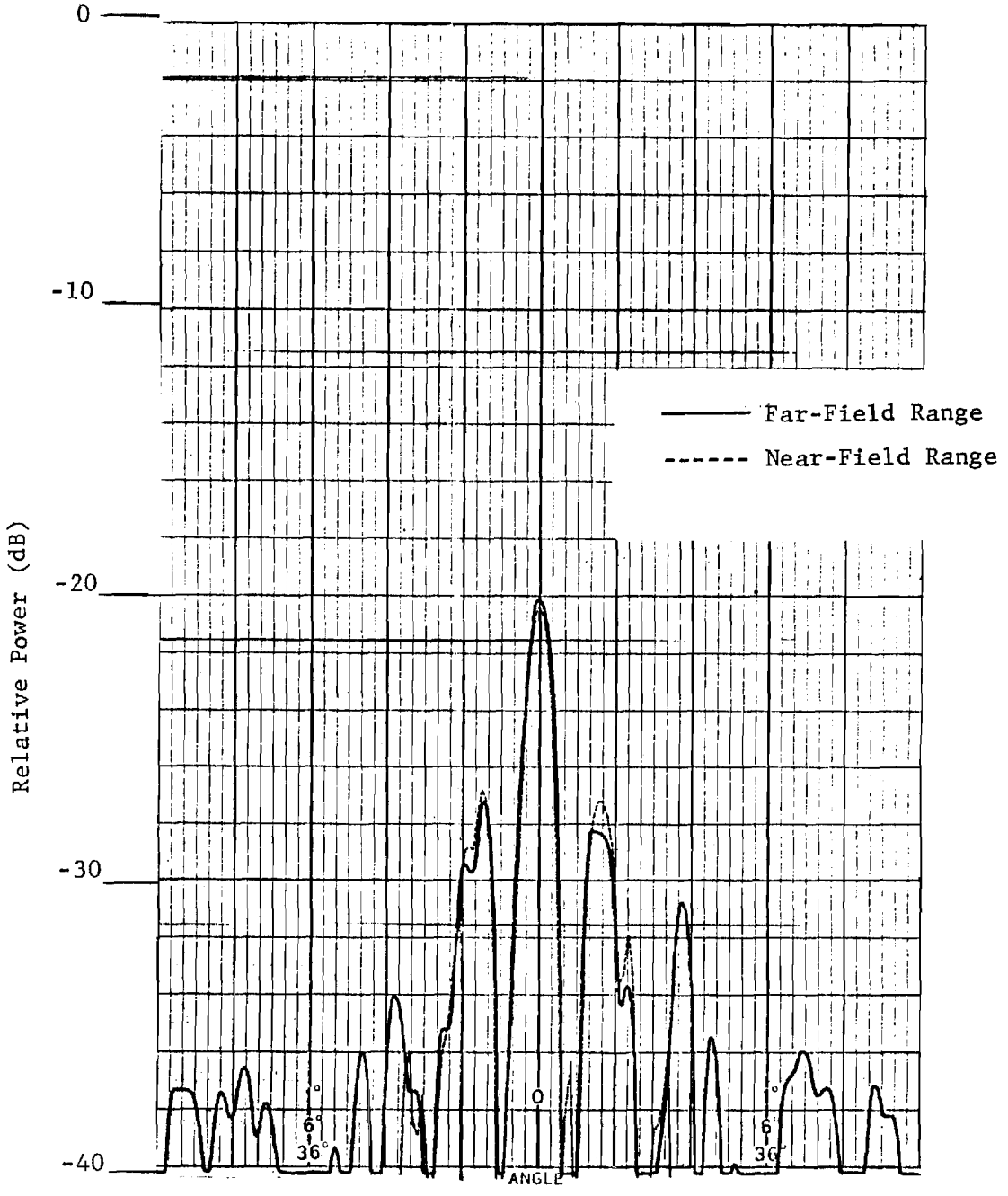

Figure 7-14. Feed 2 sum pattern azimuth cuts at elevation angle of -4 degrees taken on far-field and near-field ranges, 12 degrees per major division.

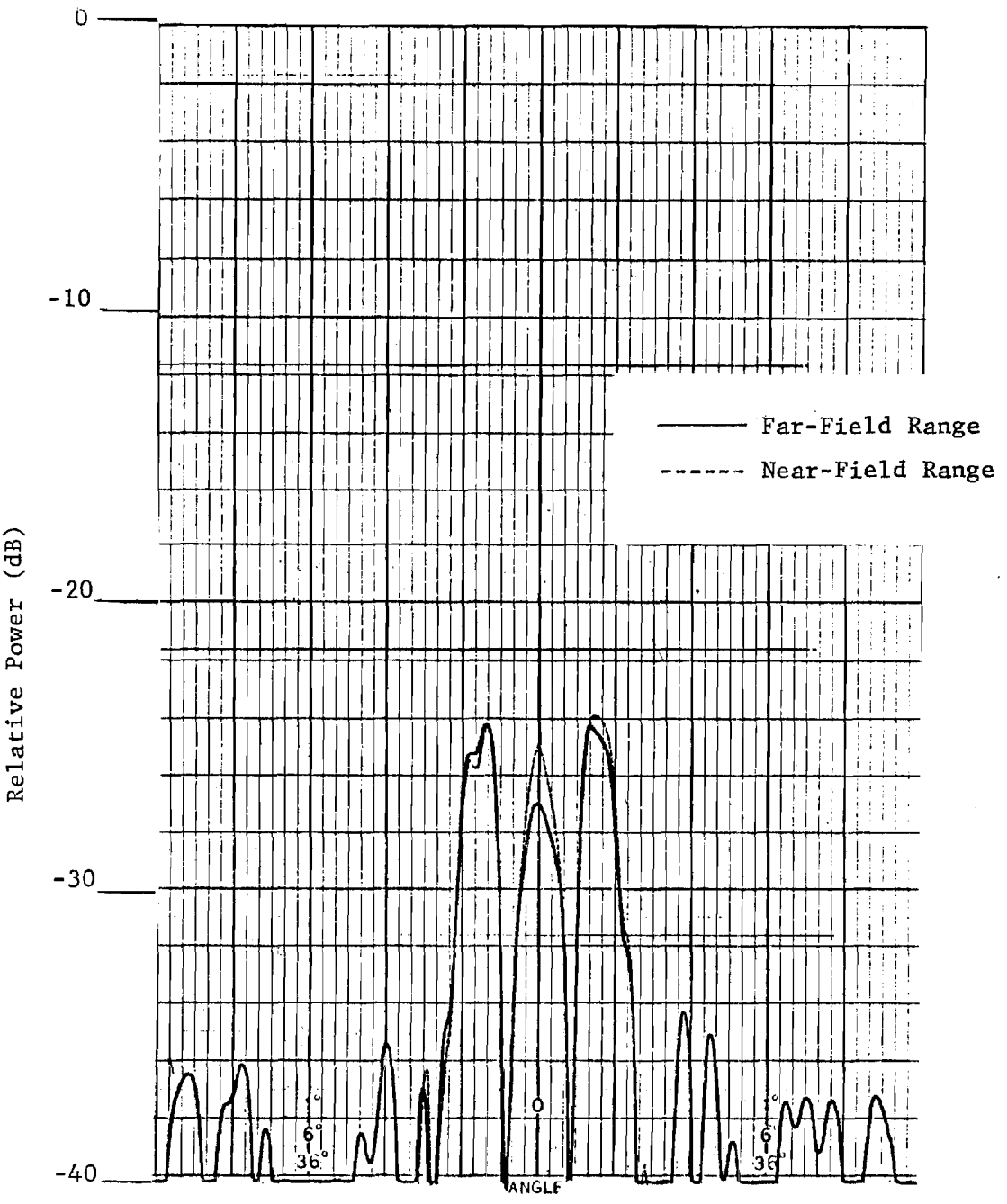

Figure 7-15. Feed 2 sum pattern azimuth cuts at elevation angle of -6 degrees taken on far-field and near-field ranges, 12 degrees per major division.

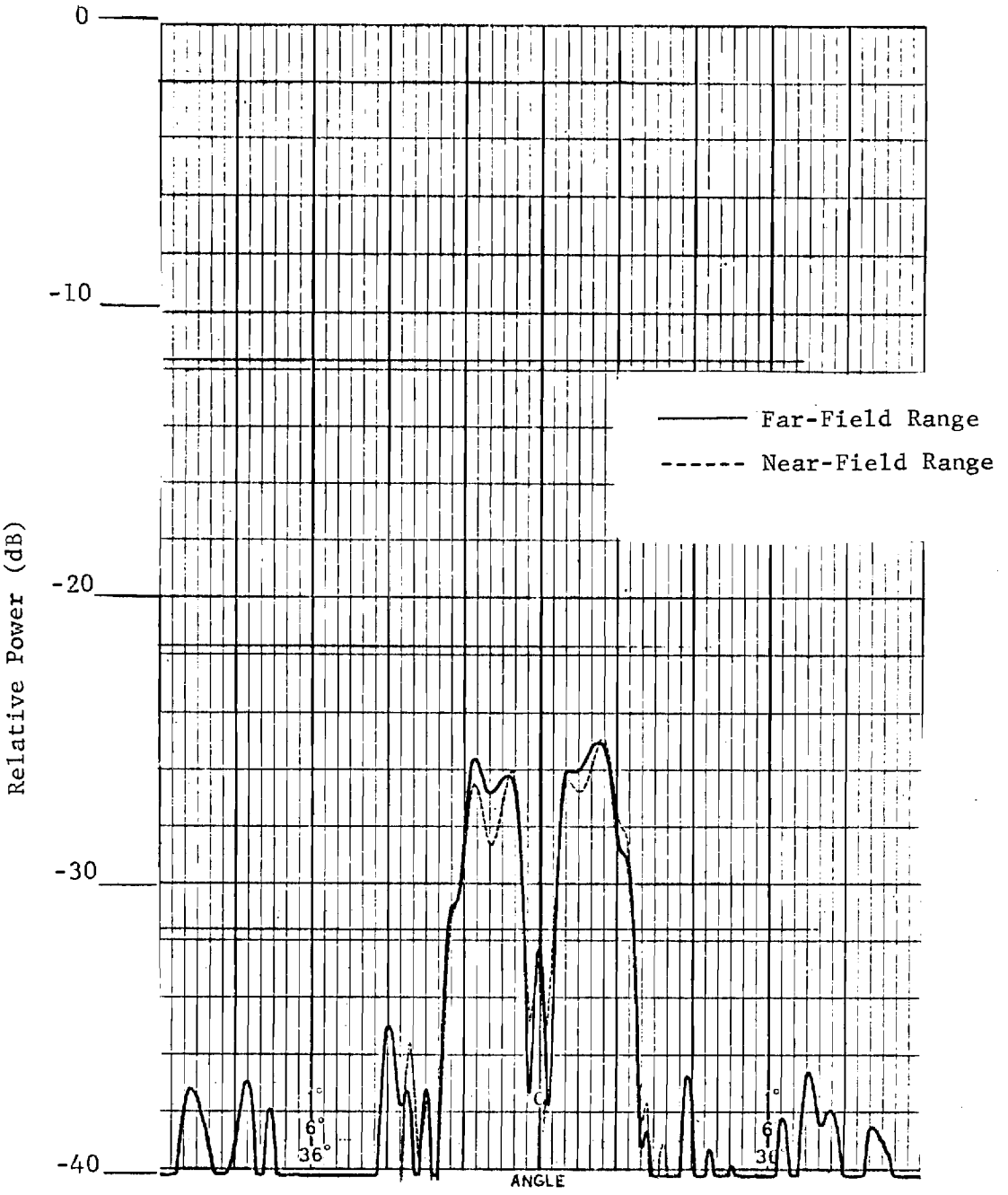

Figure 7-16. Feed 2 sum pattern azimuth cuts at elevation angle of -8 degrees taken on far-field and near-field ranges, 12 degrees per major division.

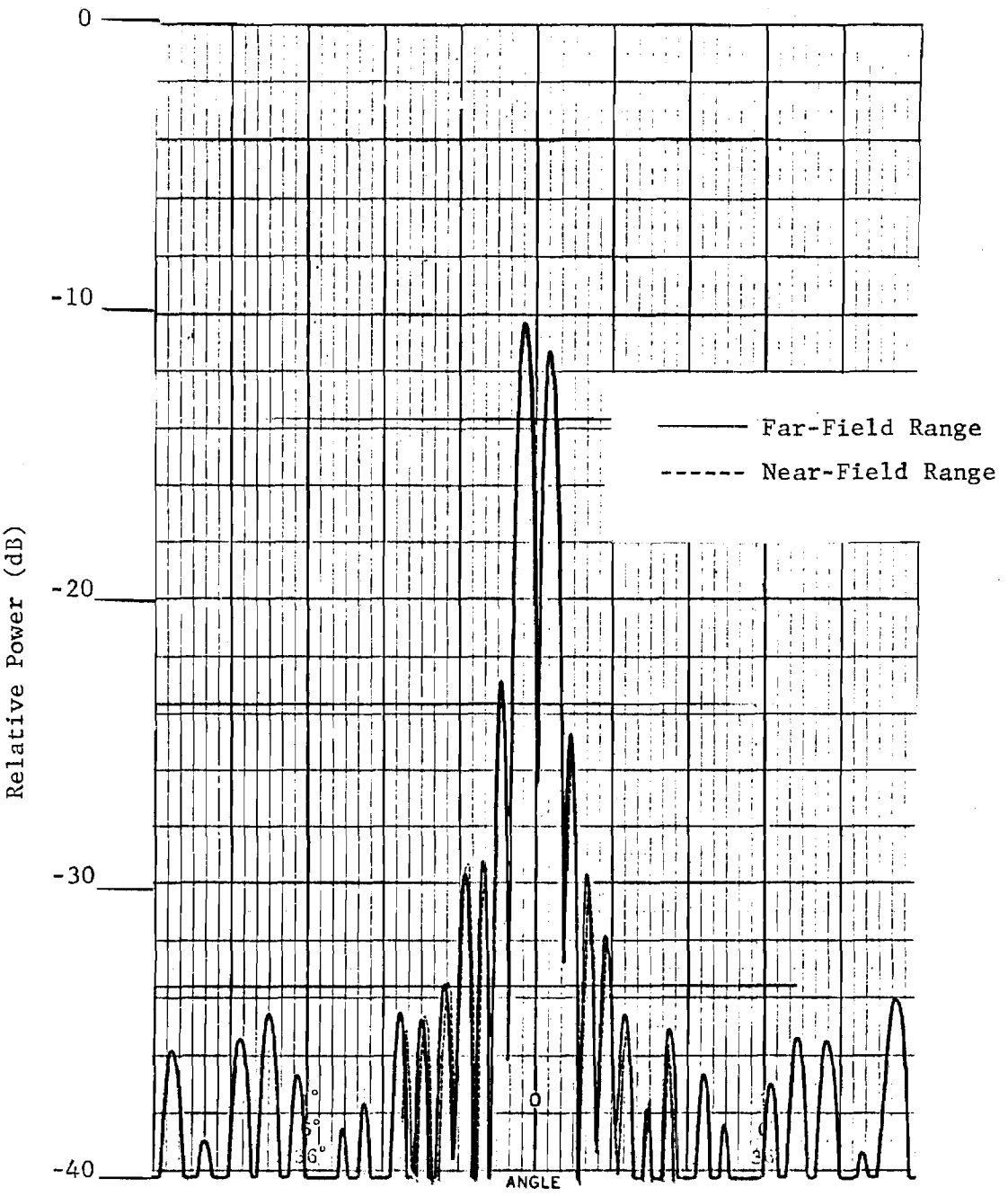

Figure 7-17. Feed 2 difference pattern azimuth cut at elevation angle of -2 degrees taken on far-field and near-field ranges, 12 degrees per major division.

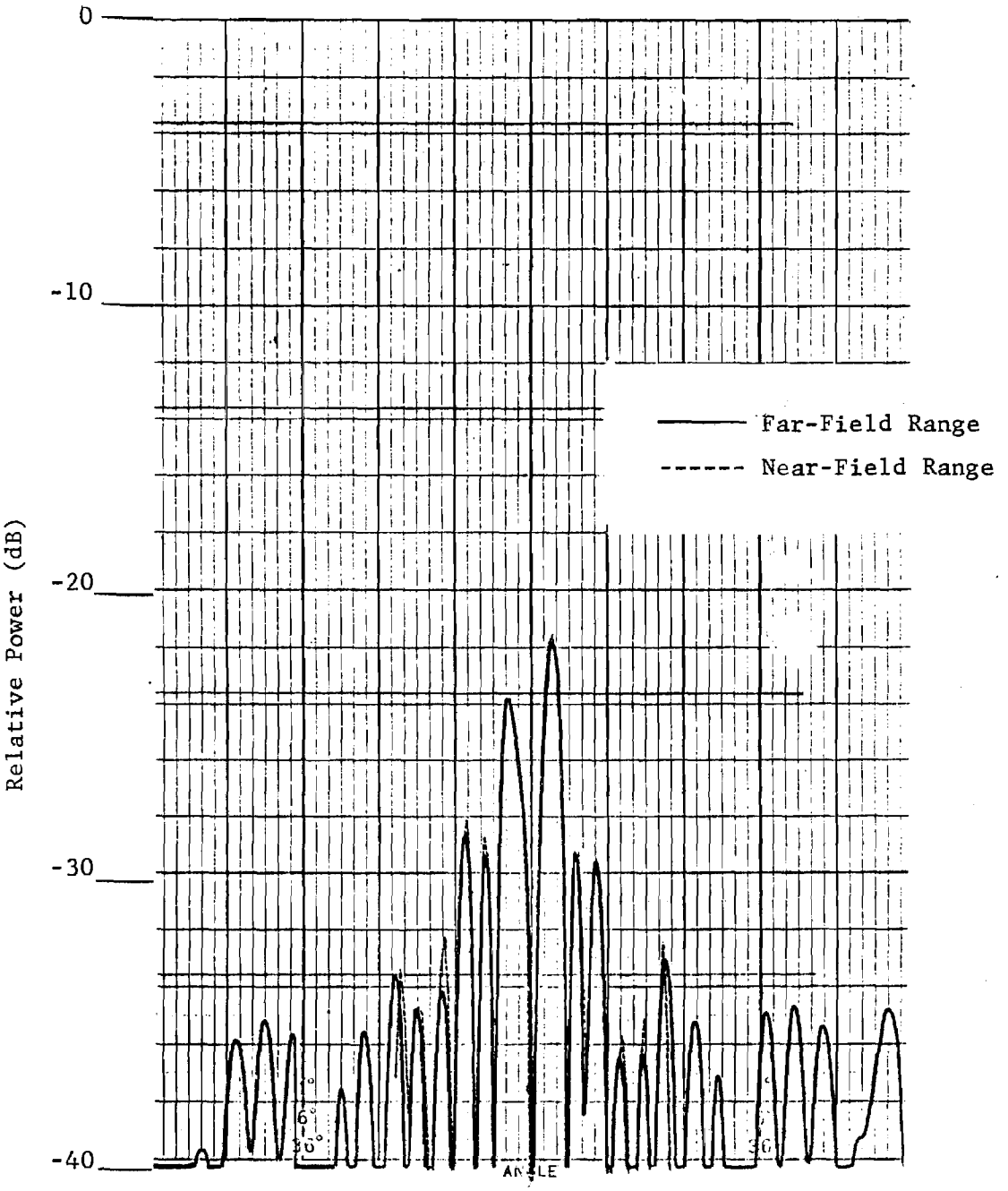

Figure 7-18. Feed 2 difference pattern azimuth cut at elevation angle of -4 degrees taken on far-field and near-field ranges, 12 degrees per major division.

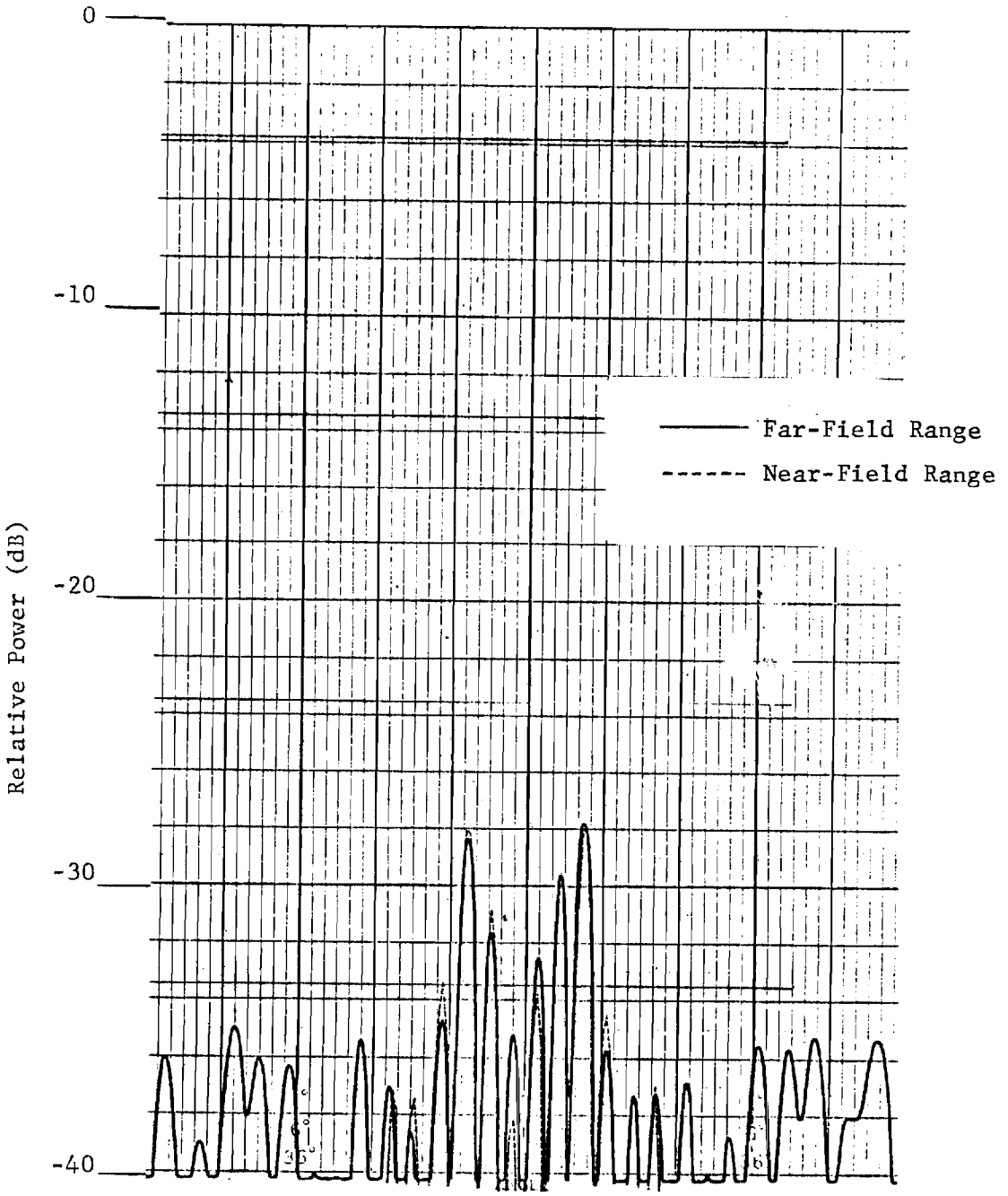

Figure 7-19. Feed 2 difference pattern azimuth cut at elevation angle of -6 degrees taken on far-field and near-field ranges, 12 degrees per major division.

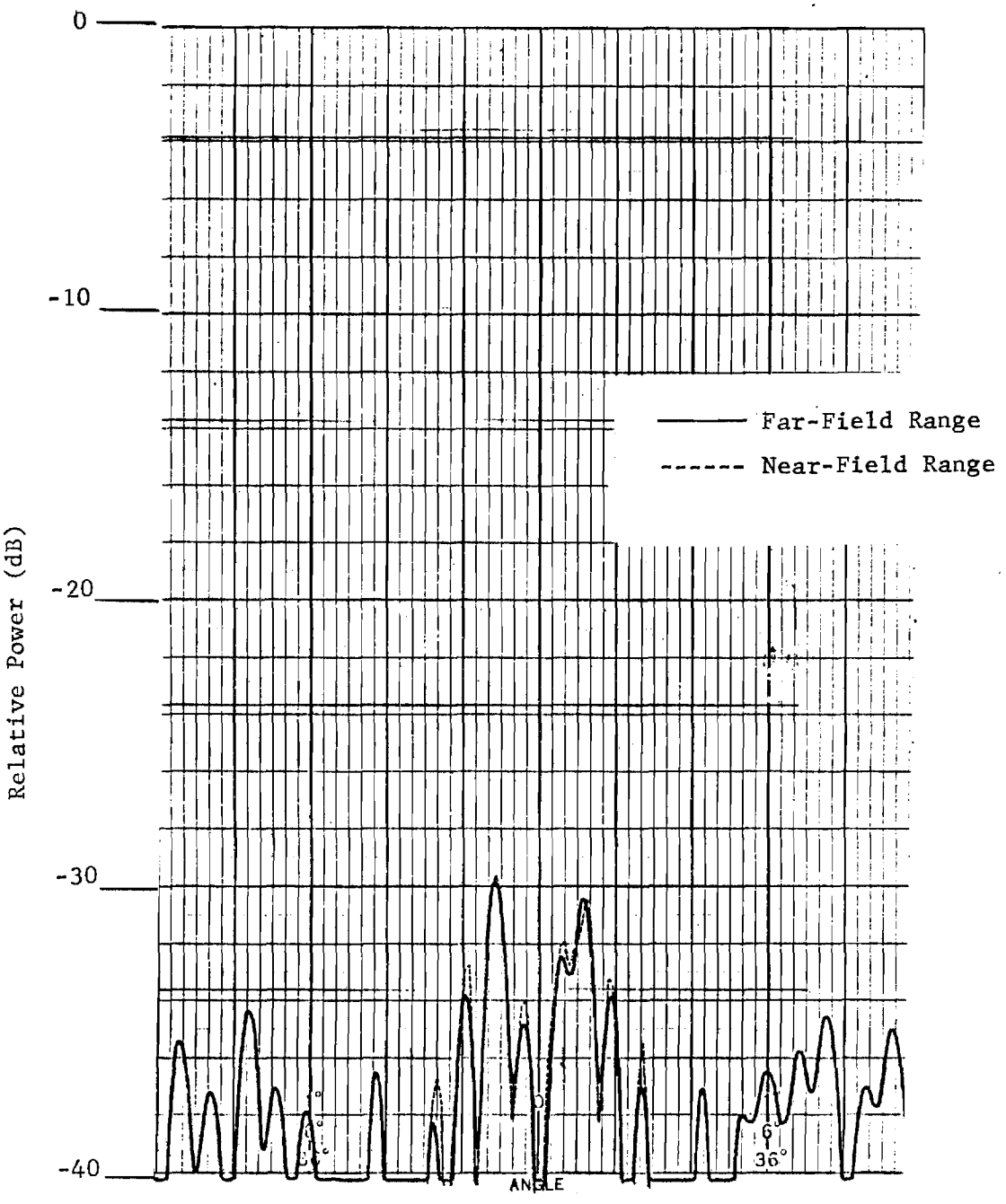

Figure 7-20. Feed 2 difference pattern azimuth cut at elevation angle of -8 degrees taken on far-field and near-field ranges, 12 degrees per major division.

of resolution. Note particularly the excellent agreement in Figures 7-19 and 7-20 at elevation angles of -6 and -8 degrees, respectively. The details of these rapidly varying sidelobes 30 to 40 dB down are reproduced with remarkable accuracy.

Off-axis cuts over 20 degree x 20 degree segments were taken at half degree steps to obtain values for RMS sidelobe levels. These results are summarized in Table 7-1. The azimuth angular region was +20 degrees and +40 degrees for the difference pattern. Two regions of the sum pattern were scanned (azimuth -20 degrees to zero degree and zero degree to +20 degrees). The elevation area covered an angular spread -20 to -40 degrees for both sum and difference channels. Forty cuts were made at half degree steps over this range on both sum and difference patterns. Shown in this table is the comparison of RMS sidelobe levels calculated for each of three regions. The two far-field ranges agree within approximately 0.5 dB for both sum and difference patterns, while the near-field data shows a consistently lower value of sidelobe level. The near-field results are consistently low by about 1 to 2 dB.

This error in computed sidelobe values deduced from the near-field data can be attributed to two potential sources. The first possible source is the point-to-point nature of the near-field plots. As earlier mentioned, these lead to inherently lower values on the slopes of sidelobes where such cuts frequently fall. If the calculated points were connected by a smooth curve, the points or sidelobes would tend to be raised uniformly. Also by increasing the number of plotted points in the far-out RMS sidelobe region an increase of the sidelobe level would occur due to the inherently greater resolution achieved.

TABLE 7-1. RMS SIDELOBE COMPARISONS

DIFFERENCE PATTERN

AZIMUTH VARIATION: +20 degrees to +40 degrees

ELEVATION VARIATION: -20 degrees to -40 degrees

FAR-FIELD #1	FAR-FIELD #2	NEAR-FIELD	$\triangle$
-38.5 db	-39.0 db	-40.7 db	1.9 db

SUM PATTERN

AZIMUTH VARIATION: -20 degrees to 0 degrees

ELEVATION VARIATION: -20 degrees to -40 degrees

FAR-FIELD #1	FAR-FIELD #2	NEAR-FIELD	$\triangle$
-34.9 db	-35.4 db	-37.1 db	1.9 db

AZIMUTH VARIATION: 0 degrees to 20 degrees

ELEVATION VARIATION: -20 degrees to -40 degrees

FAR-FIELD #1	FAR-FIELD #2	NEAR-FIELD	$\triangle$
-36.1 db	-36.3 db	-37.3 db	1.1 db

The other possible explanation for this discrepancy lies in an unresolved question with respect to the manner in which cross-polarization components are handled in the computer program.

The method of near-field probe compensation incorporated into the far-field computation process performs well for nearly linearly polarized antennas. More work on this compensation process still must be done, however, for antennas with appreciable cross polarization components. Recent work has shown that when the cross component is approximately equal to the principal component as much as a -3 dB error could be incorporated into the present computation process. This error would predict far-field levels lower than actual. The effect of this error on the approximately linearly polarized test antenna used in this research is most noticeable in the low level sidelobe regions of the far-field pattern, for it is here that the cross component and the principal component are approximately equal.

Cross polarized components of sum and difference patterns were also measured on the Scientific-Atlanta range and calculated from near-field measurements. Figures 7-21 and 7-22 show these results for sum and difference channels respectively. Here the detailed agreement is poor, though the level of cross polarized components is in good agreement. It is felt that a large portion of this discrepancy can be attributed to angular inaccuracies, since measured cross polarized patterns are most dependent on the exact orthogonality of antennas on the far-field range.

7.2 Feed 1 Comparisons

Figure 7-23 shows a comparison of the far-field patterns obtained

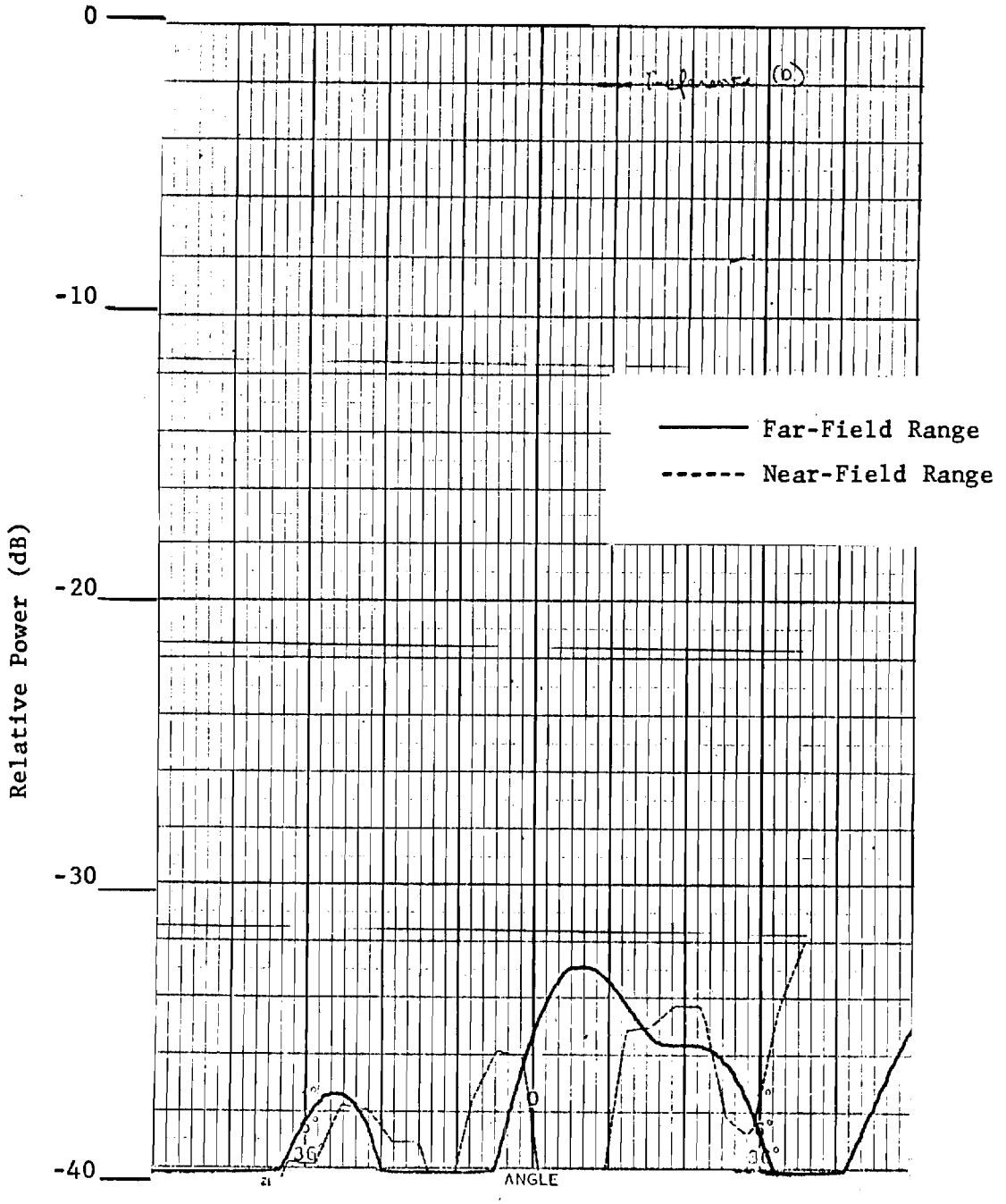

Figure 7-21. Feed 2 sum pattern, cross polarized, azimuth principal plane cut taken on far-field and near-field ranges, 2 degrees per major division.

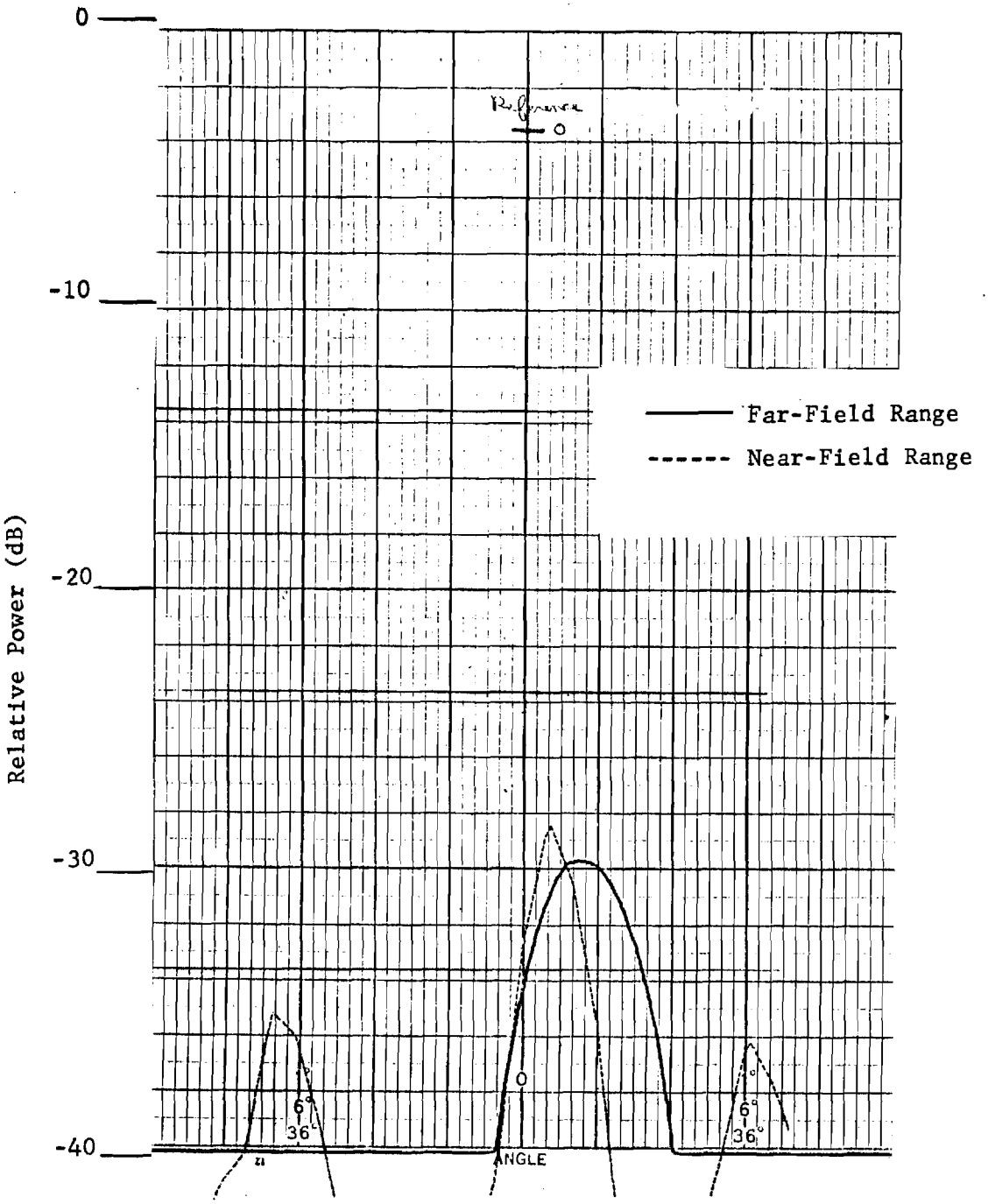

Figure 7-22. Feed 2 difference pattern, cross polarized, principal azimuth plane cut taken on far-field and near-field ranges, 2 degrees per major division.

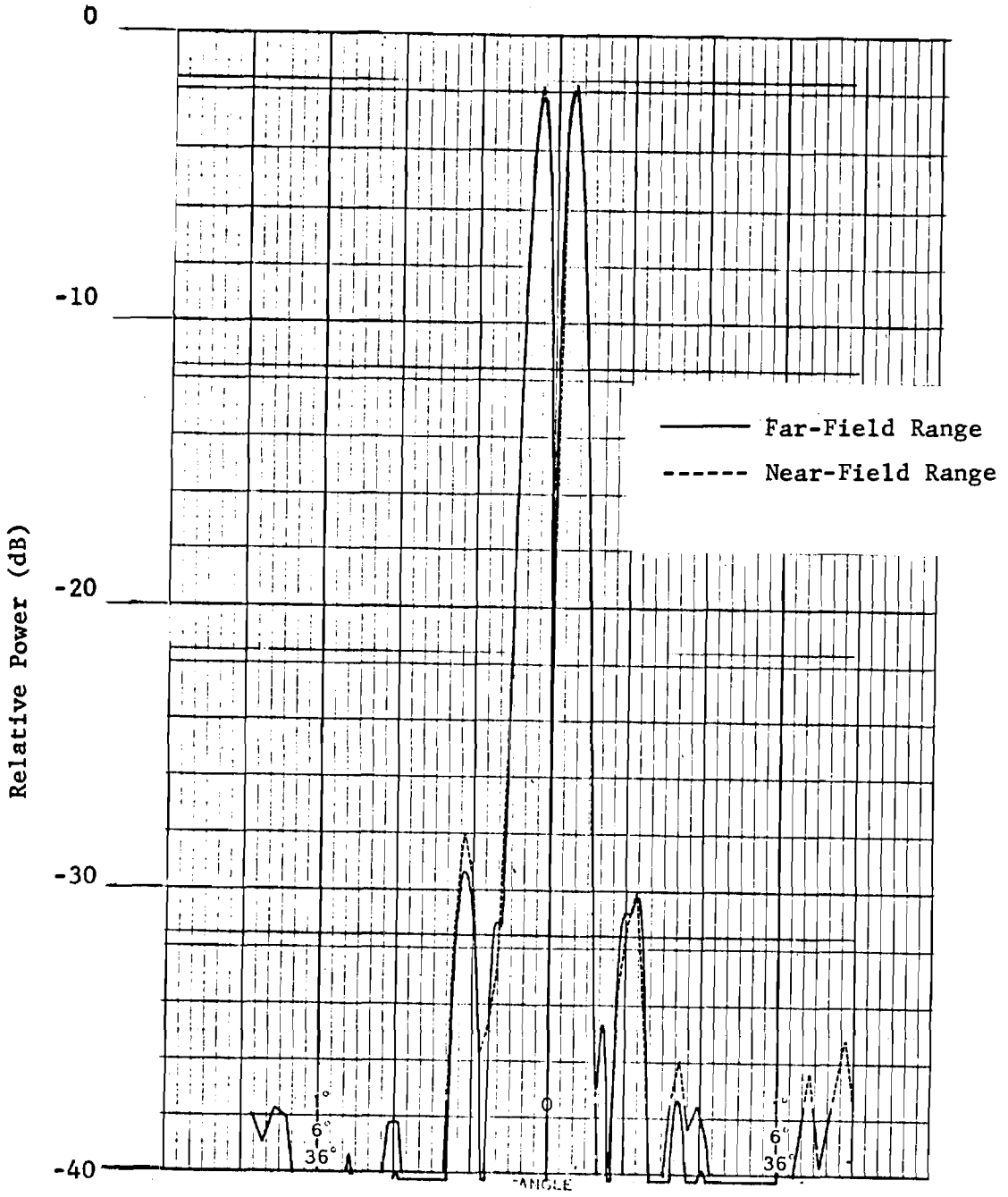

Figure 7-23. Feed 1 difference pattern principal azimuth plane cuts taken on far-field and near-field ranges, 12 degrees per major division.

from near-field measurements and from far-field measurements on the antenna using Feed 1 in the difference mode. The far-field cut (solid line) shown here was taken on the Georgia Tech range. The near-field measurements (dotted line) are distinguishable on the basis of their point-to-point nature. Agreement over this principal plane is excellent, and errors in sidelobes are on the order of 1.5 dB. Figure 7-24 shows greater detail near boresight. Again the features of the principal lobe are in good agreement in detail, with the exception that the null of the near-field derived data is not as deep as that of the far-field range data. The near-field null drops to only 20 dB below the maximum of this difference pattern while the outdoor range data shows a null more than 30 dB down. The depth of this null can be improved by further filtering of the near-field data as will be shown in subsequent figures. Errors in the sidelobe levels are again on the order of 1.5 dB. Figure 7-25 is a plot of the detail of the difference pattern null with further smoothing of the near-field data. This represents the results of three filtering processes which result in an increase in null depth from -20 dB to approximately -31 dB. Figure 7-26 shows the difference pattern null of the near-field data when four filtering processes are used to increase the resolution. Here the difference pattern null drops to approximately -35.5 dB, which agrees within 2 dB of the depth of null obtained on the far-field range. The distortion of the near-field results near $\pm$ 2 degrees arises from the effects of filtering and is always seen at band edges.

Figure 7-27 is a comparison of near-field and far-field determinations of the sum pattern elevation cut. The far-field angular

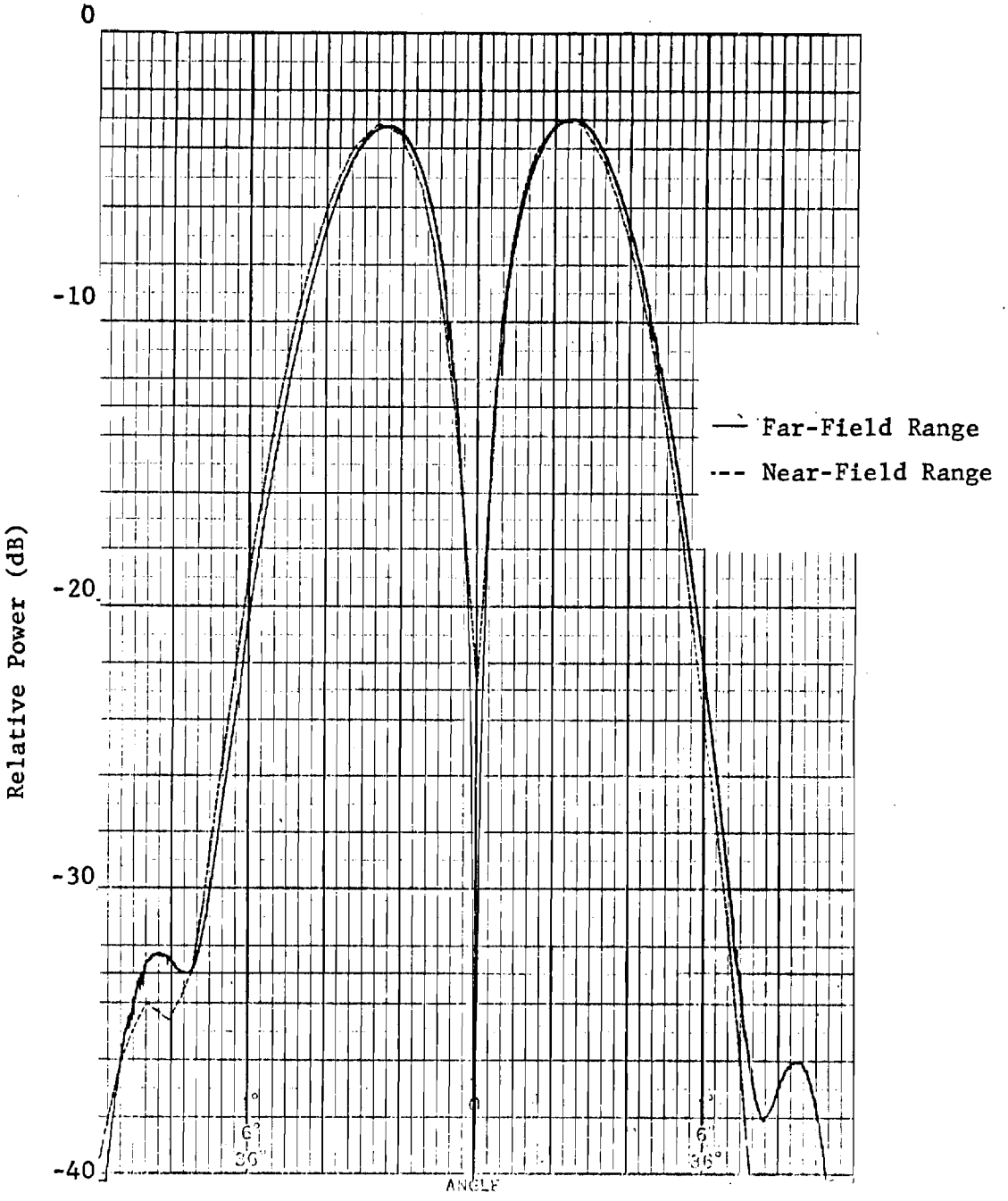

Figure 7-24. Feed 1 difference pattern principal azimuth plane cuts taken on near-field and far-field ranges, 2 degrees per major division.

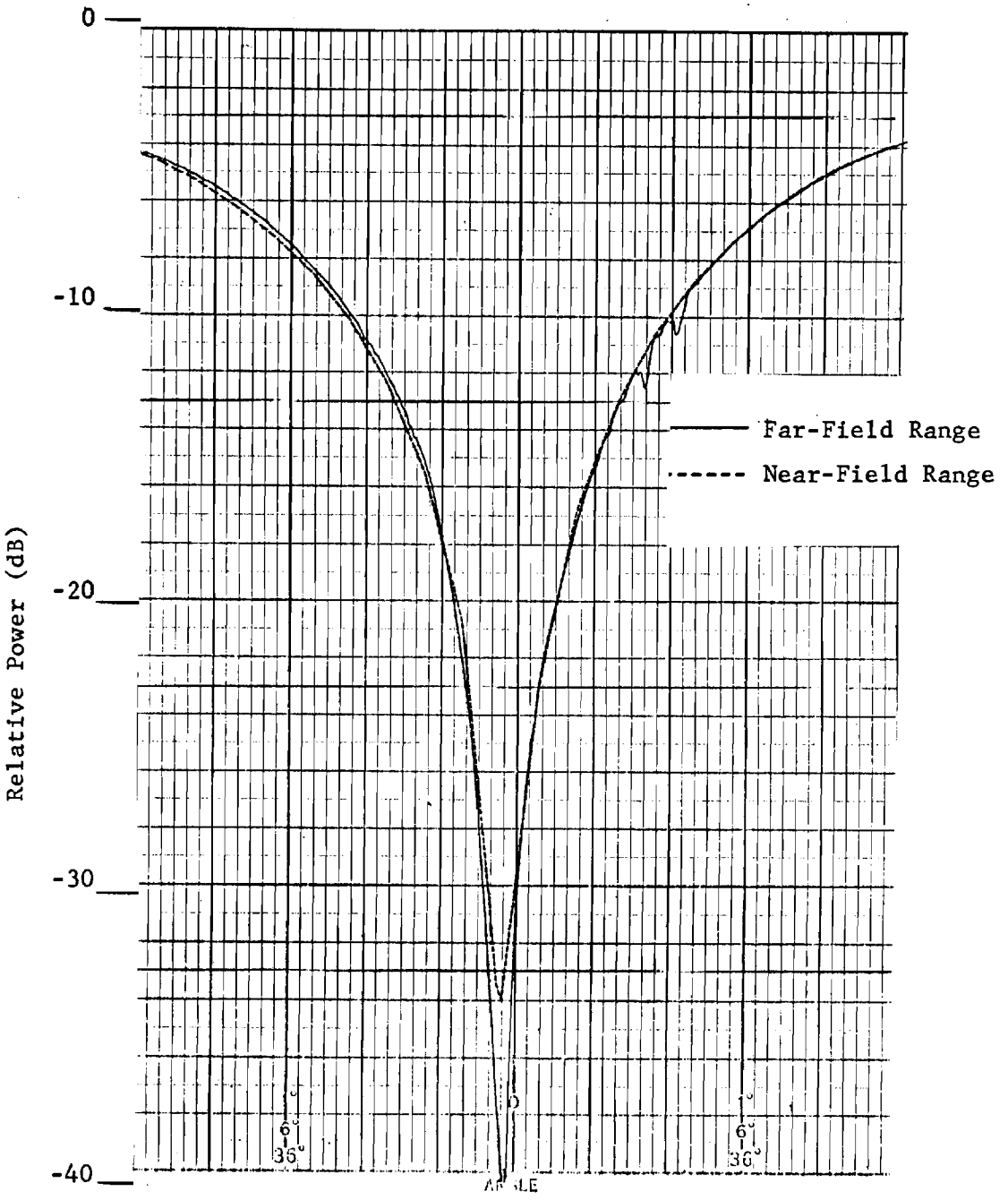

Figure 7-25. Feed 1 difference pattern principal azimuth plane cuts taken on near-field and far-field ranges, 1/3 degree per major division.

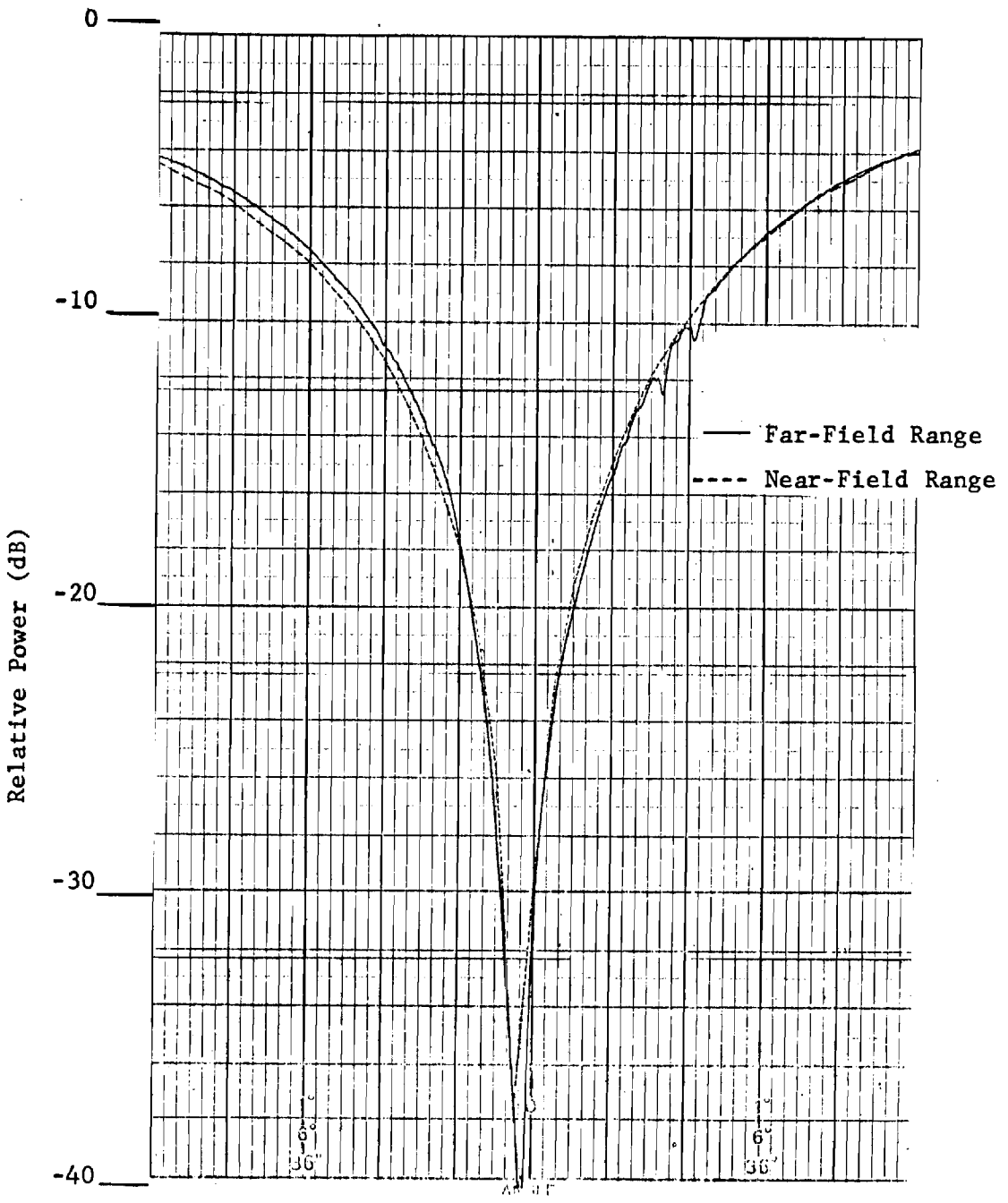

Figure 7-26. Feed 1 difference pattern principal azimuth plane cuts taken on near-field and far-field ranges, 1/3 degrees per major division and increased resolution in near-field.

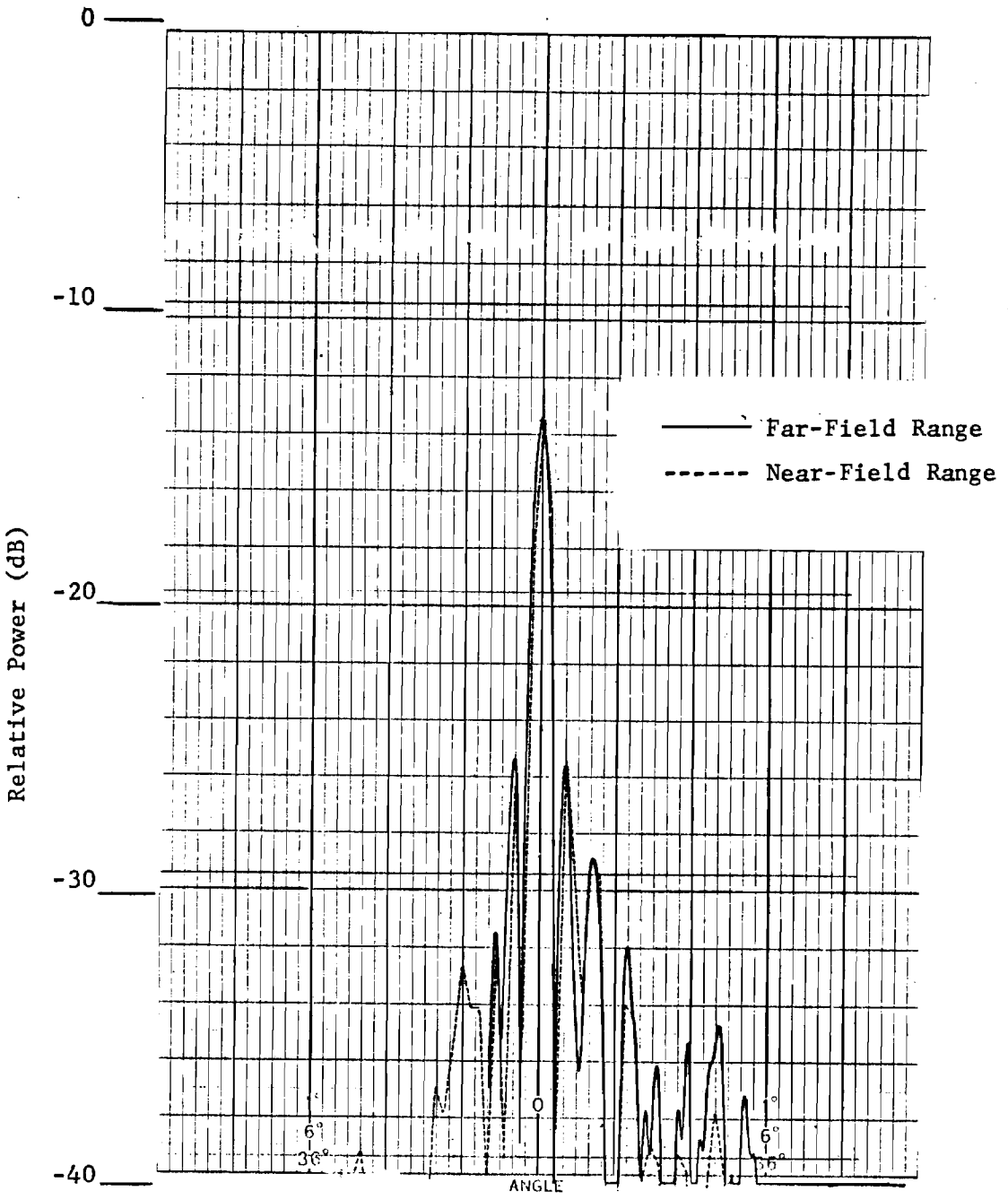

Figure 7-27. Feed 1 sum pattern principal elevation plane cuts taken on near-field and far-field ranges, 12 degrees per major division.

coverage here is +10 degrees and -36 degrees, and again the location of sidelobes is in excellent agreement. The sidelobe levels are found to agree within approximately 3 dB at roughly the -30 dB level. The noticeable point-to-point characteristic of the near-field based results is due to the wide angle coverage and therefore the low density of points is given angular spread. Figure 7-28 is a comparison of azimuth plane cuts of the sum pattern on this first feed design. The dip in the main beam is due to the low cross-over of the feed horns as described in Section 4. It is interesting to note that the double peak character of the main beam and the first sidelobes, which results from this low cross-over design, is reproduced in the near-field data, even for this low resolution plot that includes angles from roughly +50 degrees to -50 degrees. The sidelobe agreement is in this case the order of 1.5 dB over most of the range examined. Some distortion at band edges is apparent in the near-field results. Location of sidelobes is in exact agreement. Figure 7-29 illustrates the improved resolution obtainable from near-field data when filtering is employed. This plot can be compared with the far-field results of Figure 7-28 over the range from roughly $\pm$ 24 degrees. Notice that the shapes of the sidelobes, as well as some of the lower peak heights are now in much better agreement than those of the preceeding figure and that the relative amplitude of the twin peaks of both sidelobes are now in much better agreement.

To summarize, the results of these comparisons on Feed 1 indicate that good agreement can be obtained in null depths even down to levels as low as -35 dB.

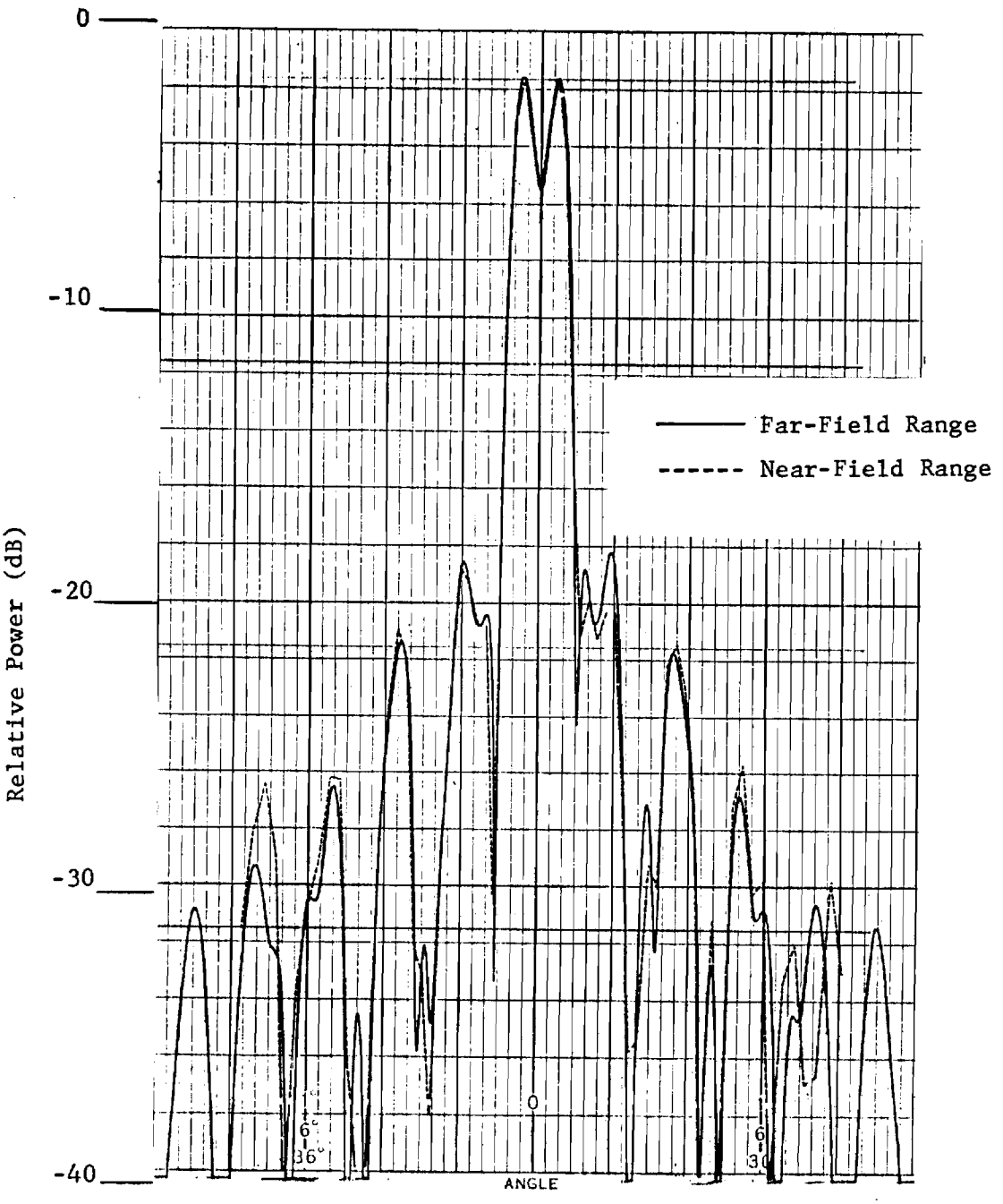

Figure 7-28. Feed 1 sum pattern principal azimuth plane cuts taken on near-field and far-field ranges, 12 degrees per major division.

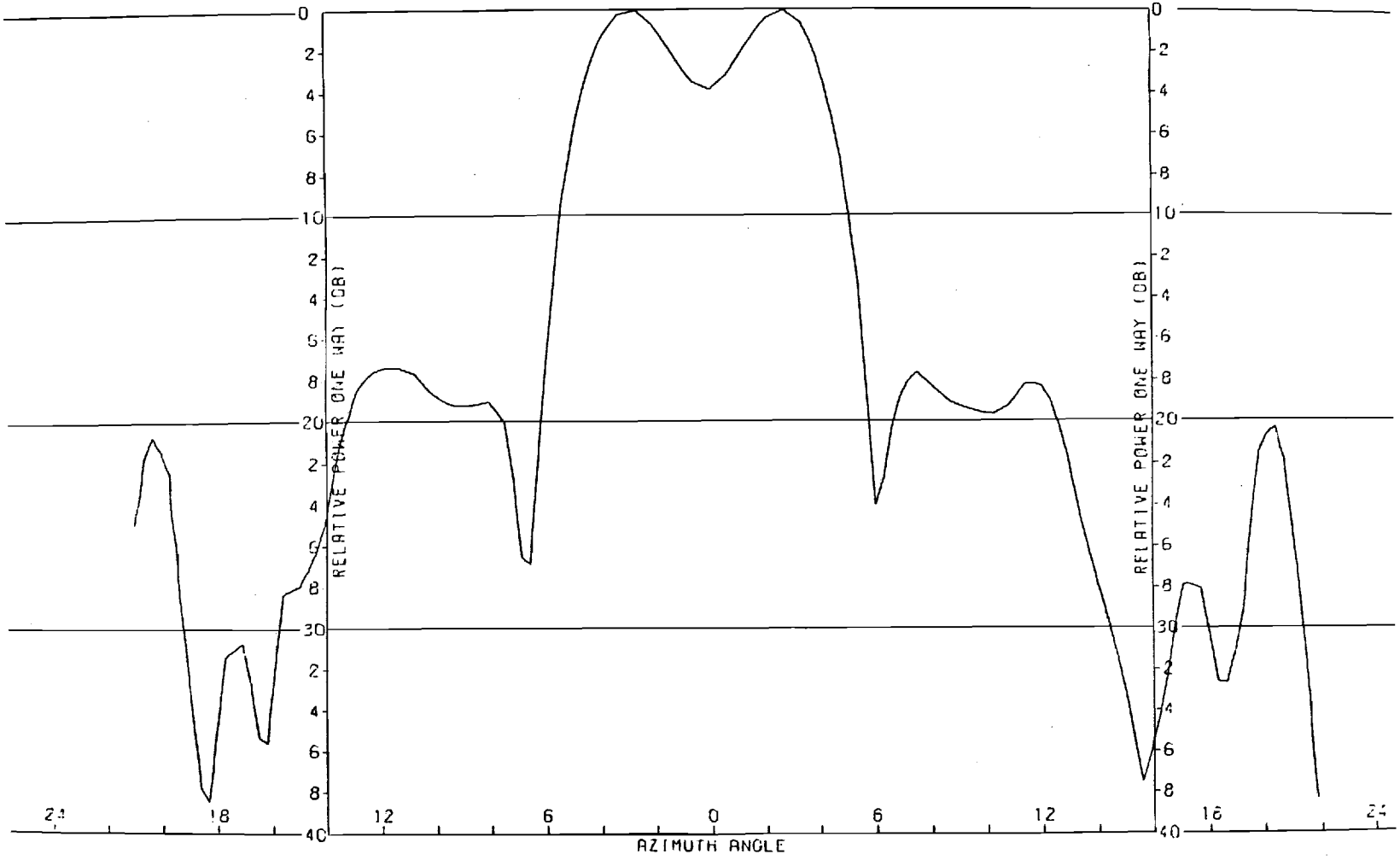

Figure 7-29. Feed 1 sum pattern principal azimuth plane cut from near-field range data processed for increased resolution.

7.3 Summary

Table 7-2 summarizes comparable accuracies achieved on the near- and far-field ranges. Over the width of the main beams no difference is observed in the various pattern determinations. The first few sidelobes that fall in the range of -20 dB show errors on the order of 0.25 dB. On sidelobes at the -40 dB level errors in the order of 2 dB are observed. The null depth of the difference pattern is determined to better than 1 dB at the -25 dB level. Boresight error is on the order of .02 degree or .5 milliradians. The accuracy with which the difference pattern null can be determined could be improved by more resolution in the system. Similarly the RMS sidelobe values could also be improved with greater resolution and possibly with a clearing up of the manner in which cross-polarized components are treated.

The cuts and tables summarizing the results indicate that the near-field technique is indeed capable of measuring antenna pattern parameters to an accuracy comparable to those encountered on far-field ranges. Moreover, the details of pattern obtainable, particularly with respect to cross-polarized components, is considerably greater on the near-field than is normally achievable on a far-field range.

TABLE 7-2

NEAR-FIELD/FAR-FIELD COMPARISON

MAIN BEAM	NO DIFFERENCE
FIRST FEW SIDELOBES	0.25 db
BORESIGHT	0.02 DEGREES
NULL DEPTH	1 db at -25 db LEVEL
RMS SIDELOBES	2 db at -40 db LEVEL

SECTION 8

COMPARISON OF NEAR- AND FAR-FIELD MEASUREMENT APPROACHES

8.1 Comparison of Measurement Methods

Virtually all antenna patterns have historically been measured on far-field ranges, and few engineers argue about its credibility. The several recent advances referred to in Section 2 of this report have made it now possible to achieve results of at least comparable accuracy on a properly constructed near-field range. The technical results as shown in this work can be made equal. A choice between one or the other technique must be based on such questions as physical size of antenna, amount of pattern documentation required, existing available facilities, schedule, etc.

It is clear that if the antenna to be measured is a simple horn and if only main beam gain is required, then given an available far-field range, the desired data can be most quickly obtained there. If, however, much detail is desired on the complete antenna pattern, then even for a simple horn, the near-field technique may be most expedient.

To put it in other terms, on the far-field range where the desired data is directly obtained one measures only those parameters desired; simple requirements mean small amounts of data. On the near-field range, the calculation of any single pattern parameter requires the collection of an appreciable number of data points for subsequent data reduction. Thus the near-field technique is less attractive when simple pattern parameters are desired. The great strength of the near-field measurement technique lies in its ability to collect an enormous amount of data in a highly efficient

manner. Such data, once collected, can be subsequently processed to yield output in literally any format of far-field pattern parameters. Thus as the required documentation of far-field pattern increases the near-field approach rapidly becomes a more efficient means of collecting data .

In addition to considerations of relative efficiency of data acquisition there are decided physical (and fiscal) advantages of the near-field approach.

- The measurements may be carried out indoors in an anechoic room or enclosure. In addition to the greater comfort of the range personnel this allows measurements to be conducted independent of whatever weather conditions prevail outdoors. Rain delays do not occur.
- Environmental conditions of heat or cold can be imposed on the antenna in its indoor facility by artificial means, and measurements can be taken under full environmental conditions (though propagation path affects must be independently accounted for). It is almost impossible to measure patterns on a far-field range under environmental extremes unless one is prepared to await Mother Nature's imposition of the prescribed conditions.
- Phased array antennas are designed and constructed to operate in a fixed position, and therefore measurements of their patterns are best done in a fixed position. Mechanical deformations that may take place as the antenna is rotated on a mount introduce extraneous physical changes that are not a part of the real world conditions under which the system is ultimately to function.

- In the case of very large phased arrays the sheer mass of the structure is a great deterrant to locating at a remote far-field range facility, and it is more advantageous to bring the range to the antenna instead.
- The cross polarized far-field pattern is quite tedious to record on a conventional range and as a result is frequently inadequately characterized. The importance of cross polarized sidelobes that may reach appreciable levels far off-axis should not be underestimated in ECM considerations. The near-field technique provides complete far-field cross polarized patterns "at no extra charge" as indicated by Figures 6-10 and 6-11.
- In recording elevation cuts on far-field ranges the problems encountered from main beam illumination of ground reflections lead to a requirement to physically rotate the antenna or depend on symmetry arguments. In the near-field approach the angular coverage for + and - elevation angles can be equally easily obtained.

The comparison of near- versus far-field measurements must also involve the relative capitol cost of establishing each facility. Briefly, the microwave electronics of the two facilities is essentially the same. Both utilize a source and a phase and amplitude receiver. The highly instrumented and more efficient far-field ranges also employ A-D converters and magnetic tape for recording data. The capitol equipment trade-off then is a comparison between the costs peculiar to the far-field range, namely the real estate for the range itself and the mechanical positioner for the test antenna, and those peculiar to the near-field range, that is the X-Y-Z positioner and the anechoic room.

8.2 Recommendations

In measurement capability the two techniques have been proven in this study to be equally capable in yielding point-to-point accuracy. These measurements were carried out on a simple dish antenna whose phase and amplitude are relatively well behaved. It remains to be demonstrated that equal accuracy is achievable when the fine grained near-field ripple characteristic of phased array antennas is encountered. While the theory behind the measurements clearly applies to any aperture, the effect of errors on such a near-field pattern remains to be demonstrated experimentally.

Further refinement of the near-field computational methods are necessary to smooth the point-to-point nature of the plots. It has been demonstrated in Section 6 that by continued filtering the resolution of plots can be improved at some sacrifice in angular coverage. In the present state of the theory such filtering can be accomplished only near zero wavenumber (boresight). Further development of the theory is needed to extend this capability to beams steered off boresight. Even without additional filtering, improvements in the manner of processing data could double the number of computed points of the far-field pattern and thereby improve resolution.

To make the near-field approach more acceptable to the systems engineer and more generally applicable to antenna pattern measurements several extensions of the present work are warranted.

- The theory should be further developed to allow increasing resolution at arbitrary directions. For a phased array antenna an accurate description of the details of the

difference pattern null as a function of scan angle requires that the mathematical reduction of data allow for the same degree of resolution to be achievable at arbitrary beam positions off boresight.

- Experimental verification is needed of the near-field technique applied to a phased array with its larger energy storage near the plane of the array and with its more rapid variation of phase across the face of the array.
- Limitations imposed by receiver recovery time need further examination. This limitation becomes all the more important in phased array systems where beam switching between sampling points might be employed.
- Further mathematical development is required to modify the data processing programs so as to reduce the memory capacity needed. In its present form one half of the data points are truncated in the computation of the far-field pattern, because of limitations of computer storage. Further developments of the program should make the truncation unnecessary and thus double the number of calculated points.

Because of the controlled environment in which near-field measurements can be conducted many systems problems could be conveniently studied by this technique. Effects such as spill-over and beam defocusing could be readily studied. The near-field technique promises to be an interesting test bed for such areas of antenna study.

APPENDIX A

COMPLETE SIMULATION RESULTS

The graphs contained in this appendix constitute a summary of the complete results of the simulation study described in detail in Section 3. Each point on these graphs represents one simulation run. The calculated points are connected by straight line segments to construct the curves. On each graph computed far-field parameters are plotted on the ordinate as a function of the particular near field error plotted on the abscissa. For a detailed discussion of the simulation model as well as of the modelling of various near-field errors the reader is referred to Section 3 where some of the more interesting results are also discussed.

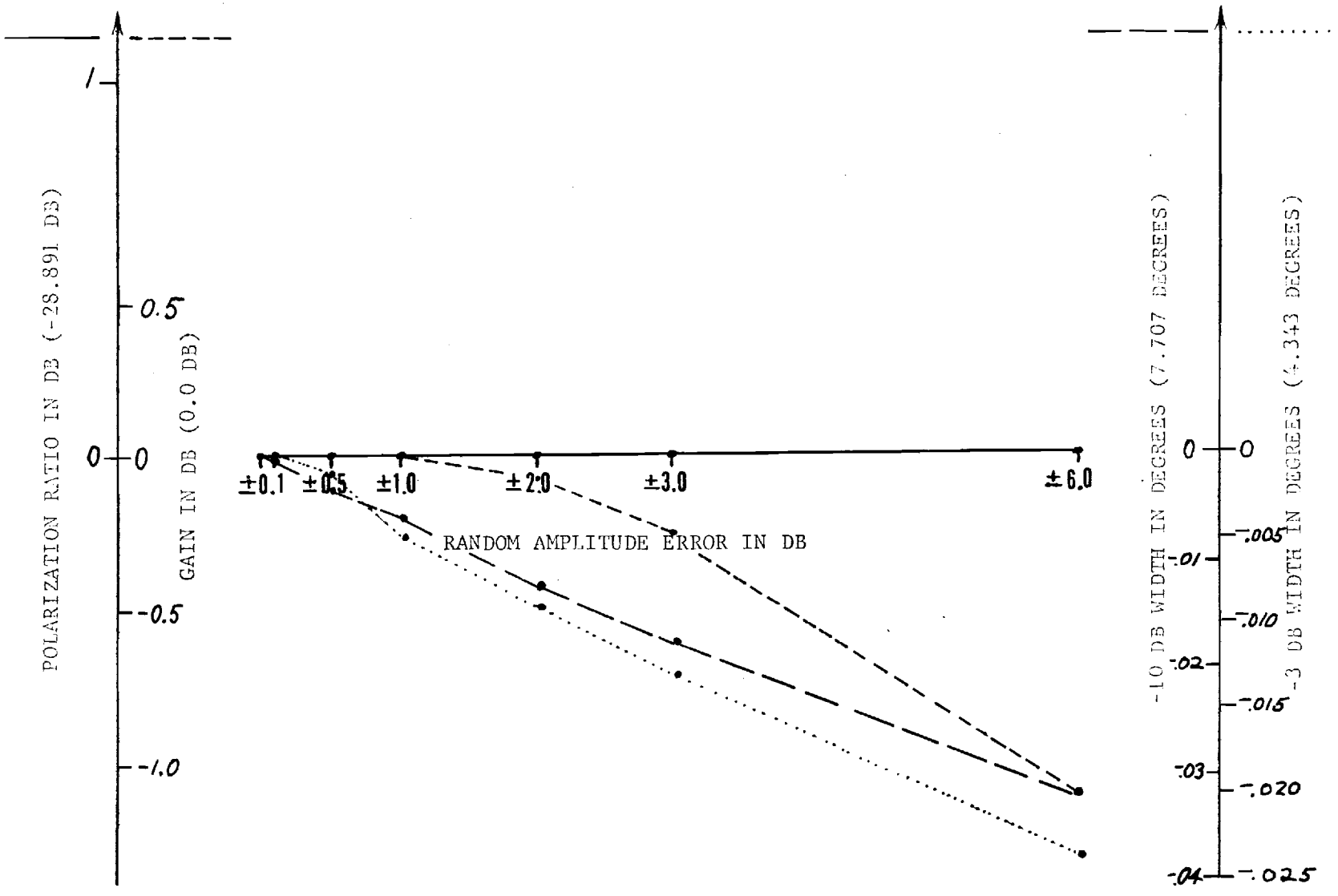

FIGURE A-1. ERRORS IN SUM PATTERN MAIN BEAM PARAMETERS (TRUE VALUES)

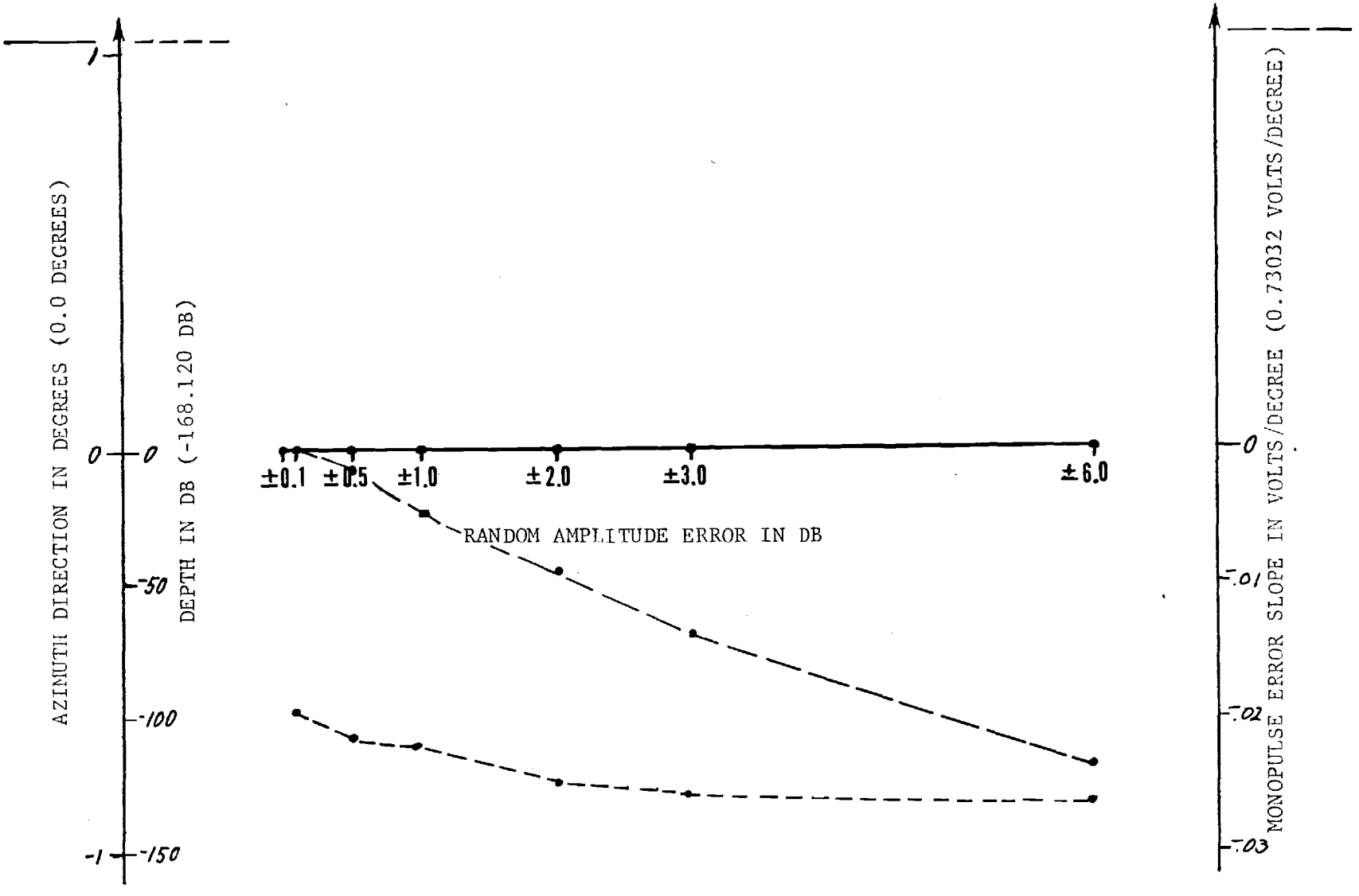

FIGURE A-2. ERRORS IN DIFFERENCE PATTERN NULL PARAMETERS (TRUE VALUES)

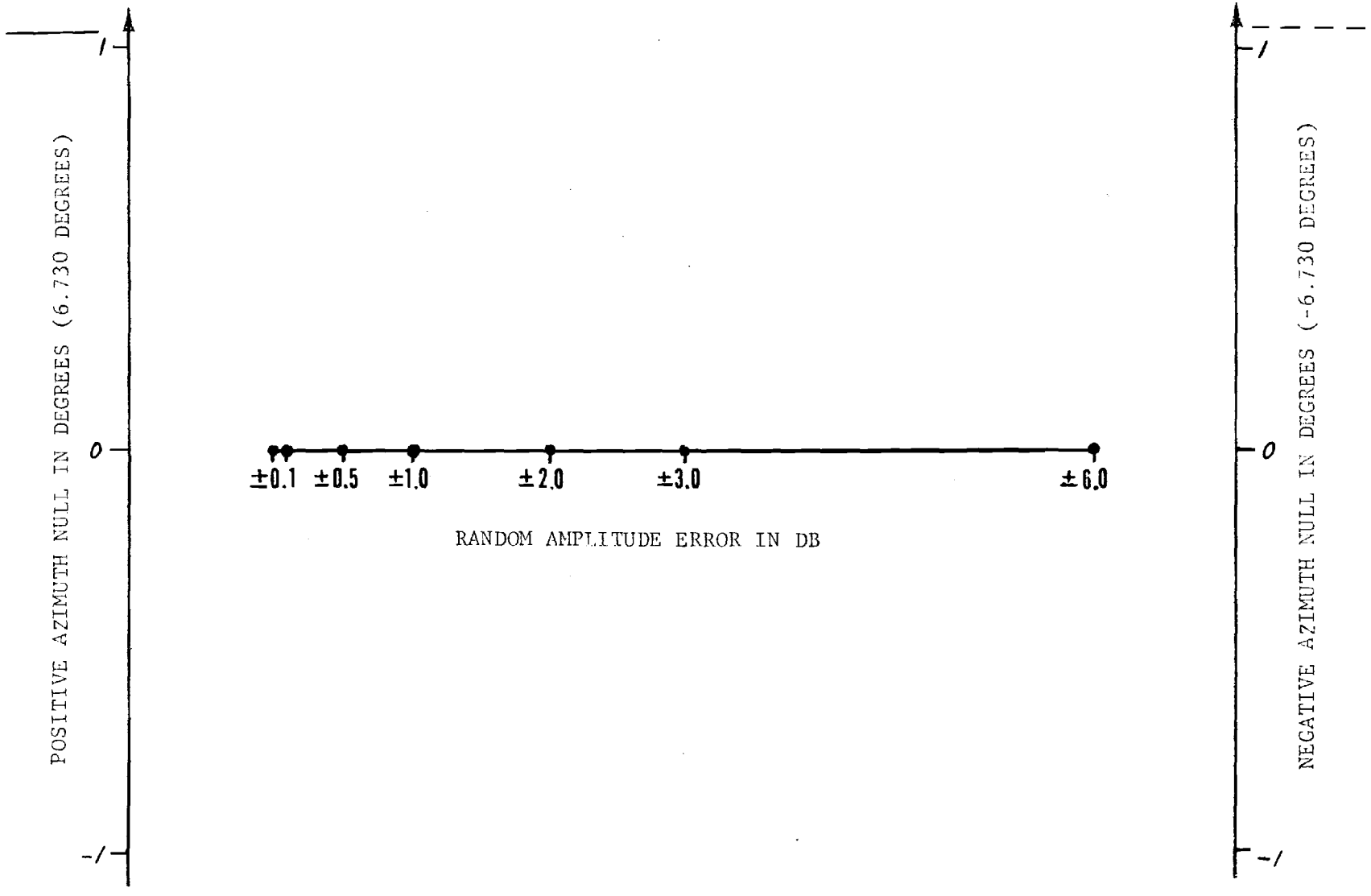

FIGURE A-3. ERRORS IN SUM PATTERN FIRST NULL LOCATIONS (TRUE VALUES)

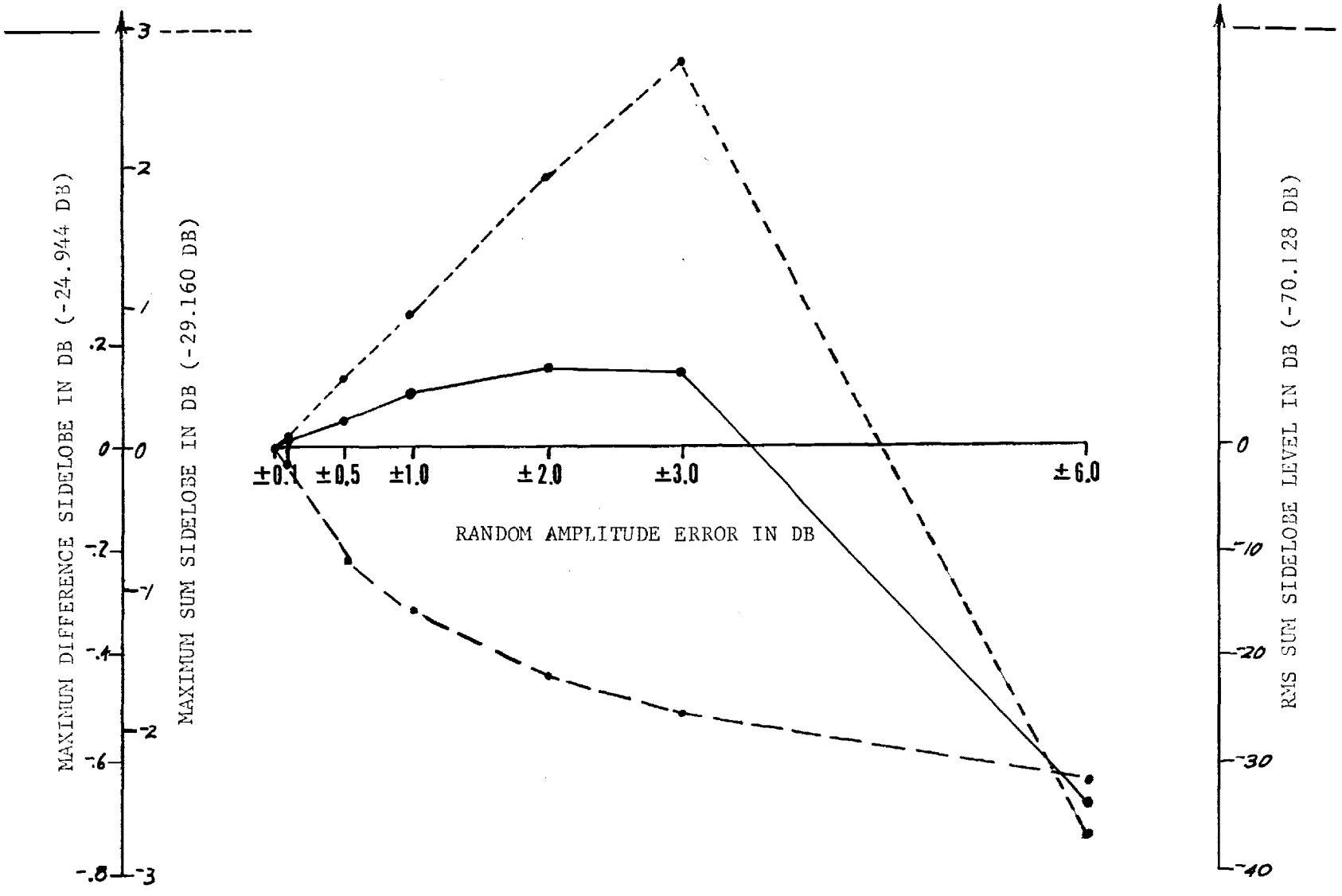

FIGURE A-4. ERRORS IN SIDELOBE LEVELS (TRUE VALUES)

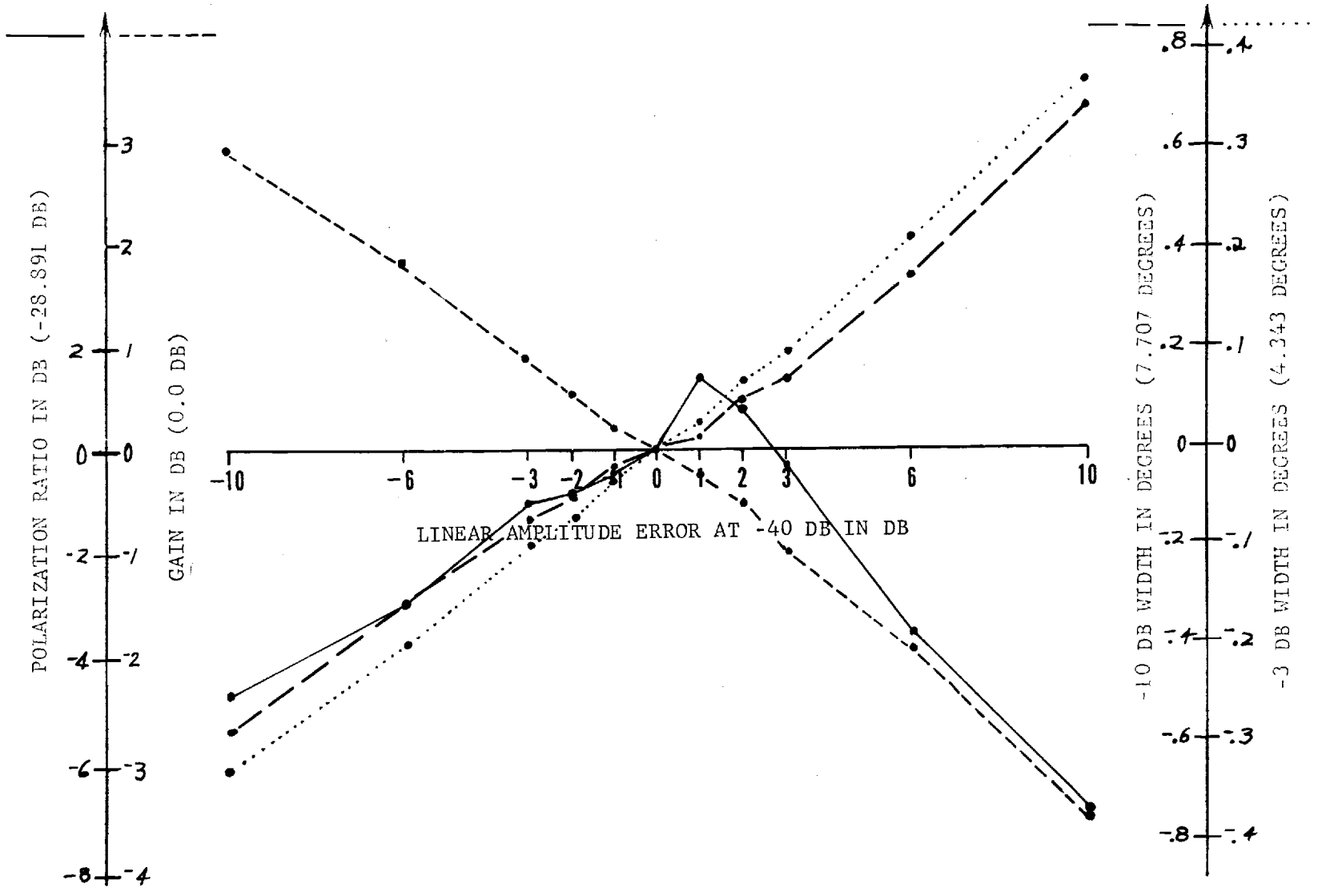

FIGURE A-5. ERRORS IN SUM PATTERN MAIN BEAM PARAMETERS (TRUE VALUES)

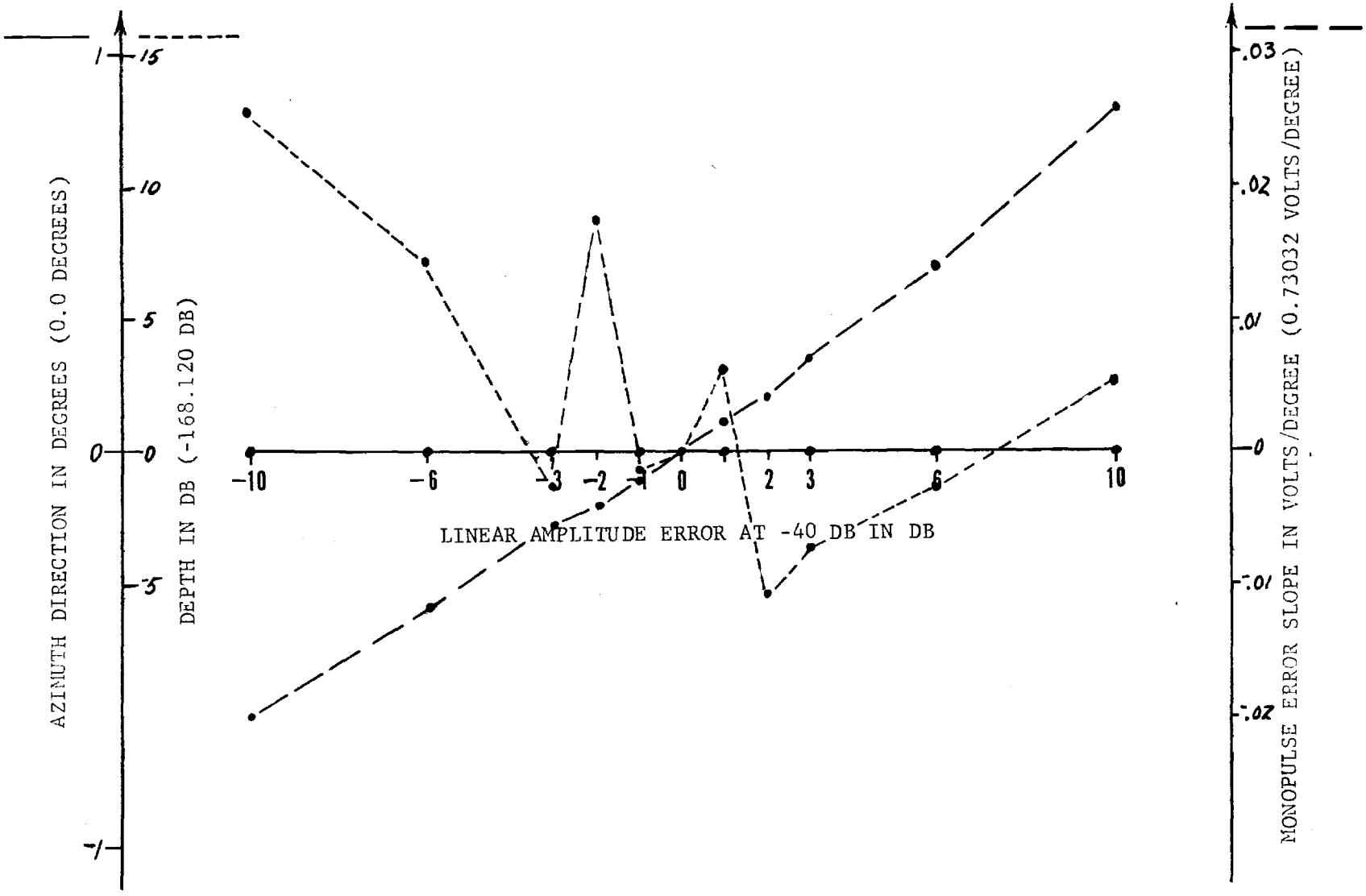

FIGURE A-6. ERRORS IN DIFFERENCE PATTERN NULL PARAMETERS (TRUE VALUES)

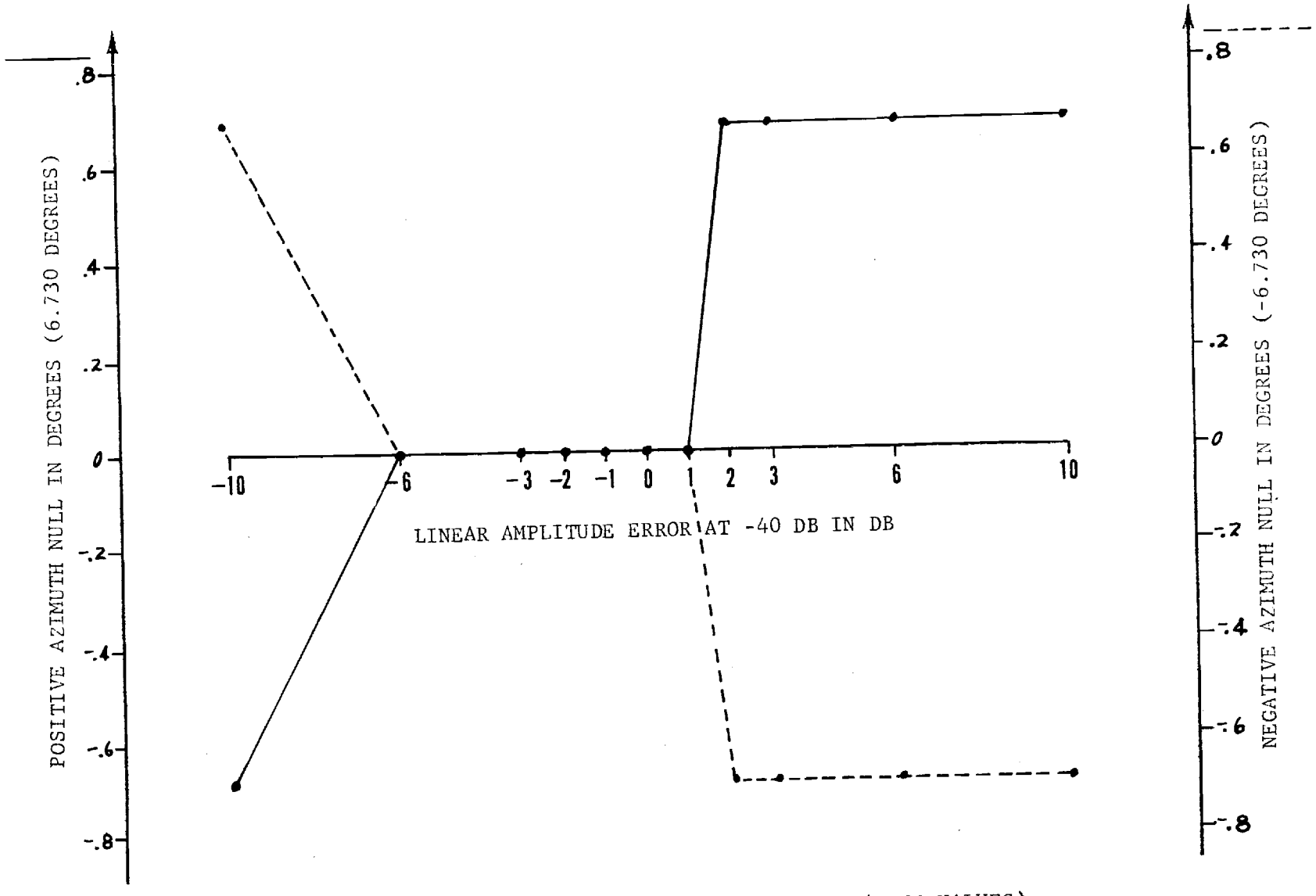

FIGURE A-7. ERRORS IN SUM PATTERN FIRST NULL LOCATIONS (TRUE VALUES)

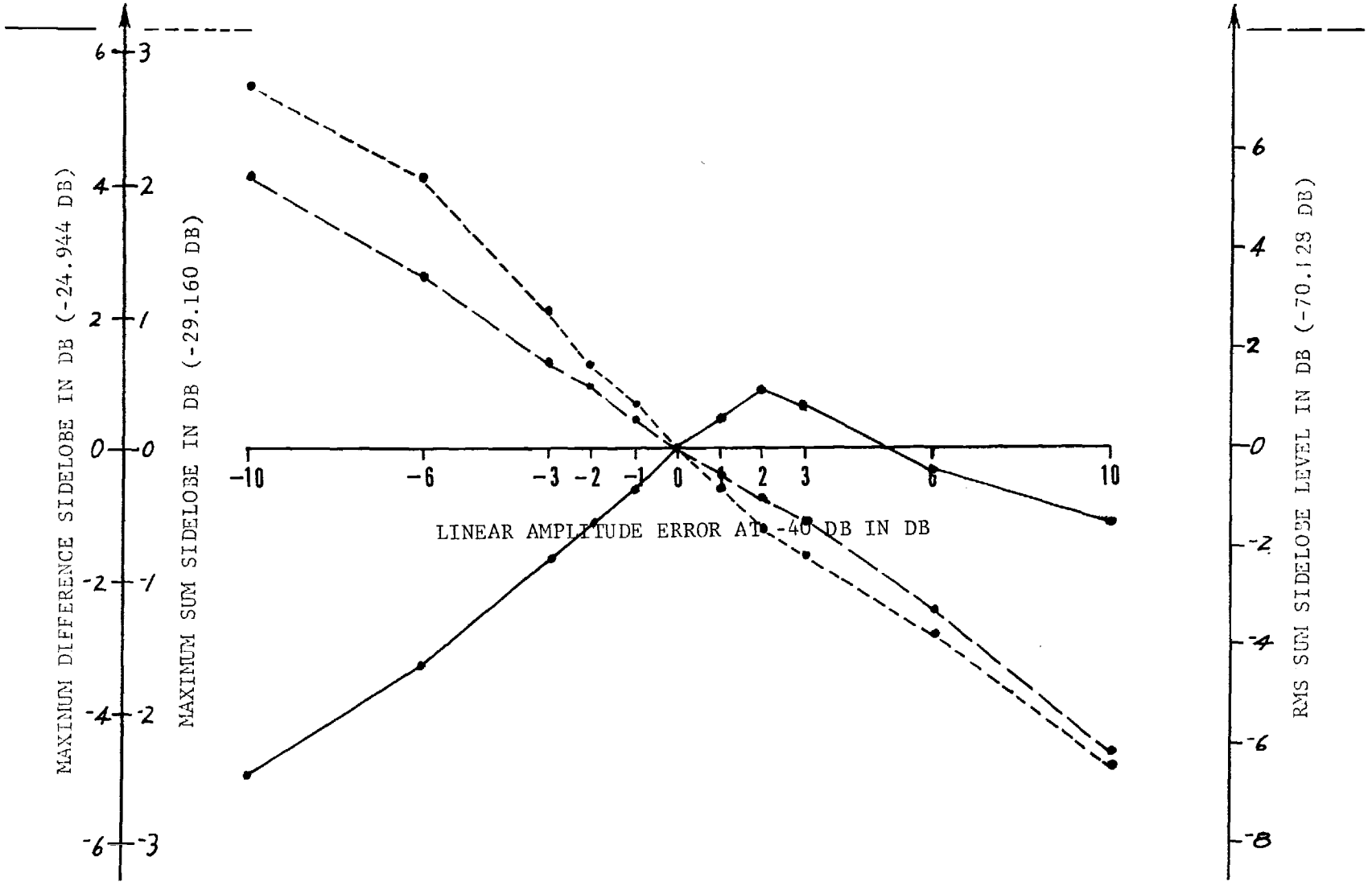

FIGURE A-8. ERRORS IN SIDELOBE LEVELS (TRUE VALUES)

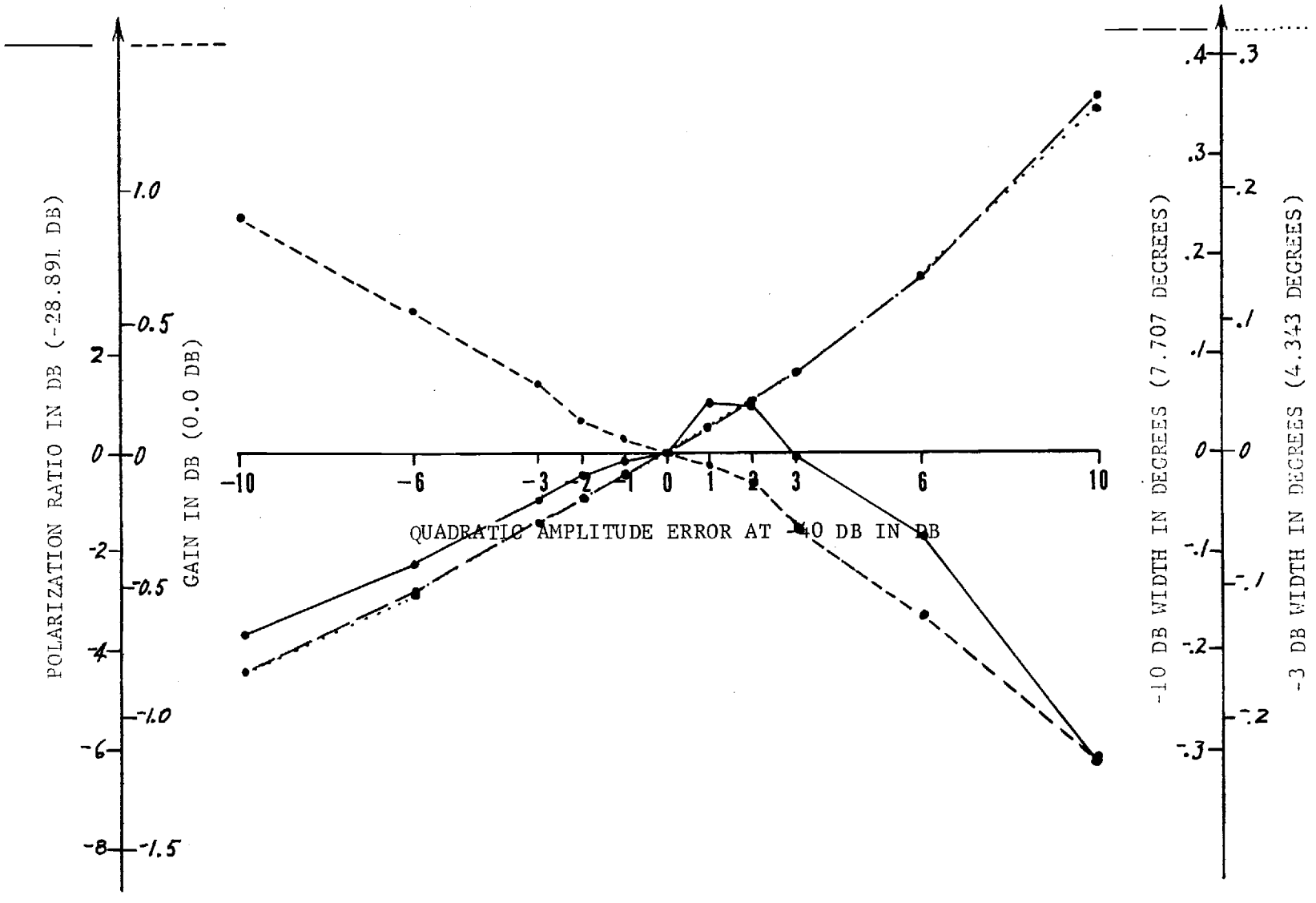

FIGURE A-9. ERRORS IN SUM PATTERN MAIN BEAM PARAMETERS (TRUE VALUES)

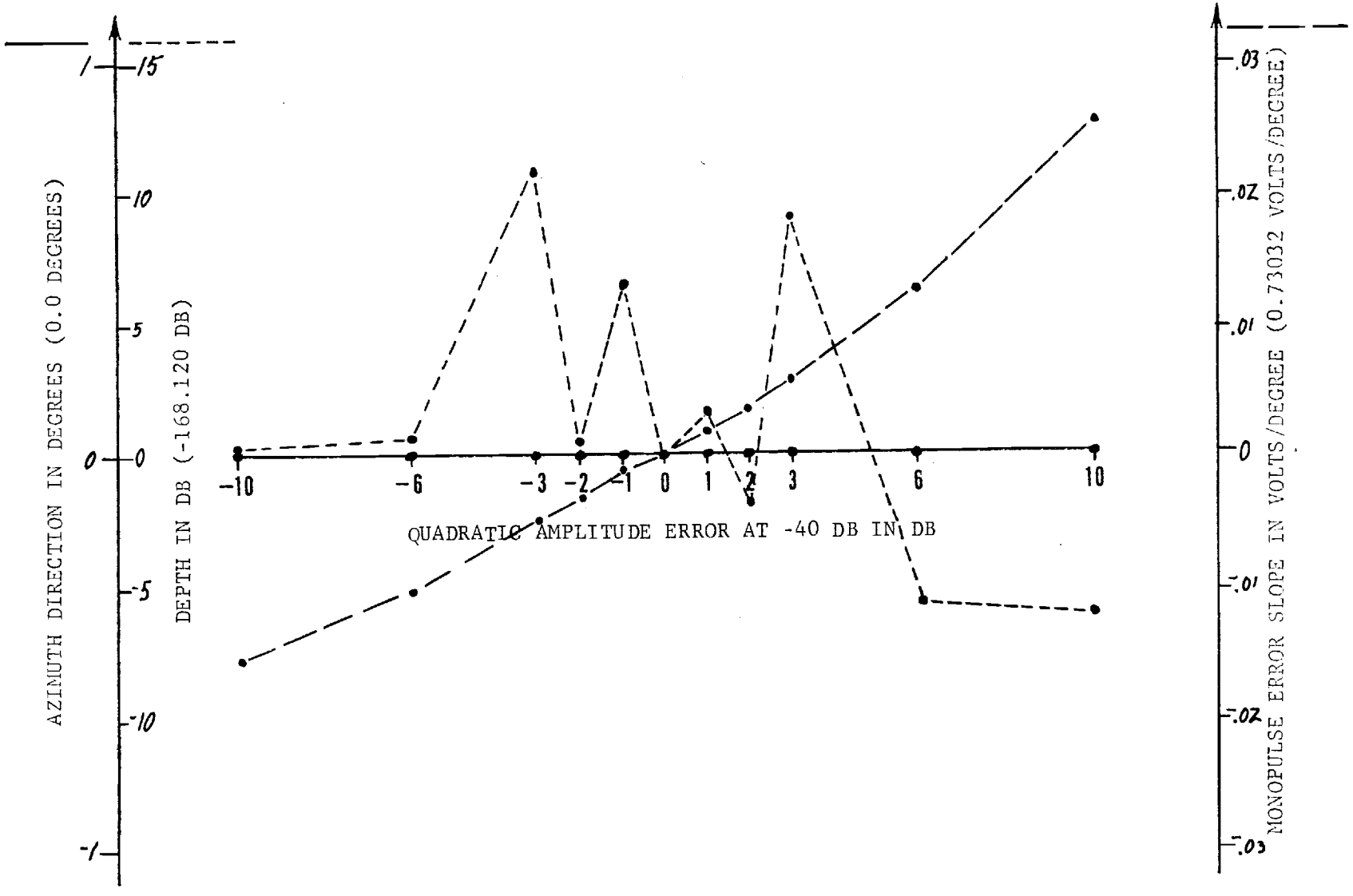

FIGURE A-10. ERRORS IN DIFFERENCE PATTERN NULL PARAMETERS (TRUE VALUES)

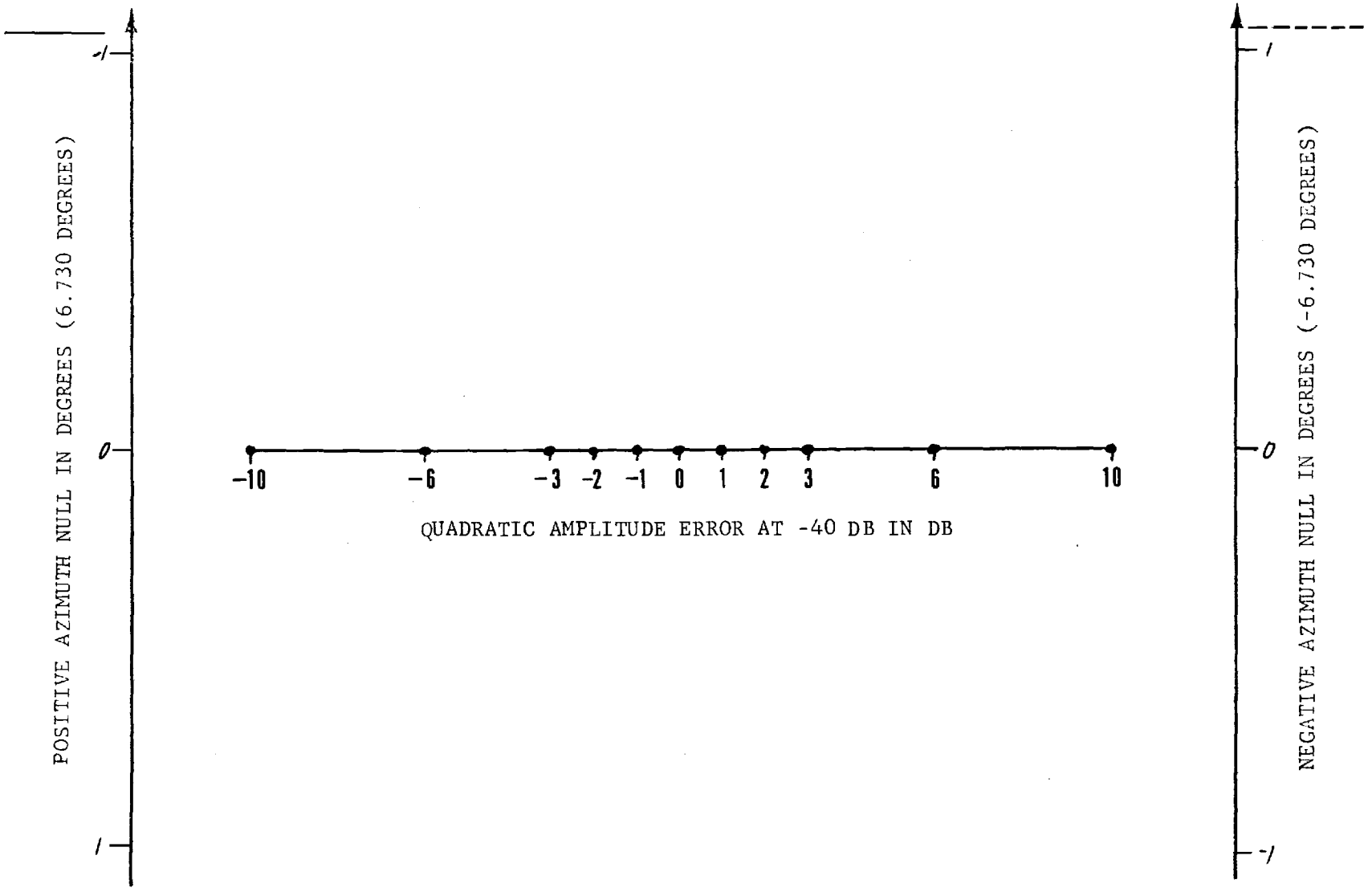

FIGURE A-11. ERRORS IN SUM PATTERN FIRST NULL LOCATIONS (TRUE VALUES)

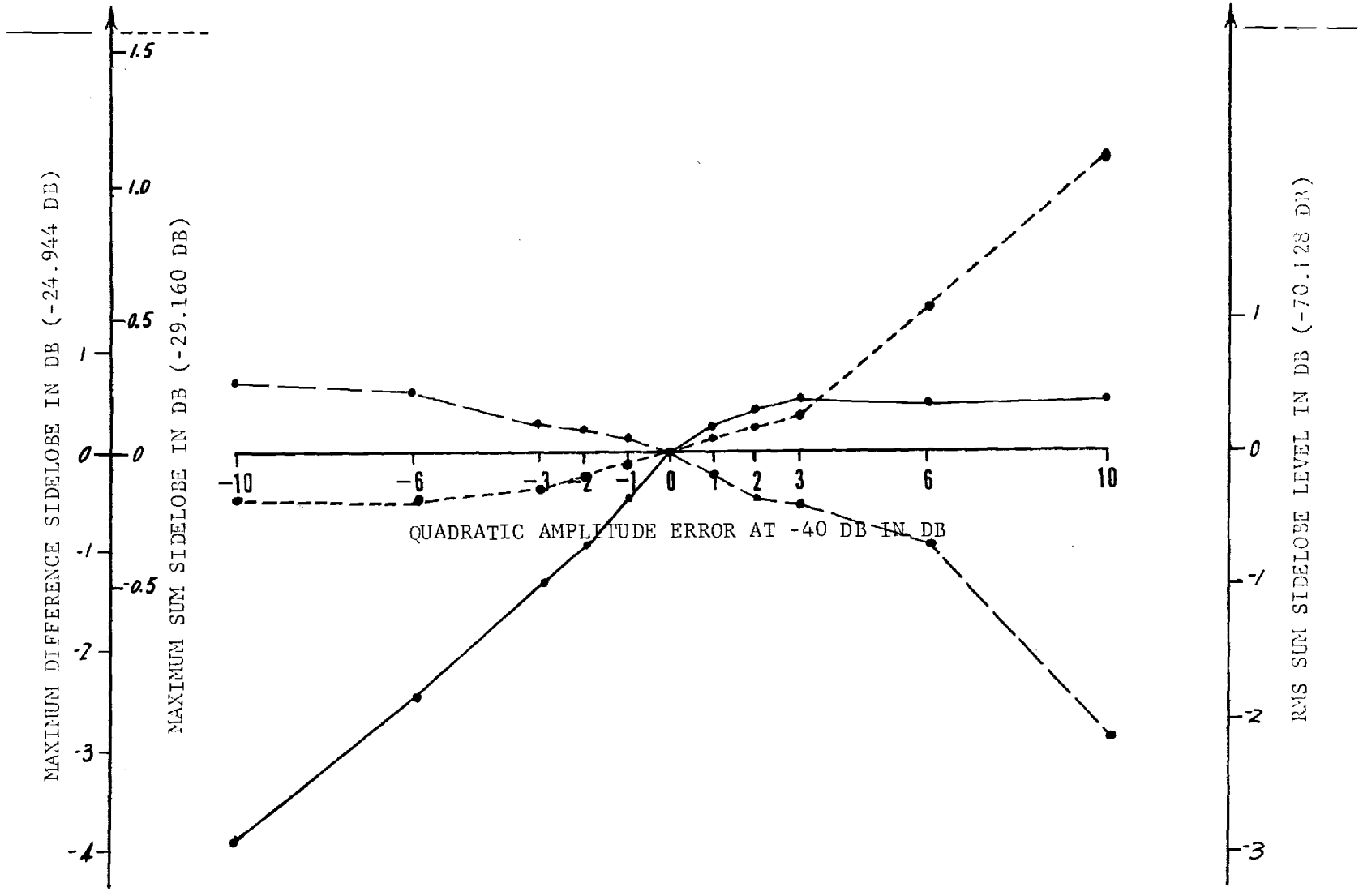

FIGURE A-12. ERRORS IN SIDELOBE LEVELS (TRUE VALUES)

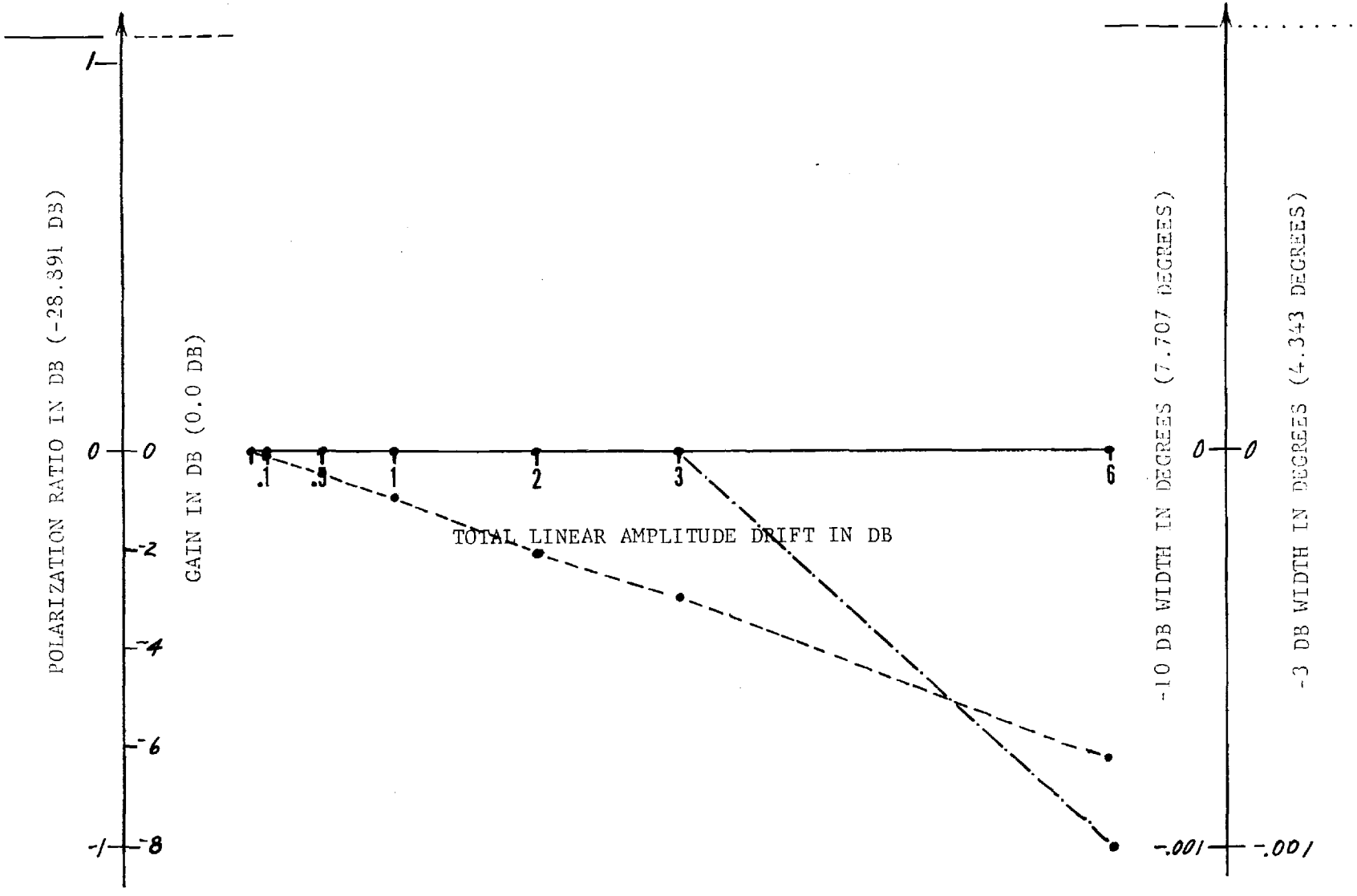

FIGURE A-13. ERRORS IN SUM PATTERN MAIN BEAM PARAMETERS (TRUE VALUES)

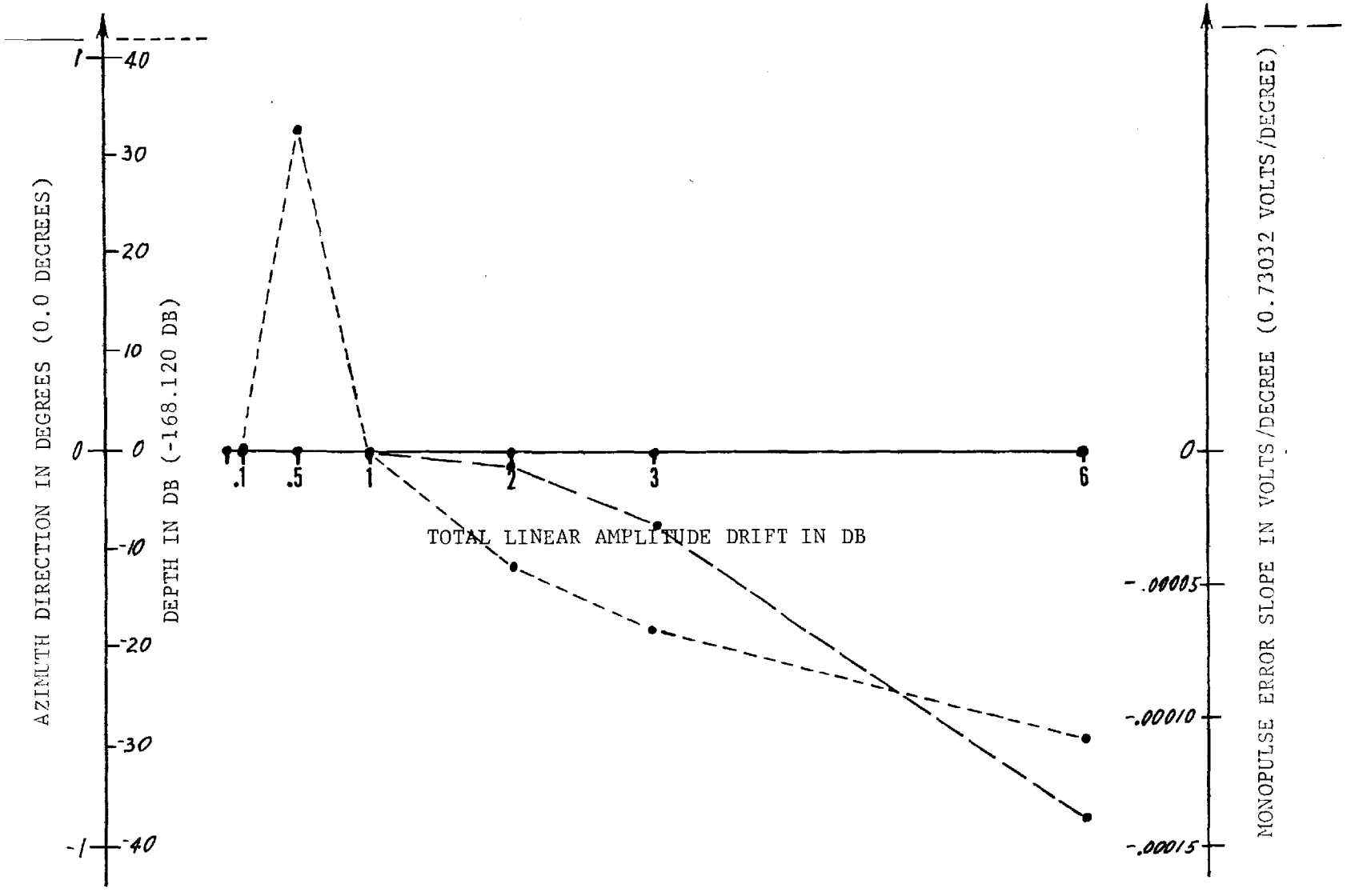

FIGURE A-14. ERRORS IN DIFFERENCE PATTERN NULL PARAMETERS (TRUE VALUES)

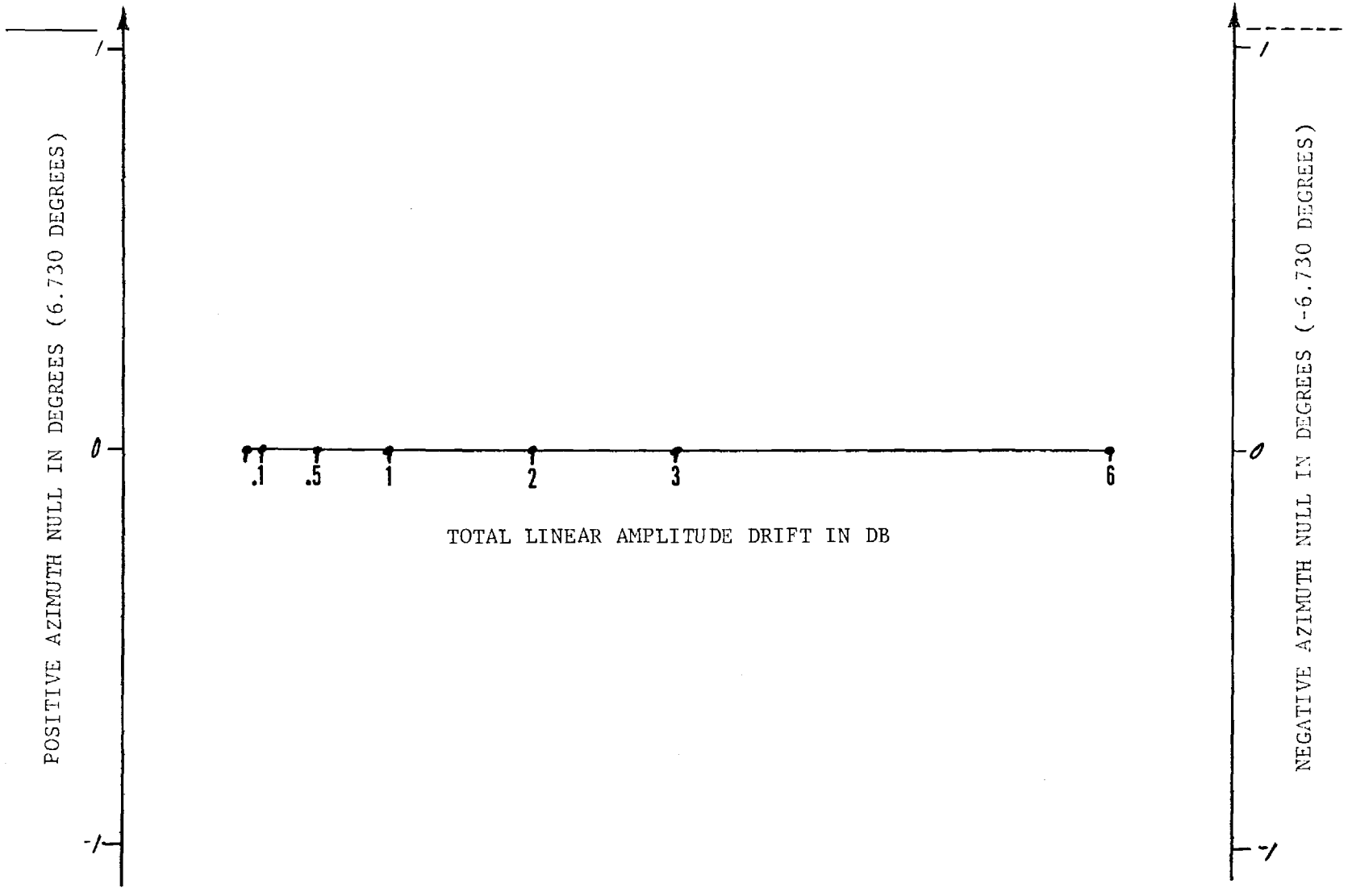

FIGURE A-15. ERRORS IN SUM PATTERN FIRST NULL LOCATIONS (TRUE VALUES)

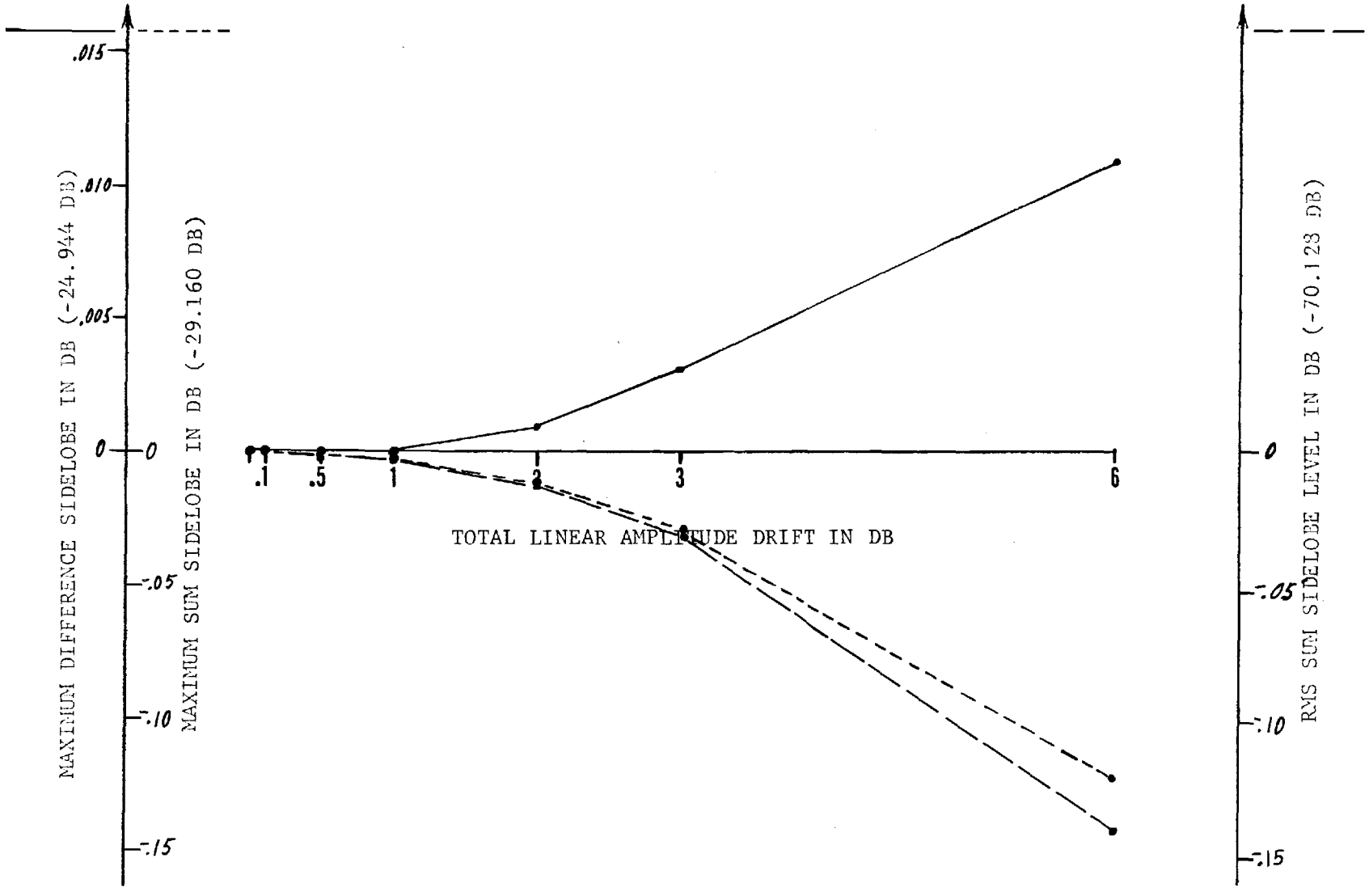

FIGURE A-16. ERRORS IN SIDELOBE LEVELS (TRUE VALUES)

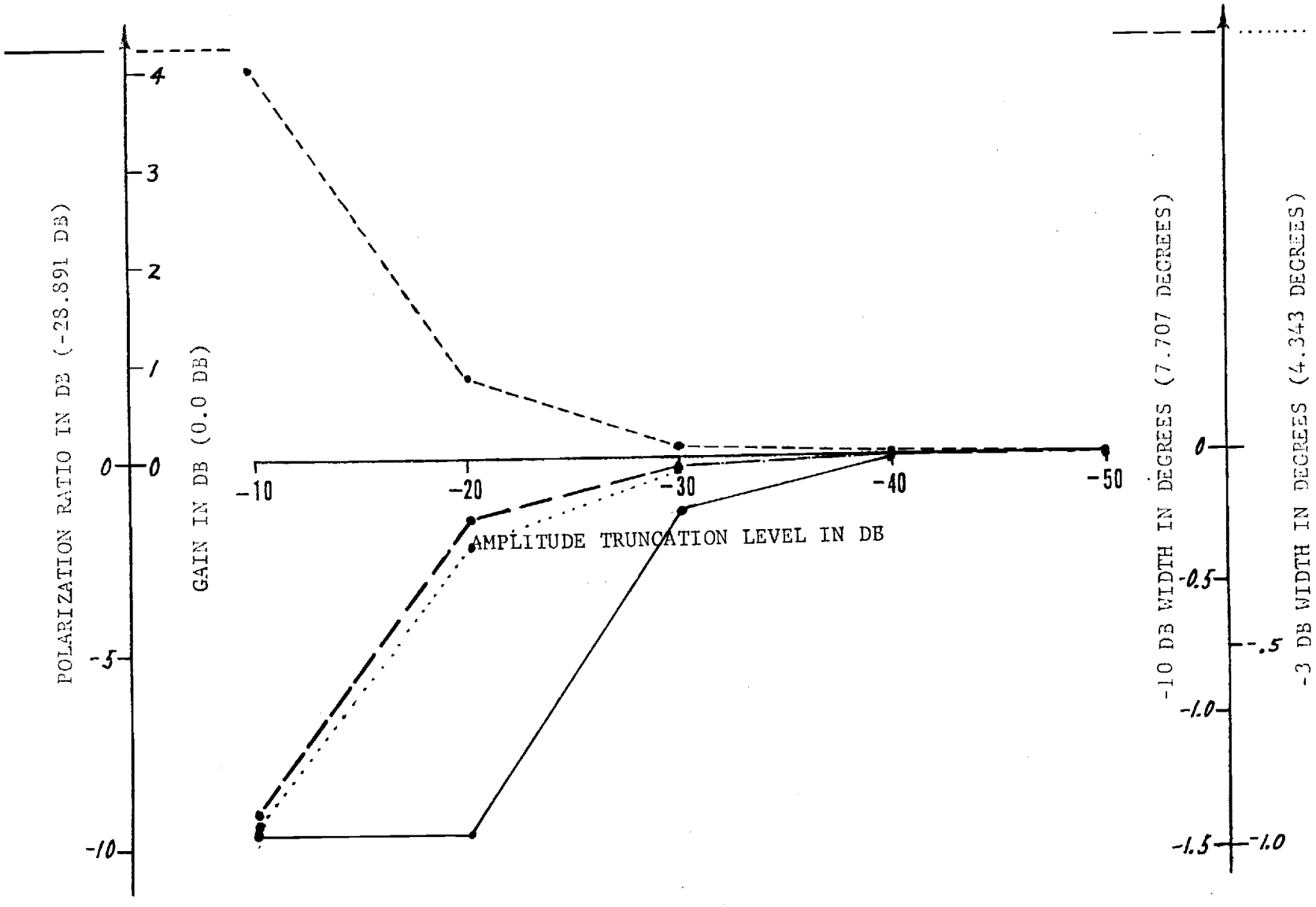

FIGURE A-17. ERRORS IN SUM PATTERN MAIN BEAM PARAMETERS (TRUE VALUES)

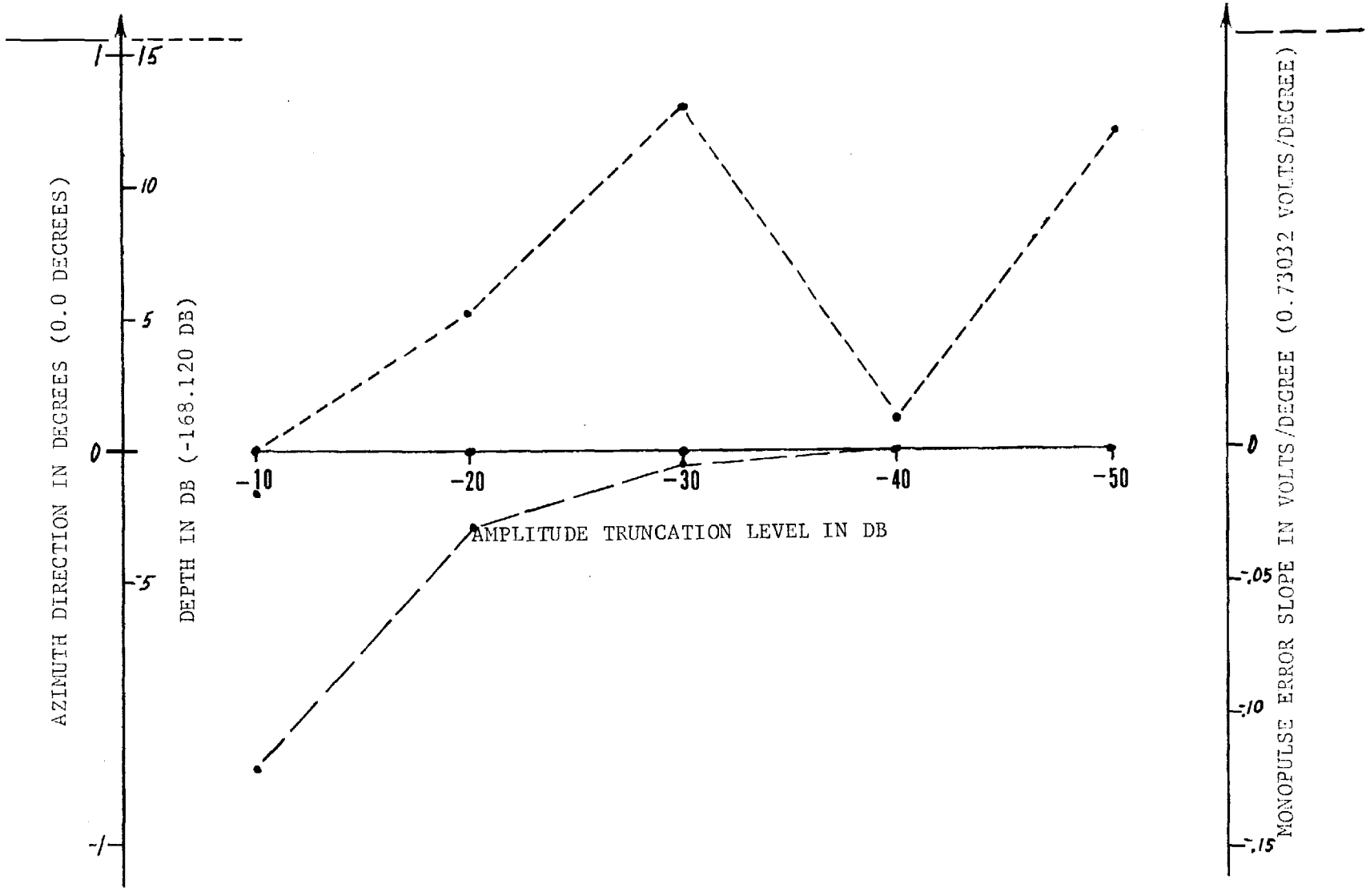

FIGURE A-18. ERRORS IN DIFFERENCE PATTERN NULL PARAMETERS (TRUE VALUES)

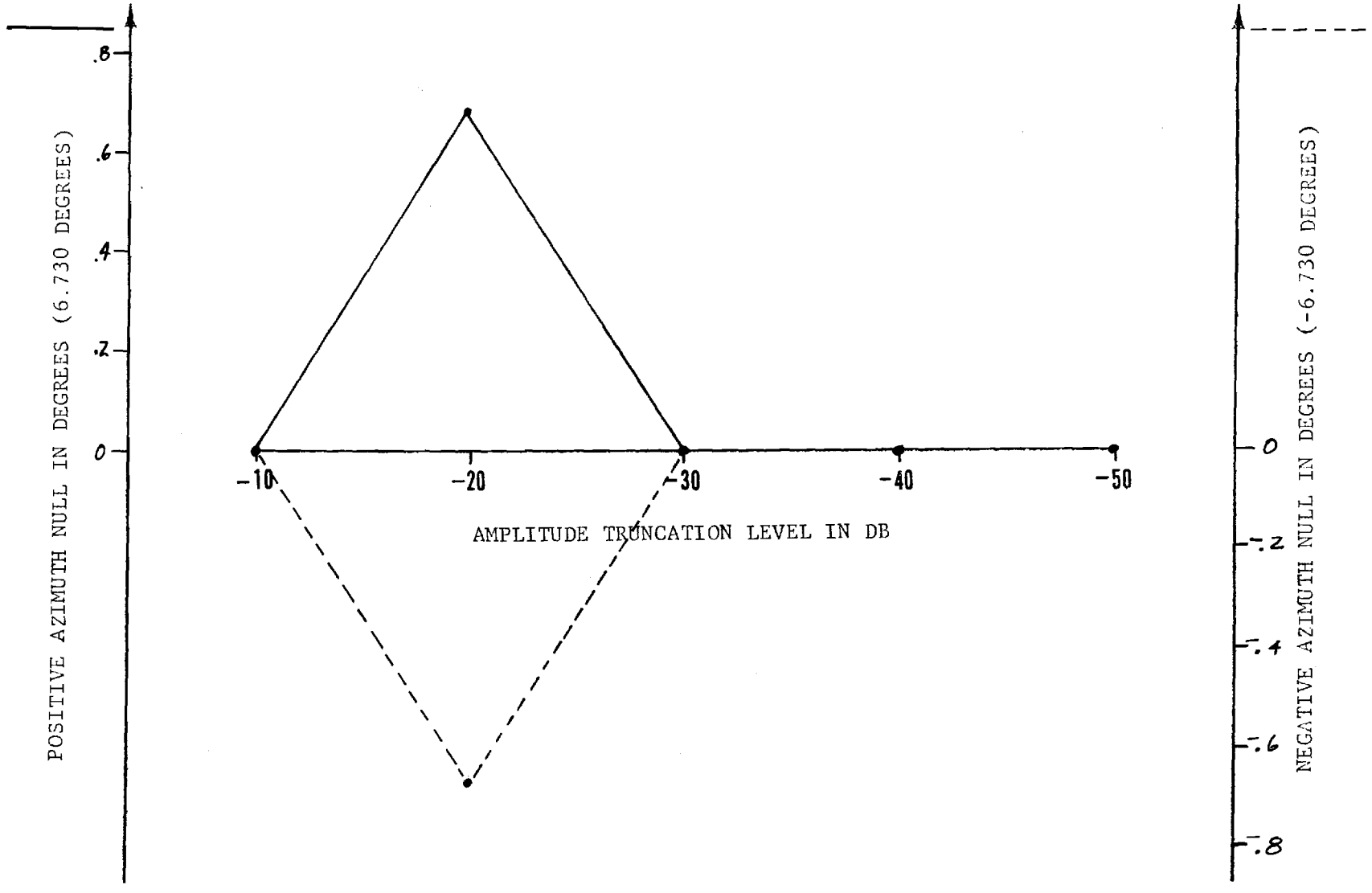

FIGURE A-19. ERRORS IN SUM PATTERN FIRST NULL LOCATIONS (TRUE VALUES)

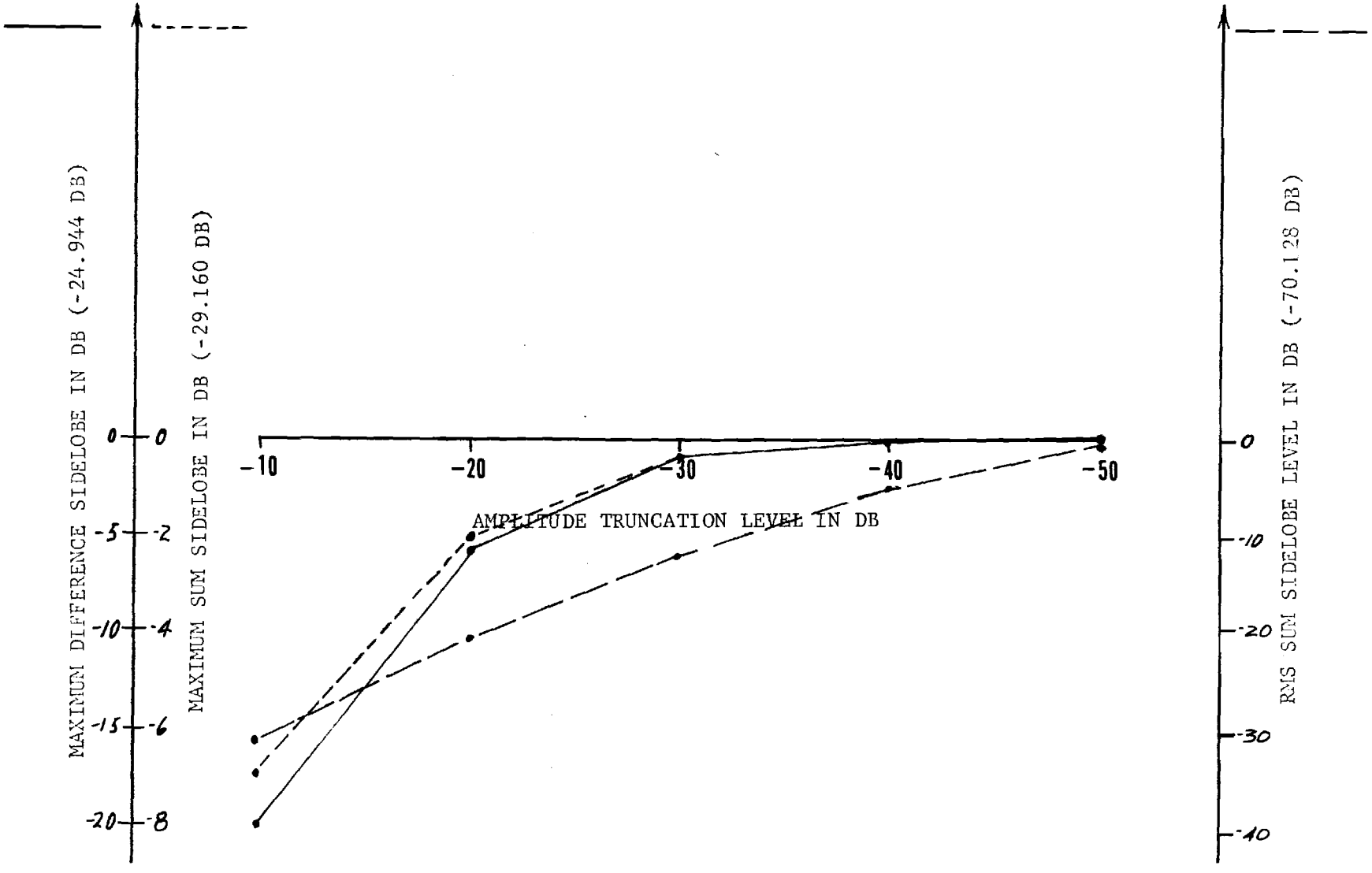

FIGURE A-20. ERRORS IN SIDELOBE LEVELS (TRUE VALUES)

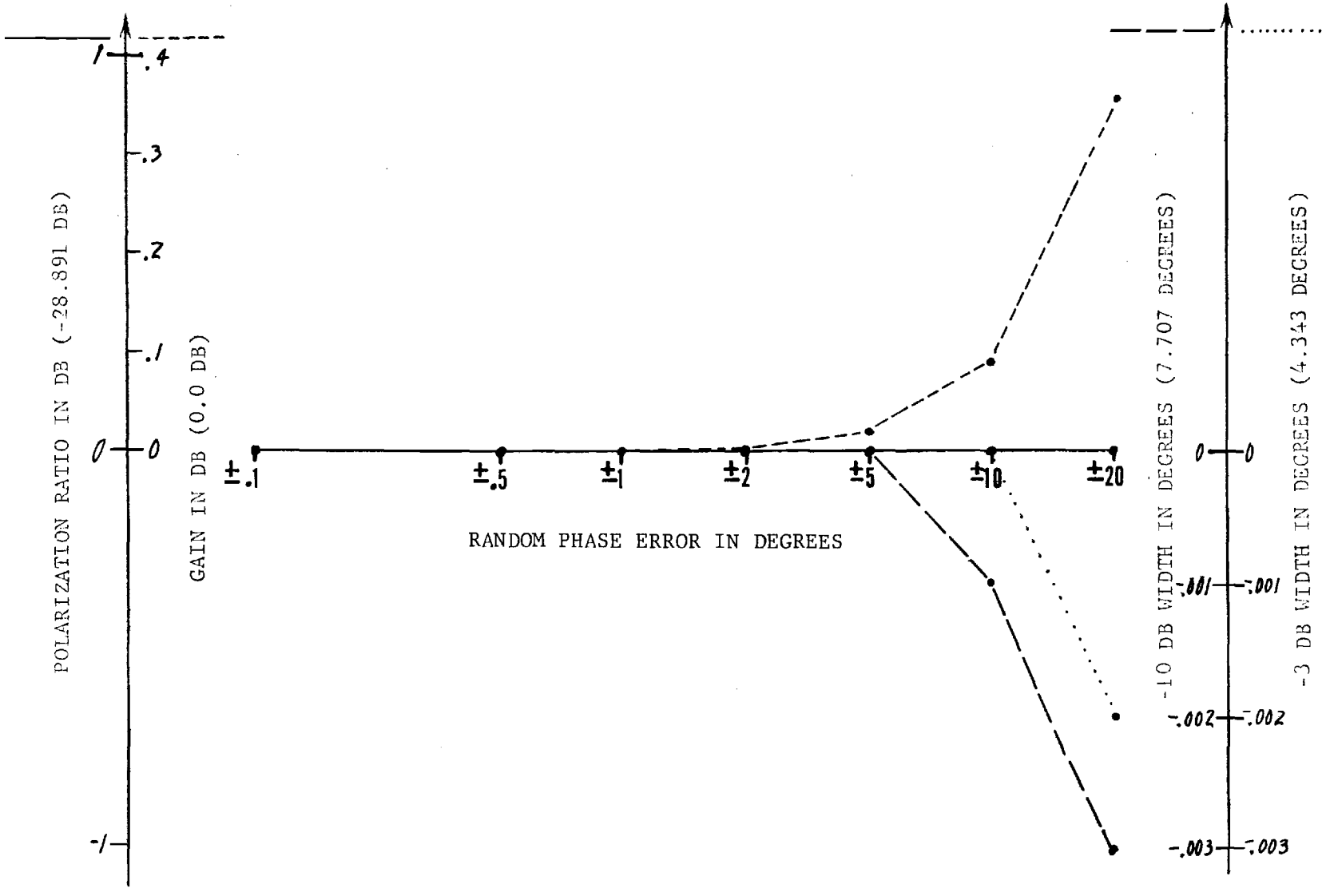

FIGURE A-21. ERRORS IN SUM PATTERN MAIN BEAM PARAMETERS (TRUE VALUES)

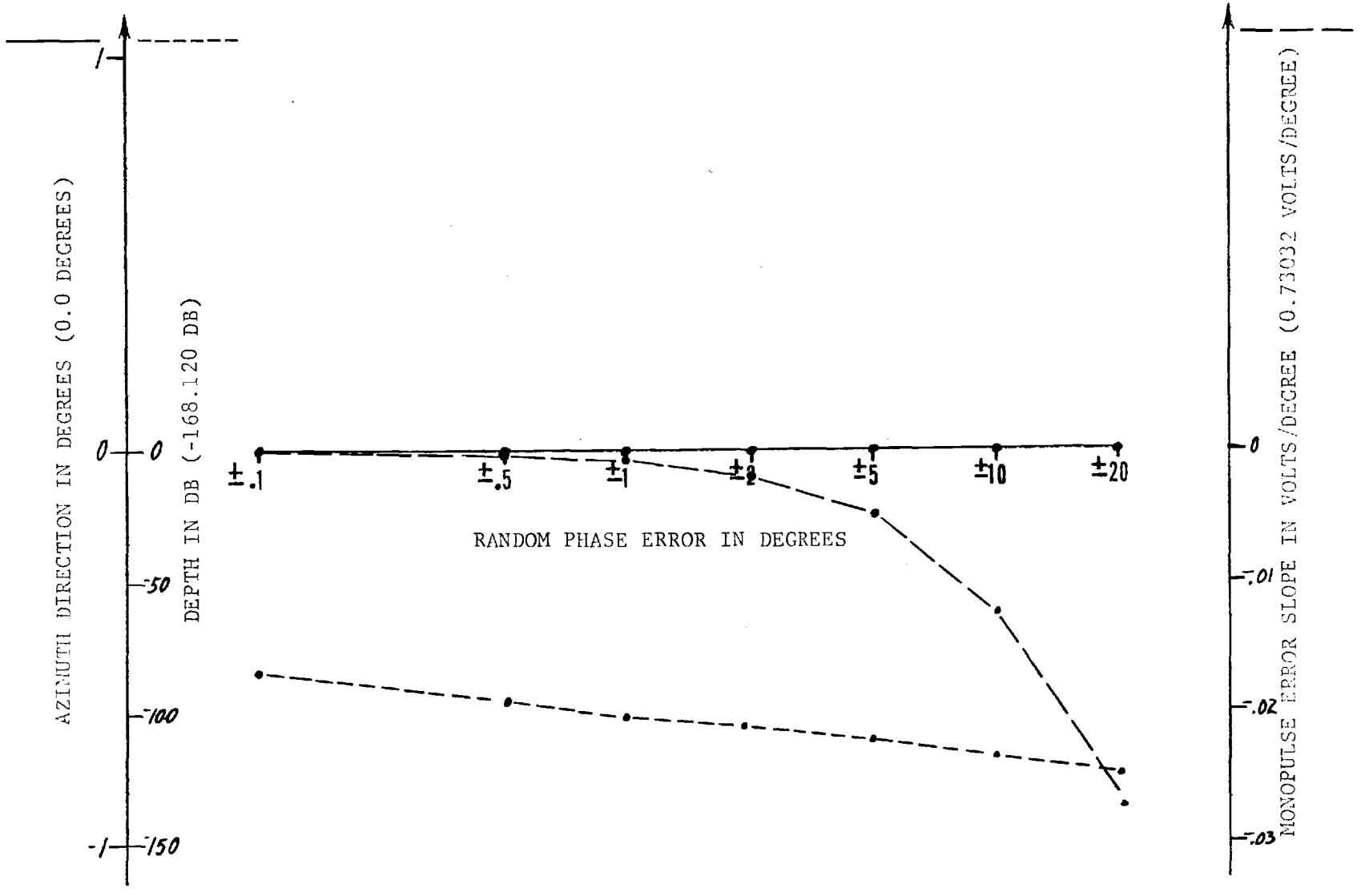

FIGURE A-22. ERRORS IN DIFFERENCE PATTERN NULL PARAMETERS (TRUE VALUES)

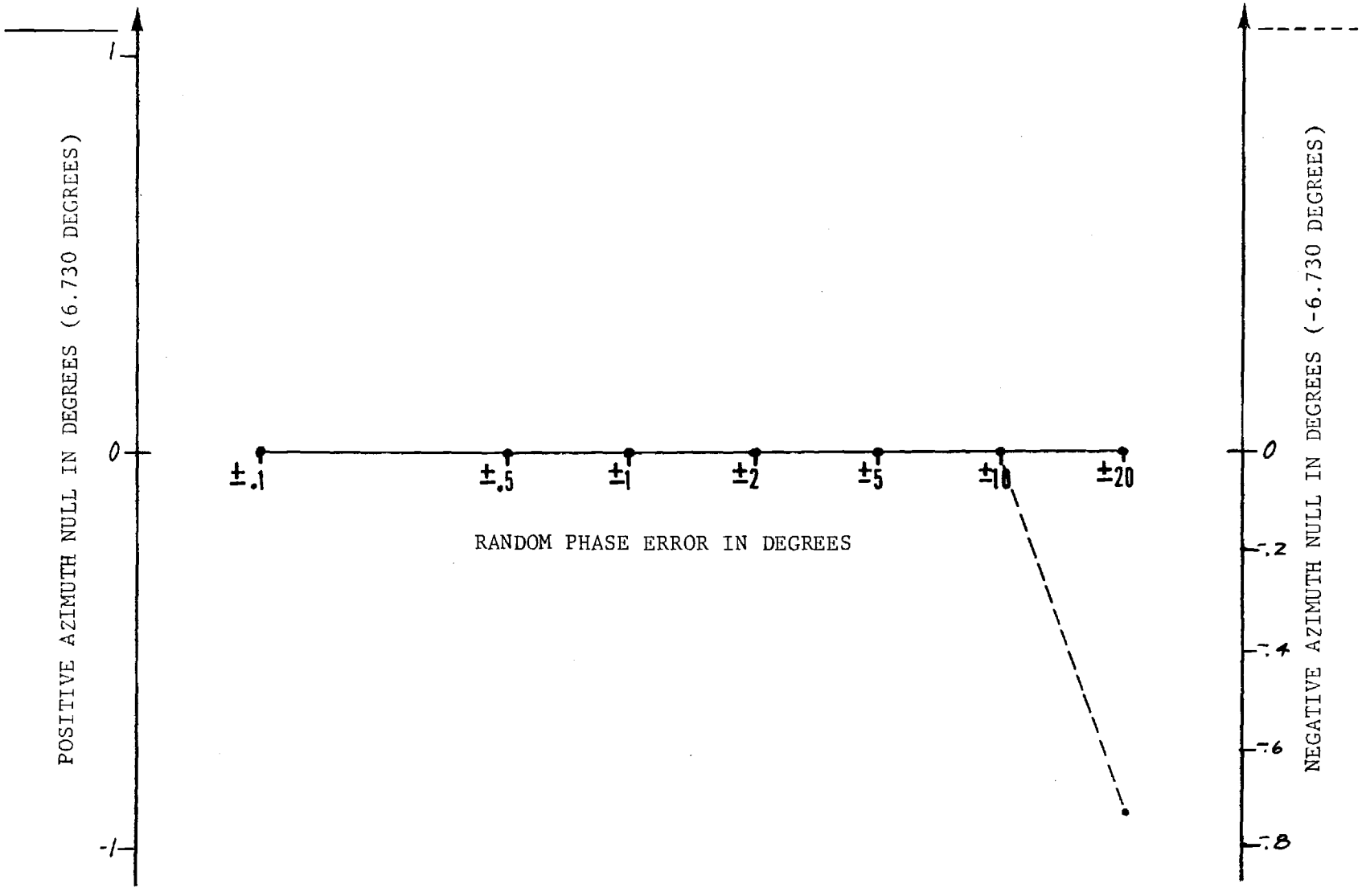

FIGURE A-23. ERRORS IN SUM PATTERN FIRST NULL LOCATIONS (TRUE VALUES)

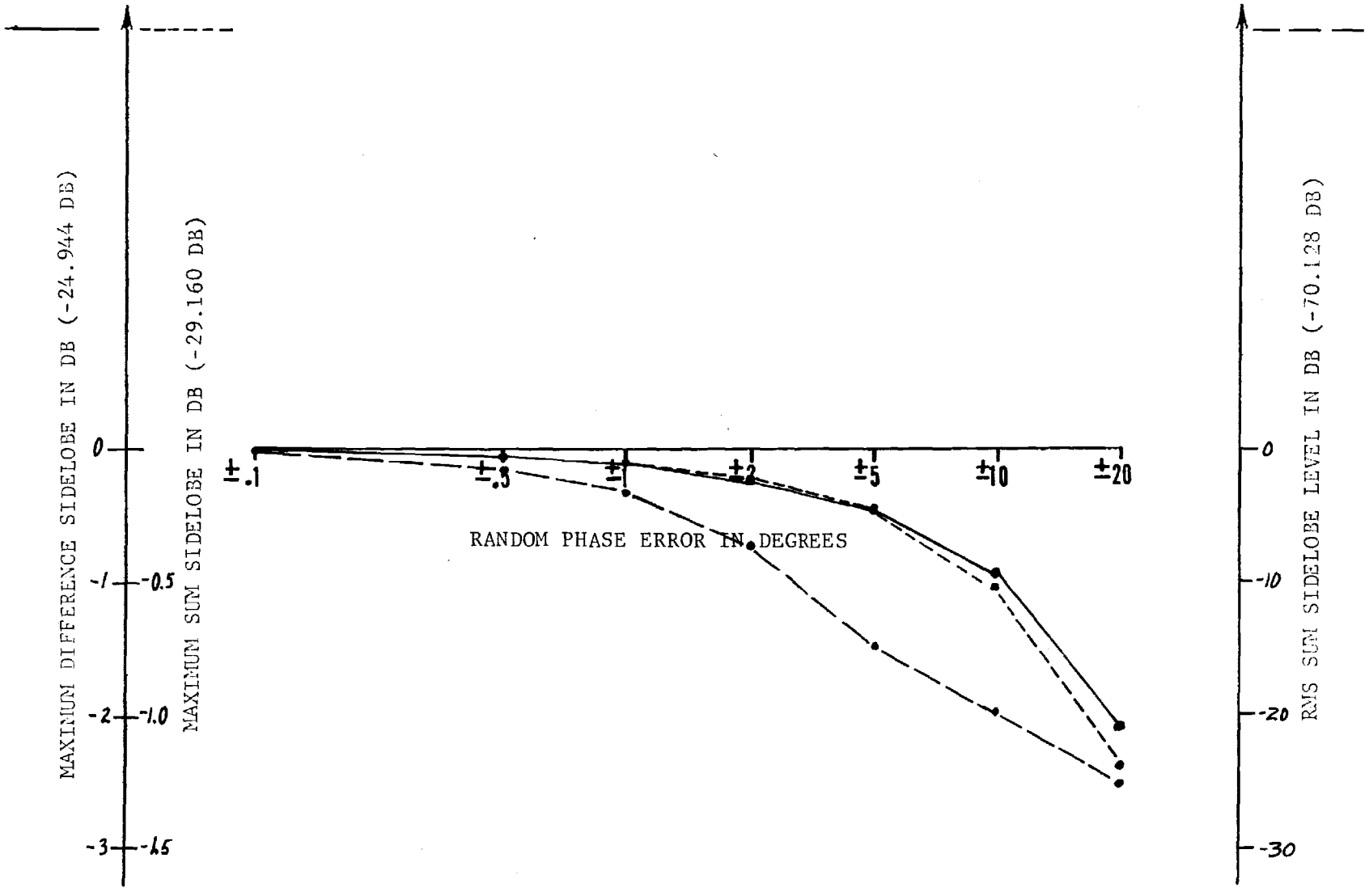

FIGURE A-24. ERRORS IN SIDELOBE LEVELS (TRUE VALUES)

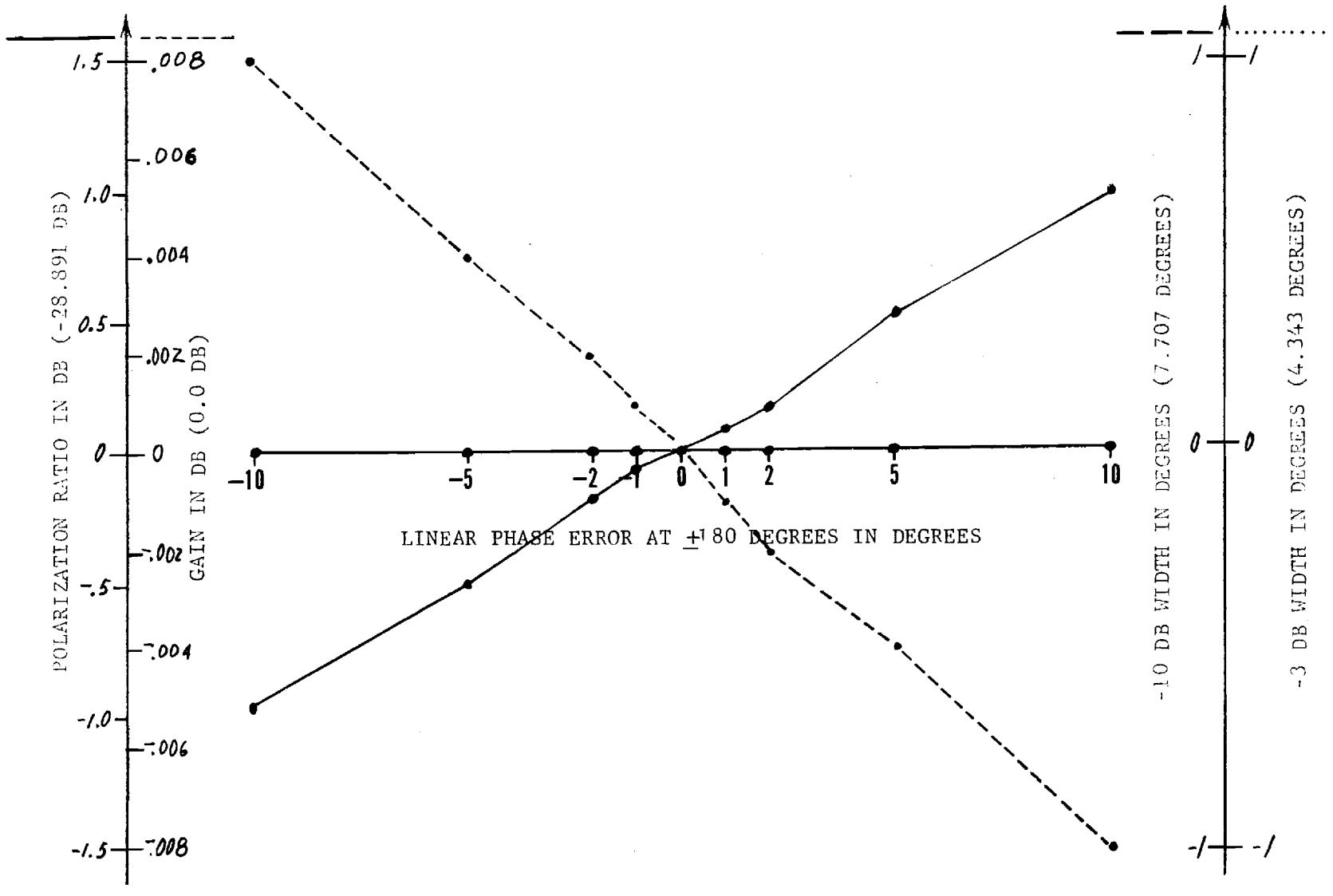

FIGURE A-25. ERRORS IN SUM PATTERN MAIN BEAM PARAMETERS (TRUE VALUES)

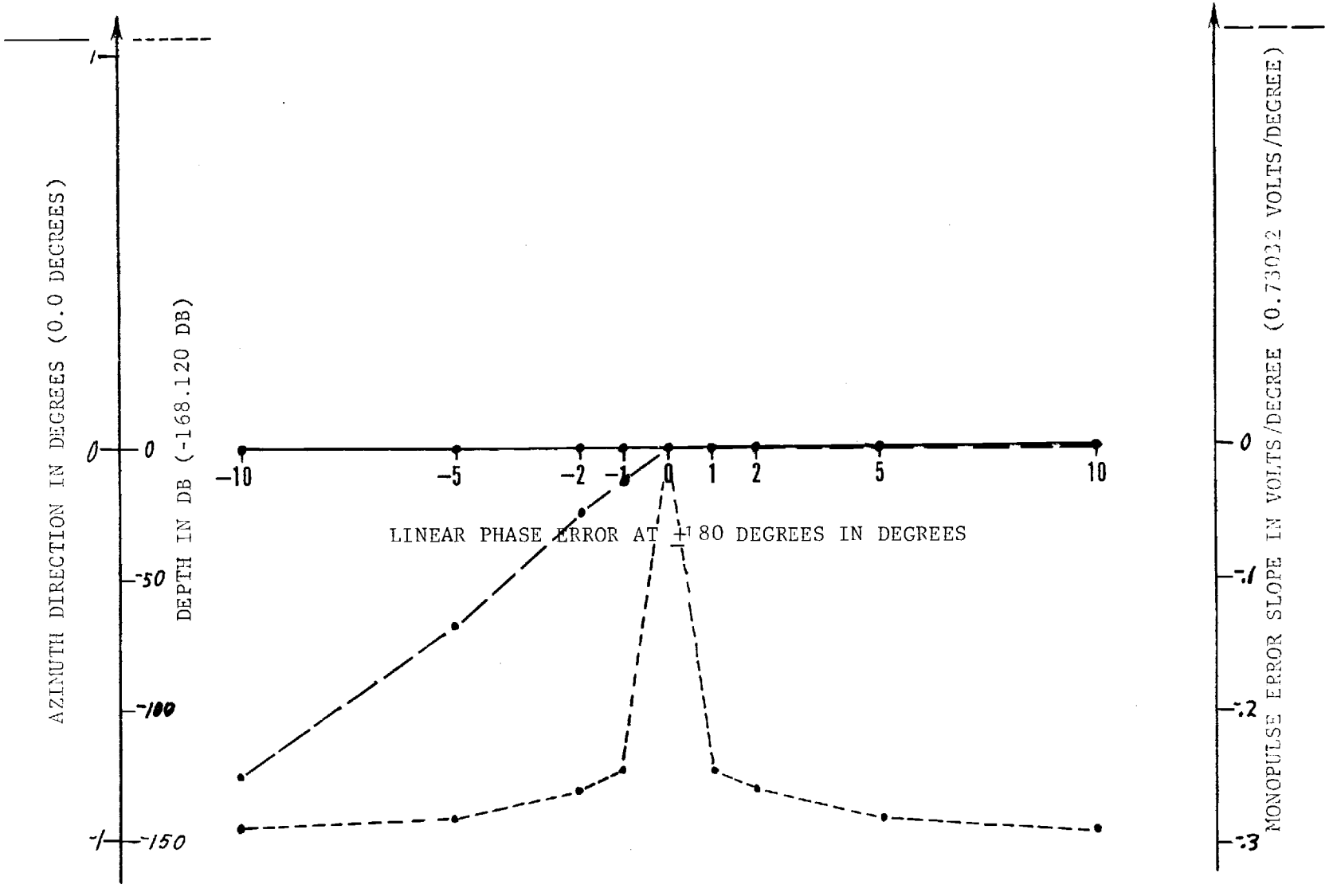

FIGURE A-26. ERRORS IN DIFFERENCE PATTERN NULL PARAMETERS (TRUE VALUES)

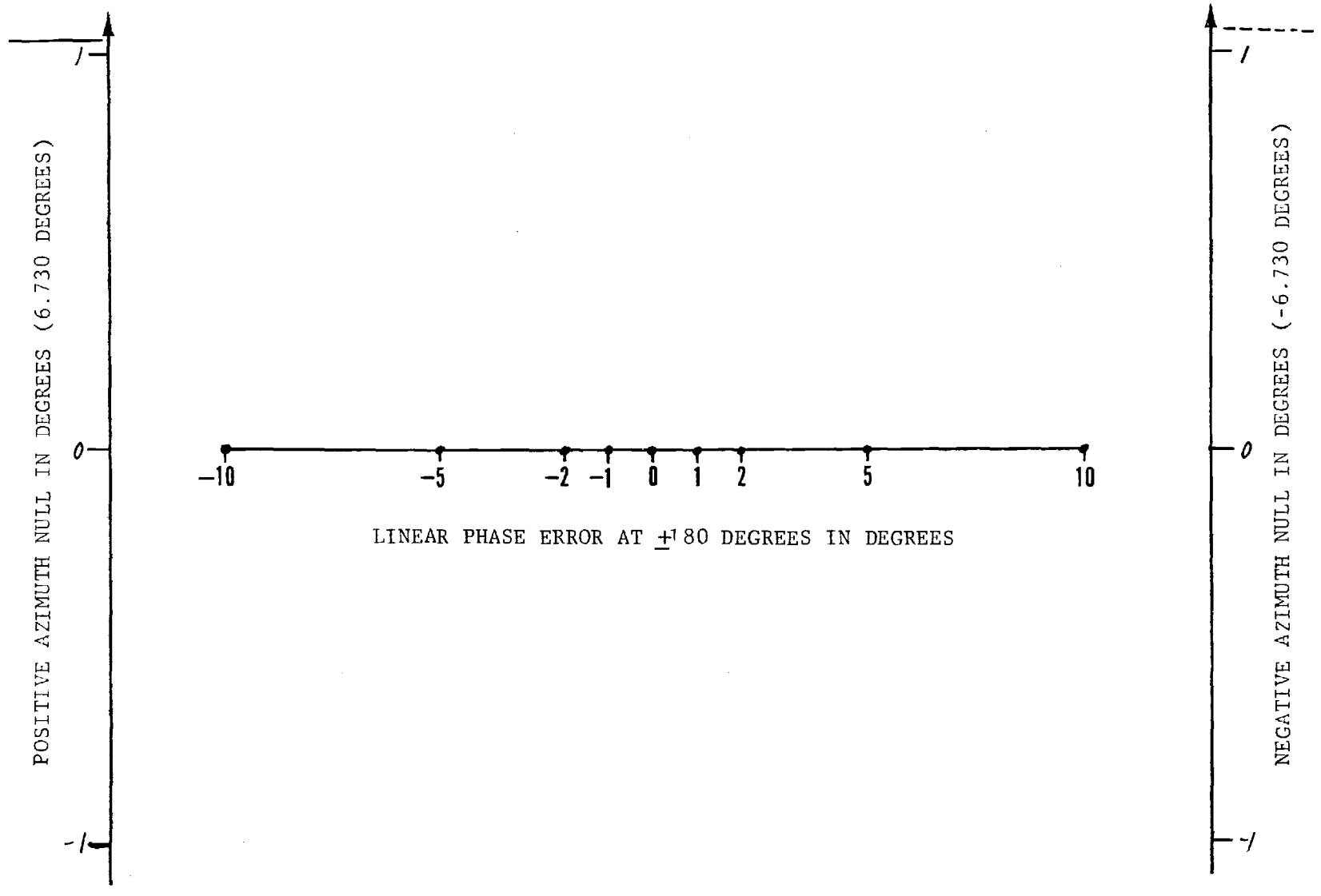

FIGURE A-27. ERRORS IN SUM PATTERN FIRST NULL LOCATIONS (TRUE VALUES)

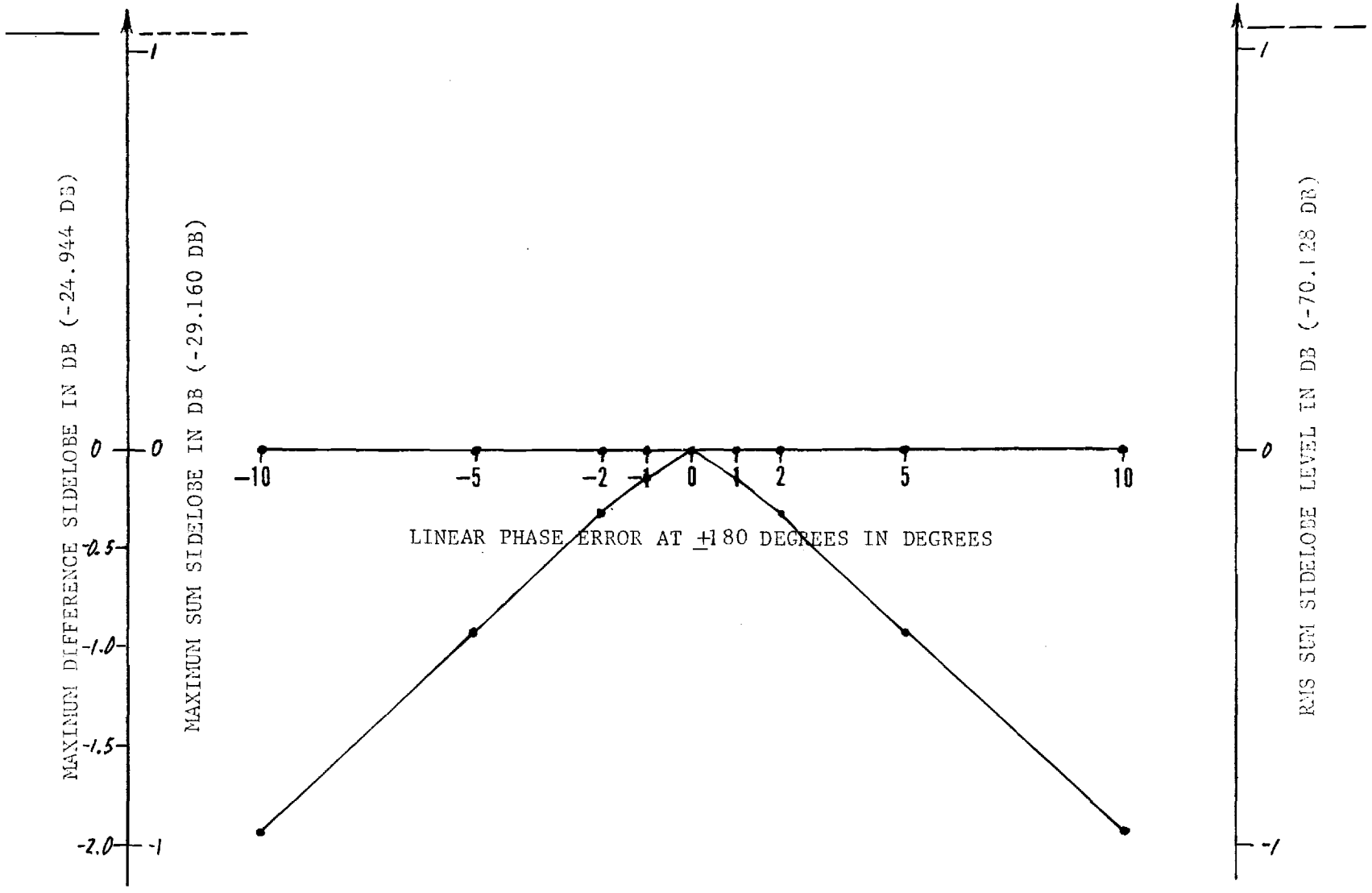

FIGURE A-28. ERRORS IN SIDELOBE LEVELS (TRUE VALUES)

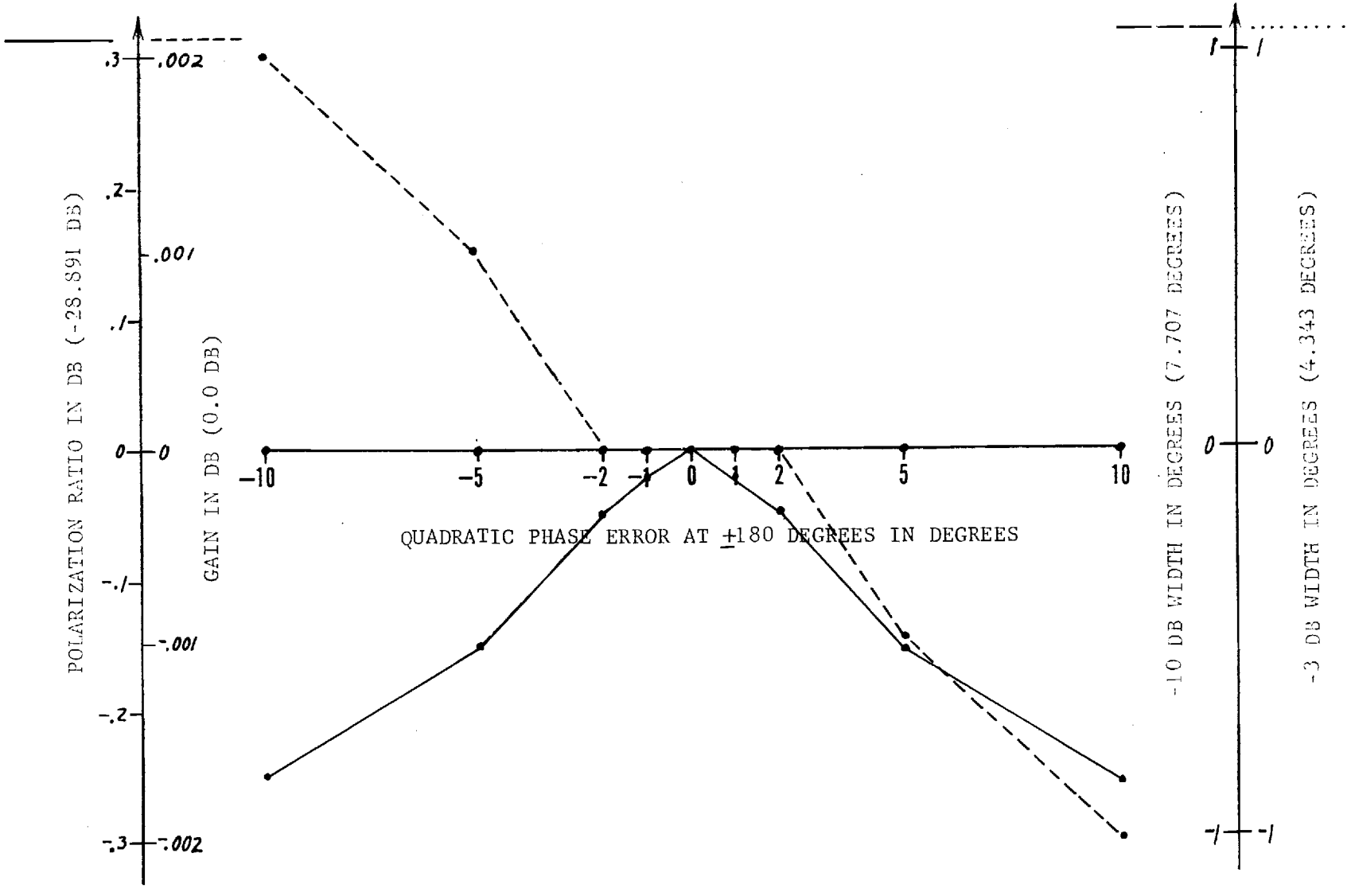

FIGURE A-29. ERRORS IN SUM PATTERN MAIN BEAM PARAMETERS (TRUE VALUES)

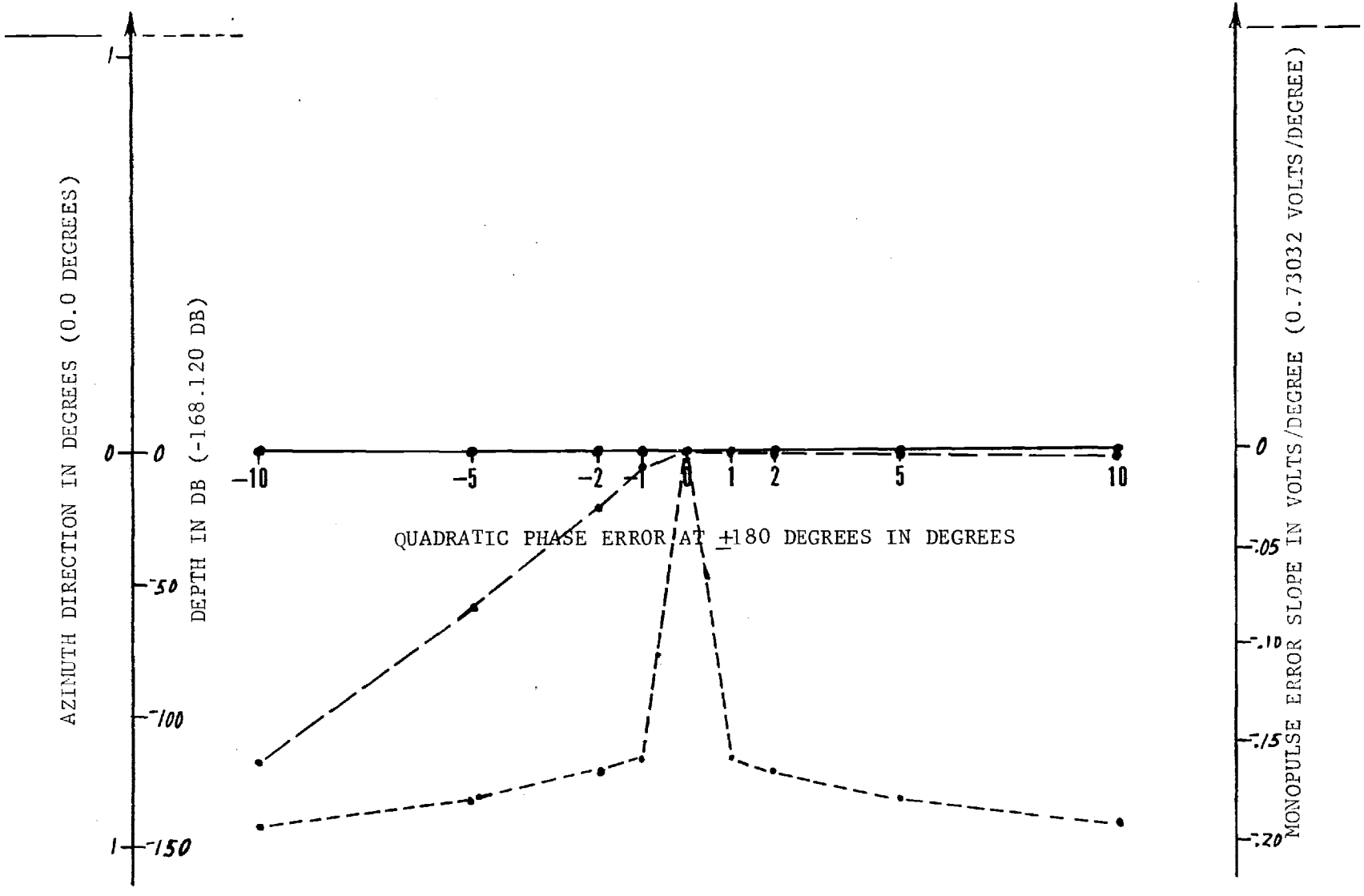

FIGURE A-30. ERRORS IN DIFFERENCE PATTERN NULL PARAMETERS (TRUE VALUES)

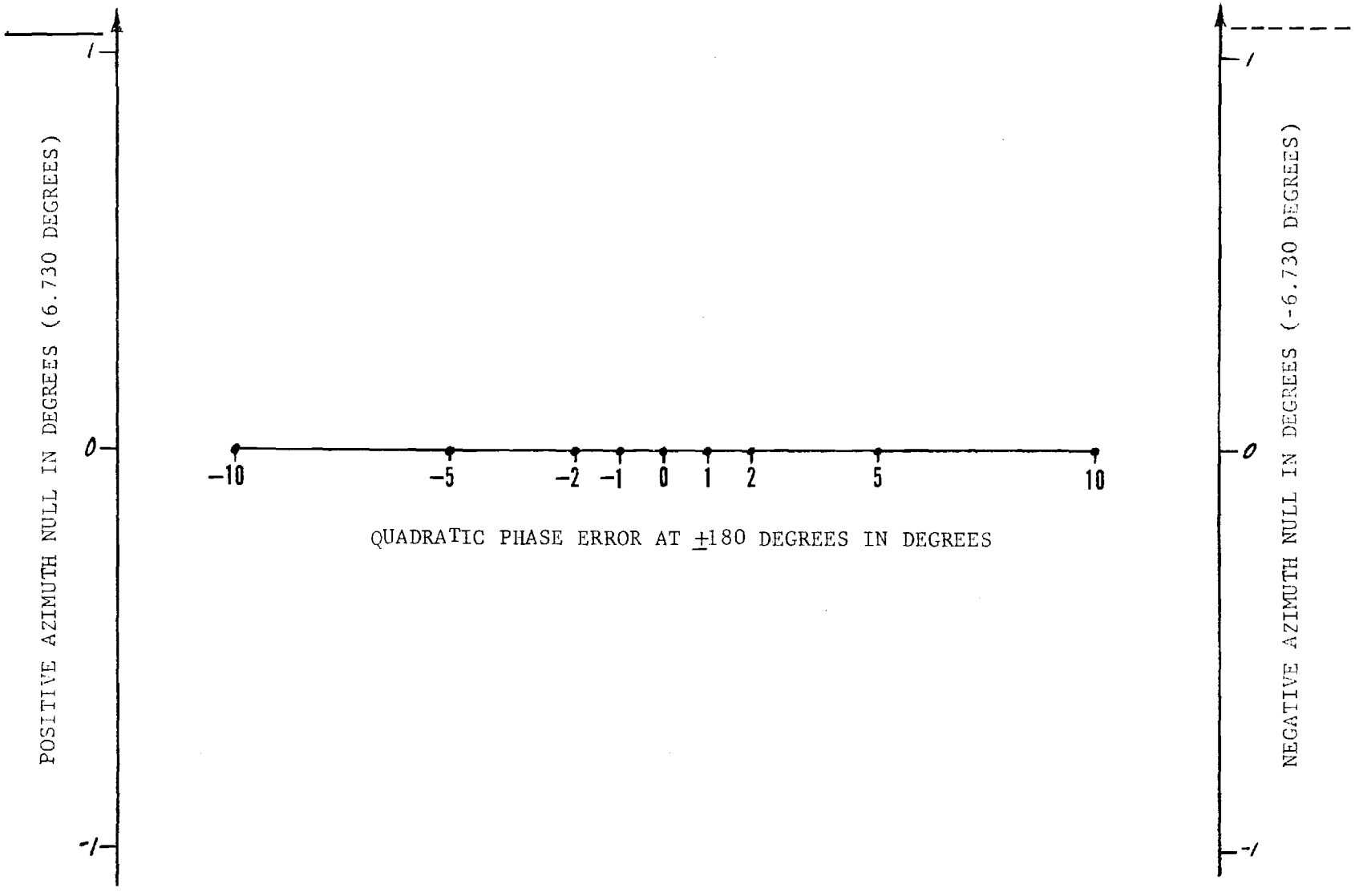

FIGURE A-31. ERRORS IN SUM PATTERN FIRST NULL LOCATIONS (TRUE VALUES)

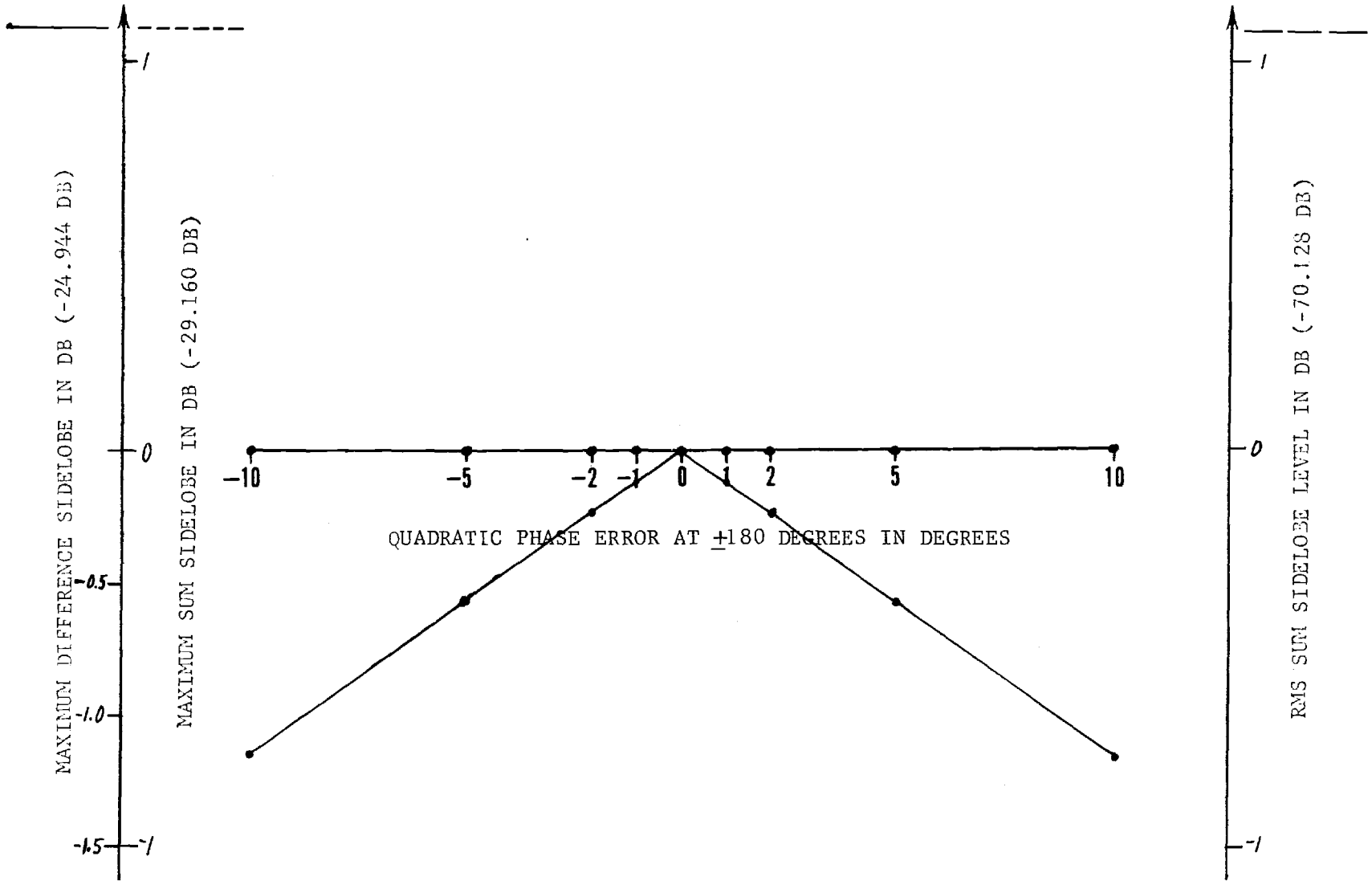

FIGURE A-32. ERRORS IN SIDELOBE LEVELS (TRUE VALUES)

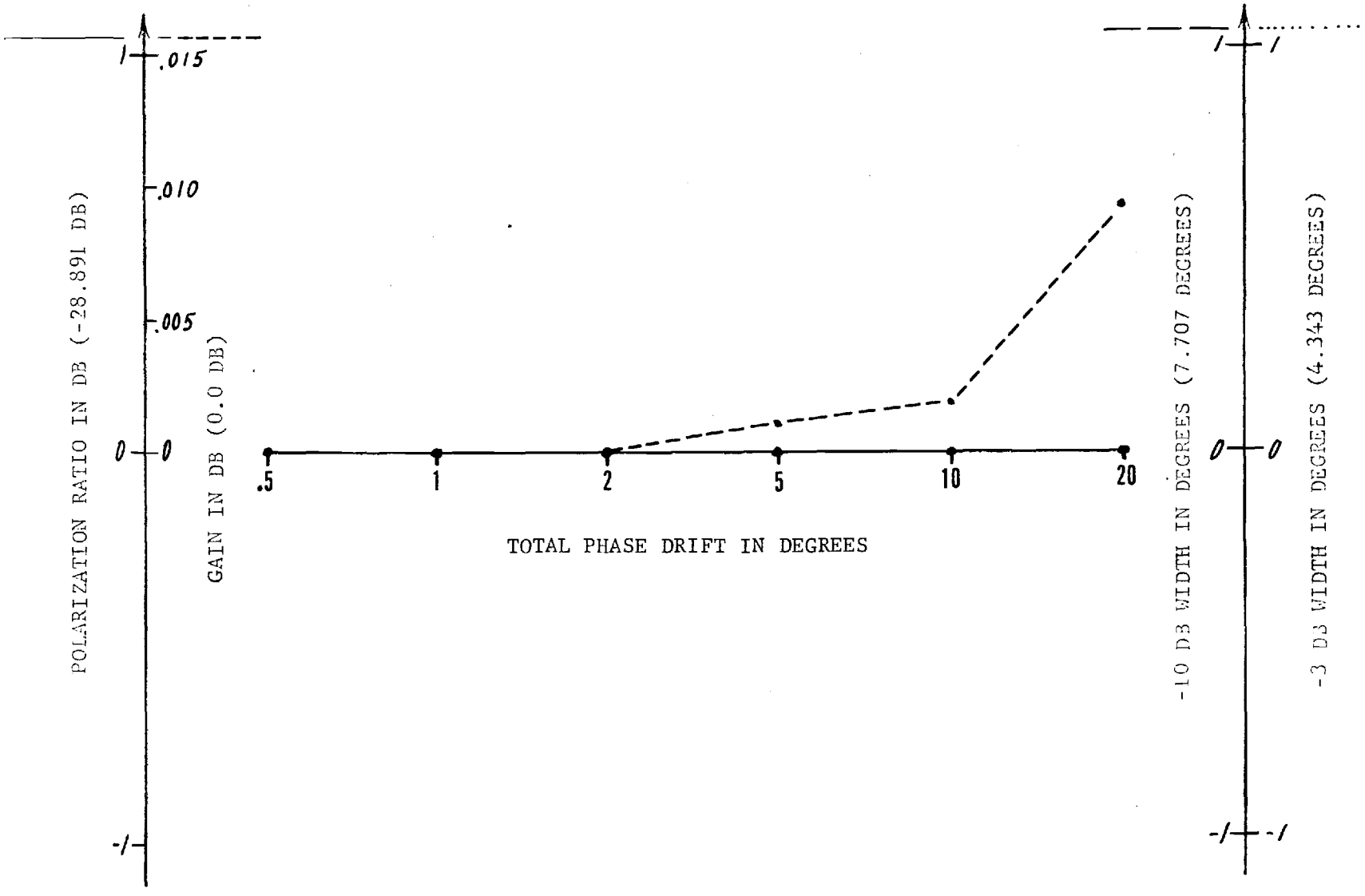

FIGURE A-33. ERRORS IN SUM PATTERN MAIN BEAM PARAMETERS (TRUE VALUES)

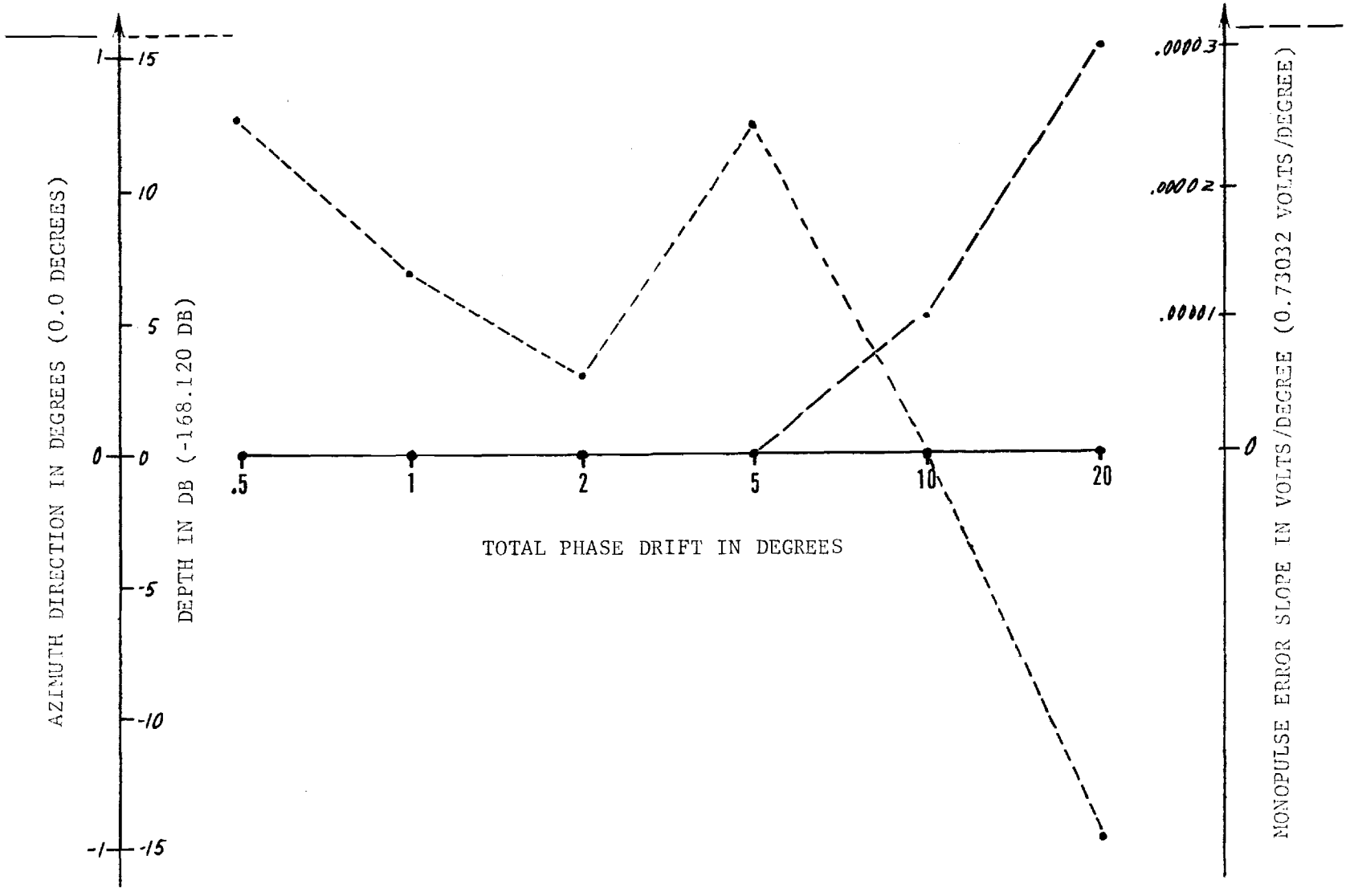

FIGURE A-34. ERRORS IN DIFFERENCE PATTERN NULL PARAMETERS (TRUE VALUES)

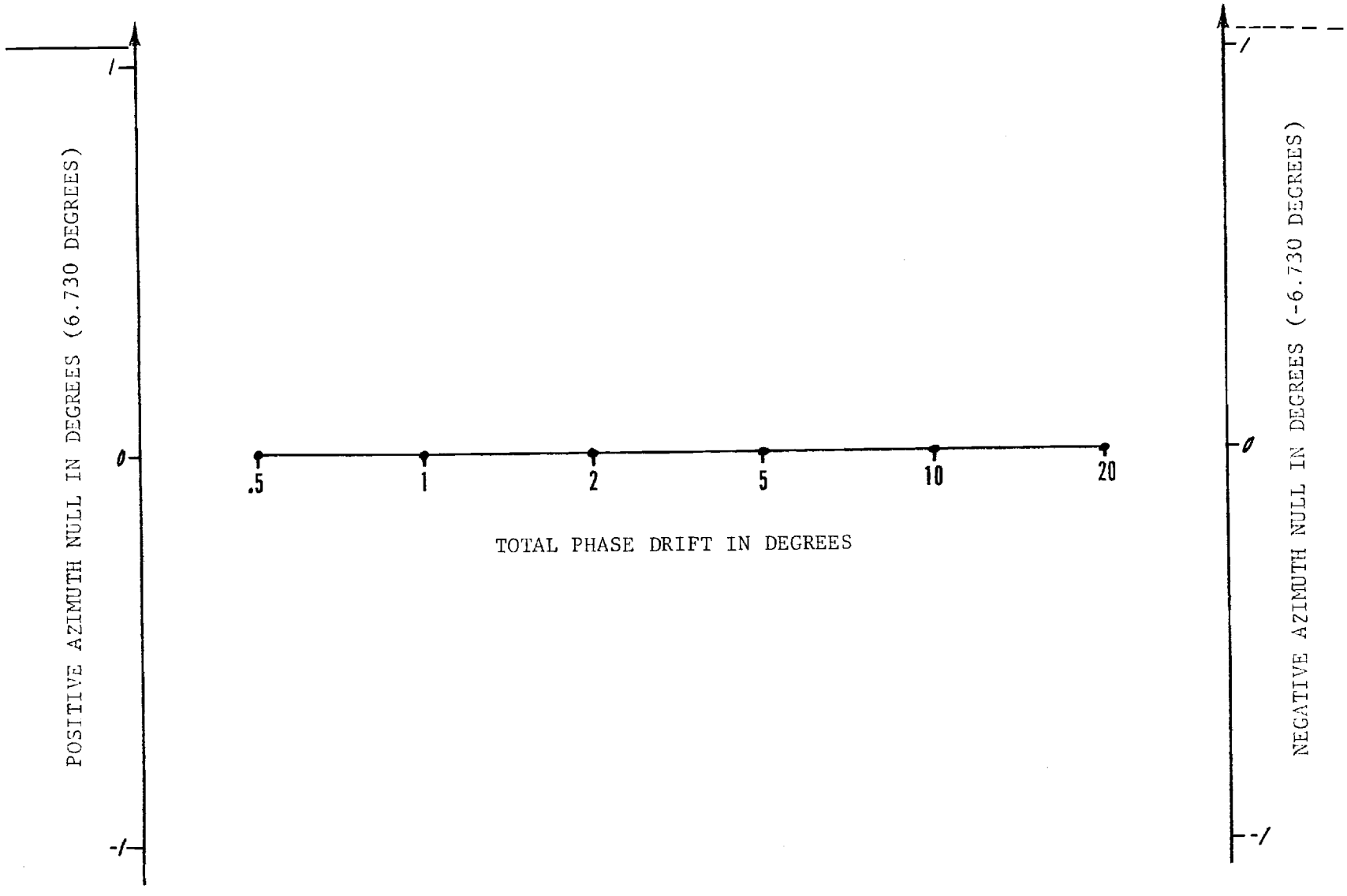

FIGURE A-35. ERRORS IN SUM PATTERN FIRST NULL LOCATIONS (TRUE VALUES)

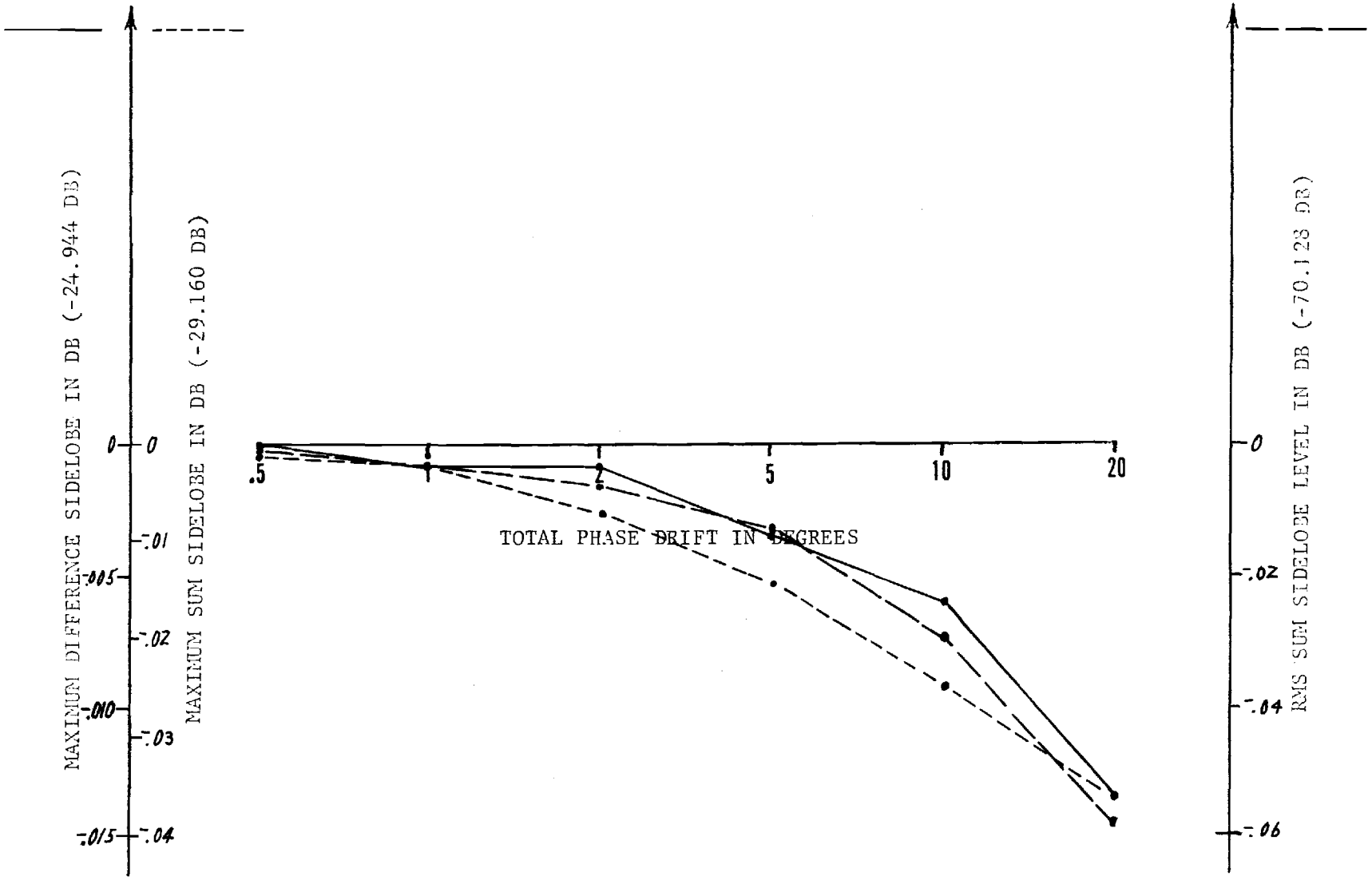

FIGURE A-36. ERRORS IN SIDELOBE LEVELS (TRUE VALUES)

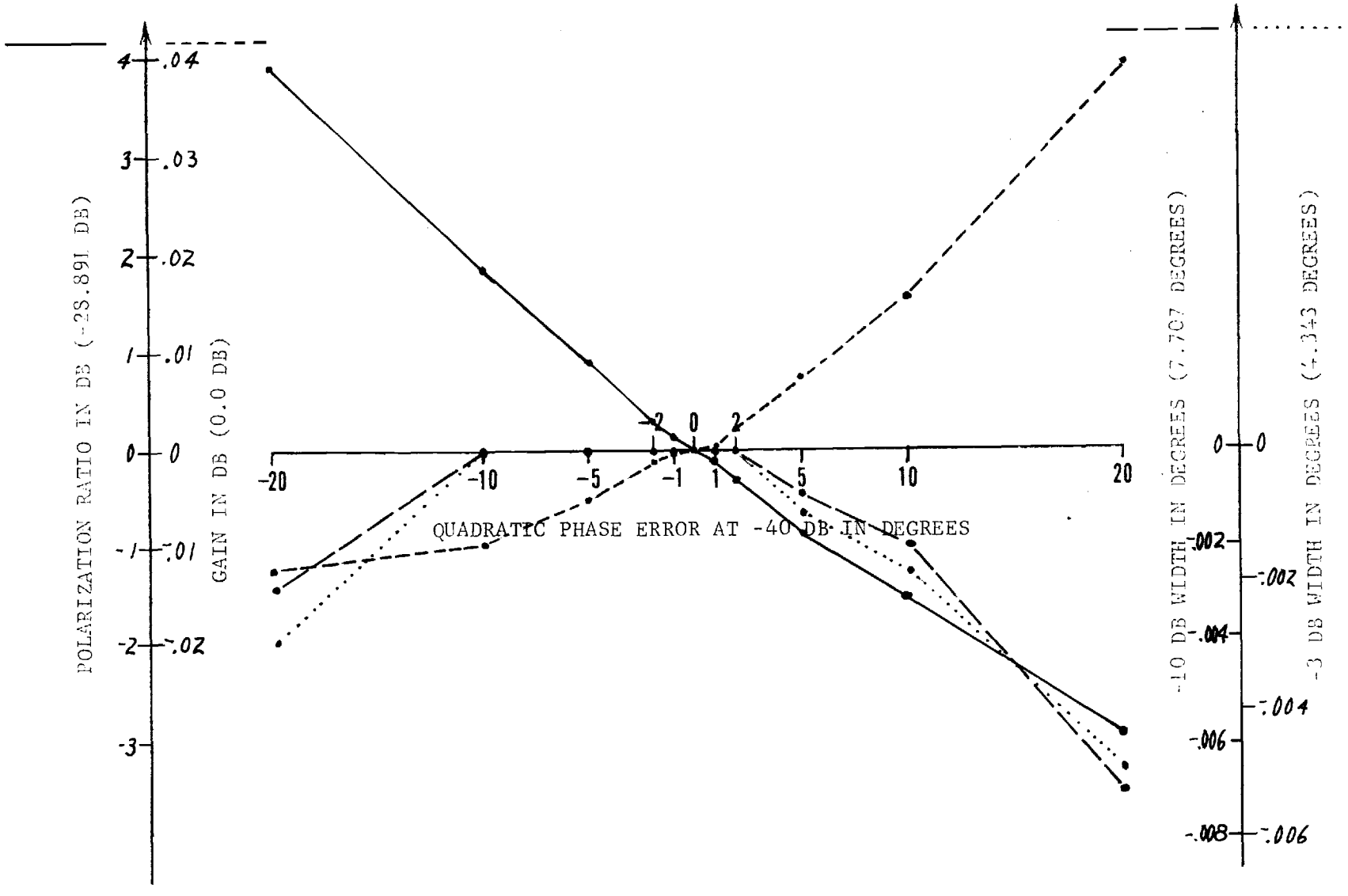

FIGURE A-37. ERRORS IN SUM PATTERN MAIN BEAM PARAMETERS (TRUE VALUES)

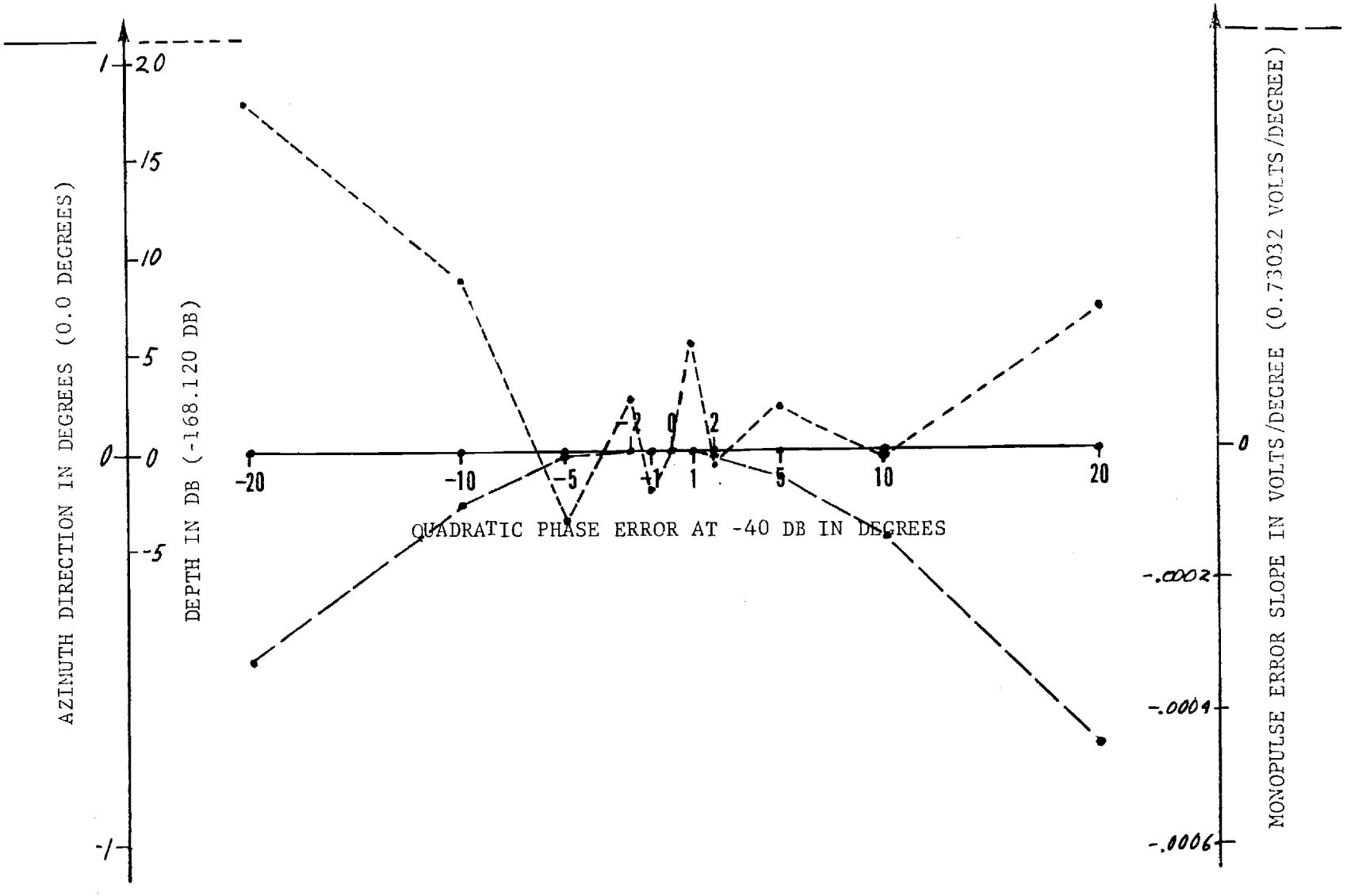

FIGURE A-38. ERRORS IN DIFFERENCE PATTERN NULL PARAMETERS (TRUE VALUES)

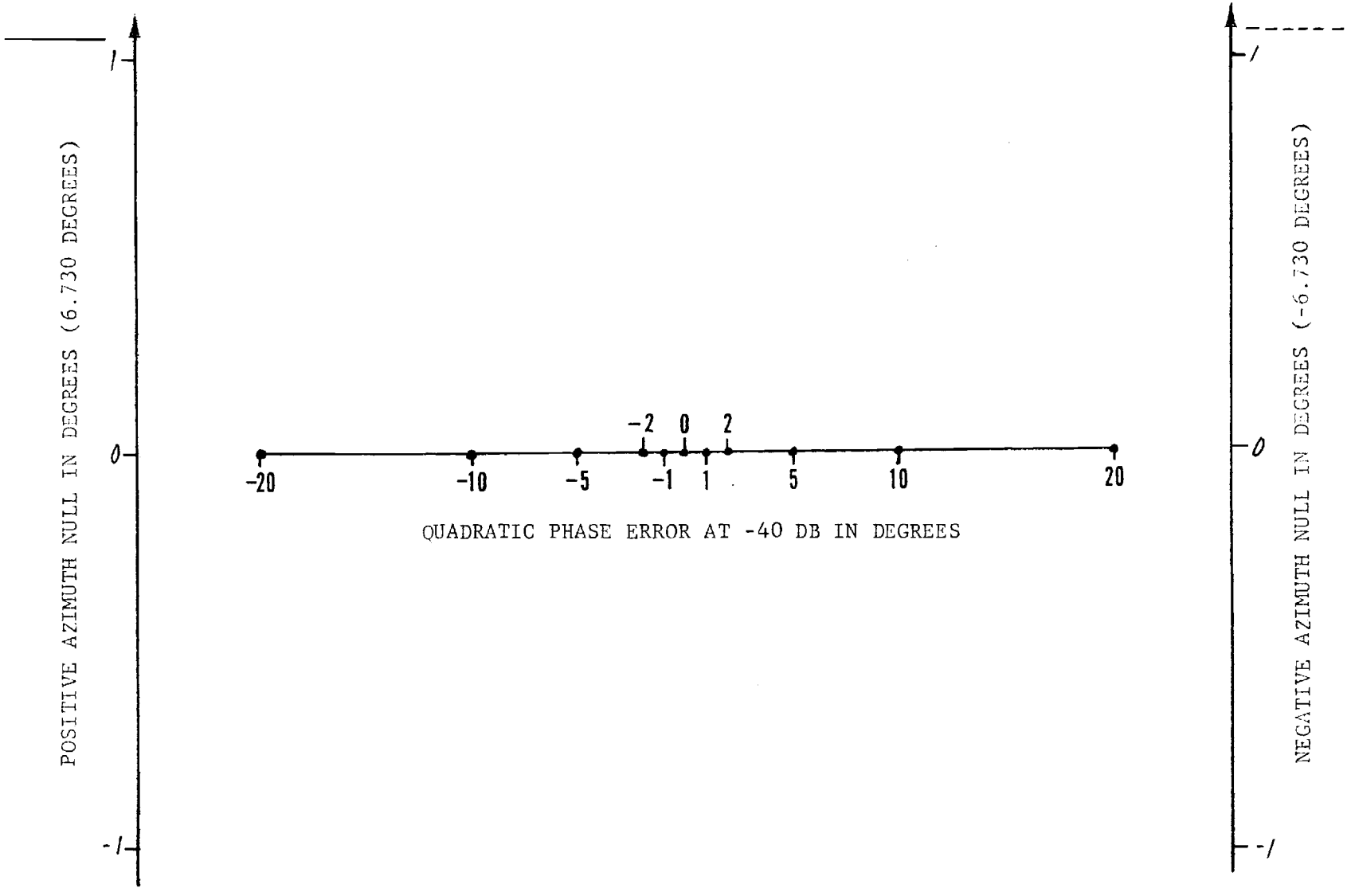

FIGURE A-39. ERRORS IN SUM PATTERN FIRST NULL LOCATIONS (TRUE VALUES)

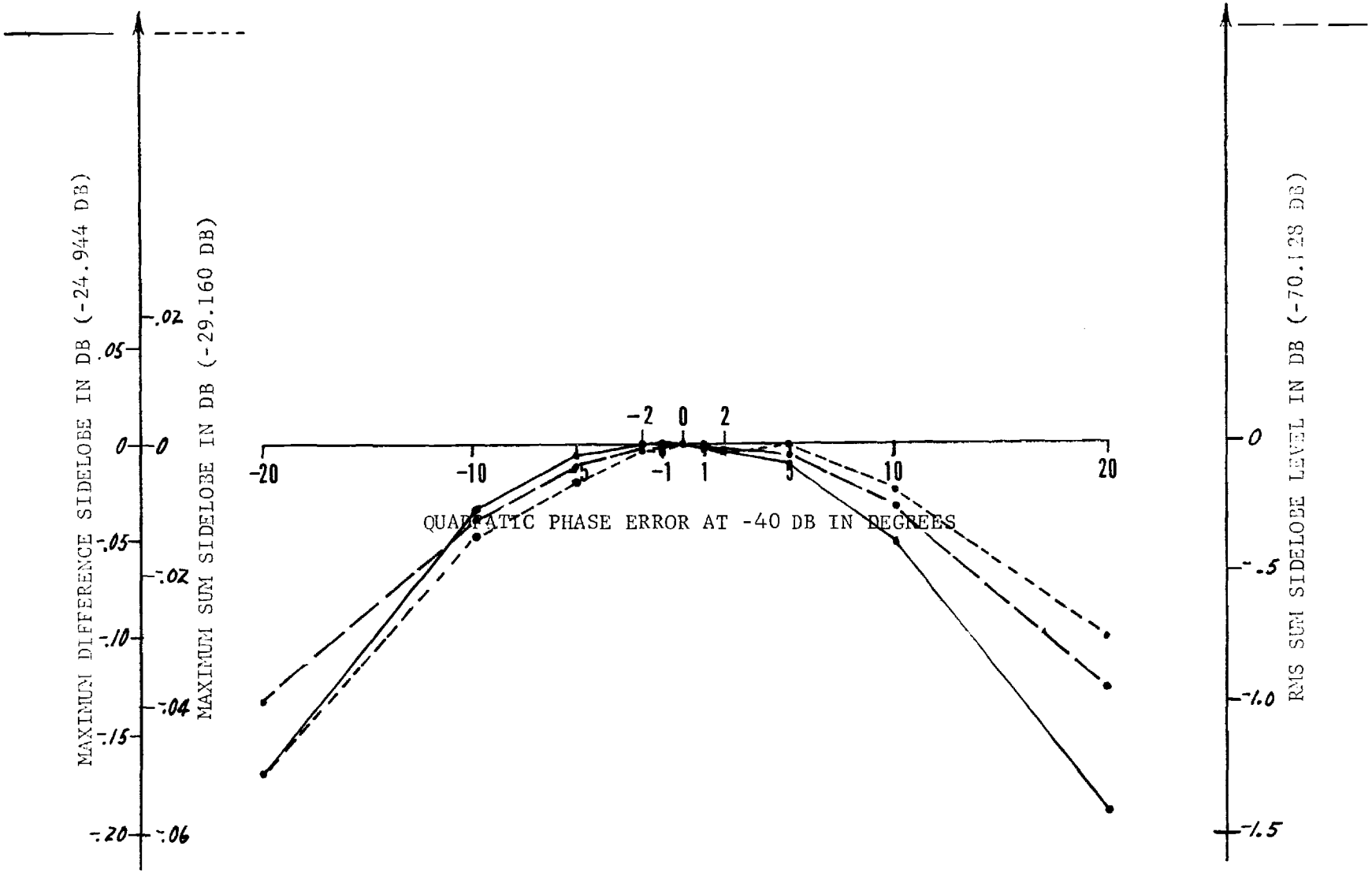

FIGURE A-40. ERRORS IN SIDELOBE LEVELS (TRUE VALUES)

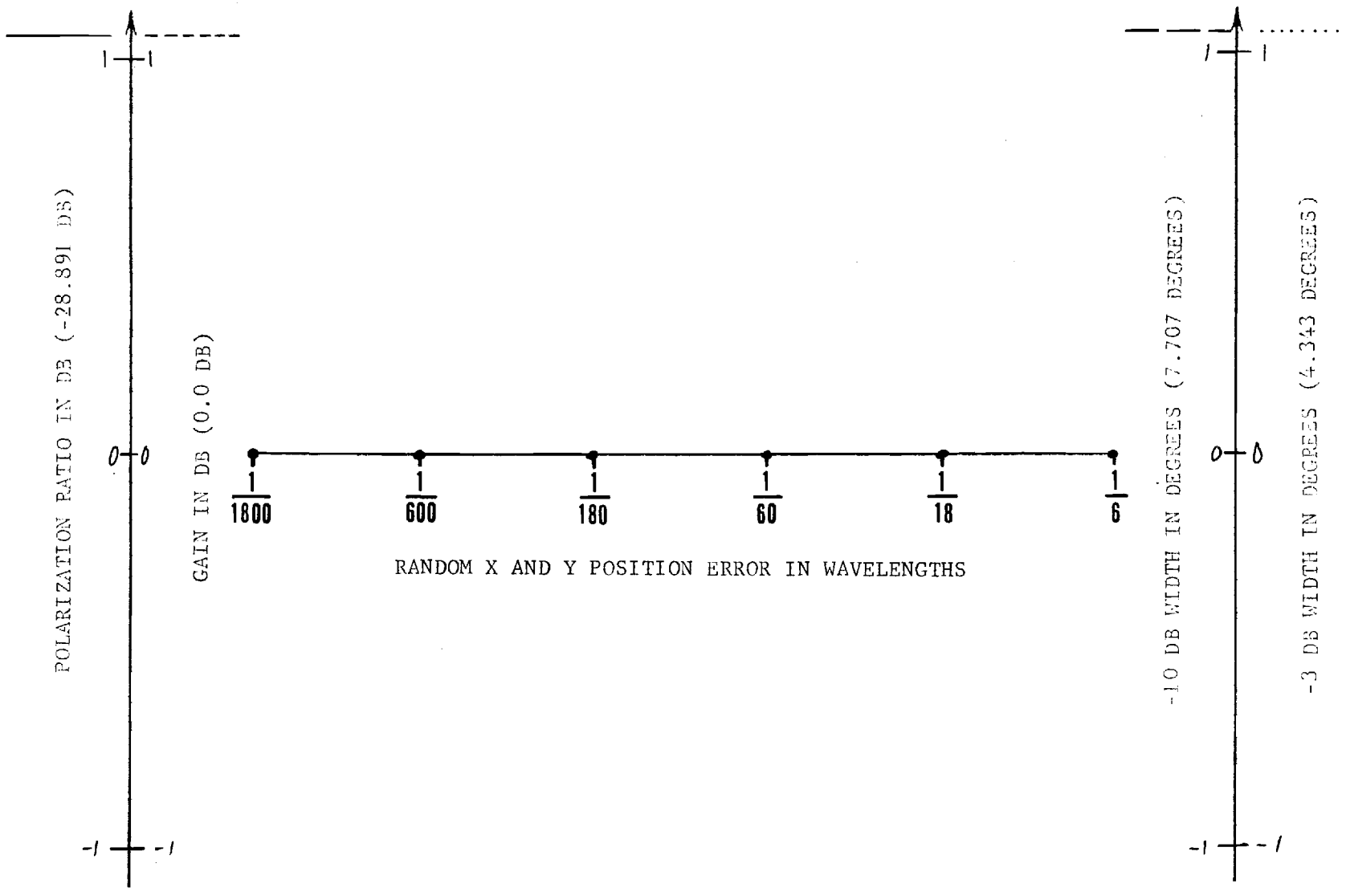

FIGURE A-41. ERRORS IN SUM PATTERN MAIN BEAM PARAMETERS (TRUE VALUES)

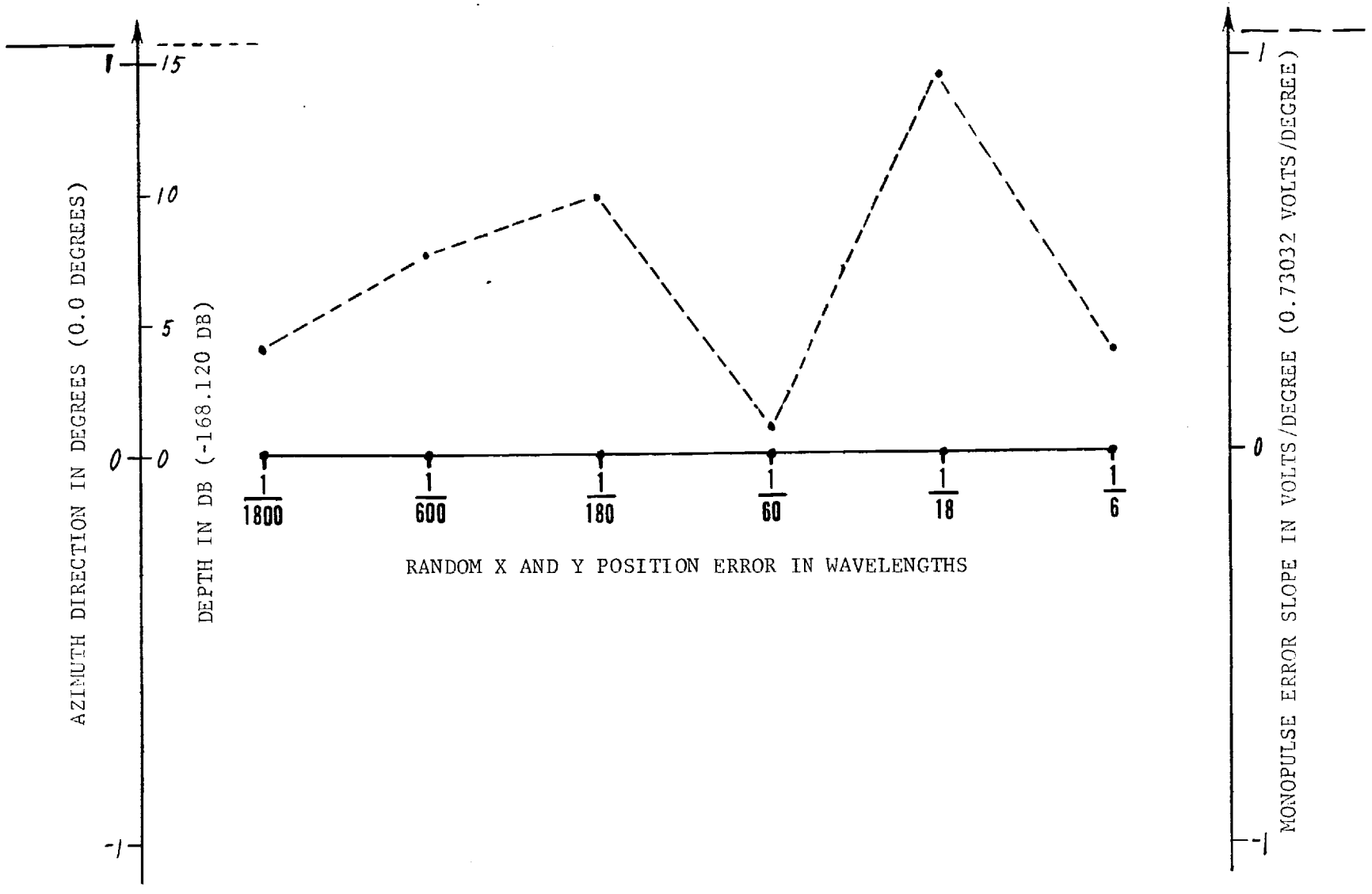

FIGURE A-42. ERRORS IN DIFFERENCE PATTERN NULL PARAMETERS (TRUE VALUES)

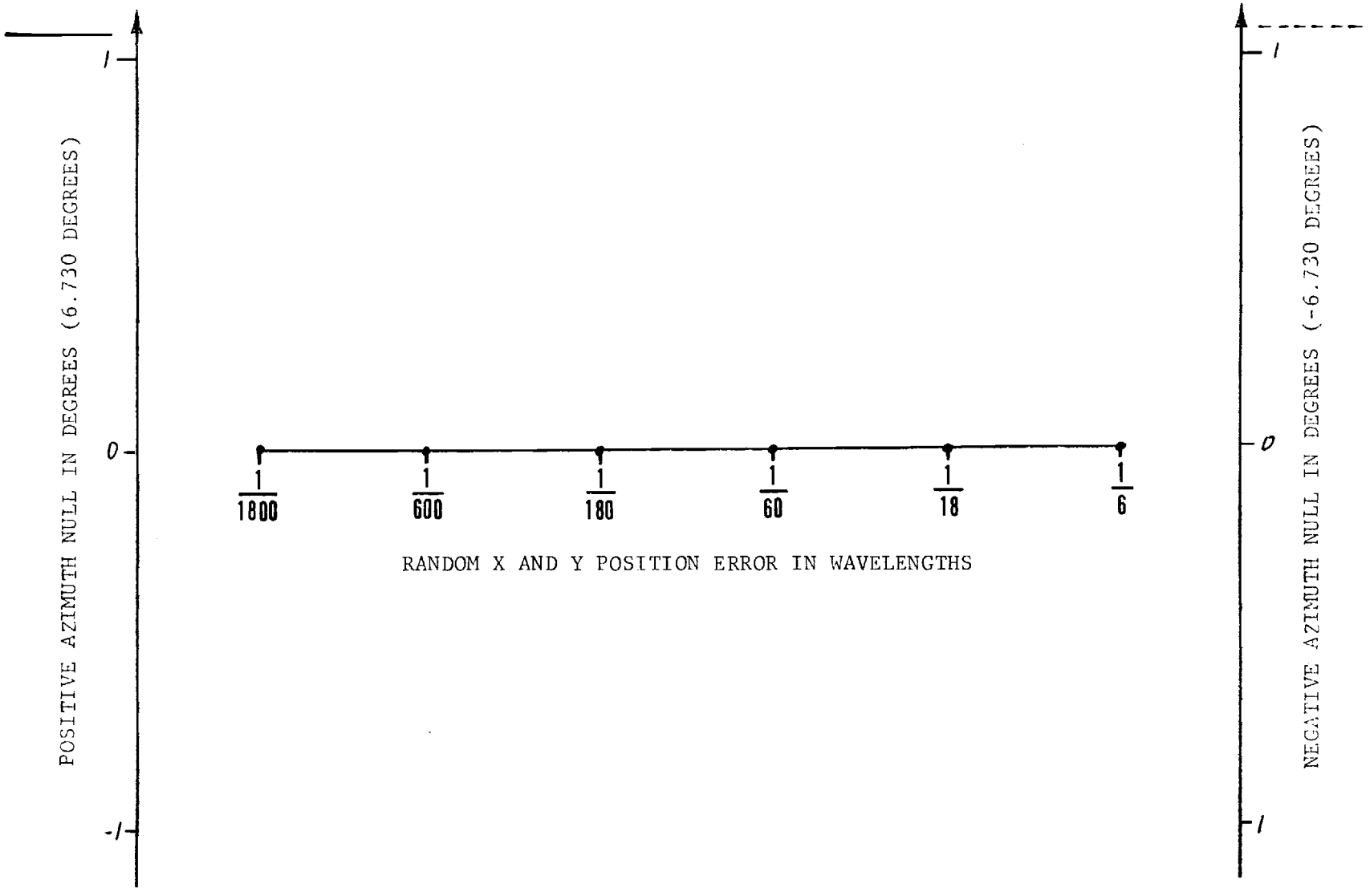

FIGURE A-43. ERRORS IN SUM PATTERN FIRST NULL LOCATIONS (TRUE VALUES)

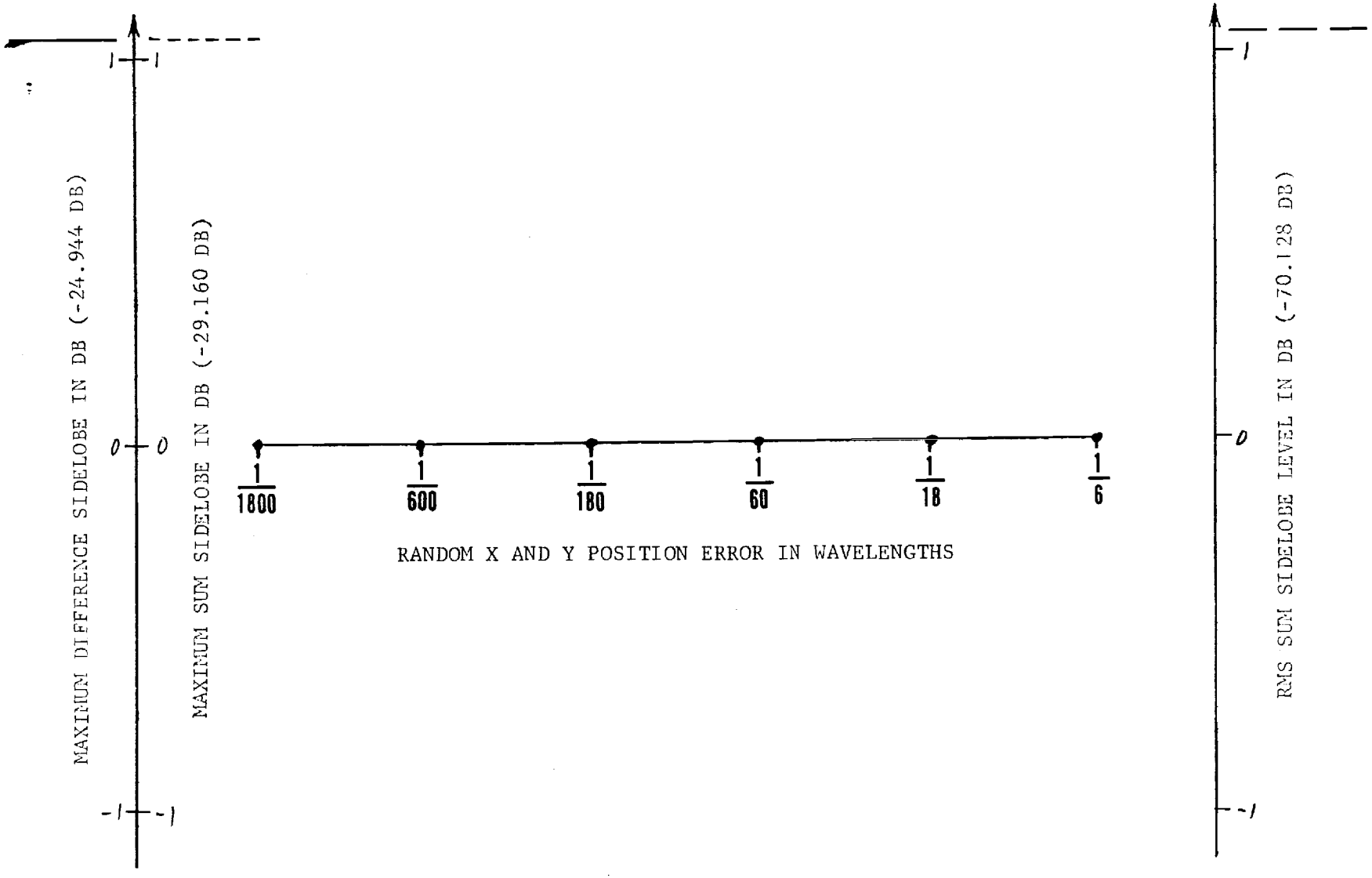

FIGURE A-44. ERRORS IN SIDELOBE LEVELS (TRUE VALUES)

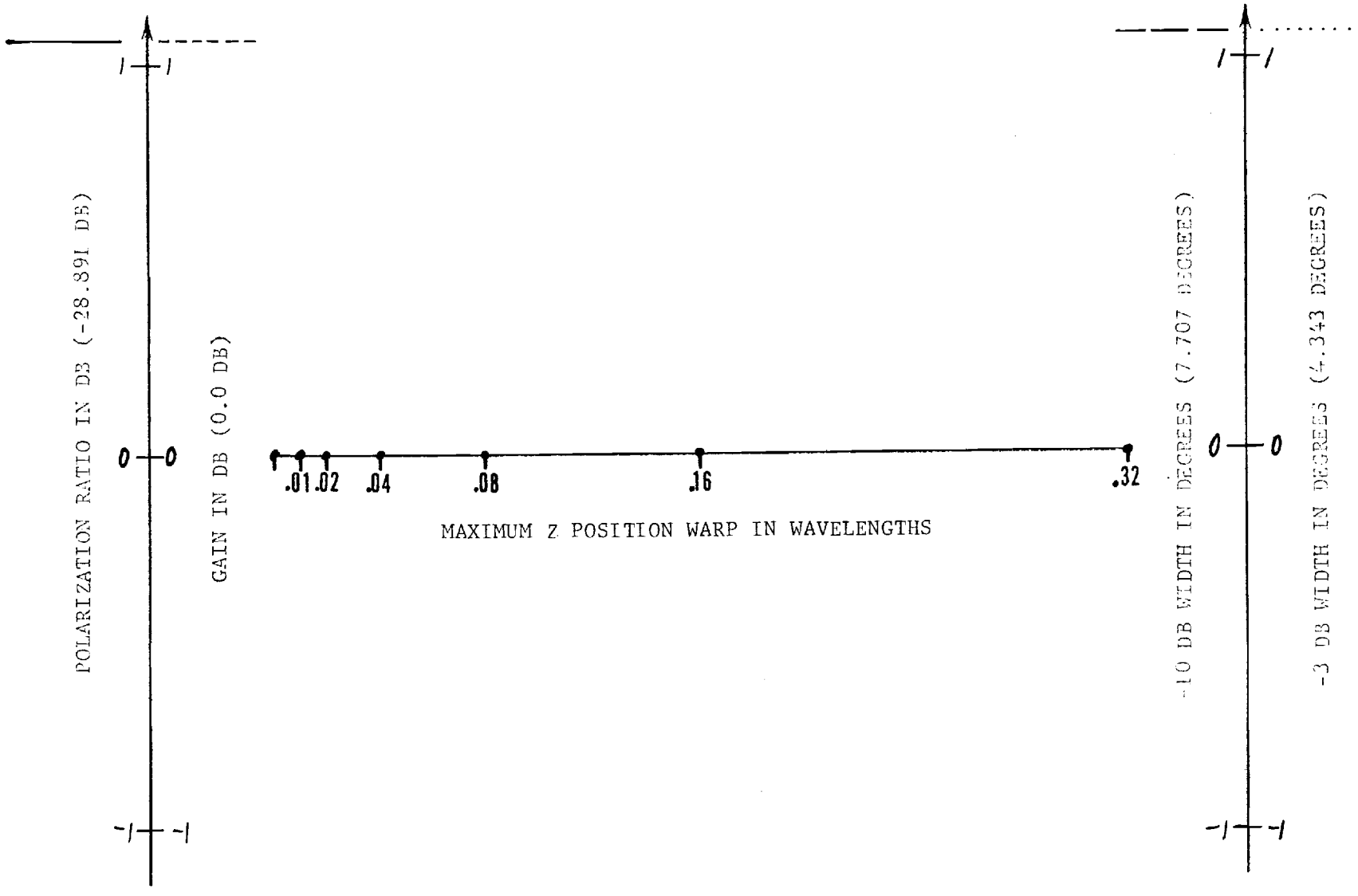

FIGURE A-45. ERRORS IN SUM PATTERN MAIN BEAM PARAMETERS (TRUE VALUES)

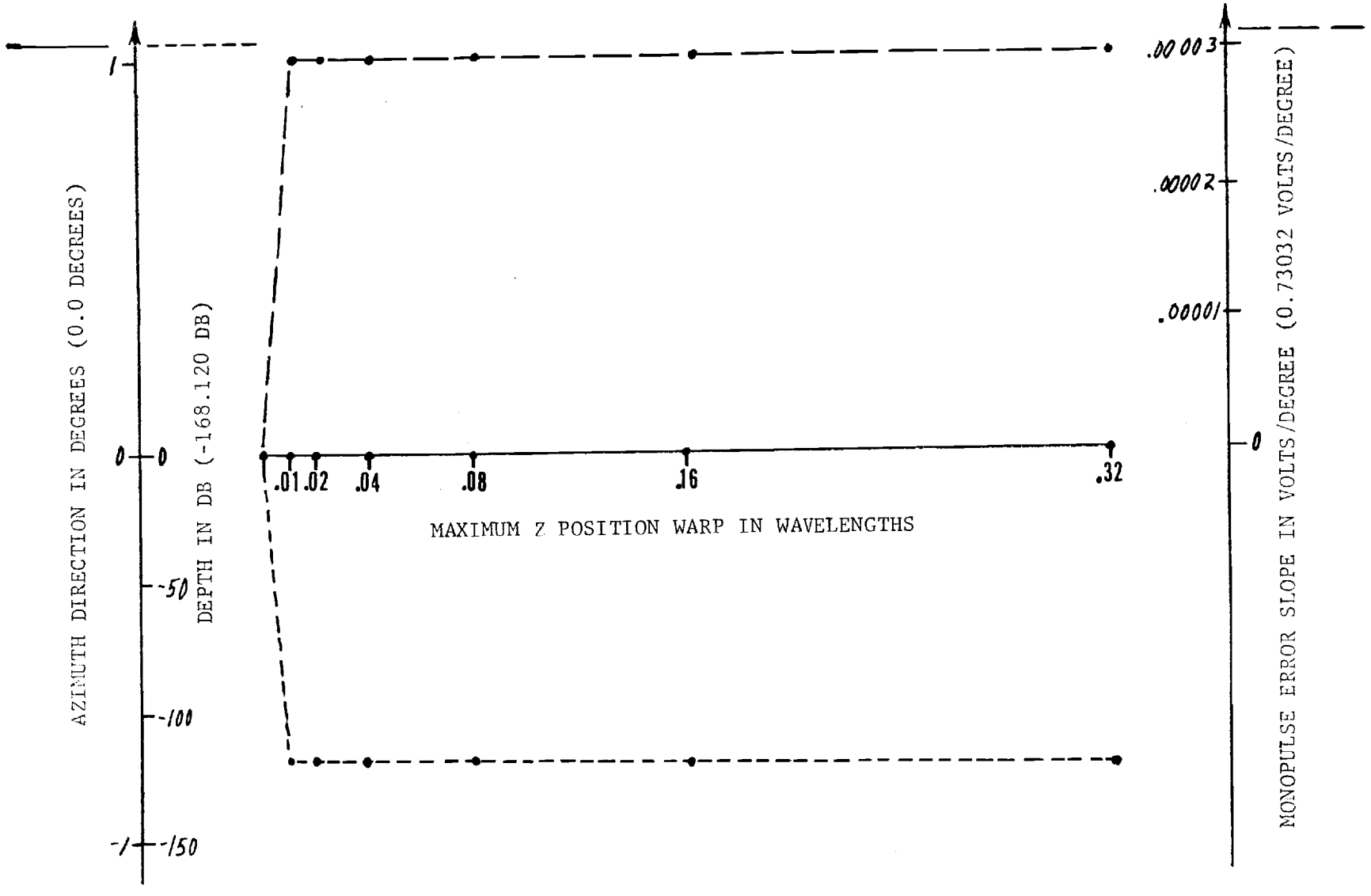

FIGURE A-46. ERRORS IN DIFFERENCE PATTERN NULL PARAMETERS (TRUE VALUES)

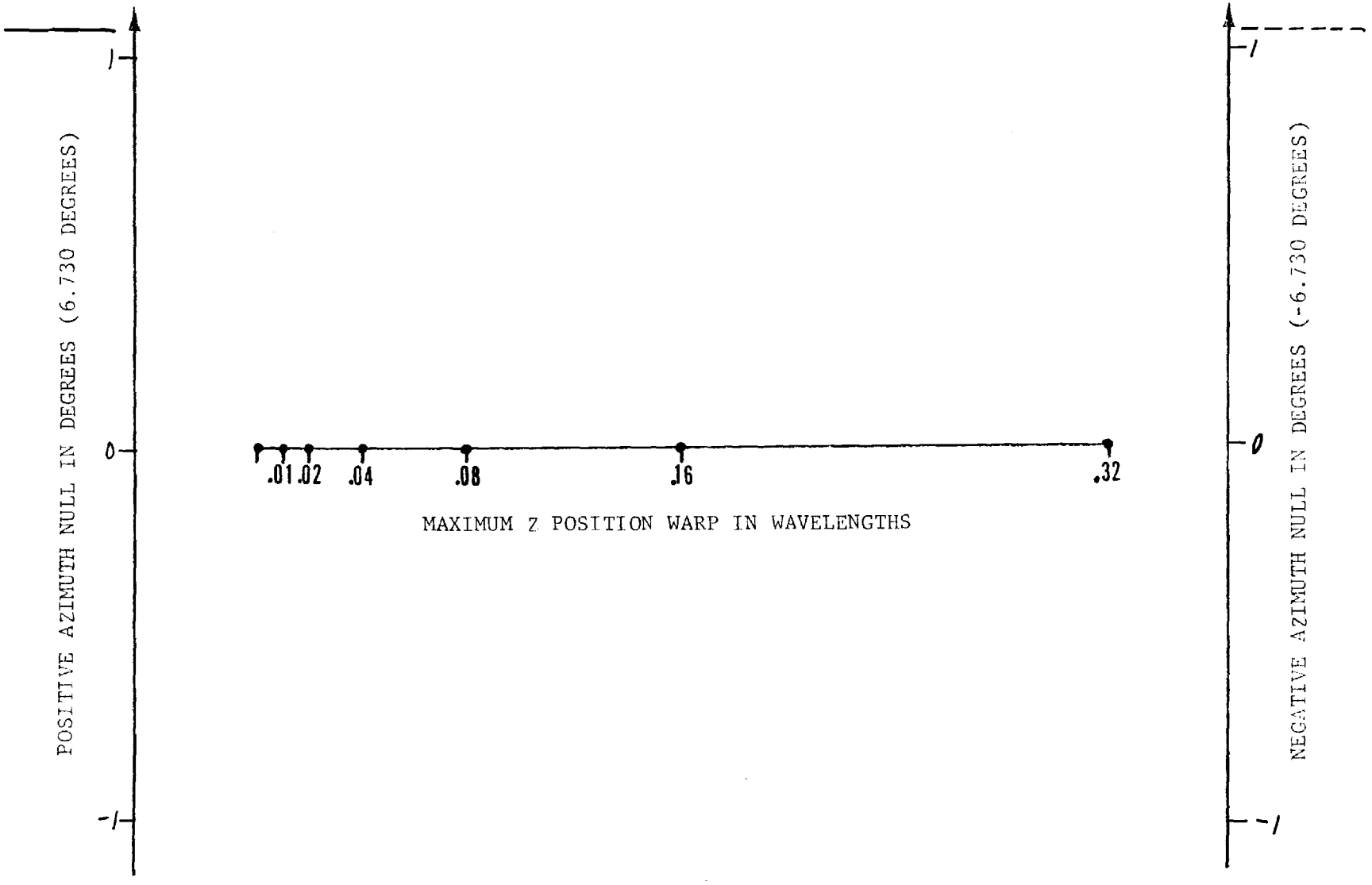

FIGURE A-47. ERRORS IN SUM PATTERN FIRST NULL LOCATIONS (TRUE VALUES)

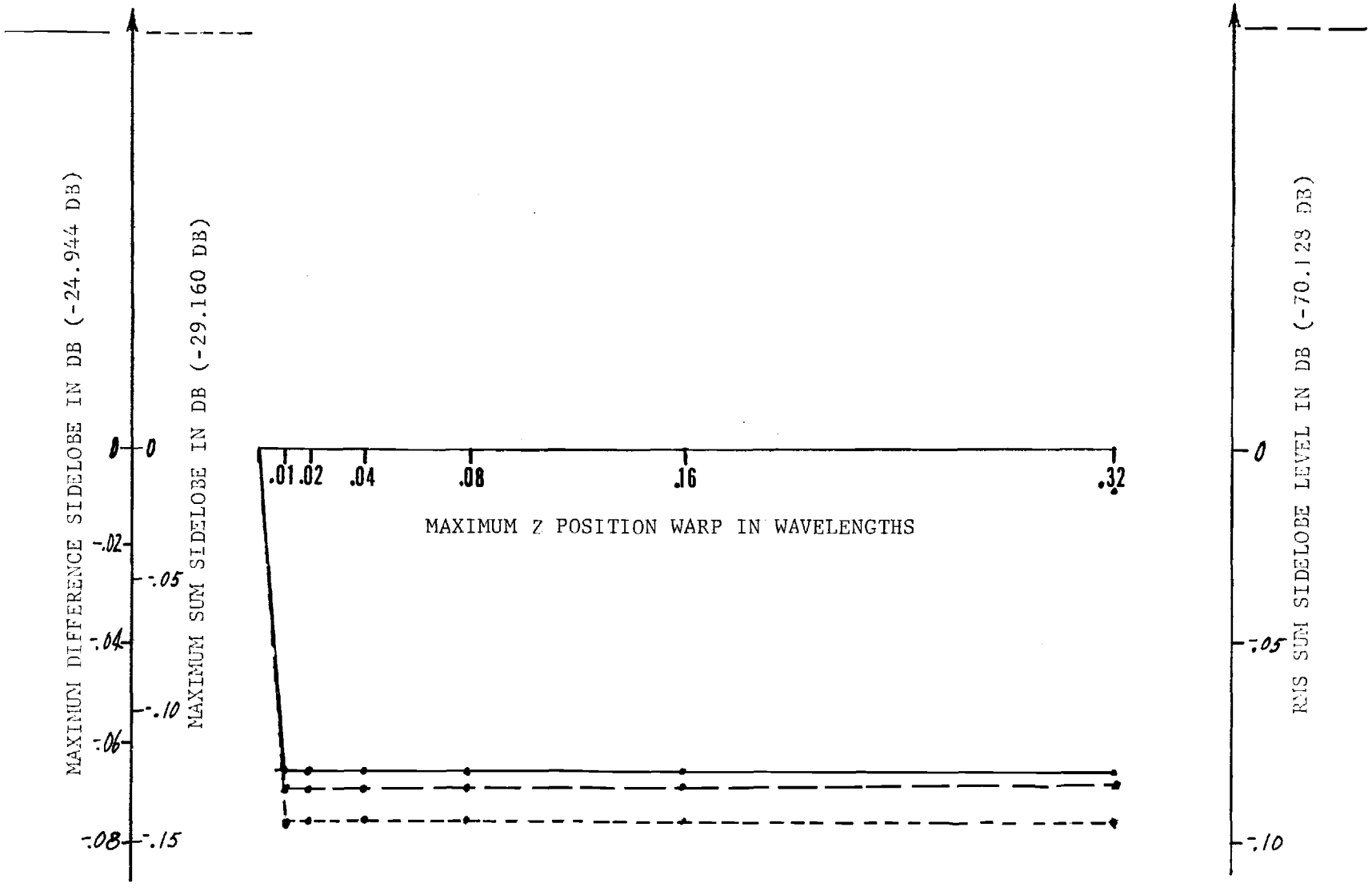

FIGURE A-48. ERRORS IN SIDELOBE LEVELS (TRUE VALUES)

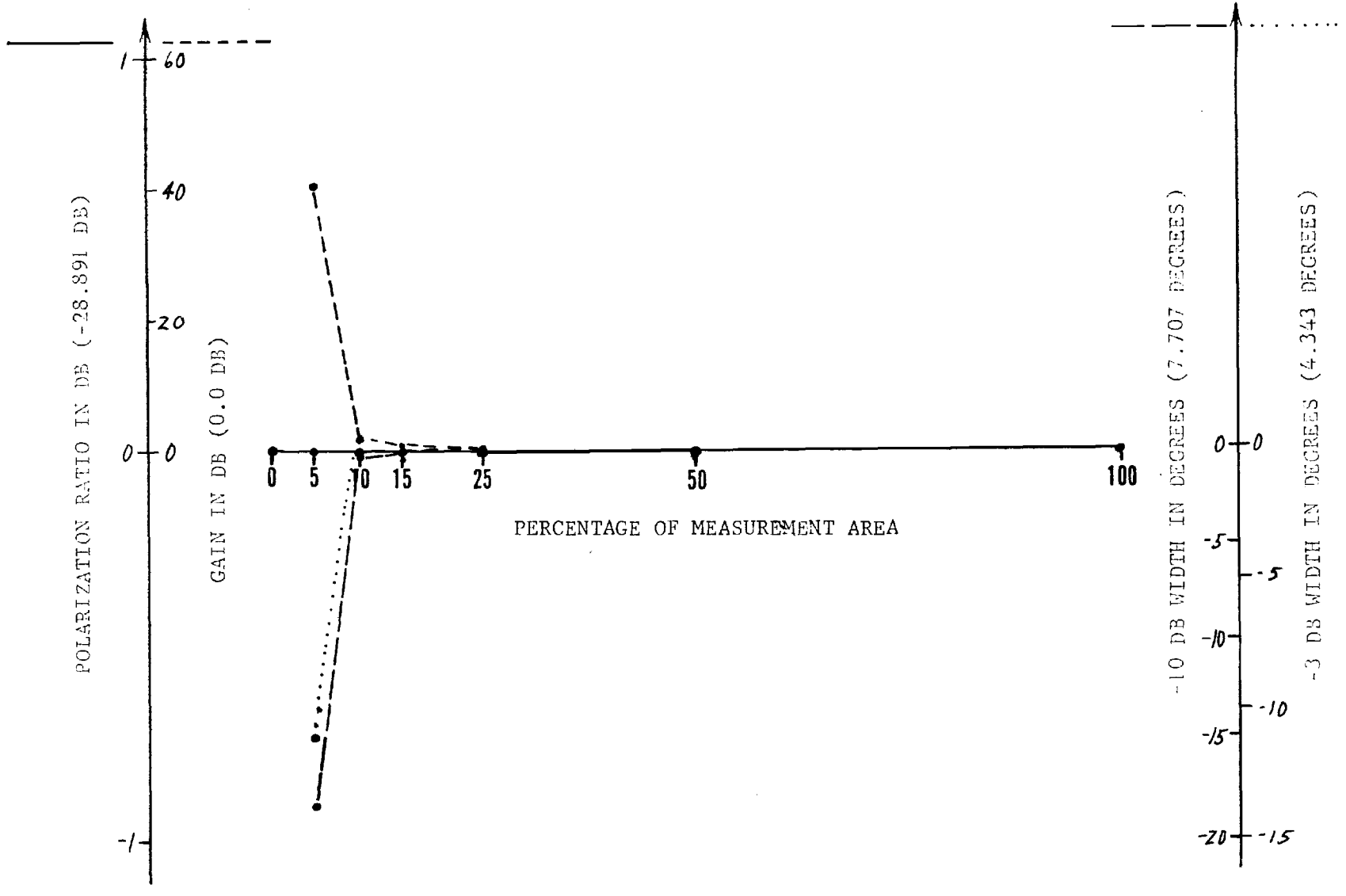

FIGURE A-49. ERRORS IN SUM PATTERN MAIN BEAM PARAMETERS (TRUE VALUES)

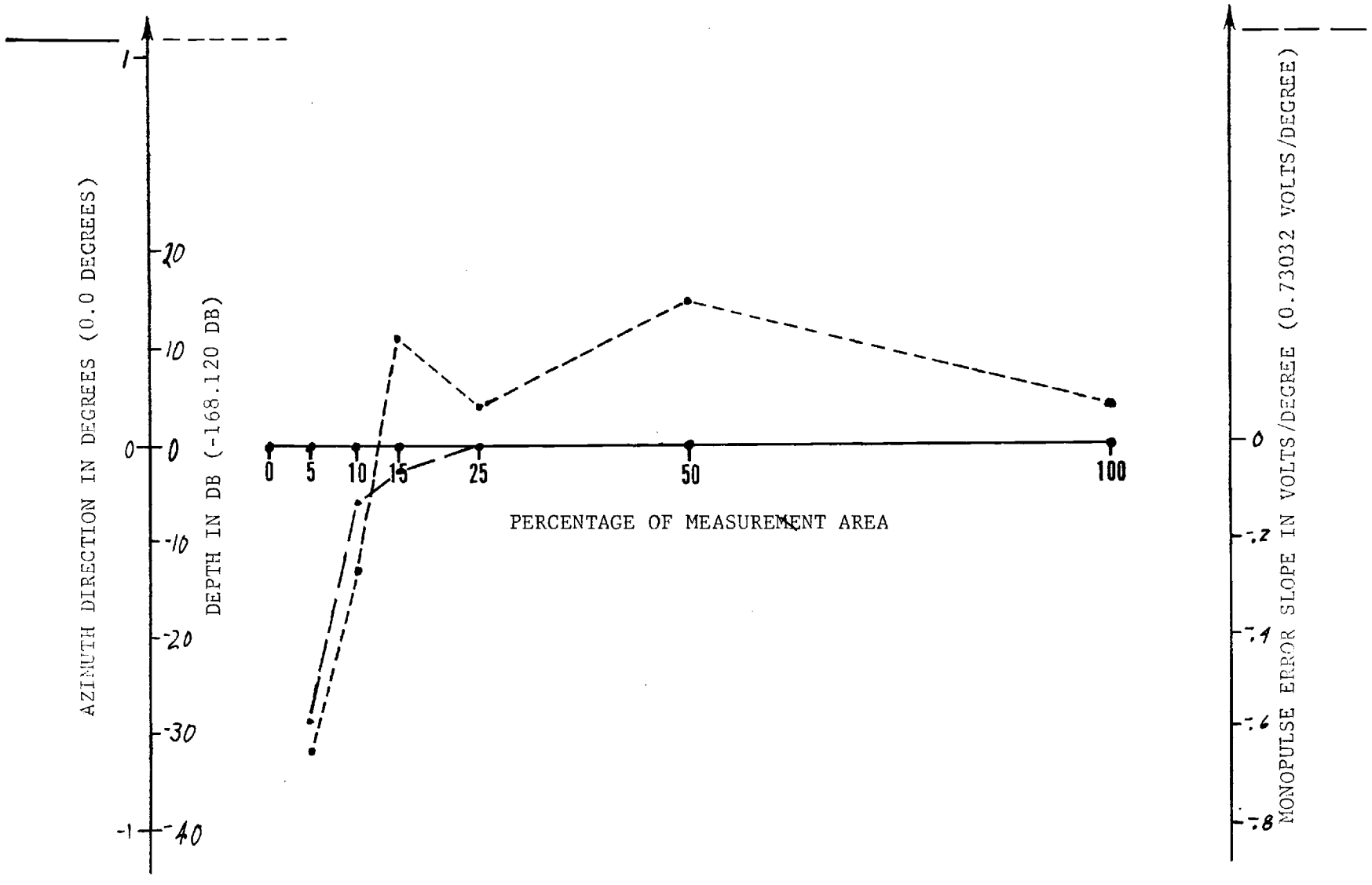

FIGURE A-50. ERRORS IN DIFFERENCE PATTERN NULL PARAMETERS (TRUE VALUES)

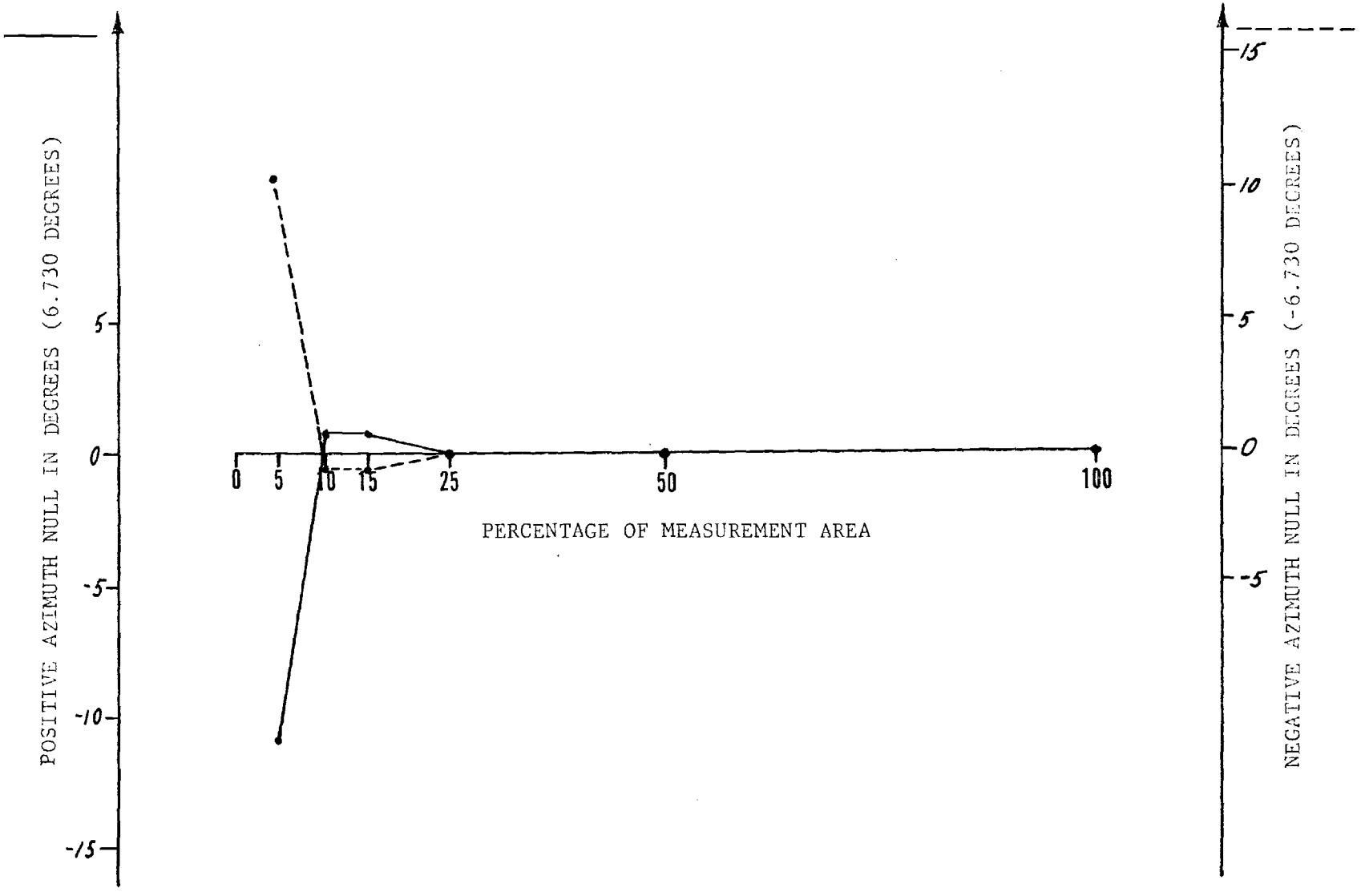

FIGURE A-51. ERRORS IN SUM PATTERN FIRST NULL LOCATIONS (TRUE VALUES)

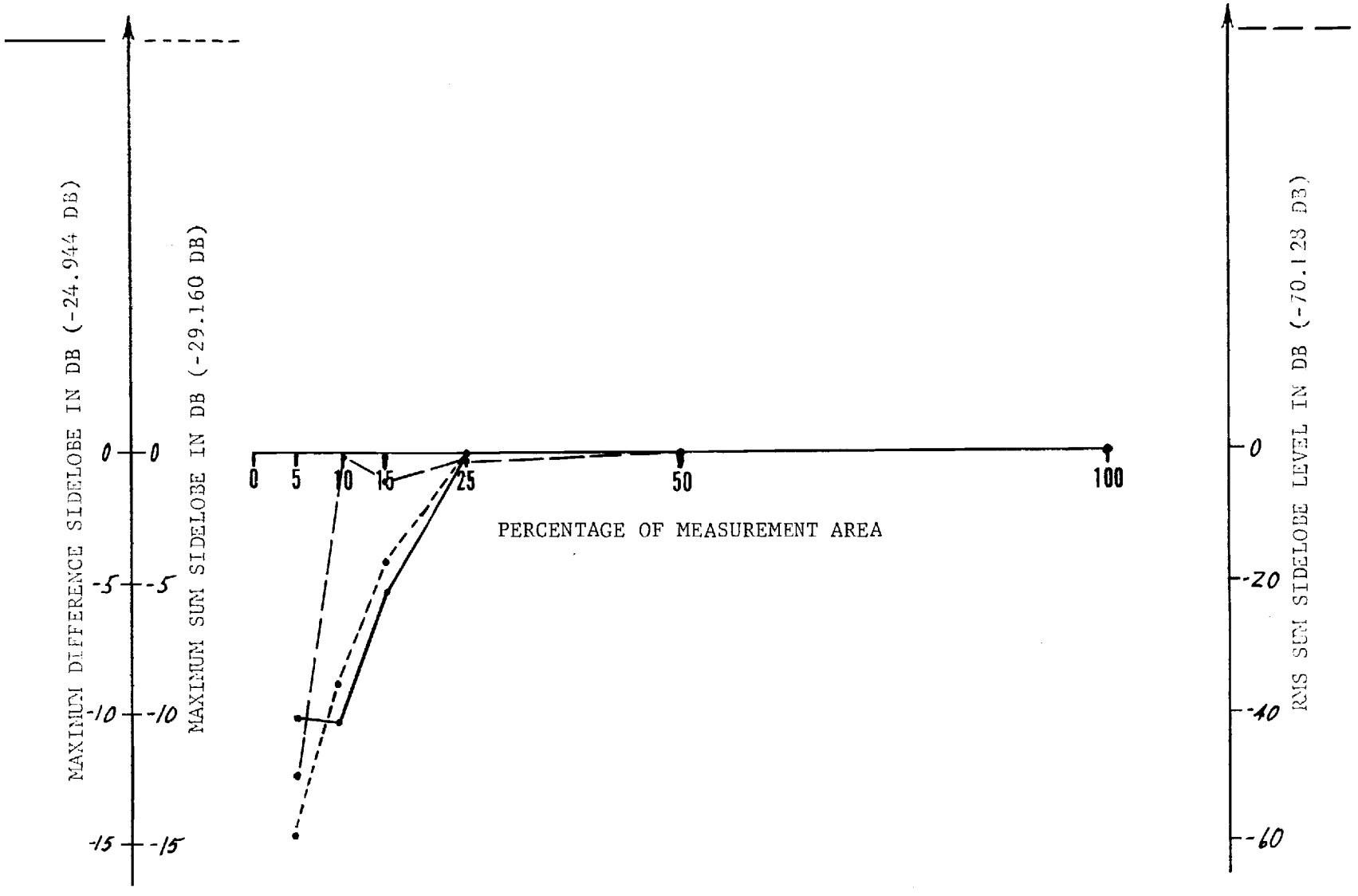

FIGURE A-52. ERRORS IN SIDELOBE LEVELS (TRUE VALUES)

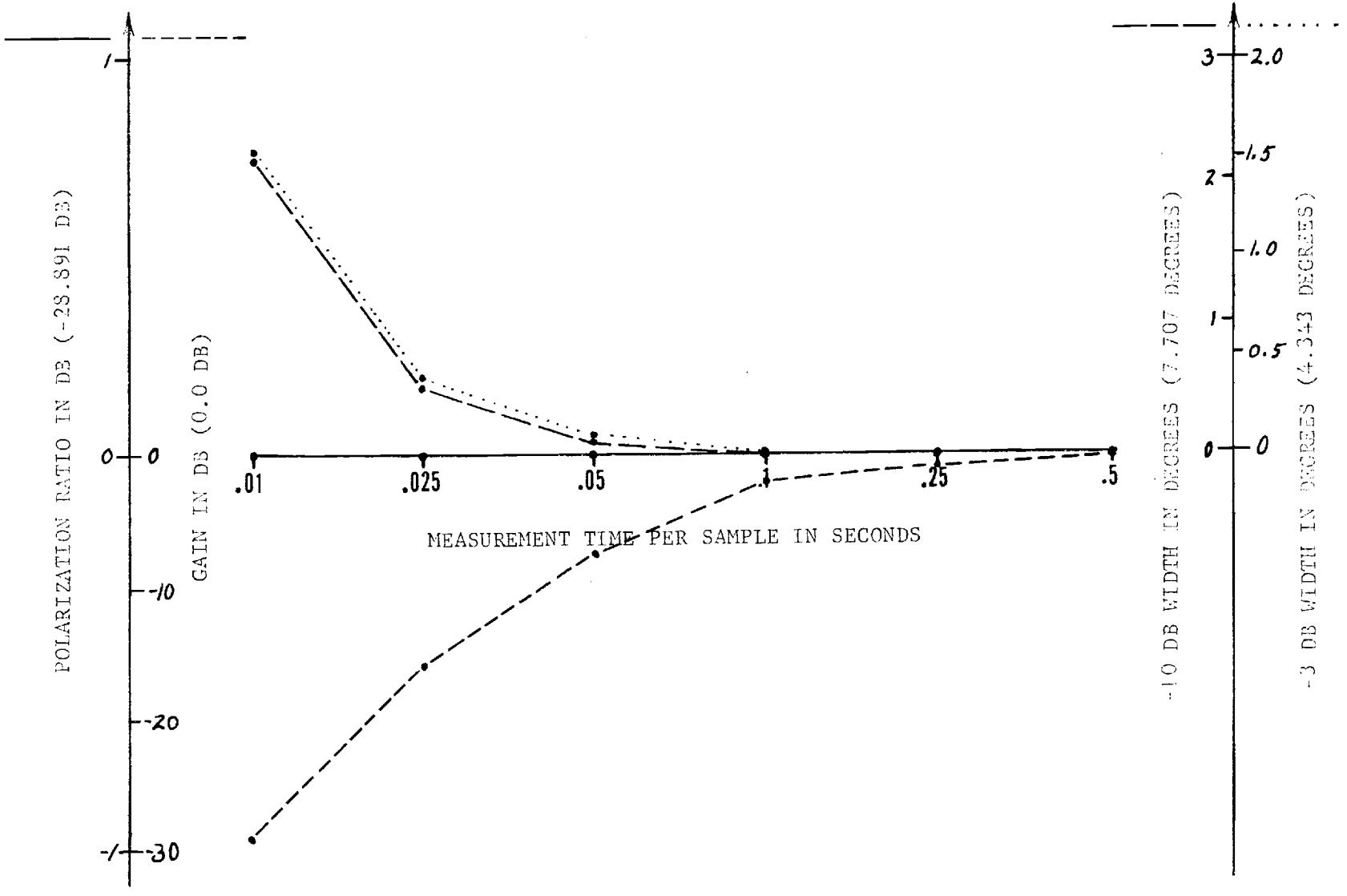

FIGURE A-53. ERRORS IN SUM PATTERN MAIN BEAM PARAMETERS (TRUE VALUES)

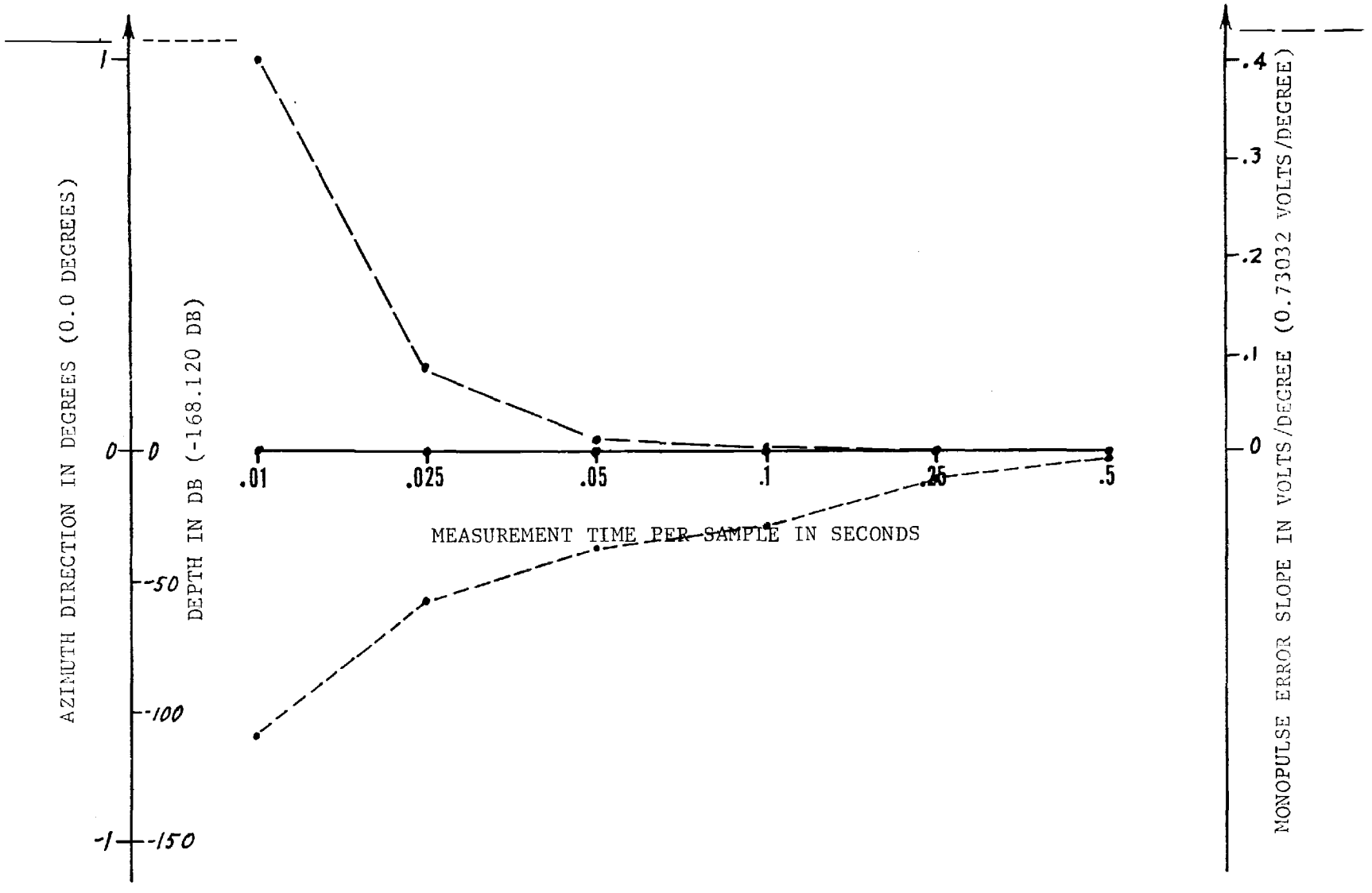

FIGURE A-54. ERRORS IN DIFFERENCE PATTERN NULL PARAMETERS (TRUE VALUES)

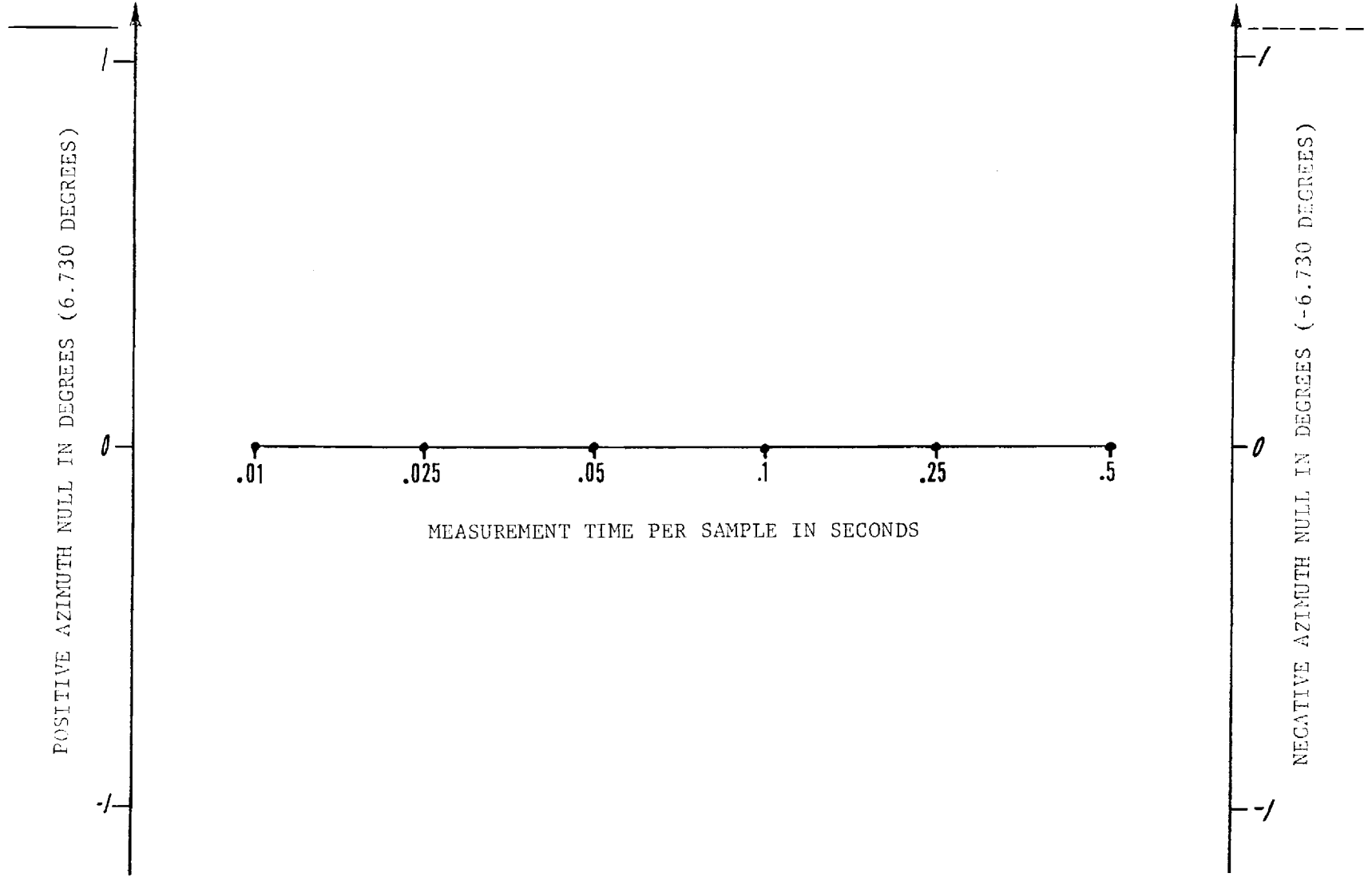

FIGURE A-55. ERRORS IN SUM PATTERN FIRST NULL LOCATIONS (TRUE VALUES)

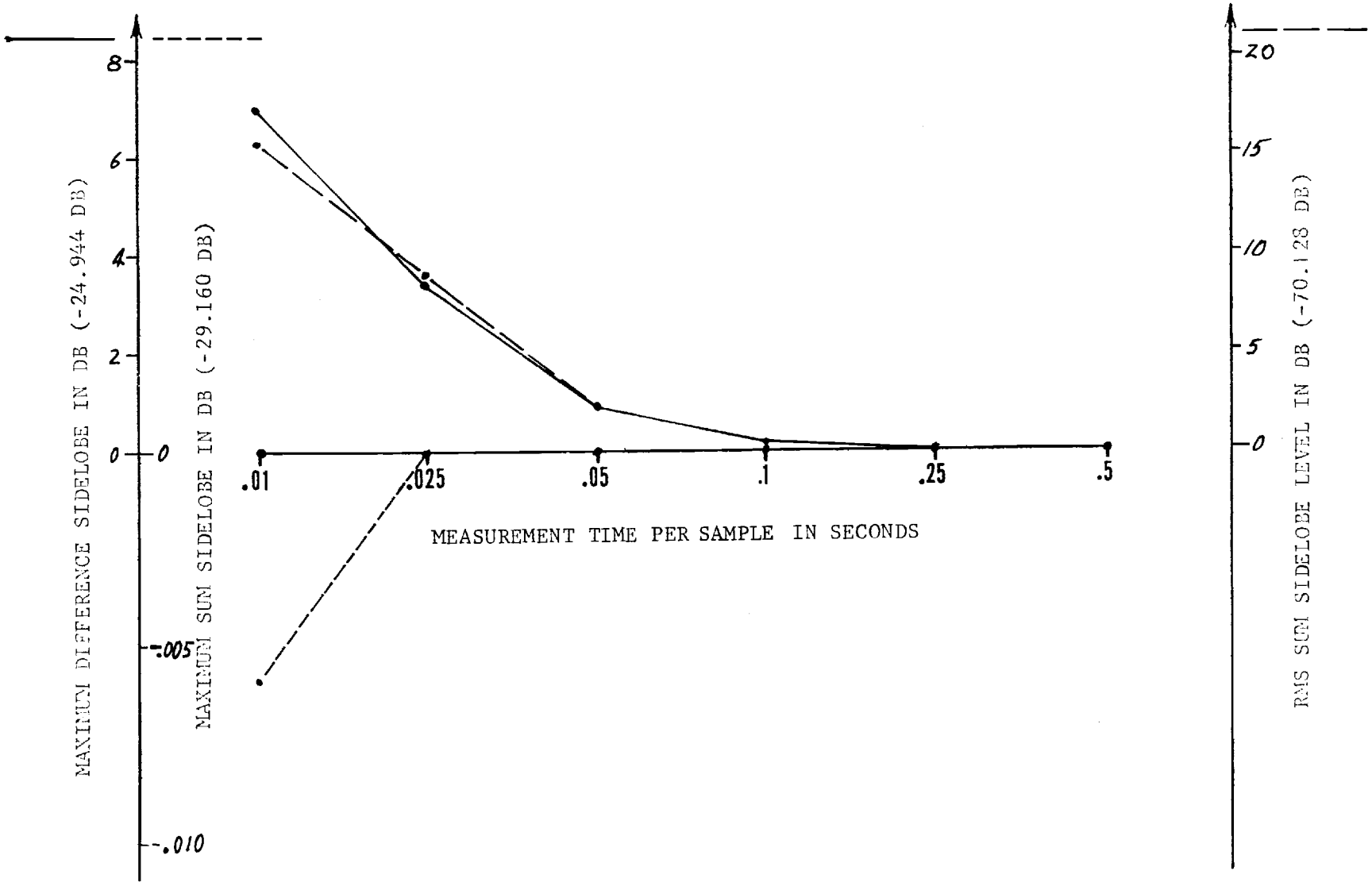

FIGURE A-56. ERRORS IN SIDELOBE LEVELS (TRUE VALUES)

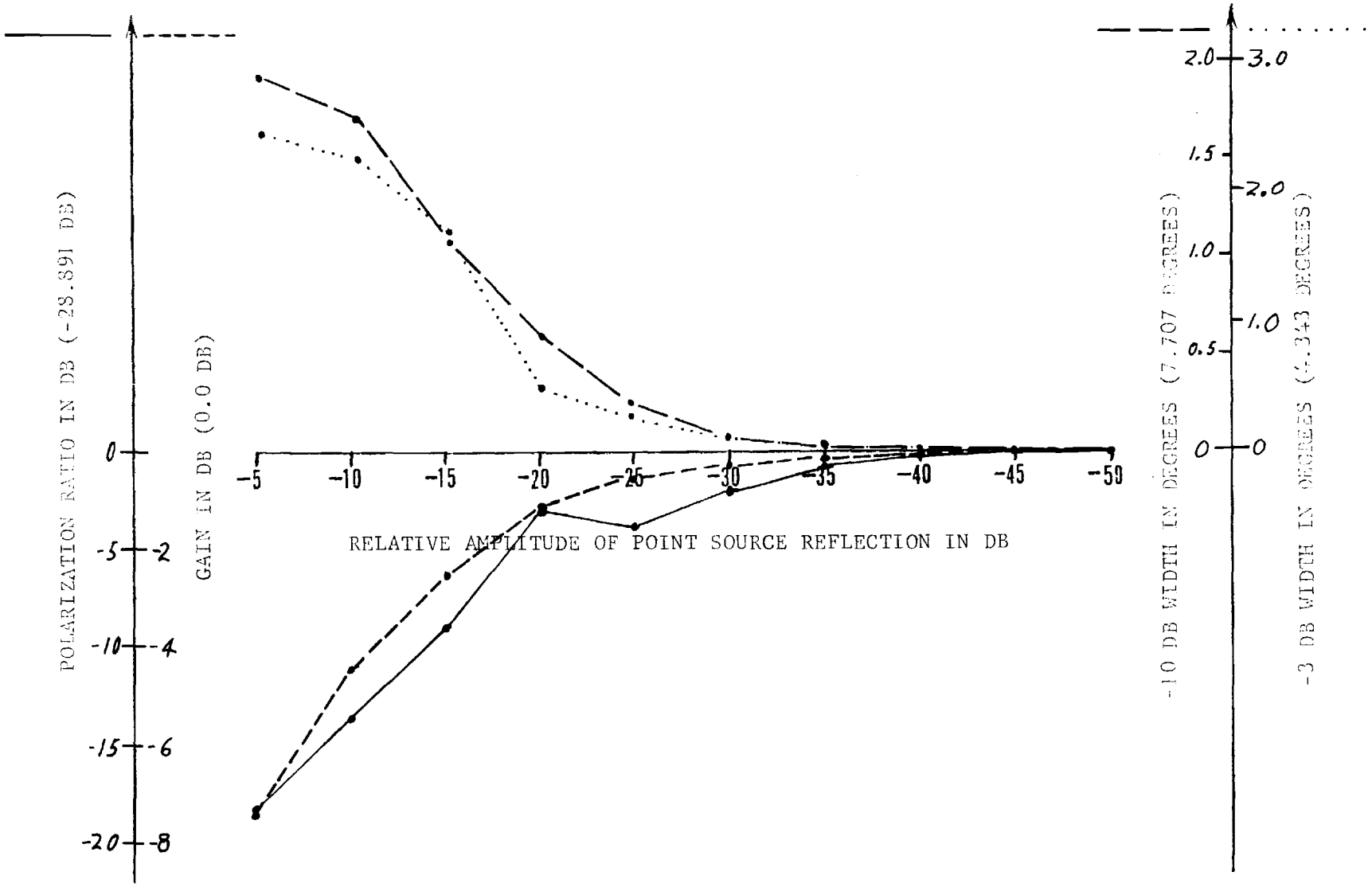

FIGURE A-57. ERRORS IN SUM PATTERN MAIN BEAM PARAMETERS (TRUE VALUES)

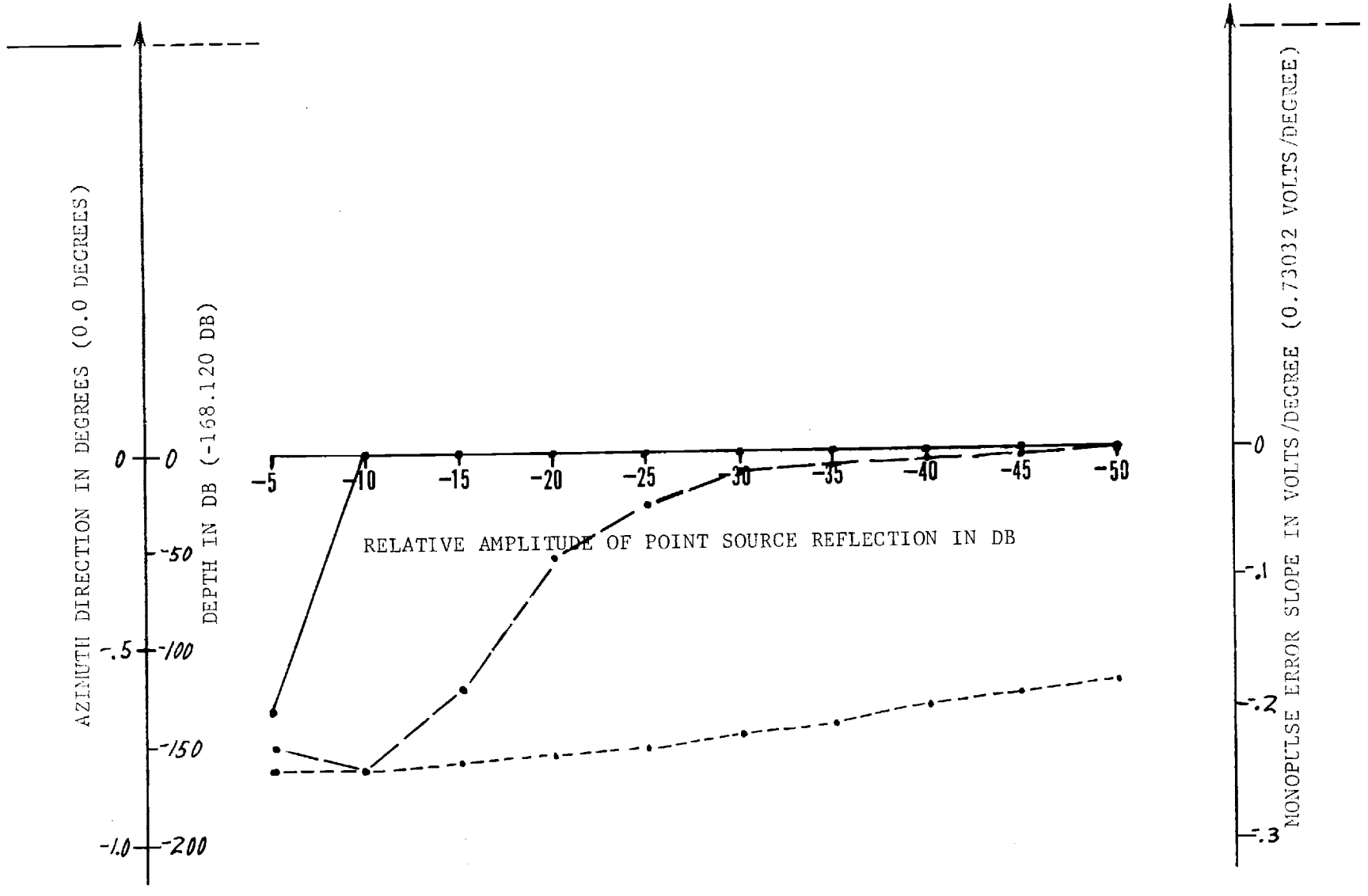

FIGURE A-58. ERRORS IN DIFFERENCE PATTERN NULL PARAMETERS (TRUE VALUES)

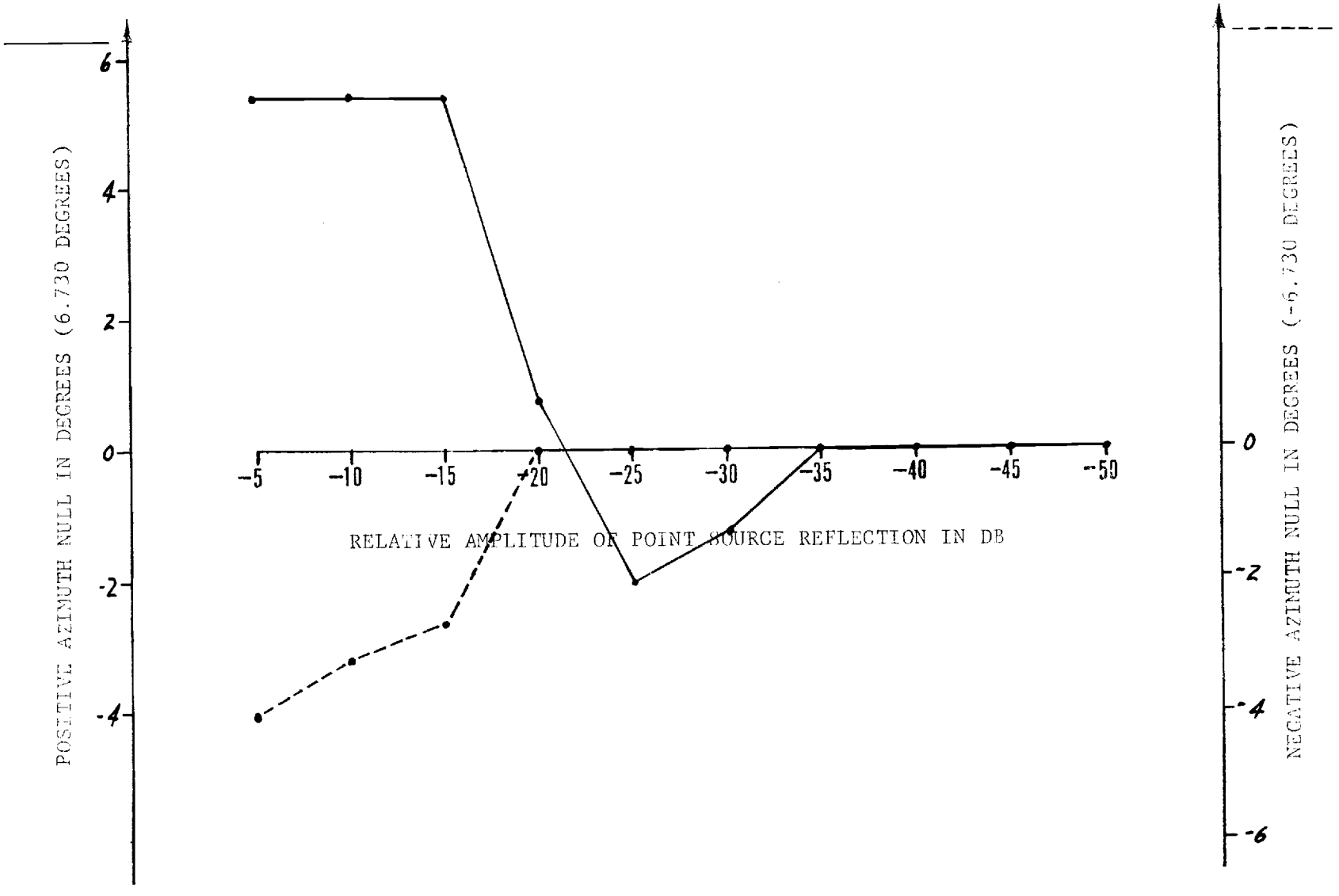

FIGURE A-59. ERRORS IN SUM PATTERN FIRST NULL LOCATIONS (TRUE VALUES)

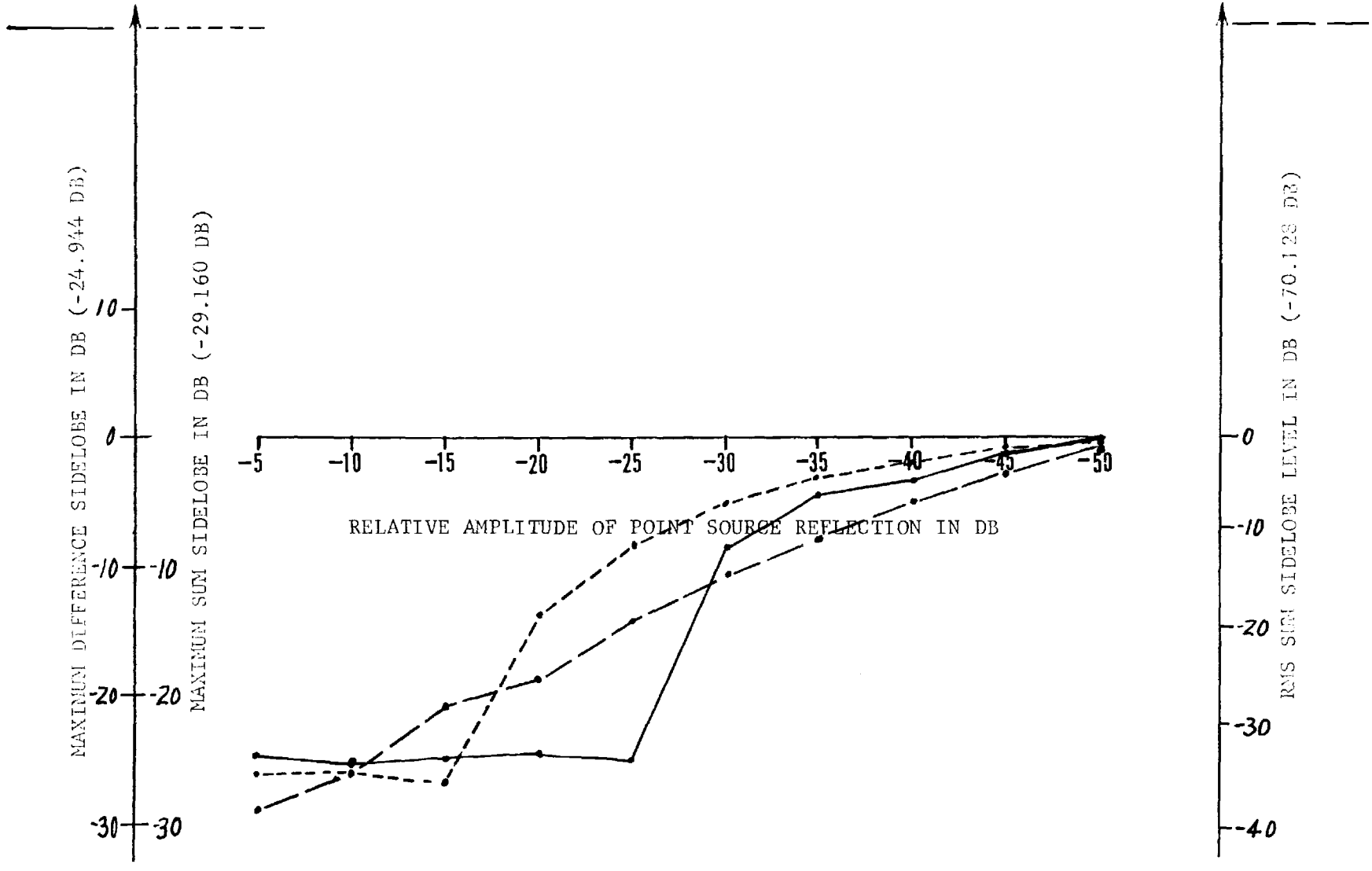

FIGURE A-60. ERRORS IN SIDELOBE LEVELS (TRUE VALUES)

APPENDIX B

ADDITIONAL FAR-FIELD PATTERN CUTS

This Appendix contains additional representative cuts of far-field antenna patterns obtained on outdoor ranges at Georgia Tech and at Scientific-Atlanta. Included here are samples of cuts not shown in the body of this report. For example, the principal plane cuts of Feed 2 are shown here over the full angular range covered, while in Sections 5 and 7 only the range of $\pm$ 48 degrees was presented. Similarly, pattern cuts off principal planes are shown here for Feed 2 while in Section 7 only principal plane results are shown. More detail on the data collected for RMS sidelobe determination is also presented here for the difference pattern of Feed 1 and the sum pattern of Feed 2.

The Appendix does not contain all far-field data collected. In the interest of efficiency only representative cuts are shown, since the program's emphasis was not on qualification of the antenna, but rather on qualification of a measurement technique.

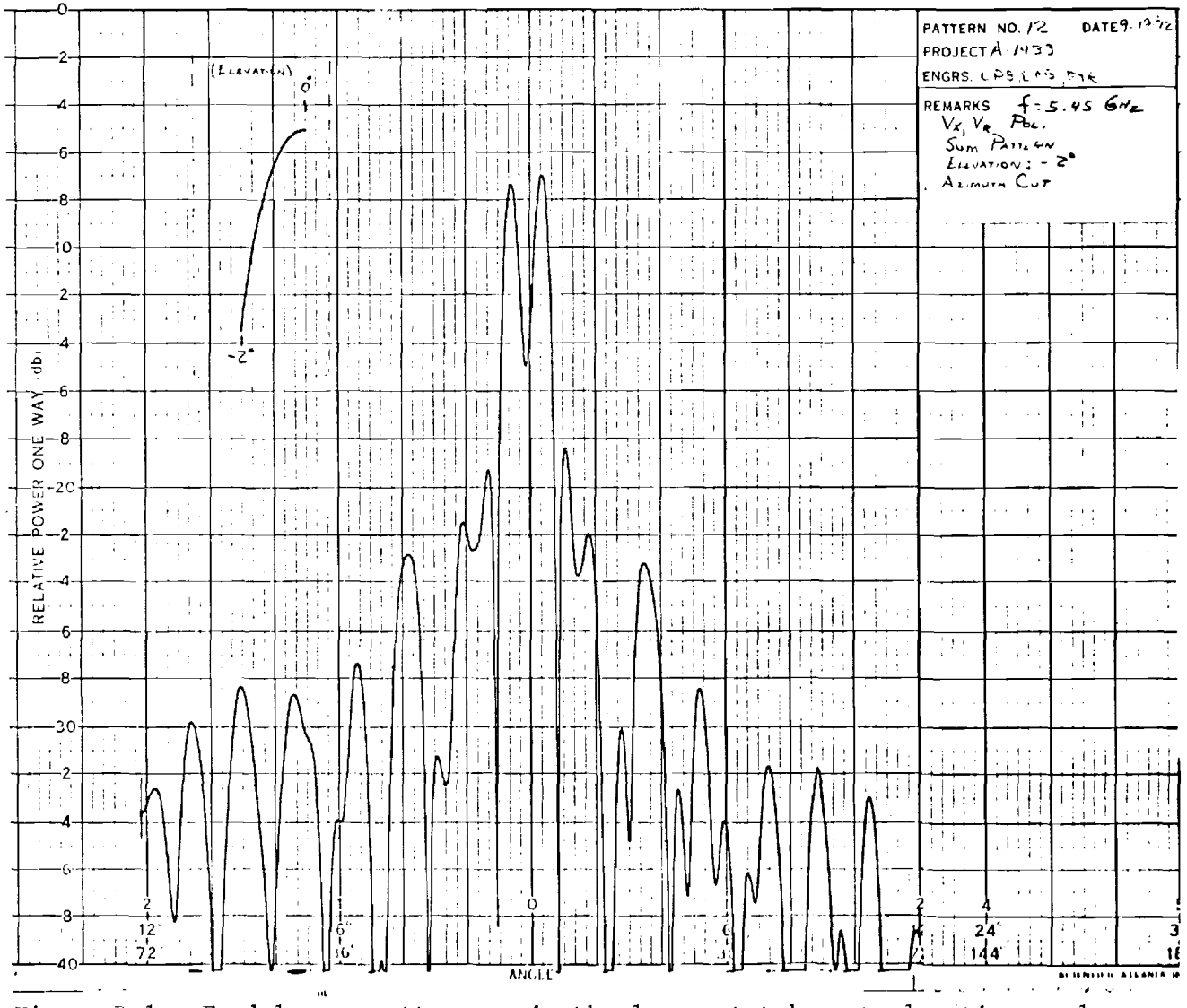

Figure B-1. Feed 1, sum pattern, azimuth plane cut taken at elevation angle of -2 degrees, 12 degrees per major division.

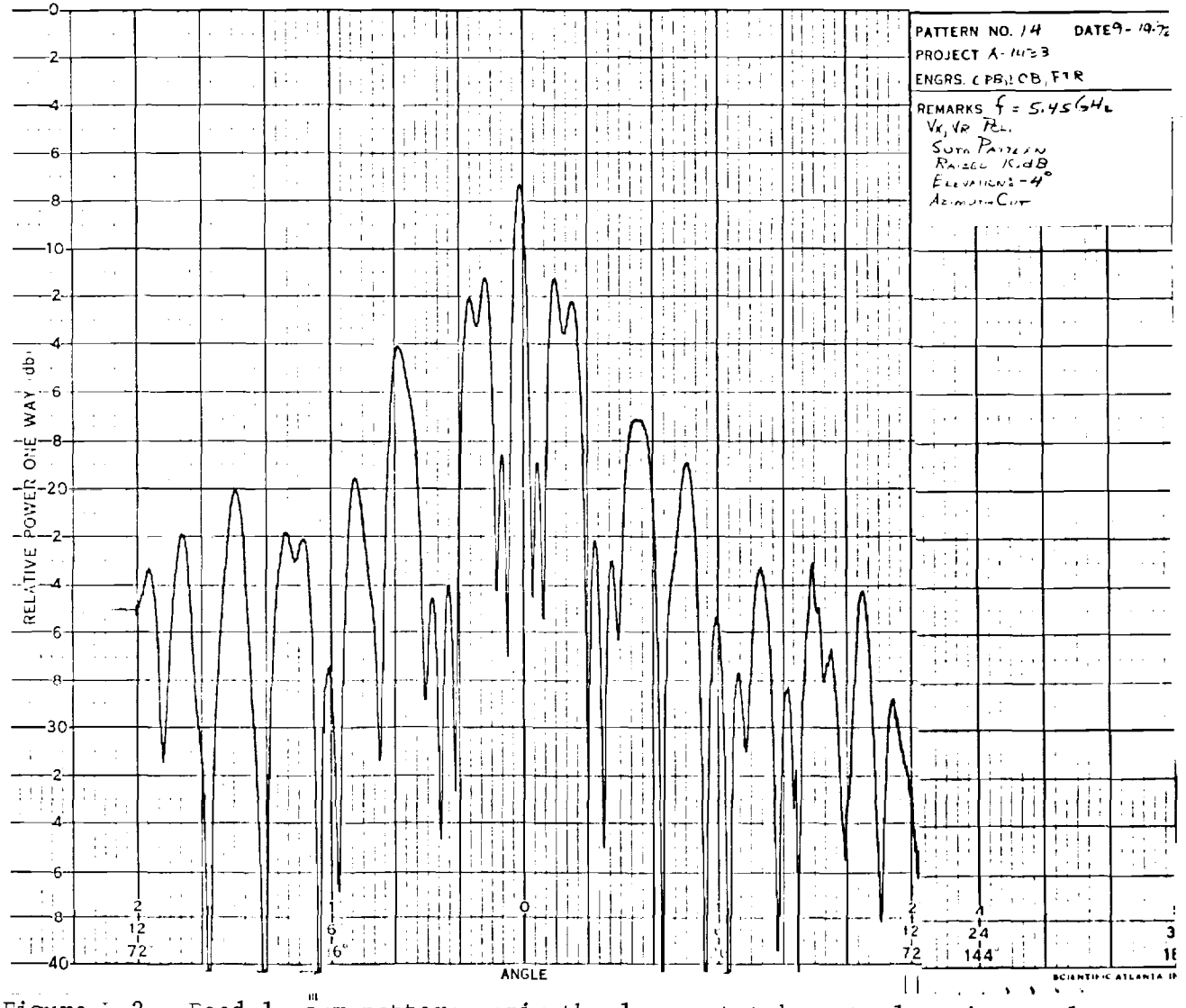

Figure B-2. Feed 1, sum pattern, azimuth plane cut taken at elevation angle of -4 degrees, 12 degrees per major division, pattern raised 10 dB.

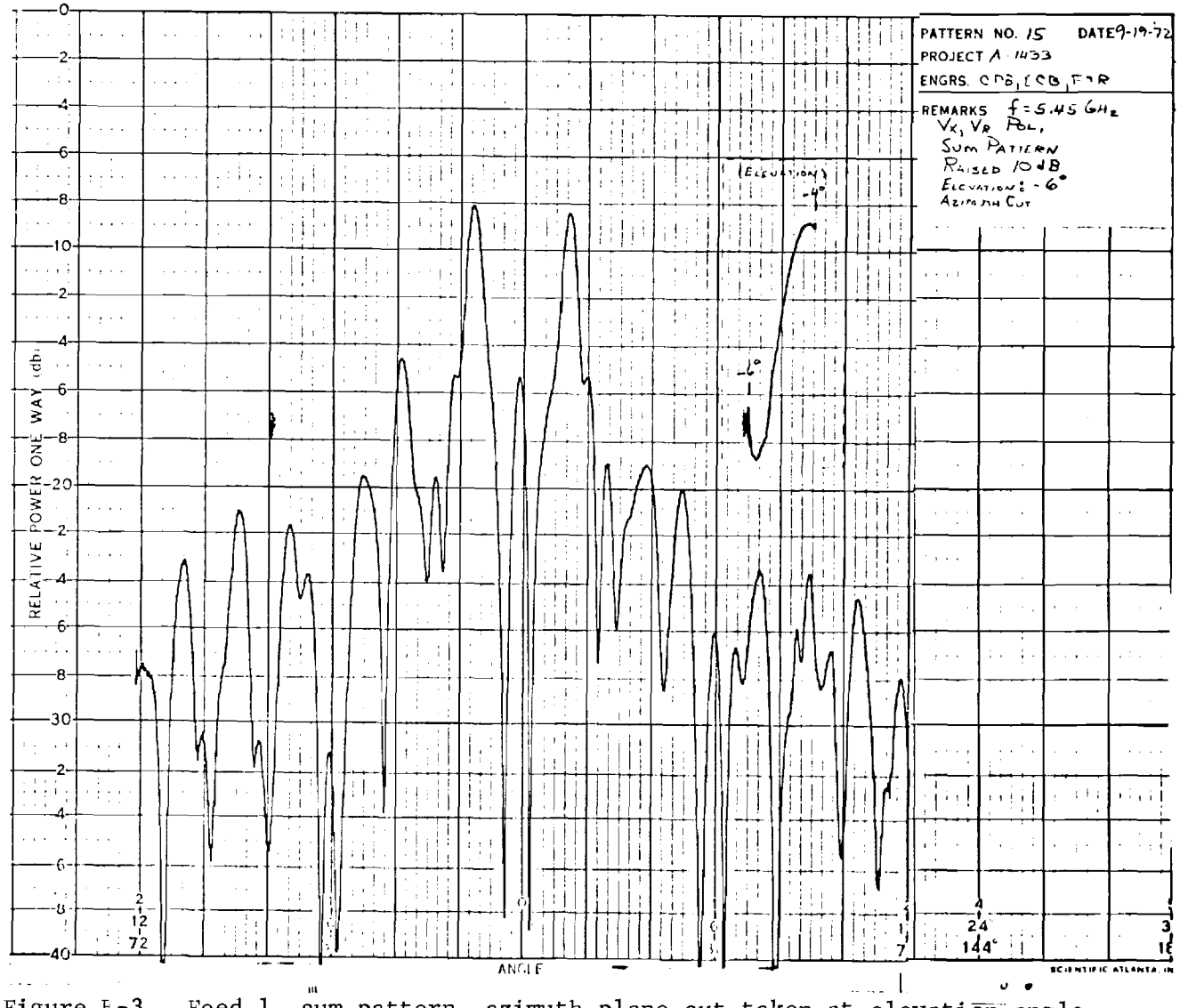

Figure E-3. Feed 1, sum pattern, azimuth plane cut taken at elevation angle of -6 degrees, 12 degrees per major division, pattern raised 10 dB.

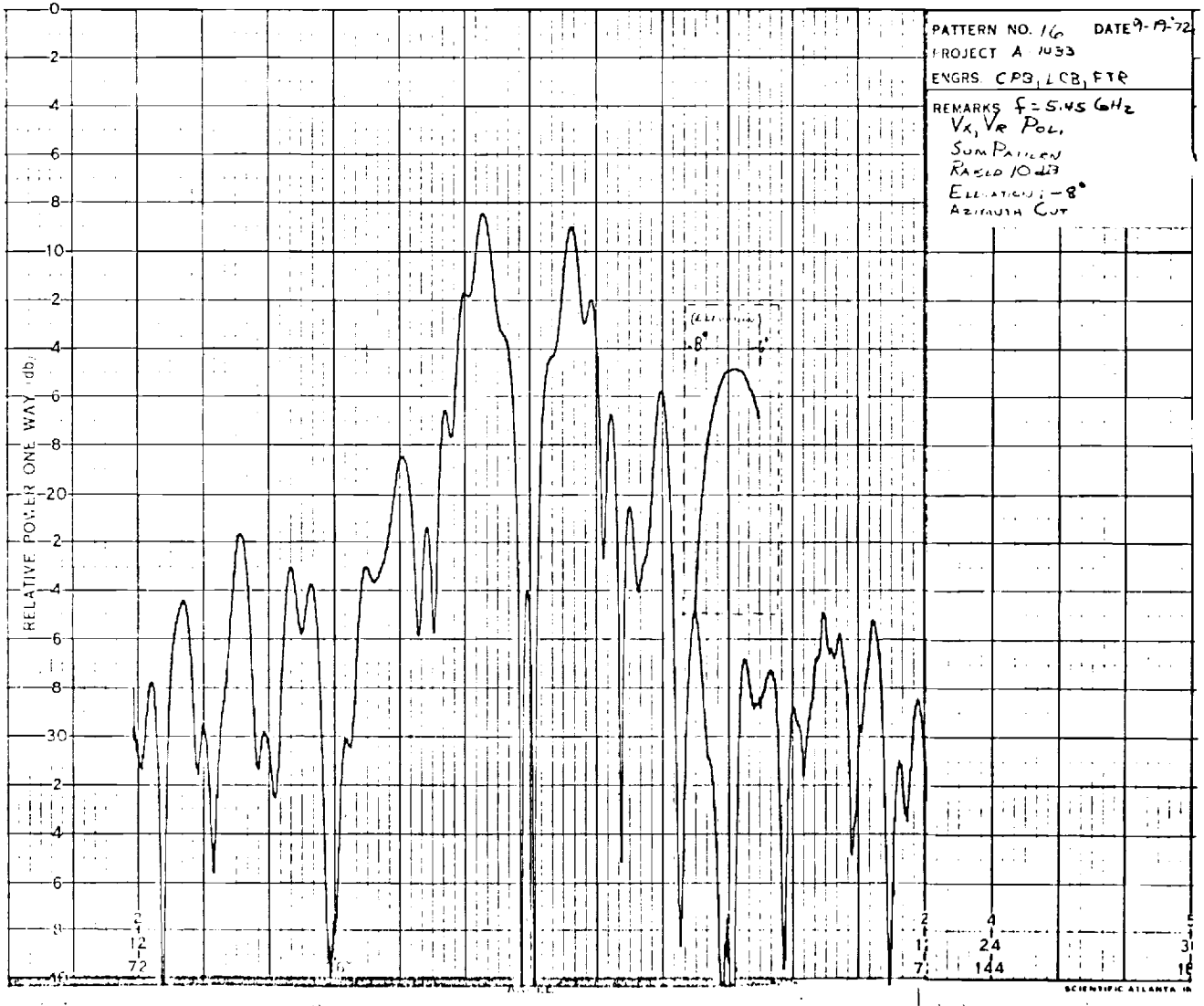

Figure 1-4. Feed 1, sum pattern, azimuth plane cut taken at elevation angle of -8 degrees, 12 degrees per major division, pattern raised 10 dB.

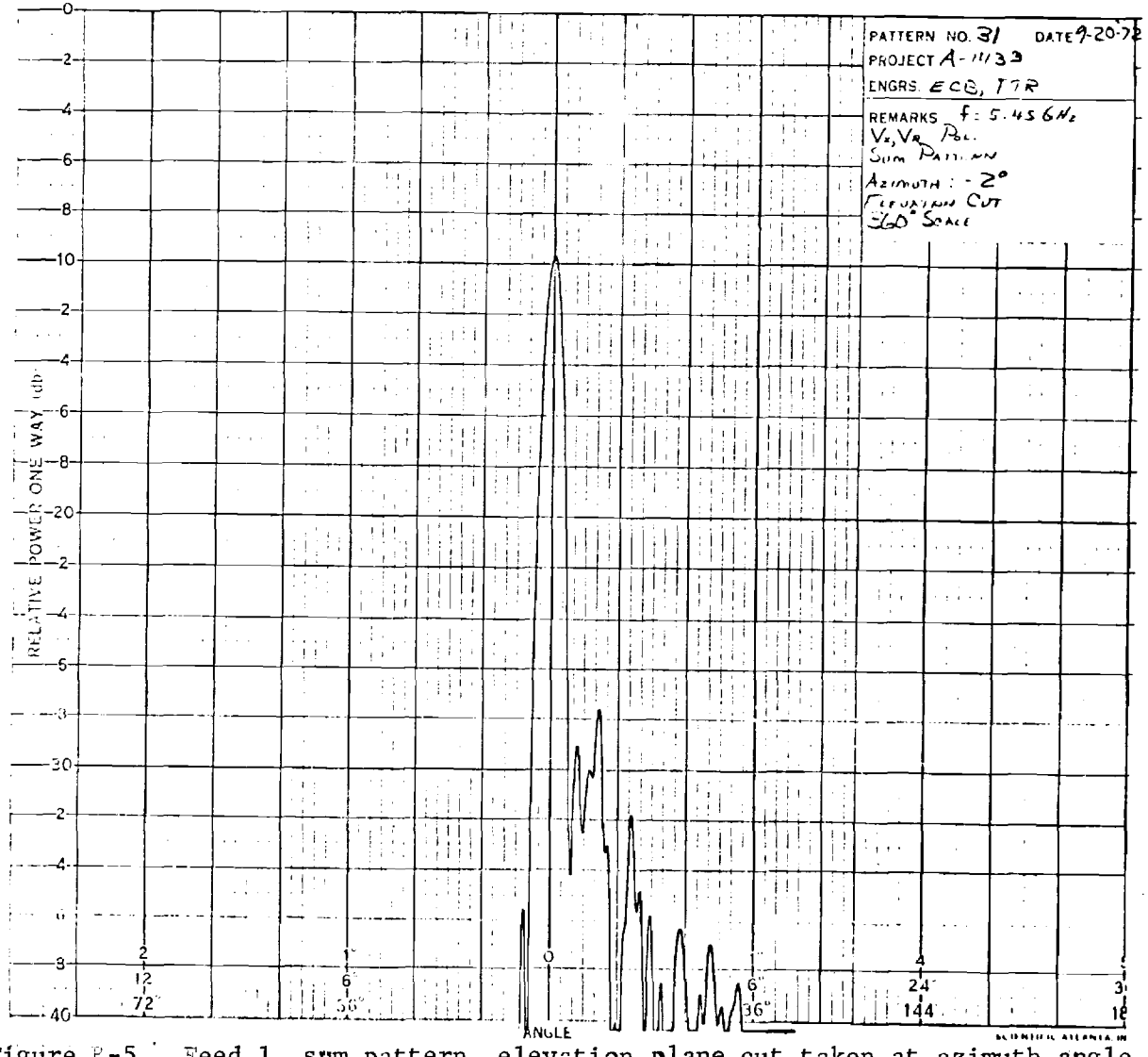

Figure B-5. Feed 1, sum pattern, elevation plane cut taken at azimuth angle of -2 degrees, 12 degrees per major division.

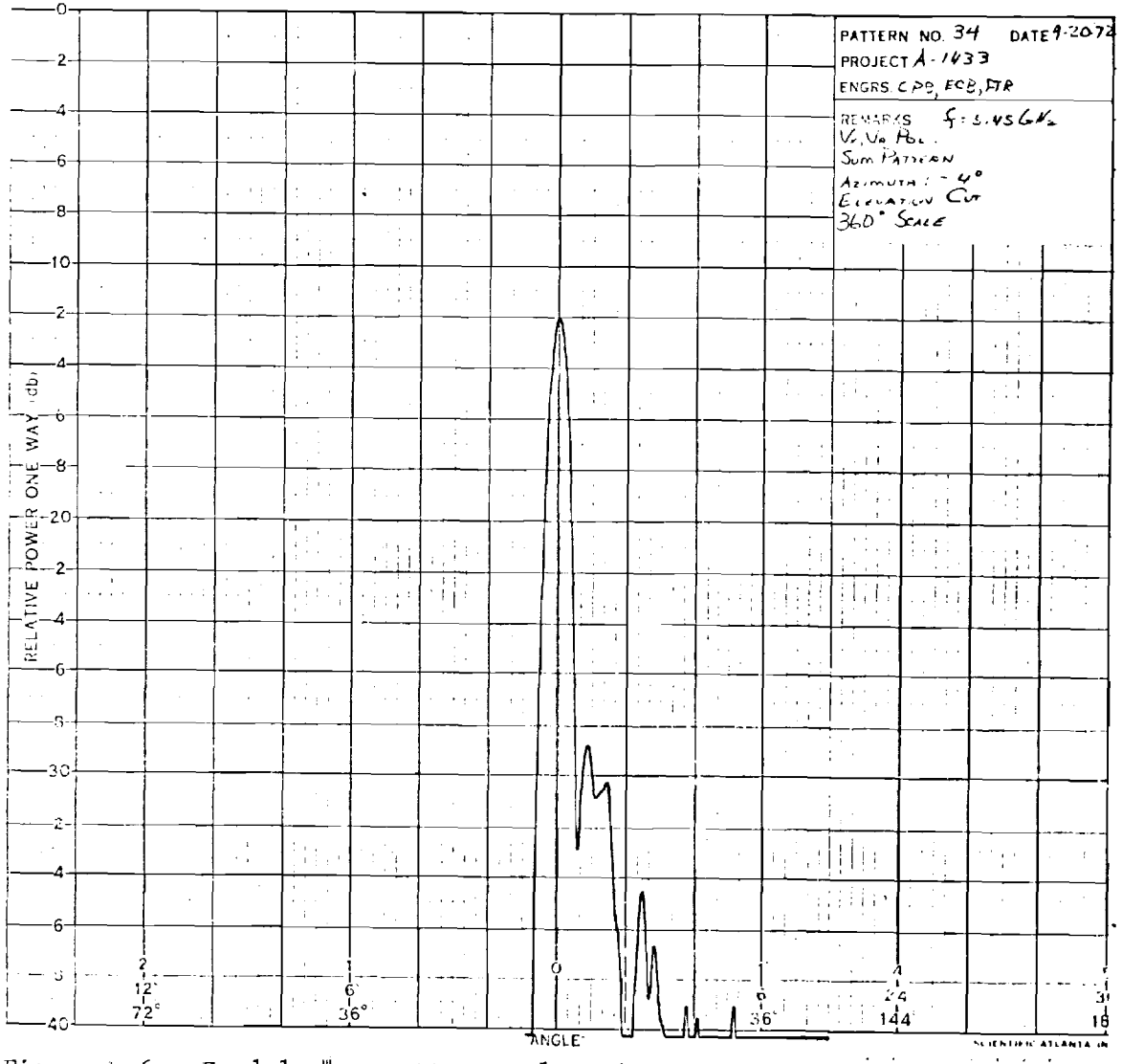

Figure 1-6. Feed 1, sum pattern, elevation plane cut taken at azimuth angle of -4 degrees, 12 degrees per major division.

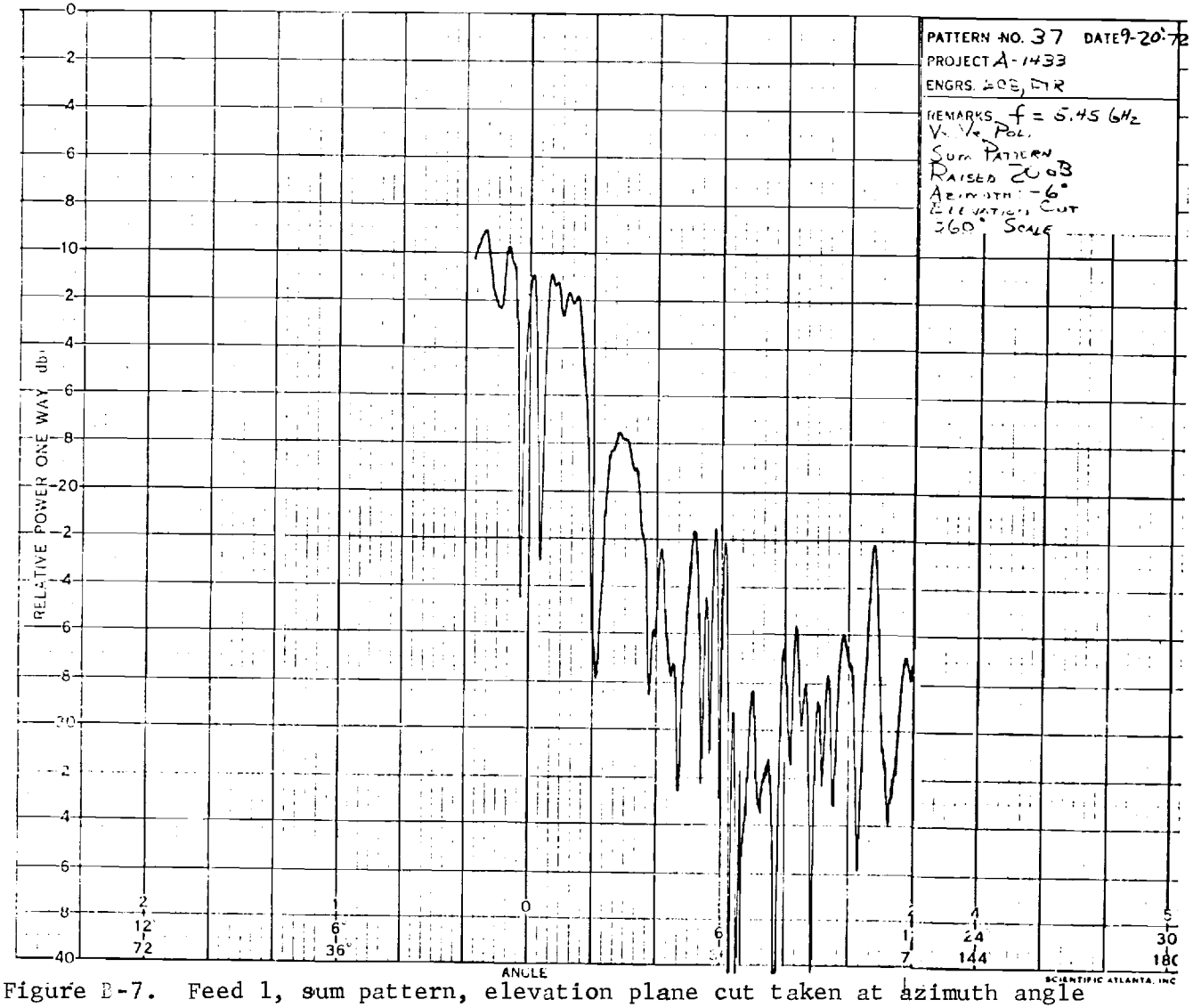

Figure B-7. Feed 1, sum pattern, elevation plane cut taken at azimuth angle of -6 degrees, 12 degrees per major division, pattern raised 20 dB.

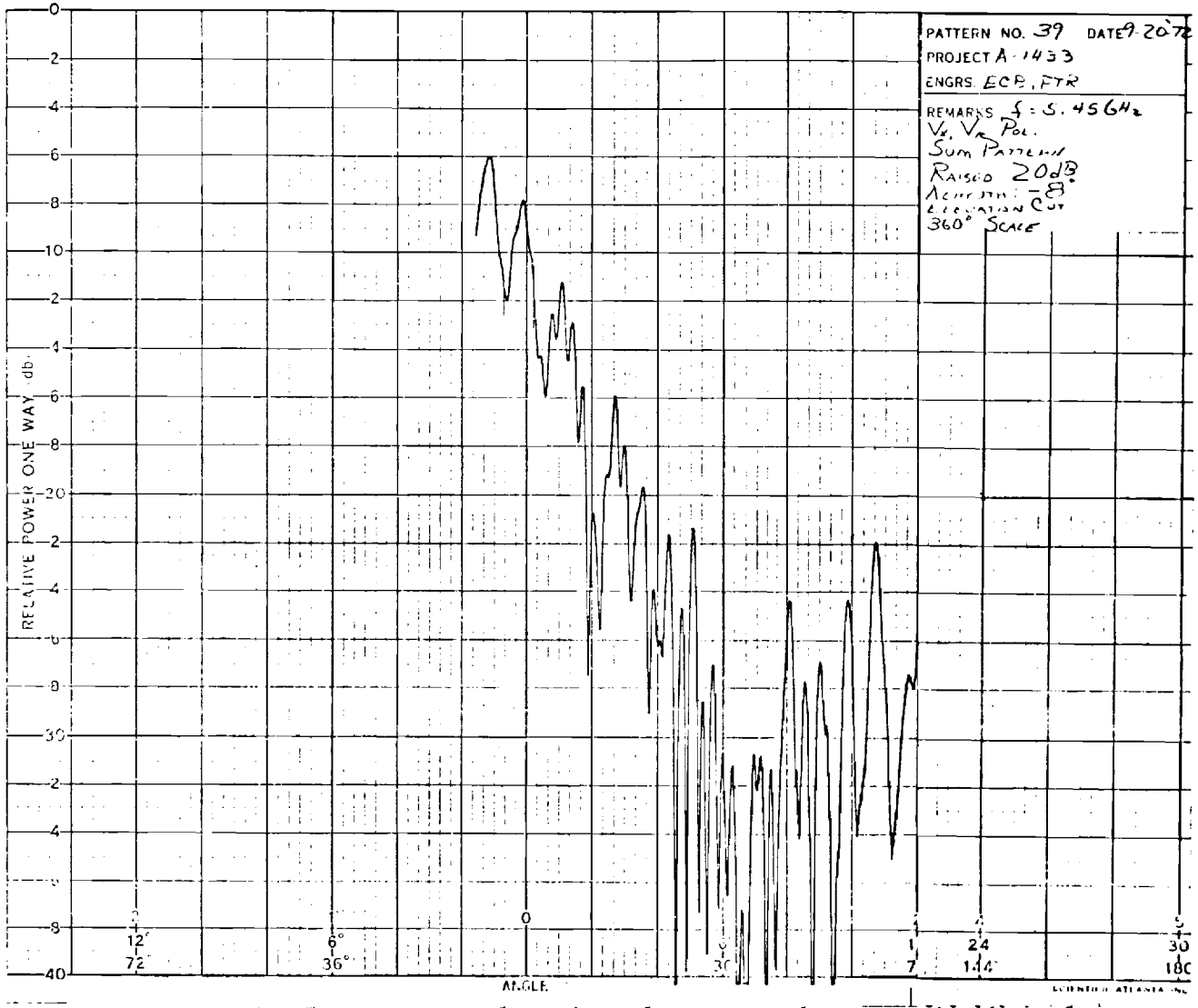

Figure B-8. Feed 1, sum pattern, elevation plane cut taken at azimuth angle of -8 degrees, 12 degrees per major division, pattern raised 20 dB.

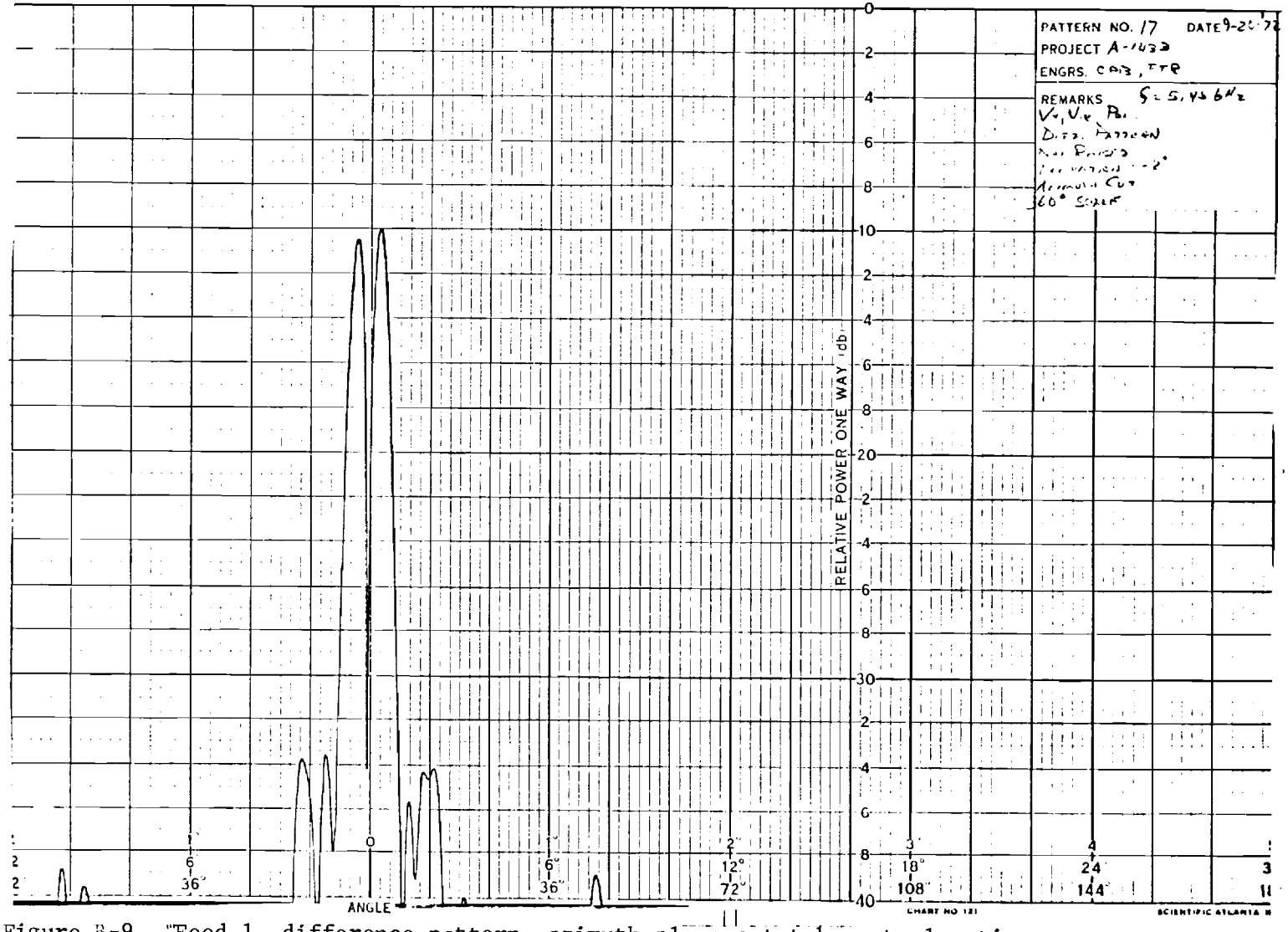

Figure B-9. "Feed 1, difference pattern, azimuth plane cut taken at elevation angle of -2 degrees, 12 degrees per major division.

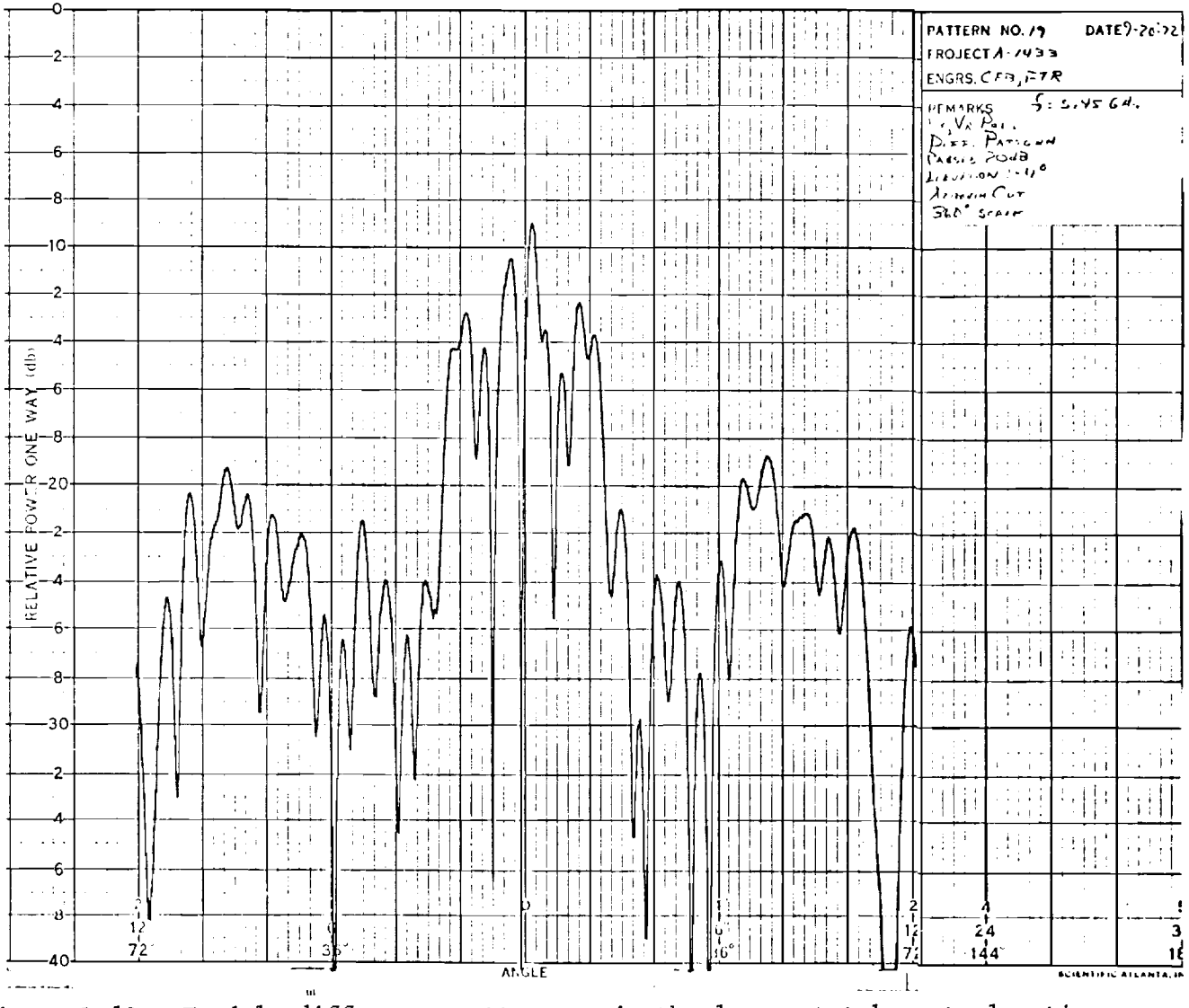

Figure E-10. Feed 1, difference pattern, azimuth plane cut taken at elevation angle of -4 degrees, 12 degrees per major division, pattern raised 20 dB.

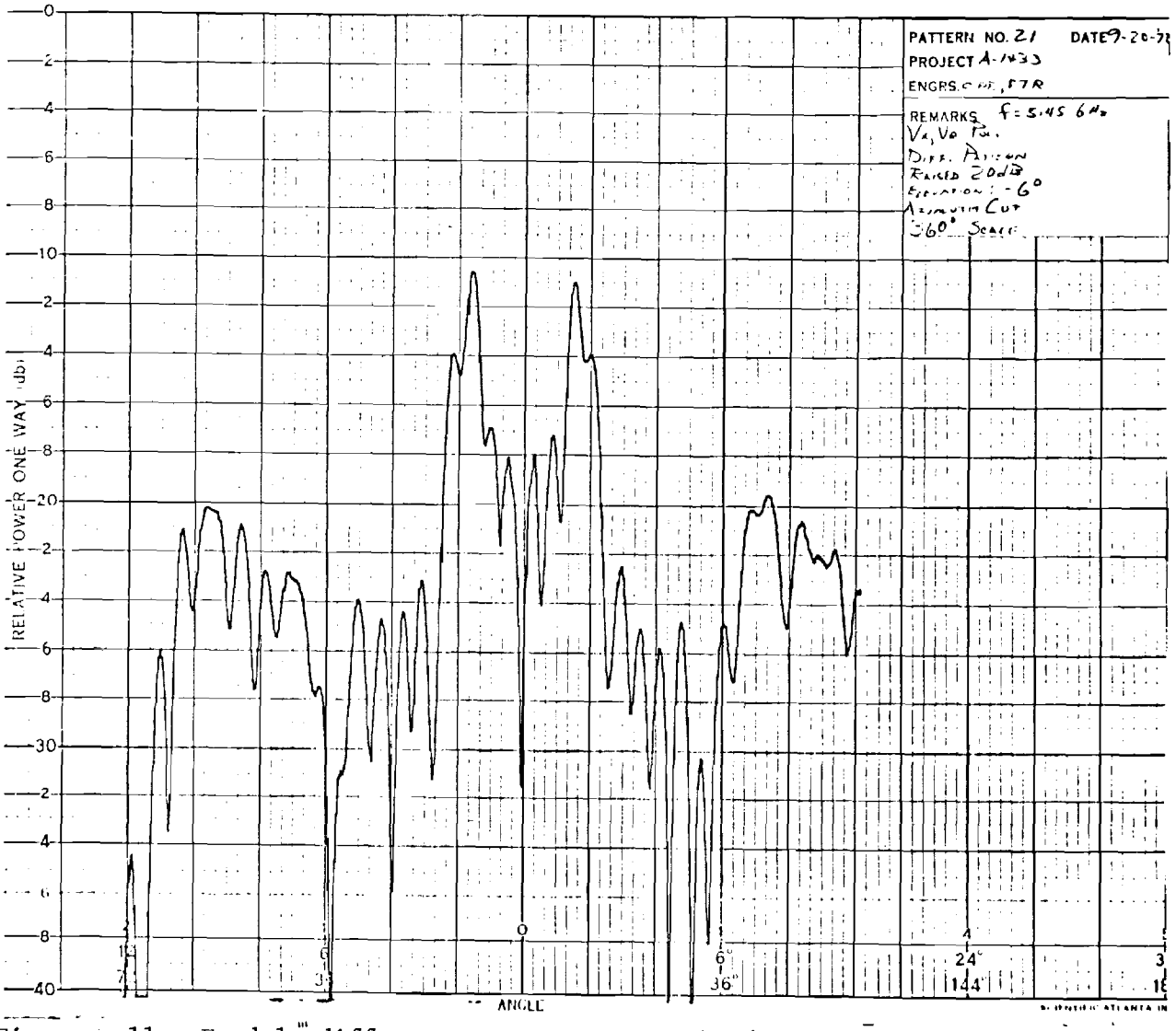

Figure 2-11. Feed 1,''' difference pattern, azimuth plane cut taken at elevation angle of -6 degrees, 12 degrees per major division, pattern raised 20 dB.

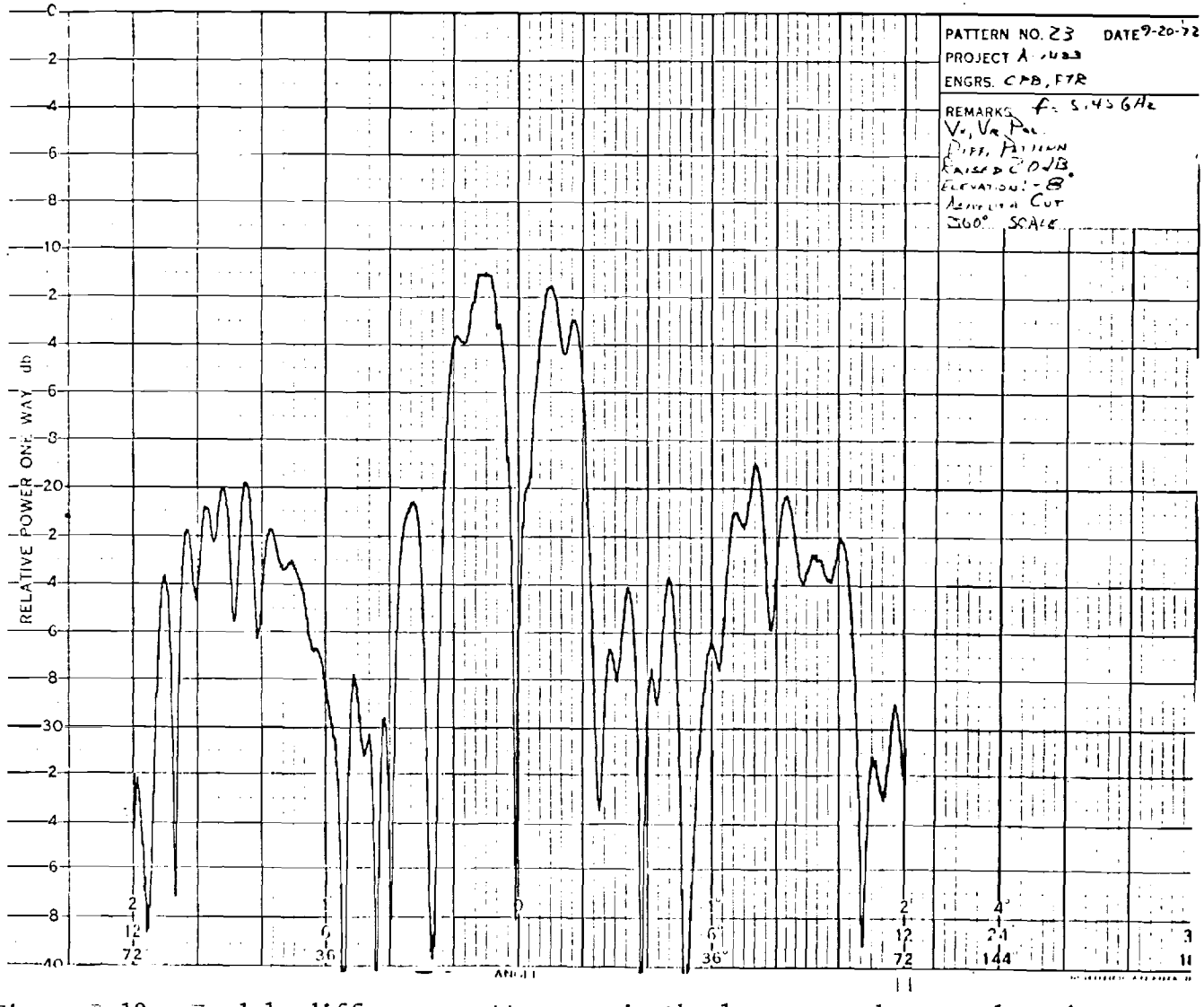

Figure B-12. Feed 1, difference pattern, azimuth plane cut taken at elevation angle of -8 degrees, 12 degrees per major division, pattern raised 20 dB.

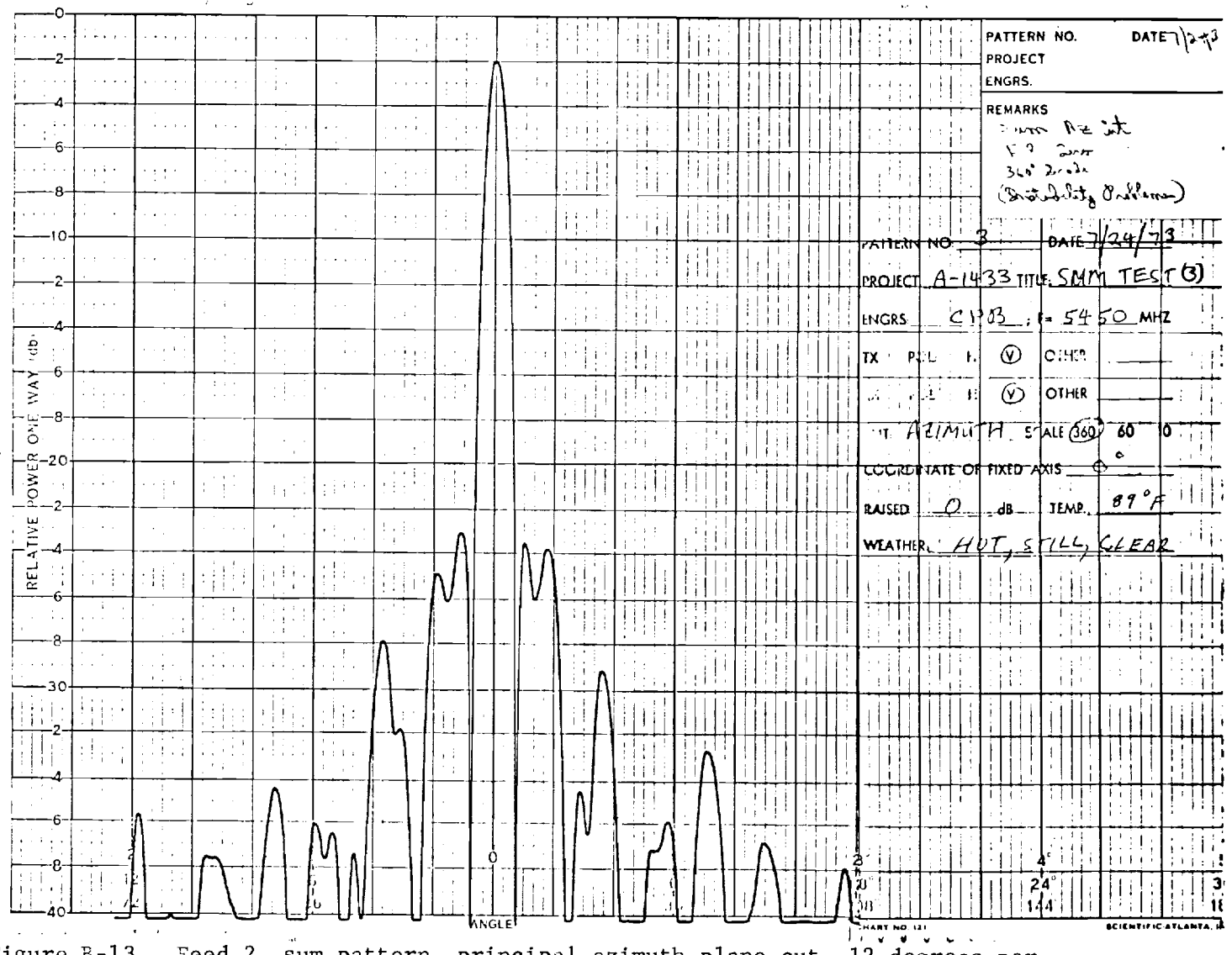

Figure B-13. Feed 2, sum pattern, principal azimuth plane cut, 12 degrees per major division.

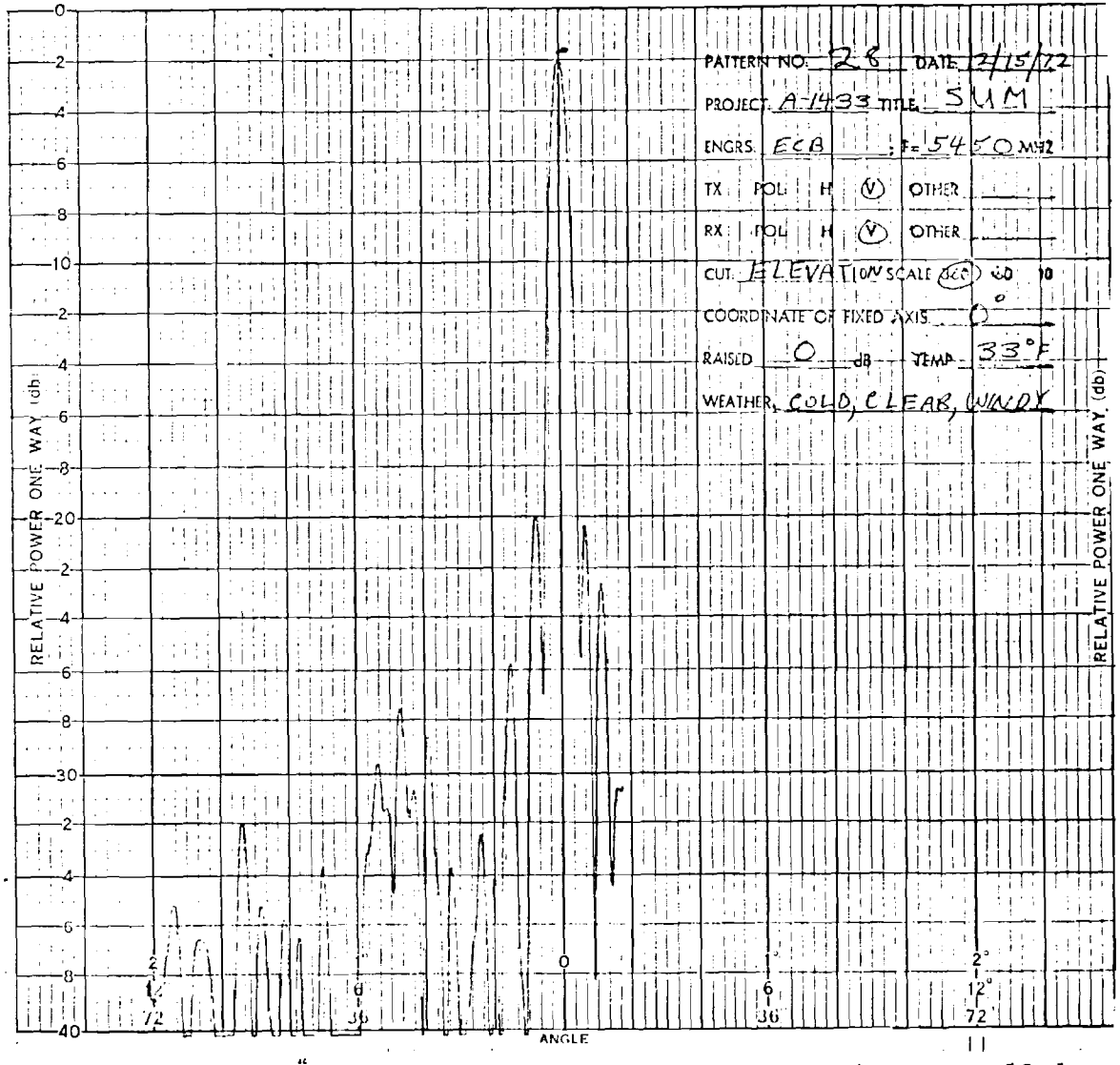

Figure 8-14. Feed 2, sum pattern, principal elevation plane cut, 12 degrees per major division.

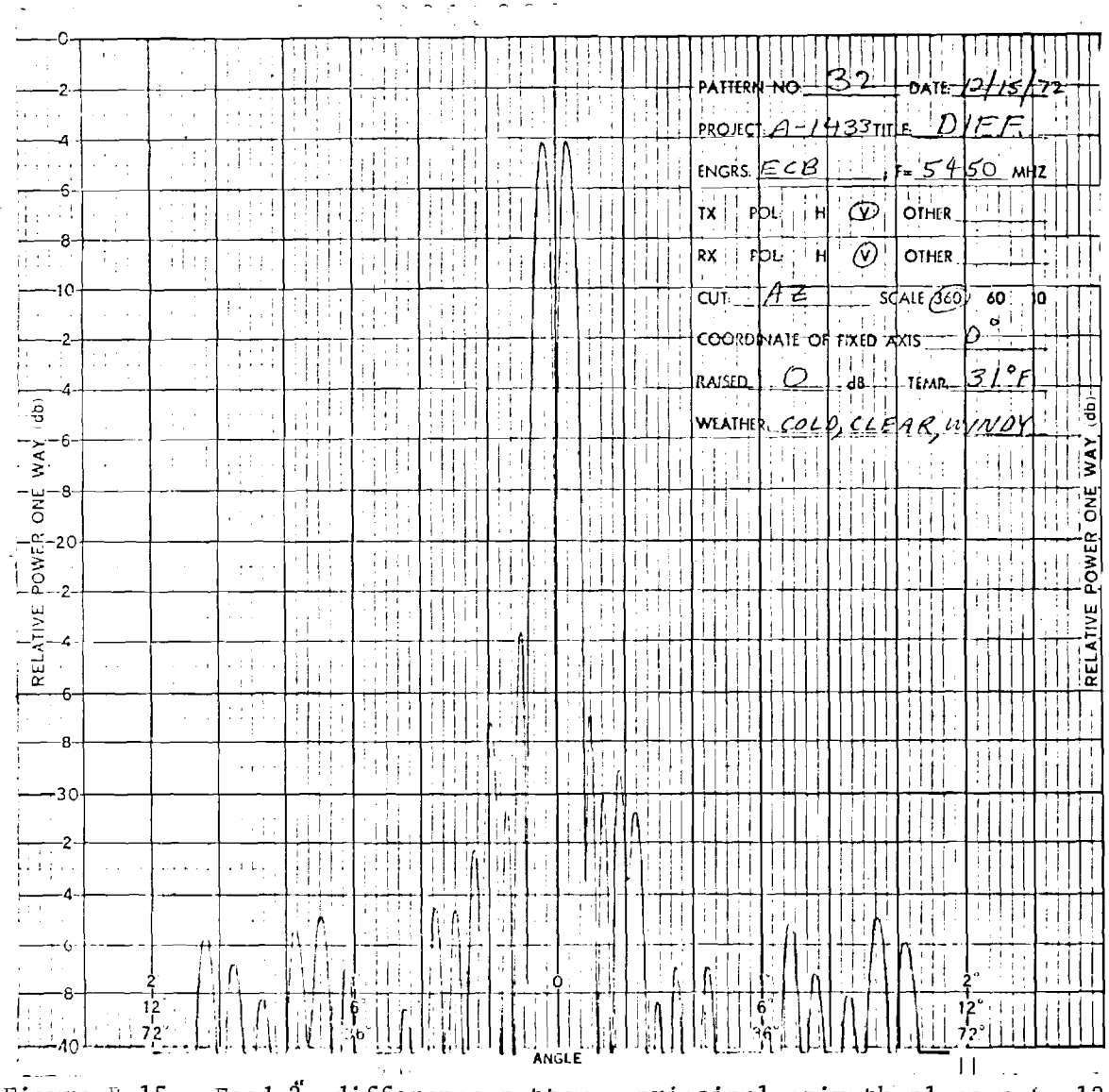

Figure B-15. Feed 2, difference pattern, principal azimuth plane cut, 12 degrees per major division.

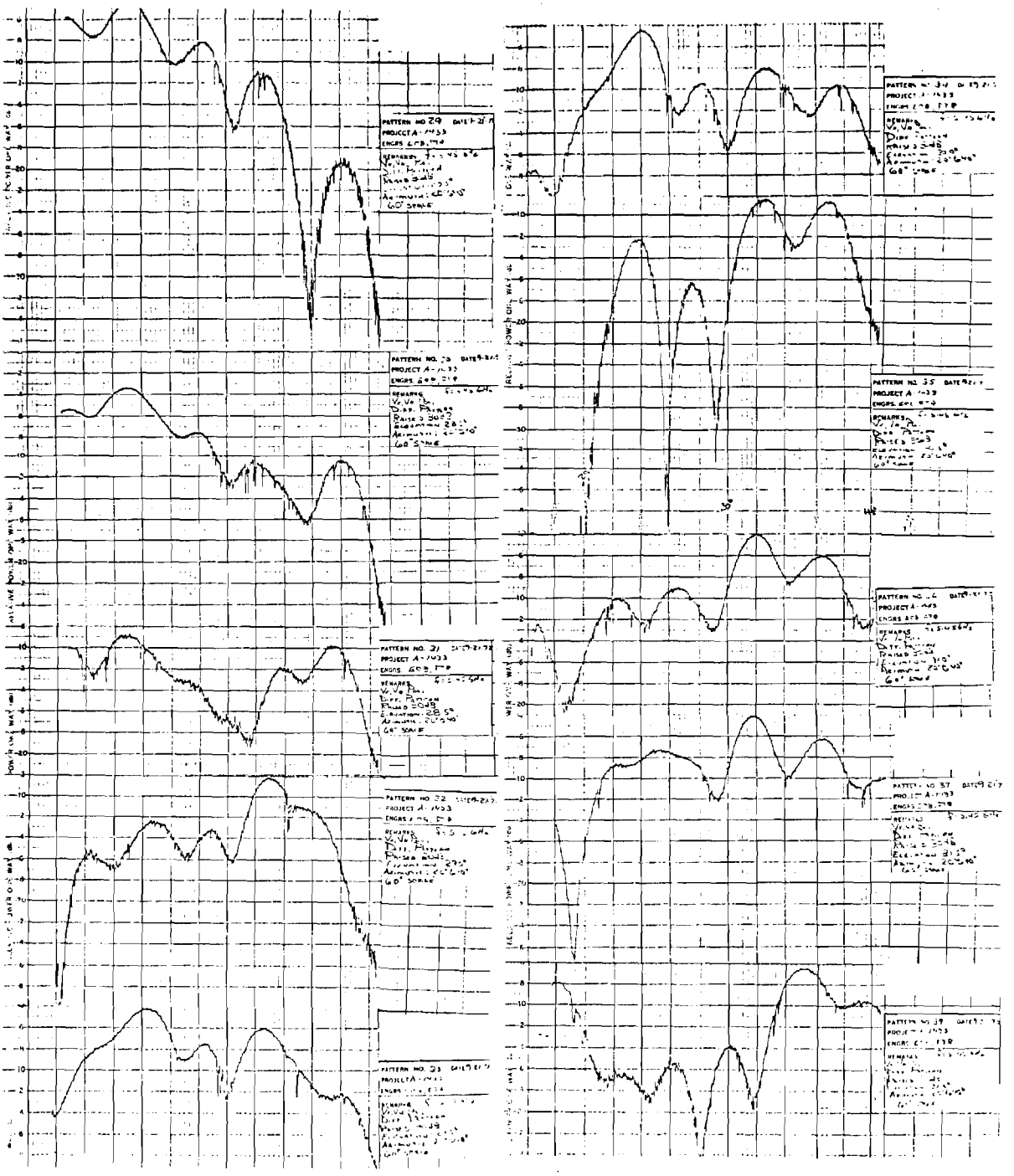

Figure B-16. Feed 1, difference pattern, azimuth plane cuts for RMS sidelobe determination taken over elevation angles of 27.5 to 32.5 degrees at 0.5 degree increments. This represents one-quarter the data collected for a single RMS sidelobe value, cuts raised 20 dB.

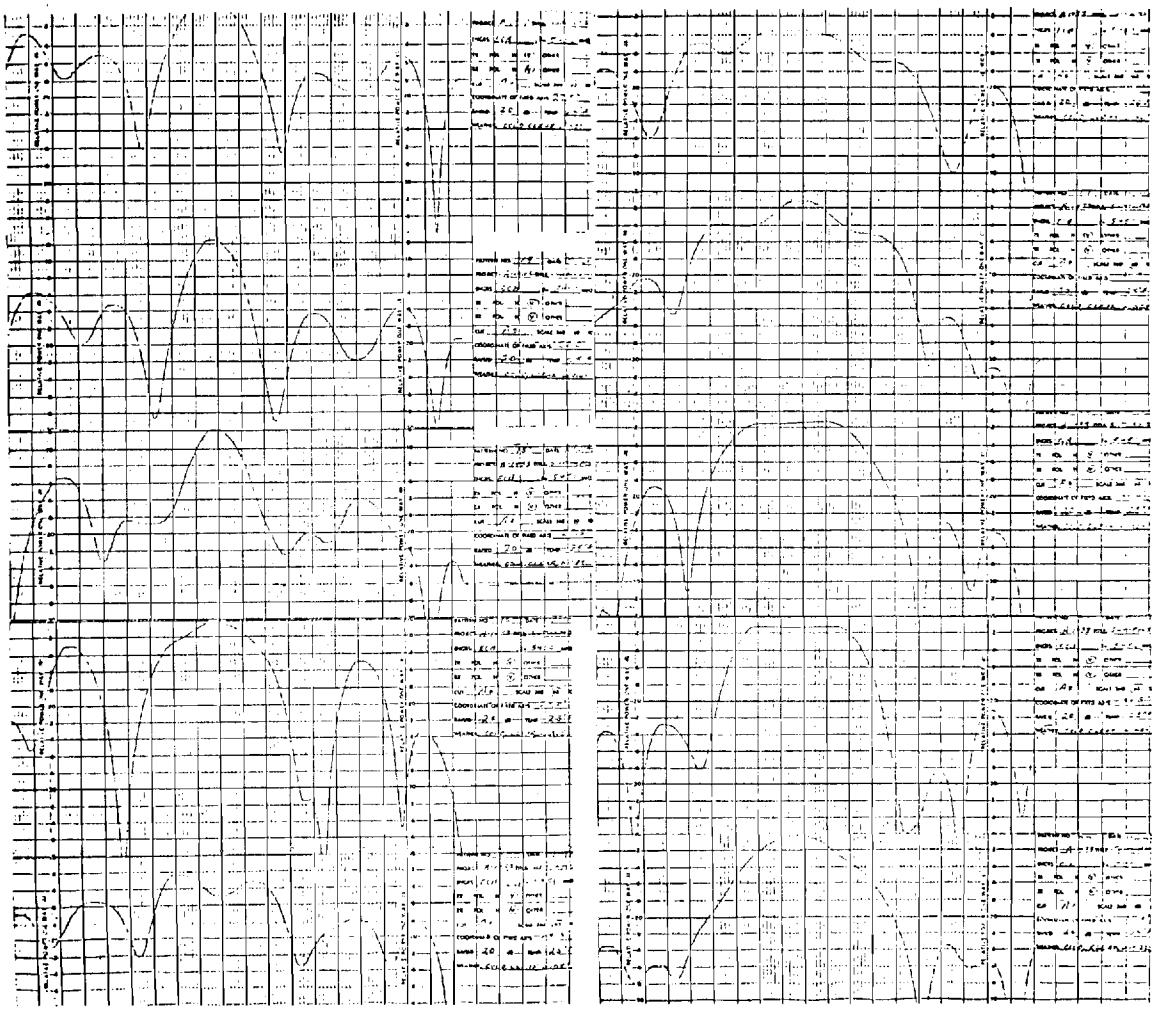

Figure B-17. Feed 2, sum pattern, azimuth plane cuts for RMS sidelobe determination taken over elevation angles of 27.5 to 32.5 degrees at 0.5 degree increments. This represents one-quarter the data collected for a single RMS sidelobe value. Cuts raised 20 dB.